Chinese Chemical Letters 37 (2026) 112243

Contents lists available at ScienceDirect

Chinese Chemical Letters

journal homepage: www.elsevier.com/locate/cclet

Metal-organic frameworks for clean water

Xiao-Hong Yi[a,1], Hong-Yu Chu[a,1], Chao-Yang Wang[b,1], Hang Ren[c,1], Li-hong Zhou[d,1], Yujie Zhao[e,1], Fu-Xue Wang[f,1], Hao Du[i,1], Yixuan Zhai[j,1], Tao Xia[k,1], Shaohua Guo[j,1], Xiaoning Wang[l,1], Yunlong Wang[m,1], Qian Wen[n,1], Ge Shen[a,1], Meng Yang[p,q,1], Yu-Hang Li[r,1], Mingjia Xu[s,1], Xiaoyuan Zhang[c,*], Hao Wang[d,*], Xudong Zhao[e,*], Yifei Sun[f,*], Yi-Lin Liu[g,*], Qingyi Zeng[g,*], Yuying Deng[h,*], Qi Wang[i,*], Xiaodong Zhang[j,*], Jie Li[k,*], Ning Liu[j,*], Chuanxi Yang[l,*], Jiansheng Li[m,*], Anping Wang[n,*], Xun Wang[o,*], Xuchun Qiu[p,q,*], Haodong Ji[r,*], Xuedong Du[s,*], Jiaxing Wu[t,*], Chong-Chen Wang[a,*]

[a] *Research center of Environmental Functional Materials, Institute of Advanced Materials, Beijing Key Laboratory of Functional Materials for Building Structure and Environment Remediation, Key Laboratory of Urban Stormwater System and Water Environment (Ministry of Education), Beijing University of Civil Engineering and Architecture, Beijing 100044, China*

[b] *Institute of Environment and Sustainable Development in Agriculture, Chinese Academy of Agricultural Sciences, Beijing 100081, China*

[c] *State Key Laboratory of Regional Environment and Sustainability, School of Environment, Tsinghua University, Beijing 100084, China*

[d] *College of New Materials and Chemical Engineering, Beijing Key Lab of Special Elastomeric Composite Materials, Beijing Institute of Petrochemical Technology, Beijing 102617, China*

[e] *College of Chemical Engineering and Technology, Taiyuan University of Science and Technology, Taiyuan 030024, China*

[f] *Key Laboratory of Agro-Forestry Environmental Processes and Ecological Regulation of Hainan Province, School of Environmental Science and Engineering, Hainan University, Haikou 570228, China*

[g] *School of Mechanical Engineering & School of Resources & Environment and Safety Engineering, University of South China, Hengyang 421001, China*

[h] *Shandong Laboratory of Advanced Materials and Green Manufacturing at Yantai, Yantai 264006, China*

[i] *Zhejiang Key Laboratory of Solid Waste Pollution Control and Resource Utilization, School of Environmental Science and Engineering, Zhejiang Gongshang University, Hangzhou 310012, China*

[j] *School of Environment and Architecture, University of Shanghai for Science and Technology, Shanghai 200093, China*

[k] *Institute of Ecological Environmental Protection and Pollution Remediation Engineering, Anhui Agricultural University, Hefei 230036, China*

[l] *Shandong Engineering Research Center of Green and High-value Marine Fine Chemical, School of Chemical Engineering and Environment, Weifang University of Science and Technology, Weifang 262700, China*

[m] *Laboratory of Jiangsu Province for Chemical Pollution Control and Resources Reuse, School of Environmental and Biological Engineering, Nanjing University of Science and Technology, Nanjing 210094, China*

[n] *Key Laboratory for Information System of Mountainous Areas and Protection of Ecological Environment, Guizhou Normal University, Guiyang, 550025, China*

[o] *School of Resource and Environment, Linyi University, Linyi 276002, China*

[p] *School of the Environment and Safety Engineering, Key Laboratory of Zhenjiang, Jiangsu University, Zhenjiang 212013, China*

[q] *Jiangsu Collaborative Innovation Center of Technology and Material of Water Treatment, Suzhou University of Science and Technology, Suzhou 215009, China*

[r] *Eco-environment and Resource Efficiency Research Laboratory, School of Environment and Energy, Peking University Shenzhen Graduate School, Shenzhen 518055, China*

[s] *Hebei Key Laboratory of Heavy Metal Deep-Remediation in Water and Resource Reus, School of Environmental and Chemical Engineering, Yanshan University, Qinhuangdao 066004, China*

[t] *Hubei Key Laboratory of Pollutant Analysis & Reuse Technology, College of Chemistry and Chemical Engineering, Hubei Normal University, Huangshi 435002, China*

* Corresponding authors.

E-mail addresses: zhangxiaoyuan@tsinghua.edu.cn (X. Zhang), wangh@bipt.edu.cn (H. Wang), zhaoxd@tyust.edu.cn (X. Zhao), sunif@hainanu.edu.cn (Y. Sun), liuyilin@usc.edu.cn (Y.-L. Liu), qingyizeng@usc.edu.cn (Q. Zeng), dengyy@amgm.ac.cn (Y. Deng), wangqi8327@zjgsu.edu.cn (Q. Wang), zhangxiaodong@usst.edu.cn (X. Zhang), lijie314@ahau.edu.cn (J. Li), liuning@usst.edu.cn (N. Liu), yangchuanxi1989@163.com (C. Yang), lijsh@njust.edu (J. Li), anping-wang@gznu.edu.cn (A. Wang), wangxunlavender@126.com (X. Wang), xuchunqiu@ujs.edu.cn (X. Qiu), jihaodong@pku.edu.cn (H. Ji), duxd@ysu.edu.cn (X. Du), wujiaxingchem@hbnu.edu.cn (J. Wu), wangchongchen@bucea.edu.cn (C.-C. Wang).

[1] These authors contributed equally to this work.

https://doi.org/10.1016/j.cclet.2025.112243
1001-8417/© 2025 Published by Elsevier B.V. on behalf of Chinese Chemical Society and Institute of Materia Medica, Chinese Academy of Medical Sciences.

ARTICLE INFO

Article history:
Received 28 November 2025
Revised 5 December 2025
Accepted 8 December 2025
Available online 9 December 2025

Keywords:
Metal-organic frameworks
Adsorption
Advanced oxidation process
Sensing detection
Clean water
Versatile applications

ABSTRACT

This review comprehensively summarizes the latest advancements in the synthesis and multifaceted applications of metal-organic frameworks (MOFs) for clean water. It systematically explores scalable synthesis methods, from solvothermal to green mechanochemical routes, and highlights the innovative transformation of waste into high-value MOFs. The article delves into the diverse functionalities of MOFs in water remediation, including the adsorptive and catalytic removal of heavy metals, organic pollutants, pharmaceuticals, PFASs, and micro/nano-plastics. Applications in sensing, radionuclide separation, oil-water separation, and advanced membrane technologies are also detailed. Furthermore, emerging roles in water capture, algal inhibition and resource recovery are discussed. Finally, the review provides a critical perspective on future challenges and opportunities, emphasizing sustainable synthesis, life-cycle assessment, and the integration of AI for the intelligent design of next-generation MOFs, paving the way for their transition from laboratory research to real-world water treatment solutions.

© 2025 Published by Elsevier B.V. on behalf of Chinese Chemical Society and Institute of Materia Medica, Chinese Academy of Medical Sciences.

1. Introduction

Chong-Chen Wang*

The global challenge of water scarcity and pollution demands innovative and efficient technologies for water purification and remediation. Among the various advanced materials explored, metal-organic frameworks (MOFs) have emerged as a revolutionary class of porous materials with unparalleled potential for addressing these critical issues [1]. MOFs are crystalline materials consisting of metal ions or clusters coordinated to organic linkers to form three-dimensional structures [2,3]. This unique hybrid composition bestows upon them exceptional properties, including record-breaking specific surface areas, meticulously tunable pore sizes, and vast structural and chemical diversity [4,5].

The intrinsic advantages of MOFs make them exceptionally suitable for clean water applications. Their ultrahigh porosity and vast surface area provide numerous active sites for the adsorption of contaminants [2,6]. More importantly, their structural and functional tunability is a game-changer: by carefully selecting metal nodes and organic ligands, or through post-synthetic modification, MOFs can be engineered with precision to target specific pollutants, enhance water stability, and introduce multifunctional capabilities. This designability allows for the creation of "tailor-made" materials that can address complex water treatment challenges far more effectively than traditional adsorbents like activated carbon or zeolites [7–9].

Consequently, the applications of MOFs in water treatment have expanded dramatically, demonstrating remarkable versatility [10]. They have been successfully deployed for the adsorptive removal of a wide spectrum of contaminants, from heavy metal ions and emerging pharmaceuticals to persistent per- and polyfluoroalkyl substances (PFASs) and microplastics [11–16]. Beyond passive adsorption, MOFs serve as excellent platforms for catalytic processes, including photocatalytic degradation of organic pollutants and Fenton-like reactions for advanced oxidation [17–21]. Their highly ordered pores are ideal for molecular sieving, leading to their incorporation into high-performance membranes for desalination and nanofiltration [22]. Furthermore, MOFs have been engineered for sensitive sensing of aqueous pollutants, selective separation of valuable resources like lithium and uranium from water brines, and even the multi-path synergistic inhibition of harmful algal blooms [23,24].

Despite the prolific research and promising results, the transition of MOFs technology from laboratory-scale curiosity to large-scale, practical water treatment solutions requires a holistic overview that connects synthesis scalability with application-specific performance. While many reviews focus on a single application, a comprehensive discussion linking sustainable synthesis strategies, particularly the valorization of waste streams, to the broad spectrum of water purification functionalities is essential to chart the future path of this field.

The purpose of this review is to provide a systematic and up-to-date summary of the multifaceted roles of MOFs in achieving clean water. We will begin by exploring the MOFs production from lab-scale to industrial-scale synthesis, with an emphasis on green and sustainable methods. A key focus will be placed on the transformative strategy of converting waste into high-value MOFs. The core of the review will meticulously detail their applications in pollutant sensing, adsorption, catalytic degradation, membrane separation, and radionuclide recovery. Finally, we will critically assess the current challenges and future prospects, focusing on the integration of life-cycle assessment and artificial intelligence to guide the rational design of next-generation MOFs for sustainable water remediation.

2. The production of MOFs: From lab scale to large scale

Xiao-Hong Yi, Hong-Yu Chu

The construction of MOFs centers on the intentional choice and assembly of metal centers and organic molecular building blocks to produce tailored architectures with precise structural features, characteristics, and functions. Fundamental principles mainly concern the strategic pairing of metal salts, ligands, solvents, and experimental parameters [25,26]. Typically, MOFs synthesis is a multi-stage procedure that encompasses three essential steps: the establishment of coordination bonds, the nucleation phase, and crystal development. In the initial step, metal ions or clusters engage with organic linkers to form coordination bonds, setting up the fundamental scaffold of the material [25]. This phase determines the core geometry and connectivity of the MOFs. Following bond formation, nucleation occurs, where tiny stable aggregates crystal nuclei appear. Environmental factors such as thermal conditions, solvent type, and reagent concentration at this juncture profoundly impact the nuclei's dimensions and quantity, thereby shaping the ultimate morphology of the framework [27]. Subsequently, crystal growth takes place as the nuclei evolve into clearly outlined, extended networks through the continuous incorporation of metal-ligand units. Regulating the crystallization speed, along with the final size and quality of MOF crystals, is achievable by tuning synthesis variables including duration, temperature, and solvent choice. Collectively, these phases determine the integral characteristics of the MOFs, such as porosity, structural integrity, and specific surface area, which are vital for its effectiveness in catalysis, adsorption, and sensing.

All these factors make the large-scale production of MOFs challenging and drive numerous researchers and engineers to actively explore and develop novel, commercially viable synthesis routes to achieve efficient, renewable, and cost-effective MOFs production [28]. This review systematically summarizes recent advances in various synthesis methods, including solvothermal, electrochemical, microwave, and mechanochemical approaches, as well as emerging techniques such as spray drying and flow chemistry for MOFs preparation, with a focus on green and sustainable strategies for scalable synthesis. Finally, based on the current research landscape, prospects and recommendations for the future development of MOF materials are provided.

2.1. Solvothermal method

In 1995, Nalco Chemical Company and Omar M. Yaghi reported the synthesis of MOFs using the solvothermal method [29]. To date, this method continues to be the most extensive and effective approach for the gram-scale synthesis of MOFs in laboratories worldwide. The process involves mixing inorganic salt and organic linker in organic solvent within a sealed reactor, followed by heating to induce crystallization and form an insoluble extended framework. DMSO (dimethyl sulfoxide), DMF (dimethyl formamide), DEF (diethyl formamide), and DMA (dimethyl acetamide) are the most frequently employed solvents in MOFs synthesis, prized for their high boiling points. The process is termed hydrothermal synthesis when water is used as the solvent.

The solvothermal method offers remarkable customizability, allowing for the systematic optimization of numerous variables including stoichiometry, temperature, solvent, pH, reaction time, precursor concentration, and counterions. This fine-tuning governs the critical properties—morphology, structure, yield, and production cost—of the resulting porous materials. Numerous MOF families, such as the MIL series, UiO series, PCN series, *etc*., have been synthesized *via* the solvothermal method [30,31].

In 1998, Akporiaye *et al.* designed a multi-autoclave system capable of conducting 100 experiments simultaneously, featuring internal polytetrafluoroethylene-lined chambers to achieve high-throughput synthesis of zeolites (Fig. S1a in Supporting information) [32]. In 2009, Biemmi *et al.* utilized a parallel multi-autoclave system for the high-throughput synthesis of 24 different solvothermal reactions, with a systematic investigation into the effects of both compositional parameters (*e.g.*, metal salt type, concentration, pH) and process parameters (*e.g.*, temperature, time) on the formation of MOF-5 and HKUST-1.

2.2. Ionothermal method

Ionothermal synthesis utilizes ionic liquids as a dual-function medium, serving as both solvent and structure-directing template under ambient pressure conditions. The ionic liquid's cations or anions actively participate in framework assembly by acting as space-filling agents and charge-balancing components during crystallization. This direct involvement enables precise structural control while simultaneously preventing pore collapse, ultimately facilitating the formation of thermally stable MOF architectures that are often unattainable through conventional synthetic routes.

In the pioneering ionothermal preparation of an organic–inorganic hybrid compound, [bmim][BF_4] (bmim = 1-butyl3-methylimidazolium) was employed as the reaction medium to obtain [Cu(bpp)]BF_4 (bpp = 1,3-bis(4-pyridyl)propane) [33]. Within the extended one-dimensional (1D) coordination polymer framework, BF_4 anions functioned to neutralize charge, and $bmim^+$ cations were retained in the liquid phase. In recent work, Azbell *et al.* employed low-melting-point metal salt hydrates, which acted simultaneously as metal precursors and reaction media, for the ionothermal synthesis of seven azole- and salicylate-based MOFs primarily comprising transition metals Fe, Co, Ni, and Zn [34]. Furthermore, the group achieved the first ionothermal synthesis of M(III) variants within the MOF-74 family, which cannot be directly prepared under conventional solvothermal conditions [34].

However, all the aforementioned methods demand high temperatures (140–225 °C) and reaction times ranging from 16 h to as long as 3 d to produce highly crystalline MOF materials. In contrast, Sang *et al.* reported that aprotic ionic liquids of the [$C_n$mim]X ($X = Cl^-$, Br^-, I^-) serve as highly effective solvents for drastically speeding up the room-temperature synthesis of Zr-MOFs [35]. Remarkably, the reaction in [Hmim]Cl finishes in 0.5 h, compared to 120 h in DMF. The formation mechanism was dynamically traced using *in situ* small angle X-ray scattering (SAXS), X-ray absorption fine structure (XAFS), and ^1H nuclear magnetic resonance (^1H NMR) spectroscopy, revealing the rapid evolution of MOF nanoparticles [35]. This rapid, IL-based method yields defective nanoparticles with small dimensions and extensive surface areas.

2.3. Electrochemistry

The electrochemical synthesis of MOFs is an innovative and efficient alternative to conventional solvothermal methods. Its fundamental mechanism involves using an electric current to generate the metal ions *in situ* directly within the reaction mixture, rather than adding pre-formed metal salts.

BASF pioneered the electrochemical synthesis of HKUST-1 in 2005 [36]. Their method involved immersing a copper anode into a solution of the organic ligand 1,3,5-benzenetricarboxylic acid (BTC) and an electrolyte. Upon applying a specific electrical current or voltage, the anode electrochemically dissolved, releasing Cu(II) ions into the solution where they coordinated with the dissolved BTC linkers (Fig. S1b in Supporting information). According to the patent, applying 12–19 V and 1.3 A for 150 min yielded HKUST-1 powder composed of 0.5–5 μm octahedral crystals. Notably, this electrochemically synthesized HKUST-1 exhibited a superior surface area of 1820 m^2/g compared to the 1550 m^2/g typical of conventional solvothermal methods.

Building upon the foundational patent, the electrosynthesis of MOFs has emerged as a highly promising methodology due to its multiple operational benefits. This approach enables continuous production of MOFs and facilitates synthesis under considerably milder conditions than conventional solvothermal techniques. A key advantage lies in the dramatically accelerated reaction kinetics, achieving framework formation within minutes to hours rather than the days typically required by thermal methods. The process further permits real-time control over crystallization through precise modulation of electrical parameters. Notably, electrochemical routes demonstrate unique capability in generating uniform thin-film deposits and coatings, while operating at ambient temperature and pressure without requiring high-pressure reactors. Additional sustainable benefits include the recycling of nitrate counterions during the process, enhancing the method's environmental profile compared to traditional approaches. Liu *et al.* employed an electrochemical approach to fabricate large-area 2D $Cu_3(HHTP)_2$ (HHTP: 2,3,6,7,10,11-hexahydroxytriphenylene) MOF films (Fig. S1c in Supporting information), establishing a robust and tunable electrochemical synthesis route suitable for industrial-scale production of MOF films, which is expected to advance their application in nanoelectronic devices [37].

2.4. Microwave-assisted method

Microwave-assisted synthesis of MOFs operates through rapid and volumetric dielectric heating, where microwave energy is di-

rectly absorbed by the reaction mixture, causing instantaneous and massive nucleation of MOF crystals due to extreme supersaturation. This is immediately followed by a self-limiting growth phase, as the precursors are quickly consumed by the vast number of nuclei, resulting in the formation of small, uniform crystals with high phase purity in a dramatically reduced reaction time compared to conventional methods [38].

Using a rapid microwave-assisted method, Ni *et al.* fabricated three zinc-based MOFs (IRMOF-1, −2, and −3) with uniform size and well-defined cubic morphology [39]. They further demonstrated that the crystal size could be precisely tailored by varying the concentration of the reactant solution. Interestingly, leveraging cobalt's excellent microwave-absorption capability, Zhang *et al.* successfully synthesized ZIF-67 using microwave irradiation without any organic solvent, completing the process within 30 min [40]. The *in-situ* growth of MIL-101(Fe) on a substrate derived from waste polyethylene terephthalate (PET) plastic was achieved by Wang *et al. via* a microwave-assisted method (Figs. S1d-f in Supporting information) [41]. This involved hydrolyzing PET flakes with ethylene glycol and sodium hydroxide to form disodium terephthalate, followed by the addition of nitric acid and an iron salt to crystallize the MOF.

2.5. Mechanochemical method

The earliest form of mechanochemistry can be broadly understood as the grinding of several solid reactants with a pestle in a mortar to promote contact and reaction between them. A typical mechanochemical reaction involves the co-grinding or milling of powdered materials, which can be carried out manually in an agate mortar or by using powered equipment such as ball mills or other grinding machinery [42]. The kinetic energy supplied during the mechanochemical process can have multiple effects on solid powders, including heat generation, reduction in particle size (increasing specific surface area or even creating fresh surfaces), formation of defects and dislocations in the crystal lattice, localized melting, and even phase transitions. It is worth noting that mechanochemical grinding, as a form of mixing, also provides an effective mass transfer process [42]. During this process, mechanical stress can increase surface area by disrupting crystals, thereby promoting interpenetration and subsequent reactions. For mechanochemical methods, controlling reaction conditions, such as grinding time, temperature, rotational speed, and even the pressure applied by the operator is crucial. Manual grinding is often subject to various unpredictable factors, including the pressure and speed applied by the operator, as well as the material of the pestle and mortar. In contrast, powered mechanical milling can deliver higher energy input, programmable control, and the possibility of systematic investigation of complex processes, making it generally suitable for laboratory-scale or commercial synthesis.

The synthesis of MOFs *via* mechanochemistry primarily relies on three techniques: solvent-free grinding (SFG), the simplest method, requiring no solvent; liquid-assisted grinding (LAG), which offers greater flexibility and speed by using a catalytic liquid to improve mobility; and ionic liquid-assisted grinding (ILAG), which further promotes formation by incorporating a catalytic liquid with minor salt additives. With these approaches enabling access to virtually all MOF families, this section will highlight key representative examples.

Pichon *et al.* pioneered the solvent-free mechanochemical synthesis of MOF, obtaining $[Cu(INA)_2]$ (INA = isonicotinic acid) by simply grinding copper acetate with isonicotinic acid for 10 min at room temperature [43]. The scope of mechanochemistry has expanded beyond the synthesis of pure MOFs to include composite materials. For instance, Wang's group prepared a series of MOF-based composites, such as g-C_3N_4/UiO-66 [44], MIL-100(Fe)/g-C_3N_4 [45], PDINH/MIL-88A(Fe) [46], *via* direct ball milling. The resulting composites not only retained the pristine morphology of the original MOFs but also exhibited enhanced catalytic activity. More remarkably, the same group valorized waste PET plastic as both a ligand precursor and a structural substrate to fabricate a PET-based MIL-53(Fe) composite (designated PSM-53) under ambient conditions, using a kitchen grinder [47]. The mechanical grinding promoted the coordination between iron and terephthalic acid derived from PET, while simultaneously inducing surface hydrolysis to generate carboxyl groups, thereby enabling the *in-situ* growth of the MOF on the PET film.

2.6. Sonochemical method

The mechanism of ultrasound-assisted MOF synthesis is primarily driven by acoustic cavitation, where the formation and violent collapse of microscopic bubbles generate extreme local conditions of very high temperature and pressure. This phenomenon dramatically enhances mass transfer and mixing between metal ions and organic linkers, while simultaneously inducing rapid and massive nucleation. As a result, the process yields highly crystalline MOFs with small particle sizes and narrow size distributions in a significantly shorter time compared to conventional methods, all often achievable under ambient conditions.

Qiu *et al.* first reported that by subjecting zinc acetate dihydrate and benzene-1,3,5-tricarboxylic acid (H_3BTC) in 20% volume ethanol aqueous solution to ultrasonic irradiation for 5.0 min at room temperature and atmospheric pressure, the fluorescent MOF $Zn_3(BTC)_2{\cdot}12H_2O$ could be obtained with a high yield (75.3% based on H_3BTC) [48]. Furthermore, as the reaction time extended from 10.0 min to 90.0 min, the yield of $Zn_3(BTC)_2{\cdot}12H_2O$ gradually increased from 78.2% to 85.3%. This demonstrates that ultrasound enables the rapid synthesis of MOFs with high yields. Moreover, Hajra *et al.* first employed an ultrasound-assisted synthesis method to prepare biocompatible cyclodextrin-based MOF materials under room temperature conditions (Fig. S1g in Supporting information) [49].

2.7. Flow chemistry

Flow chemistry, also known as continuous-flow synthesis, revolutionizes MOF preparation by transitioning from traditional batch reactions to a controlled, continuous process. Its core mechanism involves the precise pumping of separate precursor solutions, typically containing the metal salt and the organic linker, into a microfluidic reactor. Within this confined reactor, the streams rapidly mix, initiating nucleation. The key advantage is the exquisite control over reaction parameters: residence time (controlled by flow rate), temperature, and pressure are precisely maintained throughout the reactor's length. This ensures every fluid element experiences identical conditions, leading to uniform nucleation and growth. This results in highly uniform MOF crystals with superior properties, including controlled size, narrow size distribution, and high purity. The continuous nature of the process also eliminates batch-to-batch variations, enhances reproducibility, improves safety when handling hazardous reagents, and is inherently scalable for industrial production.

A pioneering study by Ameloot *et al.* in 2011 demonstrated the first application of microfluidics for constructing MOFs [50]. As illustrated in Fig. S1h (Supporting information), their method involved injecting reagent phases into an immiscible continuous fluid within a microreactor, leading to the spontaneous generation of droplets that served as isolated reaction chambers. This technique leveraged the inherent immiscibility of oil and water to template the self-assembly of hollow HKUST-1 microcapsules from copper trimesate. The crystallization was characterized as a

dynamic sequence of continual nucleation and growth, ultimately yielding crystalline MOF membranes with walls of consistent thickness.

Kim *et al.* reported a microfluidic channel-embedded solution-shearing (MiCS) technique for the rapid ($\leq$5 mm/s) and scalable production of high-quality, nanocatalyst-embedded conductive MOF (C-MOF) thin films (Fig. S1i in Supporting information) [51]. These films feature precise thickness control, achievable down to several tens of nanometers. The MiCS process facilitates the *in-situ* formation of nanoscopic catalyst-MOF particles within microfluidic channels while concurrently enabling their uniform deposition over large areas *via* solution shearing. Therefore, MiCS presents an efficient strategy for producing advanced functional porous materials.

2.8. Supercritical liquids

The synthesis mechanism of MOFs using supercritical fluids like high-temperature water (HTW), CO_2-expanded liquid (CXL), supercritical CO_2 ($scCO_2$), leverages the unique hybrid properties of substances beyond their critical points [52–54]. These fluids combine gas-like diffusivity and low viscosity with liquid-like density and solvating power, enabling them to act as exceptional reaction media. This facilitates rapid mass transfer of metal precursors and organic linkers, promoting fast nucleation and the growth of high-quality crystals. A defining advantage of this approach is its ability to integrate synthesis with activation into a single step. The supercritical fluid, particularly effective with $scCO_2$ due to its zero surface tension, can penetrate the nascent MOF pores and completely remove solvent molecules and unreacted species without inducing capillary forces that would collapse the delicate framework.

Ibarra *et al.* first demonstrated the feasibility of synthesizing MOFs using near-critical water (300 °C) as the solvent with high yield, and reported a novel Zn(II)-carboxylate material ($\{[Zn_2(L)]\cdot(H_2O)_3\}\infty$, where H_4L = 1,2,4,5-tetrakis(4-carboxyphenyl)benzene) synthesized exclusively with H_2O as the reaction medium [52]. Peng *et al.* achieved template-free assembly of mesoporous MOF by using CXL as a switchable solvent [53]. They produced mesoporous HKUST-1 with large mesopores (13–23 nm), whose pore properties could be conveniently regulated by controlling the CO_2 pressure. In addition, owing to the viscosity-reducing effect of CO_2, the reaction between metal salts and organic ligands to form the MOF was accelerated, and the resulting products could be recovered *via* CO_2 extraction. Recently, Yu *et al.* represented the first report on employing supercritical ethane (scC_2H_6) to fabricate high-pressure-tolerant ZIF-8 membranes (Fig. S2a in Supporting information) [54].

2.9. Spray-drying synthesis

Spray-drying synthesizes MOFs through a continuous, one-step process that transforms precursor solutions into solid MOF particles *via* rapid solvent evaporation (Fig. S2b in Supporting information) [55]. The mechanism involves atomizing the solution containing metal ions and organic linkers into fine droplets within a hot gas chamber. The instantaneous evaporation of solvent creates extreme supersaturation within each micro-droplet, triggering rapid nucleation and crystallization of MOF structures. This confined droplet environment ultimately produces spherical, often hollow, MOF particles with controlled morphology in a scalable continuous operation rather than batch processing.

Maspoch *et al.* reported spray-drying as a versatile strategy for assembling NanoMOFs into spherical, hollow superstructures with diameters under 5 μm, encompassing materials such as HKUST-1, Cu-BDC (terephthalic acid, H_2BDC), NOTT-100, MOF-14, MOF-74/CPO-27, MIL-88A, MIL-88B, Zn-MOF-74/Ni-MOF-74, UiO-6. They demonstrated that these resulting hollow spheres could be processed into stable colloids, which could then be disassembled *via* sonication into discrete, homogeneous NanoMOFs. Furthermore, Maspoch *et al.* encapsulated HKUST-1 within polystyrene (PS) microspheres *via* the spray-drying technique, forming an HKUST-1@PS composite to enhance its stability in aqueous environments [56].

2.10. High gravity technology

High gravity technology fundamentally enhances MOF crystallization by leveraging intense centrifugal forces in a rotating packed bed reactor to achieve instantaneous, molecular-level mixing of precursors. This creates a massive and uniform supersaturation shock, triggering simultaneous nucleation of countless crystal seeds while suppressing uncontrolled growth, which ultimately yields uniform, nanoscale MOFs with narrow size distribution in mere seconds [57].

Chang *et al.* reported the pioneering use of high-gravity technology for MOF synthesis [58]. This breakthrough method utilizes the dramatically intensified molecular mixing and mass transfer in a high-gravity field to instantaneously produce six typical MOFs in a continuous flow (Fig. S2c in Supporting information). The obtained crystals are monodispersed below 5 nm, smaller than previously reported and approaching the unit cell scale.

2.11. Liquid-phase plasma

Jiang *et al.* introduced an innovative approach for the rapid, low-energy, and environmentally friendly synthesis of MOFs under mild reaction conditions [59]. This method utilizes electric power to generate dielectric barrier discharge (DBD) plasma within the precursor mixture (Fig. S2d in Supporting information). Of significance, this DBD-driven approach is suitable for the tailored synthesis of various MOFs (MOF-5, HKUST-1, ZIF-8, UiO-66, $Mn_2(BDC)_3(DMF)_2$, Tb(BTC)(DMF), UiO-66-NH_2) and their composites (Au@ZIF-8, Ag@ZIF-8) using solvents such as DMF or alcohol. The formation of liquid-phase plasma *via* DBD promotes the generation of $DMF^{\bullet}$ radicals and free electrons, which facilitate proton removal from organic linkers by consuming released H^+ to yield H_2 or *N*,*N*-dimethyl-carbinol-amine through low-energy pathways. As a result, the crystallization of MOFs proceeds with markedly accelerated kinetics, rendering the strategy rapid, sustainable, and energy-efficient compared to conventional techniques.

2.12. Flame aerosol

Recently, Liu *et al.* established a one-step, continuous flame aerosol process for synthesizing MOFs (Fig. S2e in Supporting information) [60]. This method involves injecting a liquid precursor into a flow reactor, where it is rapidly atomized into droplets. Through instantaneous solvent evaporation and high-temperature exposure within milliseconds, the process facilitates a far-from-equilibrium, droplet-to-particle conversion. This mechanism typically yields hollow spherical particles, often trapping the material in metastable states such as nanocrystalline or amorphous MOFs, which are kinetically controlled products. The properties of the resulting MOFs can be precisely tuned by adjusting various reaction parameters like gas flow rates and precursor composition.

2.13. Other methods

Rasmussen *et al.* demonstrated a novel approach for MOF preparation by integrating $scCO_2$ with a continuous-flow system (Fig. S2f in Supporting information) [61]. In this method, $scCO_2$ is

introduced through a customized counter-current mixer, which significantly enhances heat and mass transfer to the MOF precursor materials. Using this technique, UiO-66 was synthesized at a production rate of 104 g/h. The process features an extremely short reaction time (<3 s), straightforward scalability, and the ability to recover both wastewater and unreacted starting materials.

Zhang *et al.* discovered that combining electrochemistry with ionic liquids enables the rapid synthesis of various MOFs at room temperature without external energy input (Fig. S2g in Supporting information) [62]. This was achieved in a novel ionic liquid medium, 1-octyl-3-methylimidazolium bromide (OmimBr). MOFs such as NU-1000, UiO-66, UiO-67, PCN-94, Rod-8, and MFM-300 were successfully prepared. The stable Omim• radicals present in the solution significantly accelerate the coordination between metal centers and organic linkers, facilitating fast synthesis under ambient conditions. This radical-based approach greatly streamlines MOF synthesis strategies and readily allows for structural tunability. Such a versatile, adjustable, and sustainable radical-mediated pathway holds broad application prospects.

Artificial intelligence (AI) and machine learning (ML) present powerful tools for optimizing MOF synthesis by efficiently predicting and fine-tuning key experimental parameters, such as solvents, temperature, reaction time, and concentrations, which critically influence crystallinity, morphology, and product yield. Leveraging trained models, genetic algorithms, and platforms like SyCoFinder, these approaches markedly reduce synthesis time, improve material quality, and facilitate the production of novel or traditionally difficult-to-access MOF structures [25]. This integration not only accelerates the optimization of established methods but also supports the development of scalable and innovative synthetic routes, advancing MOF research and expanding their practical applications.

2.14. Large-scale production of MOFs

By optimizing the synthesis in a 200-L Hastelloy C-276 reactor, Seo *et al.* enabled the scalable production of fluorine-free MIL-100(Fe) using solvothermal method, achieved a batch yield of 15.6 kg (Fig. 1a) and a space-time yield (STY) of ~450 kg m^{-3} day^{-1} [63]. Crawford *et al.* achieved remarkable STYs in the synthesis of HKUST-1, ZIF-8, and Al-fumarate *via* a twinscrew extruder by using the mechanochemical method, reaching 144,000, 144,000, and 27,000 kg m^{-3} day^{-1}, respectively, as illustrated in Fig. 1b [64]. To date, numerous benchmark MOFs, including HKUST-1, ZIFs, UiO-66, MOF-74, and IRMOF-5, can be synthesized rapidly and in bulk *via* mechanochemical methods.

Among various synthesis techniques, spray-drying stands out due to its established industrial applications in sectors like food and pharmaceuticals, along with inherent scalability. A collaboration between David Farrusseng, Axel'One, Maspoch, MOFApps, and under the ProDIA project successfully demonstrated the large-scale spray-drying production of HKUST-1 and ZIF-8 (Fig. 1c), highlighting the potential of this method [55]. Using a custom-built pilot-scale spray-dryer, 158 kg of an aqueous precursor slurry was processed to produce 18 kg of high-quality MOF beads, achieving an exceptional mass yield of 99 % and a solvent recovery rate of 95 %, with an estimated STY of 1000 kg m^{-3} day^{-1}. The resulting



Fig. 1. (a) Photograph of a 70 L transparent container containing the dried MIL-100(Fe)_NF8 powder produced in a 200 L batch. Copied with permission [63]. Copyright 2012, Elsevier. (b) Twin screw extruder with key parts highlighted. Copied with permission [64]. Copyright 2015, Royal Society of Chemistry. (c) Pictures of the industrial-scale spray-drying facility at Axel'One and the crystalline HKUST-1 product. Copied with permission [55]. Copyright 2020, American Chemical Society. (d) The synthesis of MOF-303 was scaled up to a 3 kg yield in a 200 L reaction vessel. Copied with permission [65]. Copyright 2020, Springer Nature.

HKUST-1 material exhibited a high specific surface area exceeding 1600 m^2/g, confirming the industrial viability of this process.

Notably, several well-known MOFs, including MOF–5, MOF–74, MOF–177, HKUST–1, ZIF-67, ZIF–8, can be synthesized under ambient conditions through the simple blending of their precursors. This approach, often referred to as a direct precipitation reaction, highlights that the crystallization of certain MOFs occurs over a very brief timescale. Yaghi and his colleagues designed a setup for large-scale MOF production using base-assisted direct precipitation, as shown in Fig. 1d [65]. The vessel has a reaction volume of 200 L. First, the organic ligand 1*H*-pyrazole-3,5-dicarboxylate ($H_2PZDC{\cdot}H_2O$) was dissolved in an aqueous sodium hydroxide solution, with the molar ratio of NaOH to H_2PZDC maintained at 3:1 to maximize the yield. Subsequently, an aqueous solution of $AlCl_3{\cdot}6H_2O$ was slowly added into the vessel through a feeding funnel. With stirring, the white precipitate MOF-303 gradually forms (inset in Fig. 1d). In consideration of the material's potential commercialization, their method proved capable of manufacturing 3.5 kg per batch with a 91 % yield. Moreover, the MOF-303 produced on this large scale exhibited analogous crystalline quality and moisture absorption performance to its lab-scale counterpart.

The separation of MOFs, particularly nanosized crystals, poses significant challenges including inefficient solid-liquid separation due to their colloidal nature, high solvent consumption during washing, and risks of framework damage. Isolating prepared MOFs from large-volume mother liquor (>3 L) poses a major bottleneck for industrial scaling, with conventional centrifugation and Buchner funnel filtration being inefficient, time-consuming, and energy-intensive due to transfer difficulties, long processing times, and slow drying. Membrane separation, particularly using robust PVDF membranes, offers a promising continuous solution by rejecting particles *via* size exclusion while permitting solvent permeation. This principle was successfully demonstrated by Goethem *et al.*, who separated various MOFs from suspension using a crosslinked PVDF flat membrane [66]. Chu *et al.* demonstrated the effective separation of MOFs from large-volume suspensions using an automated, custom-designed apparatus equipped with off-the-shelf PVDF hollow fiber membranes [67]. Evaluation with industrial-grade MIL-88A(Fe) revealed dramatic reductions *versus* centrifugation: a 62 % drop in investment, 82 % in operating costs, complete elimination of labor, 90 % shorter processing time, and a 36 % lower unit price. The separated MIL-88A(Fe) powder, easily removed by gentle vibration, maintained high crystallinity and morphology, and showed superior performance in photo-Fenton degradation of contaminants. The membrane itself could be reused instantly without cleaning. More encouragingly, the method's applicability was successfully extended to other frameworks like ZIF-8 and ZIF-67, confirming its promising prospect for the practical, high-throughput manufacturing of MOFs.

Finally, the steps of activation and purification are essential but often neglected in the mass production of MOFs. Activation generally entails eliminating solvents or opening pores to reveal the internal surface of the frameworks. Sustainable methods, such as supercritical CO_2 drying, vacuum-assisted thermal activation under mild conditions, and microwave-assisted drying, can lower energy use and limit solvent waste. In purification, switching from DMF to ethanol, water, or bio-derived solvents for washing helps lessen environmental harm. Sustainability can be further improved through closed-loop solvent recovery and membrane-based filtration techniques. A promising future approach involves creating integrated one-pot synthesis–activation setups, which may simplify these procedures for scalable manufacturing.

The future of MOF manufacturing at scale is poised to transcend traditional synthesis, pivoting towards a holistic paradigm grounded in sustainability and intelligence. The primary driver will be the rigorous implementation of green chemistry principles, moving beyond mere solvent substitution to encompass waste minimization, energy-efficient processes like mechanochemistry and continuous flow, and the design of inherently safe and renewable pathways. This green transition must be quantitatively validated through comprehensive life cycle assessment (LCA), which evaluates the environmental footprint from raw material extraction to end-of-life disposal, ensuring that the pursuit of scalability does not come at an unacceptable ecological cost. The ultimate vision is a closed-loop, intelligent production system where AI guides the synthesis of green-by-design MOFs, whose environmental and economic viability is proven by LCA from the outset, thereby accelerating their transition from laboratory curiosities to impactful industrial materials.

3. Transforming waste into high-value-added MOFs

Chao-Yang Wang

Transforming waste into high-value MOFs for water treatment presents a sustainable strategy to simultaneously address the dual challenges of waste management and water pollution. However, the heterogeneity and variability of waste composition can pose challenges to the purity, crystallinity, and structural consistency of the synthesized MOFs, ultimately compromising their performance and commercial viability. This chapter systematically reviewed the waste sources encompassed a range of materials, covering the waste electronic scrap, industrial sludge, polyethylene terephthalate (PET) plastics, polylactic acid (PLA) and so on . Methodologies for MOFs fabrication was meticulously delineated, including solvothermal, mechanochemical, and microwave-assisted routes. In addition, the applications of these waste-derived MOFs in water treatment, including adsorption, catalysis, and antimicrobial treatment were further reviewed. Finally, the prevailing challenges and future research prospects are discussed, expecting to outline a path for the industrialization, commercialization, and practical application of waste-derived MOFs in water treatment.

3.1. Metal sources and organic ligands from waste

The feasibility of synthesizing MOFs from waste is contingent on a systematic strategy for valorizing complex chemical mixtures through their purification and structural reorganization into MOFs. This paradigm treats waste as a source of non-traditional "secondary raw materials". A coherent methodology for this valorization involves segregating waste into two distinct precursors aligned with MOFs composition: metal-node precursor from metal-bearing waste and organic ligands precursors from organic polymer waste.

3.1.1. Metal sources from waste

3.1.1.1. Electronic waste. Electronic waste, such as printed circuit boards (PCBs), discarded cell phone, lithium-ion batteries (LIBs) and photovoltaic (PV) panels, constitutes a rich urban mine for metals like aluminum (Al) copper (Cu), zinc (Zn), nickel (Ni), and cobalt (Co) [68,69]. The conventional recover route involves hydrometallurgical processes, where acid leaching (*e.g.*, using HNO_3 or H_2SO_4) dissolves these metals from the crushed waste into ionic form [70]. The resulting leachate often requires purification (*e.g.*, *via* solvent extraction or precipitation) to remove interfering impurities like lead or tin before being directly employed in solvothermal synthesis. Mojtaba Yeganeh *et al.* demonstrated a circular approach by recovering Cu from waste PCBs through a combined leaching-electrochemical process, followed by the synthesis of a magnetic MOF (Cu) (mag-MOF(Cu)) and TiO_2/mag-MOF(Cu) composite [70]. This integrated strategy employed a synergistic $CuSO_4$-H_2SO_4-NaCl leaching system coupled with potentiostatic electrodeposition to selectively recover and purify Cu from waste printed

circuit boards. Soyeb Pathan *et al.* presented a sustainable strategy for upcycling copper foil from discarded mobile phones into electrochemically active Cu-BTC MOFs through a salt-free synthesis route [71]. This approach efficiently converted reclaimed Cu foil into Cu-BTC through a direct solvothermal process, providing a sustainable alternative to conventional salt-based synthesis.

3.1.1.2. Industrial waste. Industrial wastes including carbon black, pickling wastewater, and metal-rich sludge provide sustainable metal sources for MOFs synthesis, enabling direct conversion into functional materials *via* tailored strategies [72]. The carbon black waste bears a high load of heavy metals (~14,500 ppm), including Ni, iron (Fe), and vanadium (V), making it a candidate for metal recovery through chemical leaching [73]. Wang *et al.* demonstrated the synthesis of vanadium-based MOFs (V-BDC) from carbon black waste [74]. V is recovered from carbon black waste through a multi-step process. The waste is first dried and then subjected to basic leaching using NaOH. V in the resulting leachate was reduced from V^{5+} to V^{3+} using sodium dithionite as the reducing agent. Zhao *et al.* developed a direct hydrothermal conversion of stainless steel pickling wastewater into Fe/Cr-MIL-100, utilizing the wastewater itself as an integrated source of metals, solvent, and acid modifier [72]. The method eliminated conventional metal salts and external acids, simplifies synthesis units, and operates robustly across varying wastewater batches and reaction conditions (150–250 g/L solid-liquid ratio, 180–220 °C). Yao *et al.* proposed a "site reorganization-porous reconstruction" strategy for the direct conversion of iron-containing industrial sludge and white sludge into MOF-derived carbon materials without exogenous chemical ligands [75].

3.1.1.3. Other sources. Household metallic waste (*e.g.*, aluminum cans, eggshell and brand aluminum foil) offer targeted metal sources for MOF synthesis [76,77]. Aluminum foil, tubing, and mesh could be conversed Al-based MOFs, such as MIL-53(Al), MIL-96(Al), Ca-BTC and $Ca(BDC)(H_2O)_3$ [76–78]. Joshi *et al.* converted beverage cans and household foil into both supported and non-supported MOF topologies through tailored hydrothermal and etching routes. The prepared MIL-53(Al) achieved high yields (~83 %) and similar properties comparable to conventional benchmarks [77]. El-Shahat *et al.* constructed a Ca-BTC using eggshell waste as a sustainable calcium (*Ca*) source [76]. It demonstrated a circular approach by converting eggshell waste into active Ca-acetate precursor through acid digestion, followed by solvothermal assembly with tricarboxylic acid linkers to form Ca-BTC.

Conversion of metal-bearing wastes into high-value-added MOFs represents a strategic alignment with resource regeneration and circular economy principles. While current research underscores the technical feasibility and environmental promise of valorizing diverse waste streams, key challenges regarding complex metal separation and scalable processes should be navigated. Emerging strategies employing selective ligands and tailored synthesis protocols show significant potential for bridging laboratory innovation with practical implementation.

3.1.2. Organic ligands from waste

The pursuit of sustainable organic ligands is equally critical for the green synthesis of MOFs, as traditional linkers like H_2BDC are often derived from petrochemical sources. This section explored the principal waste streams that can be valorized into functional organic ligands, primarily focusing on synthetic polymers and biomass.

3.1.2.1. Waste PET plastic. Waste PET plastic represented a rich source of H_2BDC and ethylene glycol (EG) [79]. Notably, H_2BDC serves as one of the most widely used organic ligands in constructing various MOFs, including UiO-66 [80], MIL-88B [81], MIL-101 [82], MIL-53 and so on [83]. Conversion of waste PET plastic into high-value-added MOFs *via* chemical recycling emerges as an ideal upcycling strategy [84]. Up to now, hydrolysis methods for waste PET plastic in the synthesis of MOFs have primarily centered on acid hydrolysis and alkaline hydrolysis approaches and glycolysis [84]. Alkaline hydrolysis usually proceeds under ambient pressure without catalysts. This method generates H_2BDC through a two-step pathway involving base-driven depolymerization and subsequent acidification. Bool *et al.* synthesized MIL-53(Al) using waste PET plastic bottles through a microwave-assisted alkaline hydrolysis conversion process [85]. In the hydrolysis process, PET plastic pieces were first subjected to microwave-assisted heating in a NaOH and EG medium, leading to their conversion into sodium terephthalate (Na_2BDC) and EG. Subsequently, the product was acidified with 2 mol/L H_2SO_4 to form H_2BDC. In contrast, acid hydrolysis enables direct one-step conversion of waste PET plastic into H_2BDC under strong acidic conditions. Deleu *et al.* synthesized MIL-53(Al) and MIL-47(V) *via* acid hydrolysis approach with strong nitric acid (5–7 mol/L) [86]. However, it suffers from carbonization and intermediate instability. Glycolysis, typically performed at 180–210 °C, is enhanced by Zn^{2+} catalysis to reduce reaction temperature, providing a versatile pathway for monomer recovery suited to framework construction [87,88]. Ghosh *et al.* synthesized a Sn(II)-MOF using PET-derived H_2BDC as the organic linker [89]. The H_2BDC precursor was obtained through glycolytic depolymerization of waste PET at 210 °C for 8 h.

3.1.2.2. Waste PLA. PLA waste represents an untapped source of lactic acid for MOFs synthesis [90]. PLA has been employed as a precursor in the synthesis of lactate-containing frameworks such as ZnBLD, MOF-1201, and MOF-1203. Slater *et al.* prepared three homochiral MOFs *via* one-pot synthesis method [90].

Transformation of waste polymers into organic ligands establishes a robust foundation for sustainable MOFs production. Future work should focus on expanding the library of polymer-derived ligands, optimizing integrated recovery processes, and conducting techno-economic analyses to assess industrial feasibility.

3.2. Synthesis strategies for waste-derived MOFs

Up to now, the synthesis of MOFs from waste materials relies primarily on hydrothermal, microwave-assisted, and mechanochemical methods, with the specific strategy dictated by the characteristics of the available ligand and metal sources [71,72,86,91]. Current methodologies encompass two main routes: (1) A two-step process involving waste transformation into ligands or metal ions followed by MOF synthesis, which ensures high-purity products but involves separate stages; (2) a one-pot strategy where waste conversion and MOFs formation occur simultaneously under compatible reaction conditions [71,74,90]. Pan *et al.* Prepared a waste PET-derived MIL-53(Al) *via* microwave digestion and hydrothermal autoclave (Figs. 2a and b) [91]. Prior to synthesis, waste plastic bottles were subjected to alkaline hydrolysis for depolymerization, followed by H_2SO_4 acidification to isolate H_2BDC. Kabtamu *et al.* prepared a EPS-derived MOF MIL-53(Cr) through a facile hydrothermal method [92]. The fabrication of MIL-53(Cr) from EPS encompassed two integrated stages: sludge pretreatment involving filtration, drying, and homogenization, followed by hydrothermal synthesis at 220 °C using H_2BDC as the organic ligands. The strategy employs trace hydrofluoric acid (HF) as a crystallization modulator to construct highly crystalline microrods with optimized porosity and surface area, while achieving one-step integration of metal extraction and framework

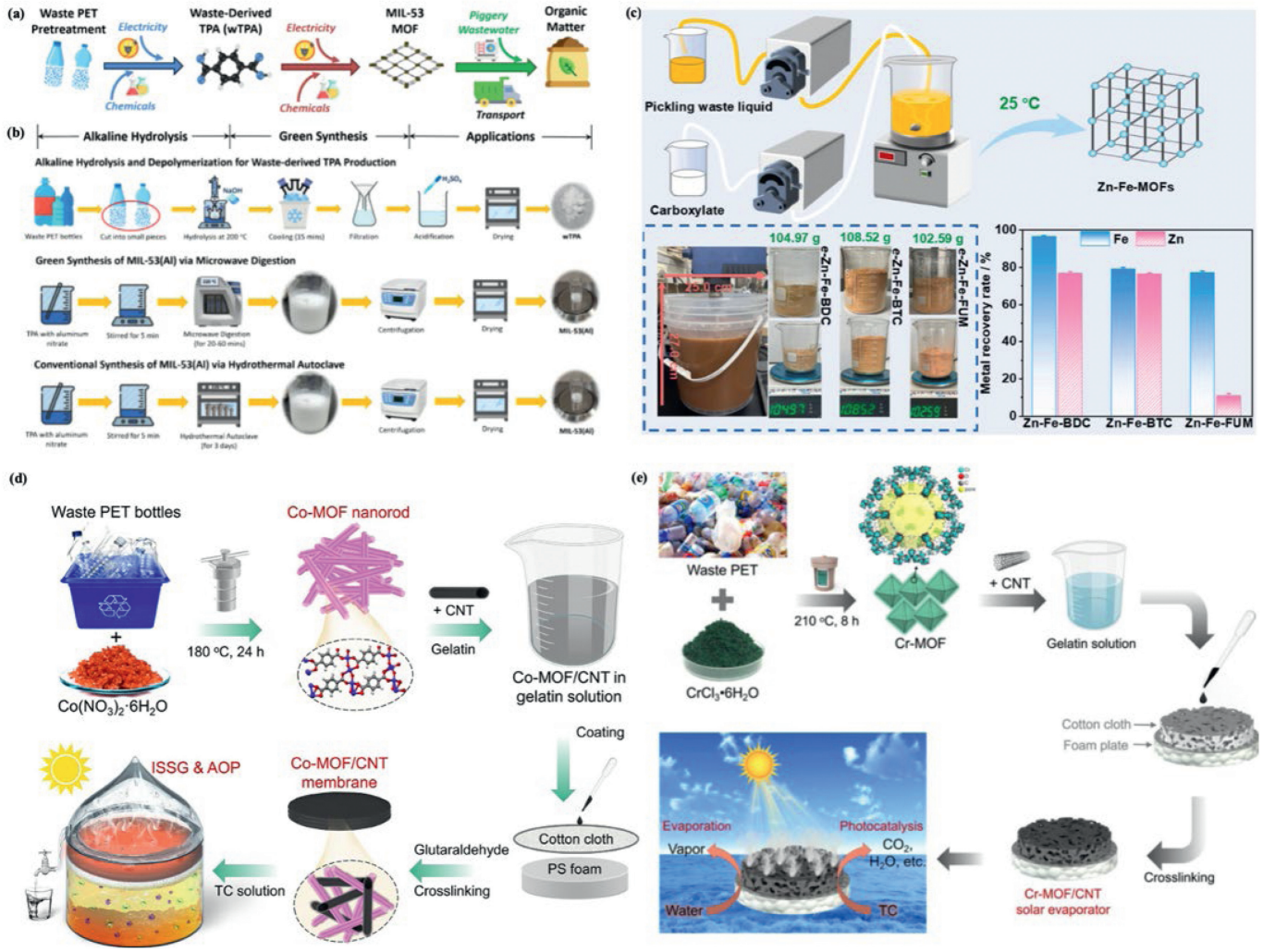


Fig. 2. (a) Scheme of synthesizing waste PET-derived MIL-53(Al) toward piggery wastewater treatment. (b) the integrated strategy employing waste PET-derived TPA for the comparative synthesis of MIL-53(Al) *via* microwave and hydrothermal methods. (a, b) Copied with permission [91]. Copyright 2024, the Royal Society of Chemistry. (c) Preparation pathway and pilot-scale evaluation of Zn/Fe-MOFs synthesized from galvanizing pickling waste, featuring metal recovery efficiencies for the Zn-Fe-BDC, -BTC, and -FUM frameworks. Copied with permission [102]. Copyright 2025, Elsevier. (d) Architectural design of a Co-MOF/CNT membrane for solar-driven evaporation and tetracycline photocatalysis. Copied with permission [103]. Copyright 2023, Elsevier. (e) Synthesis of a dual-function Cr-MOF/CNT composite evaporator from waste PET for interfacial solar water evaporation and tetracycline photodegradation. Copied with permission [104]. Copyright 2025, Elsevier.

assembly. Among these, mechanochemical synthesis stands out for its solvent-free nature and scalability, though it often yields materials with lower crystallinity [47,93]. He *et al.* developed a solvent-free mechanochemical strategy (solvent-free ball milling) for directly converting waste PET plastic into crystalline BDC-based MOFs, demonstrating kg-scale production potential and broad application prospects in energy and environmental fields [93]. Unlike conventional solvothermal methods that require toxic solvents, high pressure and temperature, this approach operated under ambient conditions with significantly reduced reaction time, while producing MOFs with well-defined crystalline structures and porous morphologies composed of agglomerated nanoparticles. Recent advances have demonstrated the rational coupling of pollutant recovery pathways with MOF synthesis protocols, enabling the design of environmentally benign MOF materials that approximate closed-loop recycling of waste resources [94]. Waribam *et al.* demonstrated an integrated approach for simultaneously valorizing waste PET bottles and heavy-metal-containing wastewater through a solvent-free synthesis of magnetic MOF composites (MagMOFs) [94]. The process involved depolymerizing waste PET plastic into Na_2BDC *via* ball milling, followed by one-pot microwave-assisted reaction with iron-rich wastewater to form MagMOFs featuring embedded magnetic nanoparticles and Fe-BDC frameworks.

3.3. Applications of waste-derived MOFs in water treatment

Waste-derived MOFs exhibited excellent physicochemical properties comparable to those synthesized from commercial-grade ligands and metal salts, demonstrating versatile applicability in gas storage [95], adsorption [89,96], catalysis [75], supercapacitance [97], and antibacterial applications [98]. Utilizing waste-derived MOFs for water purification simultaneously achieves high-value waste valorization and effective sewage remediation.

3.3.1. Adsorption

Waste-derived MOFs have been employed for the efficient adsorption of environmental contaminants, including dyes, heavy metals, radioactive elements and antibiotics [84,99]. Sharma *et al.* demonstrated a waste plastic bottles and waste marble-derived Ca-MOF for highly efficient removal of uranium ($U_{(VI)}$) and thorium ($Th_{(IV)}$) from contaminated water [99]. The Ca-MOF exhibited exceptional adsorption performance, achieving remarkable removal efficiencies of 98.99 % for $U_{(VI)}$ and 99.18 % for $Th_{(IV)}$ at pH 5. In

addition, novel functional structures (*e.g.*, defect sites, hierarchical porous) might be introduced into the framework, leading to enhanced adsorption performance compared to MOFs synthesized from commercial precursors [96,100,101]. Bazzi *et al.* reported an innovative approach for synthesizing hierarchical porous HKUST-1 (W) using copper hydroxide recovered from waste electric cables through a low-temperature green process [100]. HKUST-1 (W) displayed higher adsorption capability (196.16 mg/g) toward methylene blue (MB) than HKUST-1 (C) (159.86 mg/g). This difference in adsorption capacity is attributed to the structural defects and larger pore size present in HKUST-1(W), which provide additional sites for the adsorption of MB. Furthermore, researchers have advanced the practical deployment of waste-derived MOFs in adsorption applications through the strategic development of MOF-based derivatives, composite materials, and supported MOF architectures [41,89]. Ghosh *et al.* prepared Sn(II)-MOF-derived SnO_2 NPs for manganese (Mn^{2+}) ions elimination [89]. Wang *et al.* developed supported MIL-101(Fe) (MIL-101(Fe)@PET) using waste PET plastic as ligand source and support [41]. MIL-101(Fe)@PET performed higher adsorption capability toward arsenic pollutants tradition adsorbents. Furthermore, the exceptional adsorption capacity of waste-derived MOFs enables the recovery of valuable substances from wastewater, offering a sustainable strategy for simultaneous water remediation and waste valorization. Pan *et al.* demonstrated an integrated green supply chain that converted waste PET into MIL-53(Al) for use as an adsorbent in recovering organic matter from piggery wastewater [91]. The process achieved near-complete waste PET plastic depolymerization and effective wastewater treatment, reducing total organic carbon from 510 ppm to 80 ppm (85 % removal efficiency) with a maximum adsorption capacity of 129.9 mg_C/g. Techno-economic and life-cycle assessments reveal compelling advantages: the production cost of green MW process was 43 %–85 % lower than other methods, while greenhouse gas emissions were reduced by 73 %–83 %.

3.3.2. Catalysis

Waste-derived MOFs serve as efficient heterogeneous catalysts, exhibiting exceptional performance in organic transformations, pollutant degradation, and energy conversion while providing sustainable advantages over conventional catalyst systems [105,106]. Zhang *et al.* demonstrated a pioneering strategy for the large-scale (over 100 g) synthesis of Zn/Fe bimetallic MOFs under ambient conditions, utilizing industrial galvanizing pickling waste as metal precursors (Fig. 2c) [102]. This method achieved remarkable cost reduction (over 90 %) and eliminated hazardous solvents, aligning with circular economy principles. The resulting Zn/Fe-MOFs exhibited superior photo-Fenton activity for antibiotic degradation, maintaining 95 % efficiency over five cycles due to enhanced electron transfer and robust stability. Importantly, toxicity assessments confirmed significantly reduced ecological impact of degradation byproducts. This work stands as a benchmark for transforming high-volume industrial waste into high-performance environmental remediation materials while addressing both economic and sustainability challenges. Waribam *et al.* developed a magnetic MagMOF, which exhibited exceptional catalytic performance in the degradation of MB [94]. MagMOF demonstrated remarkable functionality in advanced oxidation processes (AOPs), achieving nearly complete degradation of methylene blue within 30 min *via* Fenton-like catalysis across a broad pH range (4–9). The material maintains excellent stability, retaining 84 % degradation efficiency after five consecutive cycles. It established a comprehensive waste-to-resource platform that combines green synthesis principles with practical application performance, offering a scalable solution for dual waste management and water treatment challenges while advancing circular economic objectives in materials science. The synthesis of multifunctional materials from waste-derived MOFs has emerged as a rapidly evolving frontier, attracting growing research interest for sustainable technology development. Bai *et al.* demonstrated a robust, flexible Co-MOF/carbon nanotube (CNT) evaporator using waste PET plastic (Fig. 2d) [103]. Under 1 kW/m^2 solar irradiation, the Co-MOF/CNT evaporator achieved an exceptional evaporation rate of 2.25 kg m^{-2} h^{-1} during treatment of tetracycline-contaminated wastewater, while maintaining outstanding mechanical robustness, structural flexibility, long-term stability, and scalable manufacturing potential. Chen *et al.* reported a waste-to-MOF strategy for fabricating a bifunctional Cr-MOF/CNT composite evaporator derived from waste PET bottles (Fig. 2e) [104]. The evaporator synergistically integrated interfacial solar-driven water evaporation with peroxymonosulfate (PMS) activation for simultaneous freshwater production and tetracycline degradation. It achieved an exceptional evaporation rate of 2.46 kg m^{-2} h^{-1} and a tetracycline degradation efficiency of 92.4 %, supported by its high specific surface area (896.1 m^2/g), abundant active sites, and optimized photothermal properties. It demonstrated a sustainable paradigm for converting plastic waste into advanced materials addressing water-energy challenges.

3.3.3. Microbial inhibition

The transformation of waste into antibacterial MOFs has gained significant attention as a dual-strategy approach that concurrently tackles waste accumulation and the pressing demand for effective microbial inhibition [98]. Kim *et al.* developed an eco-friendly algal control strategy *via* synthesizing support Cu-BDC chips, demonstrating effective inhibition of *Microcystis aeruginosa*. The Cu-BDC chips effectively inhibited *Microcystis aeruginosa* growth over 120 h while demonstrating significantly higher ecological safety than $CuSO_4$ algaecide in 48-h acute toxicity tests. The antimicrobial mechanism involves dual reactive oxygen species (ROS) generation pathways: Intracellular copper ions disrupt ROS-scavenging enzymes during photosynthesis, while extracellular hydroxyl radicals from Cu_2O and Cu-BDC photocatalytic reactions damage cell membranes, collectively leading to growth inhibition through ROS accumulation. Yang *et al.* presented a circular economy strategy for converting heavy-metal-contaminated biomass adsorbents into high-value antibacterial composites [107]. By employing an *in-situ* growth technique, copper ions adsorbed onto polyethyleneimine/cellulose/sodium alginate (PCS) matrices were directly utilized as metal nodes to construct HKUST-1 frameworks, achieving 88 % metal conversion efficiency. The prepared PCS@HKUST-1 composite demonstrated exceptional antimicrobial performance, with 98.14 % inhibition efficiency against *Escherichia coli*, which displayed a 20-fold enhancement compared to the original adsorbent. This approach simultaneously addresses hazardous waste management and functional material synthesis, establishing a sustainable paradigm for resource recovery and environmental remediation.

Valorizing waste into high-value-added MOFs for water treatment epitomizes a transformative strategy for sustainable chemistry, simultaneously alleviating environmental pressure and closing the materials loop with advanced functional materials. This review summarizes recent advances in the fabrication of MOFs from waste materials and their applications in water treatment. It systematically outlines the sources of waste, synthesis methodologies. The synthesis strategies have evolved from initial hydrothermal and microwave-assisted methods toward greener mechanochemical approaches, which offer reduced organic solvent usage, faster reaction rates, and enhanced potential for scalable production. The synthesis of MOFs from waste has undergone a paradigm shift: From recovering pure precursors to directly employing the waste itself as the feedstock. Benefiting from the inherent structural merits of MOFs, the resulting materials exhibit versatile performance in adsorption, catalysis, and antimicrobial applications, un-

derscoring their considerable potential to advance green and circular economies.

Future research on waste-to-MOFs conversion should shift from proof-of-concept to practical implementation, focusing on several key areas. Key areas include: (1) Developing robust, cost-effective purification protocols to handle real-world waste complexity and ensure material consistency; (2) establishing standardized life-cycle assessment (LCA) and techno-economic analysis (TEA) frameworks to quantitatively validate environmental and economic benefits; (3) advancing green synthesis routes, notably solvent-free mechanochemistry, to enhance sustainability and scalability. Ultimately, integrating this technology within circular economy models will redefine waste as a strategic resource, specifically for manufacturing advanced water treatment materials.

4. MOFs for pretreatment of water samples

Hang Ren, Xiaoyuan Zhang*

Water samples from environment are considered to contain multiple trace pollutants together with complex interfering matrices. Before pretreatment, many samples do not meet the requirements of analytical instruments, nor can they achieve the sensitivity, selectivity, or reproducibility needed for reliable analysis. MOFs are ideal materials for water samples pretreatment due to their large surface areas, tunable pore structures, and diverse surface functionalities [108,109]. These properties endow MOFs with high adsorption capacity and strong selectivity. Moreover, MOFs exhibit superior designability [110–114] and scalability [115–118], which can be easily combined with other functional materials. These create a versatile framework for developing water-sample pretreatment materials according to specific analytical requirements and water features. Recently, a number of water-stable MOFs and their derivatives, including ZIF-8 [119], MOF-5 [120], MIL-53 [121], MIL-100 [122], MIL-101 [123] and UiO-66 [124], have been extensively investigated in extraction/enrichment, separation/purification, and specific capture of contaminants in environmental water samples. In this section, we discuss the application of MOFs in water samples pretreatment to illustrate their advantages and to clarify the structure-activity relationship. We also emphasize the importance of tunable synthesis and post-synthetic modification in meeting specific analytical demands. Finally, the perspectives were provided for further studies.

4.1. Extraction and enrichment

Solid-phase extraction (SPE) is one of the most widely used techniques for the extraction and enrichment of trace pollutants from water samples [125,126]. It combines separation with preliminary purification, allowing effective removal of matrix interferences, concentration of target pollutants, and convenient solvent exchange. In contrast to adsorbents designed for pollutants removal, the SPE sorbents should also exhibit fast elution, high recovery, and good reproducibility, in addition to water stability, selectivity, and extraction efficiency. Due to the cooperation of pore-size sieving and interfacial interactions, MOFs perform satisfactory extraction and enrichment performance. Various MOFs and their derivatives have been used in solid-phase microextraction (SPME) [121], dispersive solid-phase extraction (DSPE) [127], magnetic solid-phase extraction (MSPE) [128], pipette-tip solid-phase extraction (PT-SPE) [129], stir bar sorptive extraction (SBSE) [130], in-syringe solid-phase extraction (in-syringe SPE) [131], membrane-based separations [132] and other processes. Various synthesis and post-synthetic modification strategies have been developed to improve MOFs' adaptability and specificity in SPE toward pollutants with different chemical and physical characteristics.

In 2006, MOFs were employed for pollutants extraction from water samples, when zhou *et al.* [133] used copper(II) isonicotinate, synthesized from copper ions and isonicotinic acid, as the stationary phase in an SPE column to enrich eight polycyclic aromatic hydrocarbons (PAHs). Then, many MOFs and derivatives have been investigated and applied in SPE for the extraction and enrichment of environmental pollutants, such as antibiotics, PAHs, pesticides, endocrine disrupting compounds, and heavy metal ions. Although ordered pore channels of MOFs provide a structural basis for molecular sieving, their fixed pore dimensions restrict their applicability to more pollutants. Therefore, various modification strategies for pore channels and surface have been developed to improve their selectivity.

Pore enlargement can be realized by using longer organic ligand during synthesis (Fig. 3a) [134] or applying defect engineering [135,136]. For instance, the pores of UiO-66 (7.5–11 Å) are small, which allow only short-chain PFAS to diffuse into the framework, while long-chain PFAS are less accessible. ZIF-8, with larger pores, exhibits higher adsorption but poorer elution efficiency. Better PFAS extractants were expected. The pore size of UiO-66 can be enlarged by replacing terephthalic acid with longer dicarboxylates, such as 4,4′-biphenyldicarboxylic acid. This replacement significantly enhances adsorption but result in poorer elution performance. Defect engineering provides another effective method to enlarge pores. Introducing strong acids during synthesis can generate linker or node vacancies, producing a defective UiO-66 structure with an expanded pore size of about 18.5 Å. Although this process slightly reduces the adsorption capacity, the extraction efficiency is greatly improved, enabling the rapid enrichment and recovery of up to 50 PFAS species, with optimal recoveries achieved for 33 of them.

Pore constriction strategies include interpenetrated synthesis, ligand replacement, and post-synthetic modification. Interpenetrated synthesis is particularly effective for enhancing size-selective adsorption by reducing pore cavities. For example, in MIL-101(Cr), uncoordinated carboxyl groups and triazole N atoms are distributed on the inner surface, which can strongly coordinate with rare-earth ions. However, the excessively large pores hinder effective interactions between rare-earth ions and these surface functional groups. Hu *et al.* [137] synthesized an interpenetrated MIL-101(Cr) with a reduced pores diameter of 3.2 Å (Fig. 3b), which is similar to the lanthanides metal ions in diameter. This structure enhanced the interaction between rare-earth ions and the carboxylate/triazole N atoms, achieving selective enrichment of lanthanides metal ions from transition and alkali metal ions. Similarly, pore-edge reactions, as one post-synthetic modification strategy, can modify the pore structure by introducing specific functional groups at the pore openings without significantly reduction in adsorption capacity [118]. It is worth noting that the introduction of functional groups also tunes the surface electronic structure of MOFs, changing their chemical reactivity. For example, the introduction of ethylenediaminetetraacetic acid (EDTA) into MOF-808 reduced the pore size to about 11.3 Å from 16.8 Å, enabling efficient adsorption of 22 metal ions while maintaining remarkable regeneration performance [12]. According to the requirements of extraction and enrichment, a wide range of reagents, such as urea, alcohols, amines, anhydrides, aldehydes, thioalkyl, isocyanates, and cyanides, have been utilized for surface modification. The amino groups located on the internal surfaces endow IRMOFs with strong hydrophilicity. Introducing hydrophobic alkanoyl anhydrides on surface increases the water stability and internal surface hydrophobicity, thereby enhancing selectivity toward hydrophobic pollutants [141]. Similarly, post-synthetic modification strategies have been applied to improve the recovery of long-chain PFAS on UiO-66. Luo *et al.* [138] grafted oligoalkyl-quaternary ammonium (PAOQ) chain onto amino-functionalized UiO-66, forming

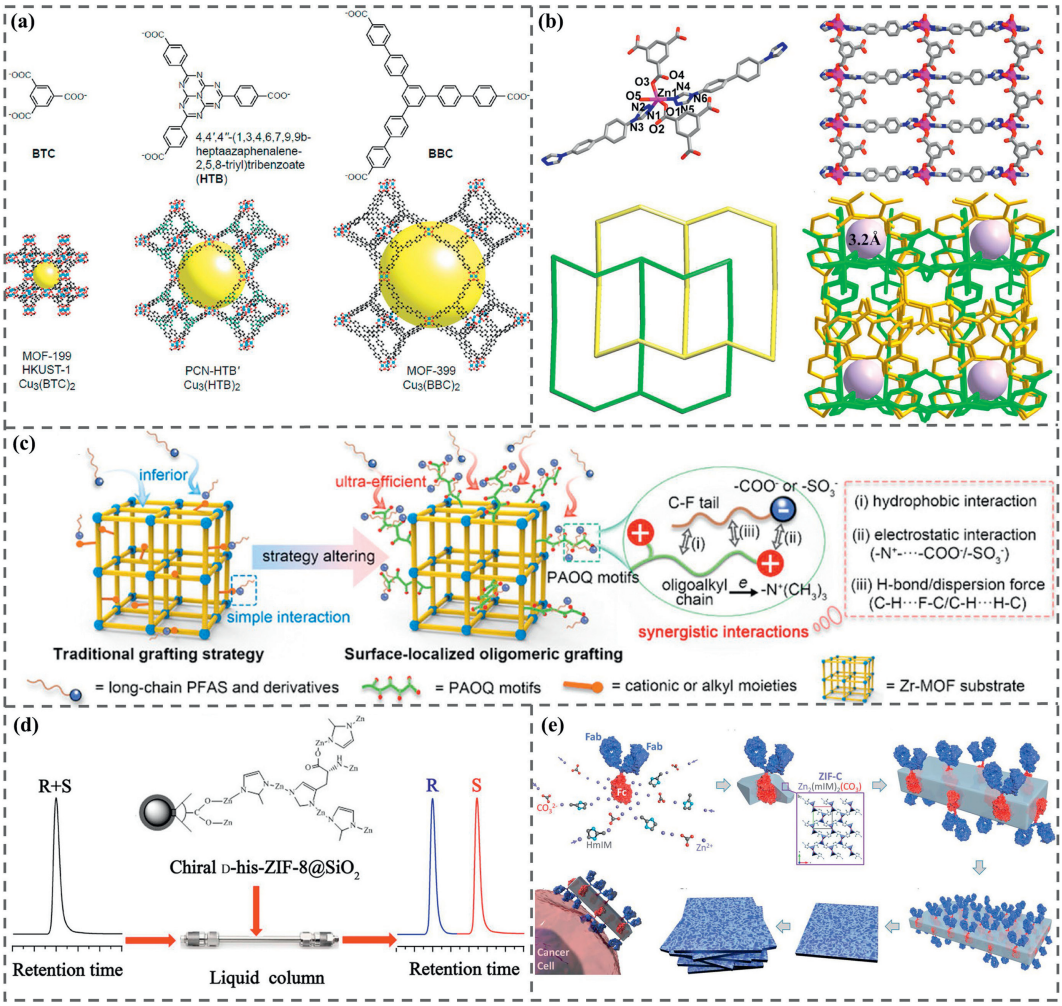


Fig. 3. Overview of MOFs application in water sample pretreatment. (a) Pore size regulation through the organic linkers of different length. Copied with permission [134]. Copyright 2011, American Chemical Society. (b) Interpenetrated synthesis strategy for narrower pore size. Copied with permission [137]. Copyright 2024, Springer Nature. (c) Surface modification through grafting. Copied with permission [138]. Copyright 2025, Wiley-VCH. (d) Silica particles functionalized with MOFs for Chromatographic separation. Copied with permission [139]. Copyright 2020, the American Chemical Society. (e) *In situ* incorporation of antibodies into MOFs during synthesis. Copied with permission [140]. Copyright 2021, Wiley-VCH.

a surface covered with proximally arranged PAOQ. The modified UiO-66 shown enhanced electrostatic and hydrophobic interactions (Fig. 3c), which became the dominant mechanism for PFAS enrichment. This UiO-66 achieved high removal (up to 94.7%) across pH 2–12 and excellent desorption efficiency (>99.6%), maintaining strong adsorption performance even after multiple cycles. Furthermore, unfavorable surface sites of MOFs can also be shielded by post-synthetic modification. For instance, polyhedral coordination cages carrying specific charges can be prepared and anchored on exposed metal sites [142]. This method regulates surface charge and electrostatic interactions with pollutants, while maintaining the internal structure and total adsorption capacity. Moreover, this process is reversible.

Besides liquid-phase extractions, MOFs with combined water, thermal, and mechanical stability—such as MOF-5, MIL-100, ZIF-8, UiO-66 and their derivatives—have also been employed as coatings in SPME for volatile organic pollutants prior to GC–MS analysis.

4.2. Separation and purification of target compounds

Chromatography is a widely used technique for separating mixtures based on differences in the interactions between the solutes and stationary phase. In contrast to SPE, chromatographic techniques demand significantly higher resolution, stability, and reproducibility. MOFs and their derivatives can also be used as stationary phases in liquid chromatography, where separation is achieved through a combination of size-exclusion effects and interfacial interactions. MOFs, including MIL-53, MIL-101, MIL-47, ZIF-8, and UiO-66, have been investigated as stationary phases for separation and purification, where they exhibit superior separation performance under suitable conditions.

The interfacial interactions and regular pore architecture give MOFs significant advantages in separations, but they also restrict their applicability to a broader range of pollutants with larger molecular sizes. In 2009, Rashid *et al.* [143] employed HKUST-1 as a stationary phase for separating aromatic compounds and PAHs. The framework features regular square pores (9 Å) that selectively adsorb aromatic molecules with smaller kinetic diameters, allowing these compounds to elute sequentially according to their interaction strengths. However, organic molecules with kinetic diameters larger than the pore size, such as 1,3,5-triphenylbenzene, cannot enter the pores of HKUST-1 and are eluted first, whereas slightly smaller molecules, such as phenanthrene and anthracene, are strongly retained within the pores. Later, MIL-53(Al) with larger pores and higher stability, was used to fabricate a reverse-phase column, exhibiting greater hydrophobicity than conventional

C18 columns in study [144]. This column performed excellent selectivity and reproducibility under both acidic and basic conditions. These studies reveal the remarkable molecular-size-dependent separation capabilities of MOFs employed in chromatography, while also highlighting their limitations in handling mixtures with broad molecular-size distributions. Environmental water samples contain diverse organic pollutants, including aromatics, PAHs, pesticides, antibiotics and dyes. These organic molecules span a wide range of molecular sizes, making effective separation difficult to achieve with a single type of MOF. Furthermore, directly packing irregular submicron MOFs particles into chromatographic columns often leads to low efficiency, poor peak shape, and high back pressure [145]. Therefore, modifying MOFs or combining them with other materials represents a promising strategy for constructing stationary phases, facilitating the development of versatile chromatographic columns for effective separation toward contaminants with a wide range of molecular sizes.

Integrating MOFs with a suitable support is an effective strategy for constructing efficient stationary phases. Silica particles [139,146,147] are a stable stationary phase for chromatographic columns, featuring uniform particle size and pore size. Their surface terminal groups facilitate the efficient immobilization of MOFs. These properties make it an ideal support for MOFs. Using silica particles modified with MOFs on surface as the stationary phase in liquid chromatography can simultaneously ensure column stability, uniformity, and selective separation performance (Fig. 3d). These stationary phases using MIL-101, ZIF-8 or UiO-66 and other MOFs on silica supports have shown remarkable separation performance for nucleosides, antibiotics, organic acids, carbohydrates, alkylbenzenes, PAHs, pesticides, and anions [146–148]. Besides covalent interaction between MOFs and silica particles, hydrogels have also been used as carrier to modify silica spheres with MOFs [147]. This strategy produces stationary phases with high column efficiency and superior selectivity. Such materials can effectively separate multiple environmental pollutants while maintaining excellent reproducibility and stability across a wide pH range.

4.3. Specific capture

Emerging contaminants and other substances of very high concern are typically present at trace levels, yet they pose considerable risks to ecosystems and human health. Therefore, specific recognition, enrichment and rapid detection is crucial for effective environmental monitoring and control. In principle, the specific recognition and capture of target pollutants can effectively minimize matrix interference and enhance sensitivity. In contrast to extraction and purification, specific capture emphasizes the selective identification and enrichment for single target pollutant. When a target molecule is specifically captured by the sites of a MOF or its composite, the interaction induces changes in the electronic structure, which in turn lead to measurable variations in its macroscopic properties [137]. Many approaches, including colorimetric, fluorescence, surface-enhanced Raman, and electrochemical techniques, have been developed using specifically designed MOF-based specific materials to enable qualitative and quantitative determination of target analytes. MOFs, with their uniform porosity, high surface area, and abundant active sites [149,150], provide an ideal platform for immobilizing molecularly imprinted polymers (MIPs) and antibodies, thereby achieving highly selective and sensitive capture of pollutants in water.

Molecular imprinting creates polymeric cavities complementary to a target molecule, which can be constructed on the surface or internal channels of MOFs. Representative MOFs such as ZIF-8, HKUST-1, and UiO-66, have been employed as carriers for molecularly imprinted polymers (MIPs). Reported preparation techniques include precipitation method, sol–gel synthesis, MOF deep eutectic solvent-MIPs, one-step synthesis, liquid crystalline, and micro-emulsion methods [149,151]. For example, MIPs templated with tetrabromobisphenol A (TBBPA) on HKUST-1 have demonstrated selective enrichment of TBBPA from water [152]. Similarly, MIL-101-based composites integrating quantum dots and surface-imprinted polymers enable fluorescence-based detection of antibiotics and pesticides [153]. After the construction of MIPs, not only the template molecules but also the MOFs used as support materials can be removed, which increases the surface area and enhances the capture of target pollutant molecules [154,155].

Immuno-recognition methods are detection approaches based on the specific binding between antigens and antibodies, enabling the selective recognition and enrichment of target pollutants in water. MOFs exhibit good biocompatibility [150,156] and can be used to protect and immobilize antibodies, enhancing their thermal, chemical, and mechanical stability [157,158], while also enabling further modification to amplify detection signal [159]. Antibodies can be incorporated into MOFs through *in situ* encapsulation during synthesis (Fig. 3e) [140] or post-synthetic modification [160] such as surface binding, grafting, or pore infiltration. MOFs commonly used for water extraction and separation, including HKUST-1, ZIF-8, MIL-53, MIL-101, IRMOF-3, and UiO-66, can also serve as carriers for antibodies. For instance, a post-synthetic modification strategy was employed to introduce Eu^{3+} ions into UiO-66-$(COOH)_2$, producing a fluorescent probe capable of the selective recognition and capture of pentachlorophenol [160]. Incorporation of pentachlorophenol-specific antibodies provided selective binding sites, yielding a fluorescence-based material for the specific capture and detection of pentachlorophenol. Similarly, monoclonal antibodies against *Staphylococcus aureus* were immobilized on a ZIF-8 support *via* Zn-S bonds, enabling the selective capture of the bacteria in water and rapid detection through bioluminescence [161].

MOFs, with well-defined structures and highly designable features, have attracted considerable attention in the pretreatment of environmental water samples and show strong potential for advanced analytical applications. Their ordered pore architectures and abundant active sites enable strong and selective interactions with specific contaminants, making them excellent candidates for enriching and purifying target analytes in complex aqueous matrices. These features also provide a solid foundation for the development of next-generation targeted analytical strategies. Nevertheless, the intrinsically fixed structures can restrict their broader applicability. One practical approach is to load MOFs onto inert supports, which allows their active sites to be fully utilized while mitigating the constraints associated with rigid pore geometries. Conversely, MOFs can also serve as hosts, where constructing specific structures within their uniform channels for pollutants recognition and capture. Looking ahead, the application of MOFs in water-sample pretreatment should be guided by specific analytical scenarios and requirements, integrating mechanistic insights with data-driven approaches to advance structural design, performance evaluation, and synthetic route optimization.

5. Sensing of aqueous pollutants in MOFs

Li-Hong Zhou, Hao Wang*

Water pollution has become an urgent global challenge threatening both ecosystem stability and public health [162]. The proliferation of industrialization and urbanization is accompanied by the persistent introduction of significant amounts of heavy metals, antibiotics, pesticides, and organic dyes into aquatic ecosystems, leading to adverse ecological and public health consequences [163]. Therefore, the development of efficient and sensitive on-site detection technologies is essential for ensuring water safety and achieving sustainable environmental management. Although conventional analytical techniques—such

as chromatography, spectrophotometry, and mass spectrometry—offer high accuracy, their high cost, complex instrumentation, and limited real-time capability hinder widespread application in field analysis. In contrast, chemical and electrochemical sensing technologies demonstrate significant advantages in sensitivity, portability, and cost-effectiveness, making them highly promising approaches for water quality monitoring. The intrinsic structural designability and chemical versatility of MOFs make them ideal candidates for constructing high-performance sensing platforms. However, most traditional MOFs suffer from hydrolytic instability and framework collapse in aqueous environments, which restrict their practical applications [164]. To address these limitations, strategies such as defect engineering, ion doping, and composite formation have been extensively employed to enhance their chemical stability and sensing performance. The primary detection mechanisms of MOF-based materials include dynamic quenching, static quenching, electron transfer, proton transfer and energy transfer. For Ln-MOFs, the common mechanisms also include the antenna effect, media effect, and second-sphere interactions. However, in most cases, the detection mechanisms are mutually reinforcing rather than operating independently.

5.1. Traditional and modified luminescent MOFs

Traditional MOFs, characterized by their high porosity, tunable coordination environments, and structural diversity, enable efficient molecular recognition and fluorescence response in aqueous pollutant detection [1]. Among them, lanthanide-based MOFs (Ln-MOFs) have become important materials for optical sensing due to their “antenna effect,” which endows them with high luminescence efficiency and selectivity. In order to improve the detection performance of MOFs, and thanks to the intrinsic adjustable structure, MOFs could also be modified by defect engineering or co-doping strategy.

5.1.1. Anion recognition

Anions play a crucial role in shaping aquatic ecosystems and influencing human health; thus, developing efficient, facile, and highly selective recognition systems is of great significance. The rod-shaped Tb-BTC MOF reported by Ding exhibits strong luminescence and specific adsorption affinity toward phosphate ions, enabling rapid and stable detection of $Cr_2O_7^{2-}$ [165]. There was a synergistic fluorescence quenching mechanism, involving resonance energy transfer arising from the spectral overlap between the anion and the emission of the phen ligand, as well as photoinduced electron transfer from the excited ligand to the anion. In contrast, the two-dimensional Co–NDC–BPY MOF reported by Bhattacharjee achieves a unique "dual-recognition integration" function through two independent optical pathways [166]: Specifically, S^{2-} forms a ground-state complex with Co(II), triggering a photoinduced electron transfer process to quench fluorescence; while HSO_4^- breaks the Co–O coordination bond through protonation, releasing the fluorescent ligand 1,4-NDC and leading to enhanced luminescence (Fig. 4a). Thus, this system can achieve distinguishable recognition of various aqueous anions by precisely regulating the metal–ligand coordination dynamics.

5.1.2. Heavy metal ions and organic pollutants

The widespread presence of heavy metal ions in environmental and food sources poses a serious threat to human health [167]. Therefore, developing efficient detection strategies for these ions is of great importance for ensuring ecological safety and protecting public health. Du combined Eu^{3+} doping with defect engineering to prepare Eu@UiO-MOFs, which enabled highly sensitive ratiometric fluorescence detection of Cd^{2+} in aqueous media (Fig. 4b) [168]. The recognition mechanism of this system relies on ratiometric fluorescence detection based on dual emission signals. Cd^{2+} coordinates with the bipyridyl groups of the ligand to form Cd–N bonds, which hinder ligand-to-Eu^{3+} energy transfer, leading to enhanced ligand emission and weakened Eu^{3+} emission. The emission intensity ratio enables quantitative determination of Cd^{2+} concentration, while missing-linker defects increase the specific surface area and pore volume, facilitating Cd^{2+} enrichment and improving sensitivity. Roh synthesized a ratiometric Tb-MOF, $[Tb_2(oba)_3(phen)_2(DMF)_2(H_2O)_4]_n$, (oba = 4,4′-oxybis(benzoic acid)) capable of specifically recognizing Cr(VI). The ratiometric signal (I_{545}/I_{362}) enhanced both detection accuracy and anti-interference capability [169]. A novel Ln-

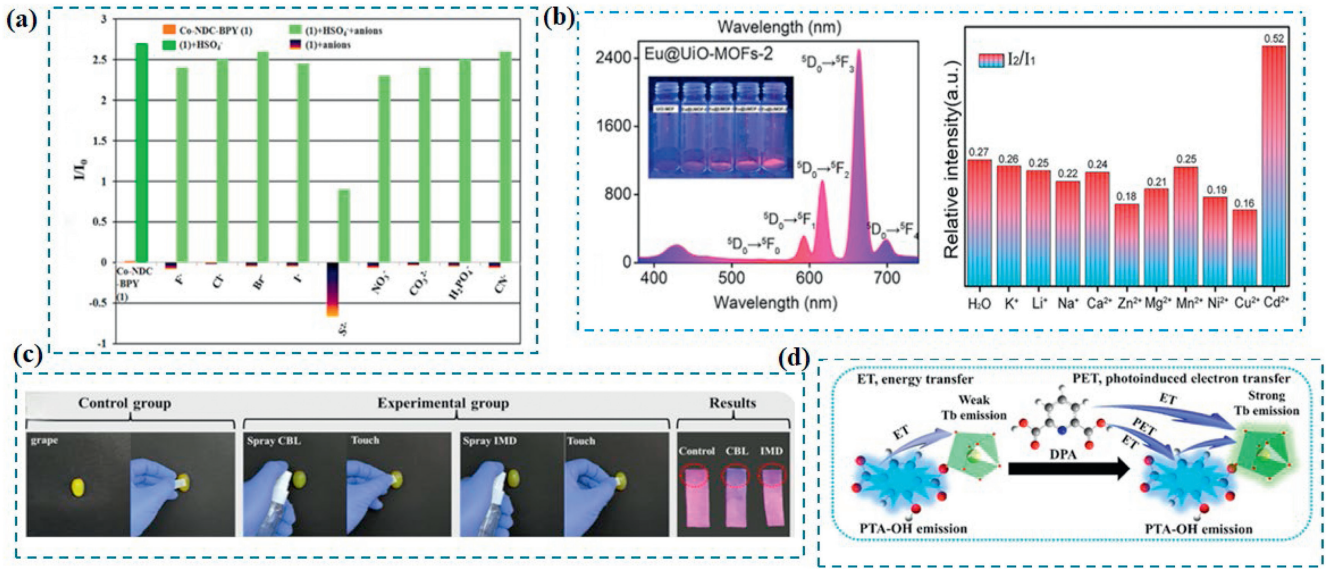


Fig. 4. (a) Cross-interference study of Co-NDC-BPY towards detection of HSO_4^- in presence of different anions monitoring. Copied with permissions [166]. Copyright 2023, Elsevier. (b) The fluorescent spectra of UiO-MOFs-2 after introducing $Eu^{3+}$and luminescence intensity responses of signal I_2/I_1 from Eu@UiO-MOFs-2 induced by Cd^{2+} and various coexisting species under the excitation of 330 nm (λ_{ex} = 330 nm). Copied with permission [168]. Copyright 2022, Elsevier. (c) EuUTDCA-based paper sensors were employed to detect CBL and IMD residues on vegetable surfaces. Copied with permission [172]. Copyright 2025, Elsevier. (d) Simplified schematic illustration of the transport process in Eu@UiO-MOFs influenced by Eu^{3+} and Cd^{2+}; the sensing mechanism of Tb-PTA-OH for DPA. Copied with permission [173]. Copyright 2022, Elsevier.

MOF (NIIC-3-Ln) was successfully synthesized, among which NIIC-3-Tb exhibited remarkable selectivity and ultra-sensitive fluorescence quenching responses toward Hg^{2+}, with limits of detection (LOD) of 0.88 nmol/L [170]. The material demonstrates high detection efficiency and excellent anti-interference capability in aqueous systems, enabling precise analysis of pollutants in complex environments. In addition, Gao constructed a two-dimensional tetranuclear Tb-organic network that achieved multi-responsive detection of Fe^{3+} and 2,4,6-trinitrophenol (TNP), maintaining stable fluorescence signals over a wide pH range (3–11) [171]. A water-stable dual-emission fluorescent sensor, EuUTDCA, was synthesized, exhibiting distinct and independent responses toward carbaryl (CBL) and imidacloprid (IMD), enabling their simultaneous quantitative detection in mixed systems. A logic gate sensor based on EuUTDCA was further constructed for accurate discrimination of the two pesticides, and the corresponding paper-based sensor was applied for the detection of CBL and IMD residues on vegetable surfaces (Fig. 4c) [172]. These findings highlight the potential of Ln-MOFs for simultaneous recognition of multiple pollutants in complex aqueous environments.

5.1.3. Biomarkers and antibiotics pollution

In the detection of biomarkers and antibiotics, MOFs also have demonstrated remarkable recognition and sensing capabilities owing to their tunable structures and excellent photophysical properties. Yu constructed a dual-emission Tb-PTA-OH MOF as a ratiometric fluorescent probe for the trace detection of the anthrax biomarker dipicolinic acid (DPA), achieving a limit of detection (LOD) as low as 13.4 nmol/L (Fig. 4d) [173]. This system enables ratiometric fluorescence sensing of DPA through both direct and indirect energy transfer mechanisms. Specifically, DPA coordinates with Tb^{3+}, and the T_1 energy level of DPA matches well with the excited state of Tb^{3+}, efficiently sensitizing Tb^{3+} emission. Meanwhile, energy transfer from DPA to the organic ligand further enhances Tb^{3+} luminescence while slightly diminishing the ligand fluorescence. Zhou *et al.* proposed a new strategy for designing water-stable MOF-based fluorescent sensors with high sensitivity and environmental stability for the efficient detection of antibiotics nitrofurazone (NFZ) and ciprofloxacin (CFX) [174]. In addition, NIIC-2-Eu and NIIC-2-Tb, were successfully synthesized, among which NIIC-2-Tb exhibited outstanding selectivity and ultra-sensitive fluorescence response toward ofloxacin (OFX) [175].

Overall, traditional and modified luminescent MOFs have achieved highly sensitive and selective detection of various pollutants through doping modulation, defect engineering, and energy transfer strategies, demonstrating excellent structure–function programmability and promising application potential.

5.2. MOF-based composite materials

Traditional MOFs suffer from limitations in water stability and electrical conductivity. By integrating MOFs with metals, carbon materials, semiconductors, or polymers, enhanced structural stability and electron transport efficiency can be achieved. MOF-based composite systems, benefiting from the synergistic effects of multiple functional components, have emerged as a key strategy for developing high-performance sensing platforms.

5.2.1. Metal nanoparticle (MNP) MOF composites

The integration of MOFs with MNPs is an effective strategy to enhance electrical conductivity and catalytic activity [176]. The introduction of MNPs not only optimizes electron transport pathways but also provides additional active sites, thereby significantly improving the sensitivity and stability of pollutant detection in aqueous systems. Chen incorporated AuAg nanoparticles into a ZIF-8 framework to form core–shell ZIF-8@AuAg and dispersed ZIF-8–AuAg composites [177]. The metal-enhanced effects facilitate the highly sensitive detection of dinitroaniline pesticides (PDA), achieving a detection limit of 4.2 nmol/L. The sensing mechanism of this system is based on binding competition and photoinduced electron transfer. PDA competes with the surface ligand (APDC) on AuAg NPs for binding sites; since APDC possesses lower HOMO/LUMO energy levels than PDA, excited-state electron transfer from APDC to PDA occurs, leading to fluorescence quenching of the ZIF-8-AuAg NPs. Dong used a bimetallic MOF precursor to construct a Co-CuSe@NC composite *via in situ* selenization [178], where the synergistic effect of the bimetallic components and the nitrogen-doped carbon matrix significantly enhanced electron conduction and catalytic activity. Furthermore, modified UiO-66-NH_2 produced **66-IS-Zn** nanozymes with a 130-fold higher turnover number *Kcat*. The activity enhancement depended on Zn–N/O coordination. With strong phosphatase-like activity and enhanced fluorescence, **66-IS-Zn** enabled a three-channel sensor array to efficiently distinguish six organophosphate pesticides [179]. This sensing platform exhibited a wide linear response range and an ultralow detection limit for OPs in complex water samples, demonstrating its practical feasibility for real-world water analysis.

5.2.2. Semiconductor oxide–MOF composites

Incorporating semiconductor components into MOFs enables the construction of heterojunction interfaces that effectively promote the separation and migration of photogenerated charge carriers, thereby improving photoelectric response and catalytic performance. Su developed a TiO_2-CeMOF hybrid nanozyme capable of signal amplification and cyclic detection *via* PFOA-induced hydrophobic regulation [180]. This system maintained excellent stability and reproducibility even in high-salinity water samples. Furthermore, the core–shell Fe_3O_4@PDA@Eu-MOF [181] composite achieved multifunctional integration through multilayer structural design. This hybrid system integrates the superparamagnetism of Fe_3O_4, the interfacial adhesion of PDA, and the fluorescence recognition of Eu-MOF. Benefiting from the "antenna effect," it exhibits enhanced luminescence for efficient tetracycline detection and removal, while the Fe_3O_4 core enables rapid magnetic recovery (<2 min). This provides a simple and efficient solution for high-performance pollutant recognition and recyclable application in complex water environments.

5.2.3. Polymer/biomolecule-integrated MOF composites

Polymer and biomolecule composite strategies have further expanded the application potential of MOFs in terms of flexibility, selectivity, and biocompatibility. Such systems achieve highly selective detection of pollutants in complex aqueous environments through molecular recognition and interfacial modulation. Chen encapsulated alkaline phosphatase (ALP) within a hydrophilic ZIF-90 framework to construct a bioenzyme composite system (ALP@ZIF-90) [182]. This material maintained enzymatic activity while improving thermal and chemical stability, enabling highly sensitive colorimetric detection of methyl paraoxon (MPO) in aqueous solutions. Zhang *et al.* further developed a flexible solid-state fluorescent membrane by *in situ* compositing carbon dots with ZIF-8 (E-CDs@ZIF-8), achieving rapid and visual detection of Cu^{2+}[183]. In addition, the Eu-based metal–organic framework Eu(2,6-NDC)(COO) (BUC-88) exhibited distinguishable fluorescence intensity and color responses toward quinolone and tetracycline antibiotics on the composite film [184].

These studies demonstrate that composite strategies effectively enhance the conductivity and water stability of MOFs, providing a sustainable material platform for the detection of multicomponent pollutants.

6. Adsorptive removal of metal ions in MOFs

Yujie Zhao, Xudong Zhao*

Metal ions are broadly distributed in diverse natural and artificial water media, such as seas, salt lakes, and industrial wastewater (*e.g.*, electroplating and acid pickling effluents) [185]. Owing to their toxicity (*e.g.*, mercury), scarcity (*e.g.*, rare earth metal), or high value (*e.g.*, noble metal), it is essential and urgent to remove or extract these metal ions from aqueous solutions, to ensure environment safe and support the circulation of metal sources. Among the current separation methods for metal ions, adsorption technique holds the distinct features especially in selectivity and applicability toward trace concentrations [186].

The adjustable regular pore structures and variable chemical natures endow MOFs with suitable transport channels and adsorption sites for metal ions, respectively. Since the first report of metal ions adsorption in MOFs in ~2009, the past sixteen years have witnessed a tremendous historical development process in this area. Multiple classes of metal ions including alkali, alkaline earth, transition, rare earth, and actinium series have been widely and systematically studied for their diffusion behaviors and detailed anchoring modes in MOFs, to successfully establish the structure-performance relationship.

In this section, we will review the representative works in the field of metal ions adsorption by MOFs. The adsorption behaviors and mechanisms will be discussed and analyzed through closely associating to the framework structure and chemical microenvironment of MOFs. For a smooth reading and convenient induction and analysis, metal ions are roughly classified into metal cations and metal anions. Meanwhile, the cases of nuclides such as uranyl and thorium ions will be discussed in Section 8, and thereby was not introduced herein.

6.1. Adsorption of metal cations

6.1.1. Alkali and alkaline earth metal ions

These two classes of metal ions possess a prominent feature apart from other ions, *i.e.* saturated and stable valence shells, leading to their difficult coordination on traditional individual organic functional group. Aiming at these coordination-inert ions, a strong chelation interaction from synergistic multiple groups or active atoms with lone-pair electrons is required. Meanwhile, the differences in charge, bare ion diameter, hydrated ion diameter, and hydration energy usually result in their different diffusion and adsorption behaviors [187].

The first work in this field dates back to 2009, when T. Bein *et al.* reported an open and flexible framework with exchangeable Na^+ ions, lanthanum(III)tetrakisphosphonate [188]. In the hydrated and expanded form, each Na^+ ion coordinates with three phosphonate oxygens and two water oxygens, as well as the fourth phosphonate oxygen with a weaker interaction. In the dehydrated and contracted form, each Na^+ ion connects with five phosphonate oxygens. It is interesting that Li^+ and K^+ ions can replace Na^+ ion to form both expanded and contracted states; however, the Rb^+-exchanged sample remains only the contracted from even with the hydration attempts, due to the lower hydration enthalpy and higher matching degree for the contracted form of this larger bare ion. Other ions including Cs^+, Mg^{2+}, Ca^{2+}, Sr^{2+}, and Ba^{2+} can hardly or slightly exchange with the Na^+ ion, caused by their too large bare diameter (*e.g.* Cs^+), hydrated diameter, or hydration energy (*e.g.*, Ca^{2+}, Mg^{2+}). Thus, this finite flexibility of the trap induced its selective affinity toward smaller bare ions. Recently, our group developed a novel 1D-channel framework, TYUST-8, featuring the inert wall A and active wall B with Pockets I and II (Fig. 5a) [189]. The small 1D channel (*d*, ~7.5 Å) permits hydrated Li^+, Na^+, and K^+ ions passing through but intercepts the migration of hydrated Mg^{2+} and Ca^{2+} ions. Meanwhile, the ion pockets especially for Pocket II in the active wall match better with Li^+ ion in size than Na^+ and K^+ ions. Benefiting from these features, TYUST-8 exhibits a large capacity (76.1 mg/g) and excellent selectivity for Li^+ ion based on ion sieving mechanism.

It is known that multiple-oxygens micro-environments are common in the supramolecular systems, such as cyclodextrin, crown ether, and calixarene [190]. The incorporation of these molecules or their quasi-phases into MOFs has been demonstrated to be a promising strategy. As a typical example, in a cyclodextrin-like Zn-MOF framework [191], two hydroxyls of each glycerol are coordinated but the third one is free. In its 1D channel, six free hydroxyls circle to form a supramolecular adsorption unit with a suitable cavity size for bare Li^+ diameter, leading to the selec-

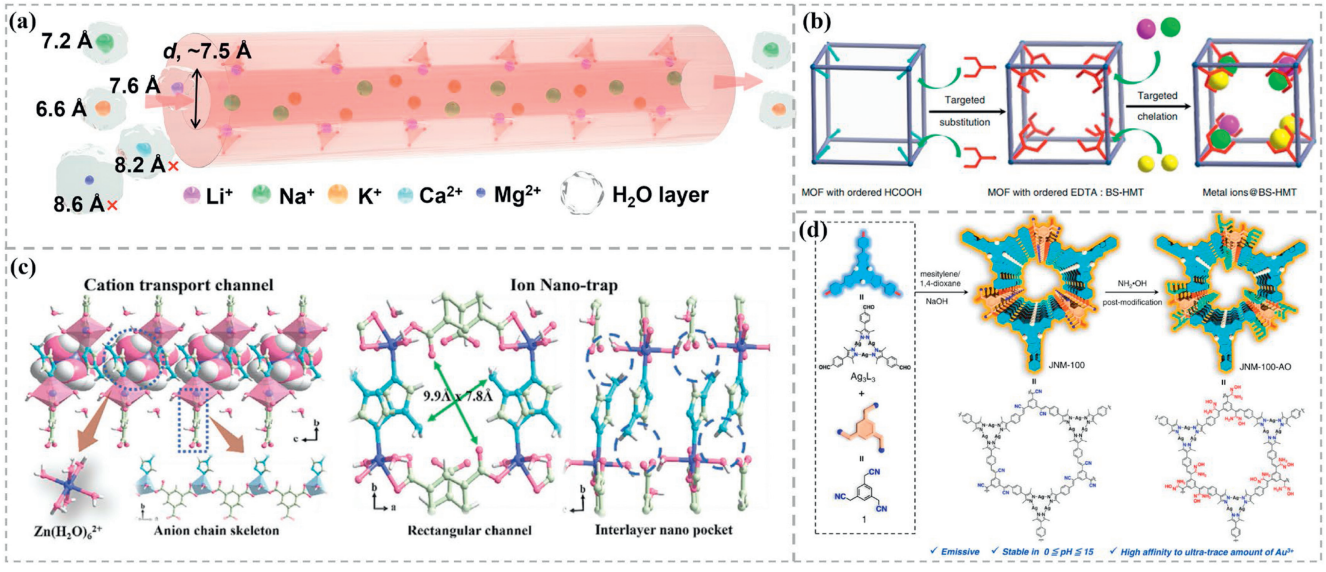


Fig. 5. (a) Schematic of ion sieving in 1D channel of TYUST-8. Copied with permission [189]. Copyright 2025, Wiley-VCH. (b) Schematic of design and synthesis of MOF-808 with ordered EDTA molecules. Copied with permission [12]. Copyright 2018, Springer Nature. (c) Cation transport channel and ion traps of ATZ-BTC-Zn. Copied with permission [195]. Copyright 2025, Wiley-VCH. (d) Fabrication and chemical structures of JNM-100 and JNM-100-AO. Copied with permission [196]. Copyright 2022, Springer Nature.

tive adsorption over Na^+, K^+, and Cs^+ ions. The precise and adjustable oxygen-rich crown ether (CE) units endow the CE-MOFs with targeted adsorption affinity. In this respect, one of the common methods is to use CE-containing organic ligands to *in-situ* assemble MOFs. For example, a quadridentate ligand with 18-crown-6-ether (18C6E) coordinated with the transition-metal Zn cluster and Ni cluster to form the structure-interpenetrated SNU-200 and non-interpenetrated MOF-18Cr6 [192,193]. The 18C6E structure is preferable for Sr^{2+} ion, leading to the selective adsorption over K^+, Cs^+, Mg^{2+}, Ca^{2+}, and Ba^{2+}, *etc*. However, the non-interpenetrated structure endows MOF-18Cr6 with a larger pore volume and transparent 1D channel, resulting in its higher Sr^{2+} adsorption capacity (84.93 mg/g). The self-assembly of two 18C6E- and 24C8E-containing ligands and Zr-O cluster produces two highly stable frameworks, ZJU-X100 and ZJU-X102 [194]. ZJU-X100 is demonstrated to be high selective for Sr^{2+} over Na^+, K^+, Cs^+, but the adsorption of Cs^+ in ZJU-X102 is disturbed by other cations especially for K^+ and Sr^{2+}.

6.1.2. Toxic heavy metal ions

Removal of toxic heavy metal ions (*e.g.*, mercury, lead, cadmium, thallium) from aqueous solutions also remains a hot topic, due to their enormous environment risks. According to the Soft-Hard acid-base theory, Hg^{2+}, Cd^{2+}, and Tl^+ ions were classified to soft acids and Pb^{2+} ion was identified as a borderline acid [11]. As a result, soft bases or some of borderline bases will be suitable for strongly grabbing these heavy metal ions. Following this basic rule, mercapto group (-SH) as a representative owns strong adsorption affinity for Hg^{2+}. For example, the thiol-abundant UiO-66-$(SH)_2$, derived from the 2,5-dimercapto-1,4-benzenedicarboxylic acid and zirconium-cluster, can eliminate the Hg^{2+} ions from 10 mg/L to 0.01 mg/L in an acidic media, achieving an ultrahigh removal ratio of >99.9% [197]. Sulfur-bearing amino acids or their variants are capable of building functional BioMOFs with the unreacted amino acid residues. In a typical example of this route, an oxamide ligand derived from L-methionine was applied to construct a 1D-channel CaCu-MOF whose supramolecule-like channel is decorated by the dangling methylmercapto groups [198]. The soft sulfurs afford a high $HgCl_2$ capacity of 0.9 g/g and moderate CH_3Hg of 0.166 g/g. Similar to this route, an isostructural CuCa-MOF derived from *S*-methyl-L-cysteine amino acid was prepared for an in-depth removal [199]. Meanwhile, the encapsulation of the two CuCa-MOFs crystal particles into a membrane matrix achieves an efficient static and dynamic removal performance for Hg^{2+}, solving the drawbacks of powder-state MOFs in real application. A promising powder-shaping method based on sodium alginate was also reported to achieve effective Pb^{2+} ion adsorption [200]. A combination of serine and methionine oxamide ligands was performed to construct a multivariate (MTV) MOF bearing uncoordinated -OH group (from serine) and methylmercapto group (from methionine) [201]. Single crystal analysis reveals the two groups are alternately arranged in the 1D channel wall. Three toxic ions of Hg^{2+}, Pb^{2+}, and Tl^+ are all selectively removed over Cu^{2+}, Ni^{2+}, and Ca^{2+}, Mg^{2+}, *etc*. Compared with perfect crystals, defective species owns more open ion transport channel and thereby higher utilization efficiency for active sites. Just recently, Li *et al.* reported a solvent-assisted evaporation route to construct amorphous a_{gf}BNU-1(Zn) and a_{gf}BNU-1(Cd) glass foams [202]. The mercapto and triazole nitrogen from the ligands synergistically coordinate to Hg^{2+} ion. Compared with the crystalline BNU-1, these amorphous species exhibit sharply enhanced adsorption performance both in capacity and kinetics, benefiting from the disordered defects.

Besides the ions discussed above, the capture of other heavy metal ions (*e.g.* Cu^+) also attracts wide concerns. Introduction of Lewis base sites is considered as one of most feasible methods. MOF-808 is famous for its large pore and abundant exchangeable formic acid or acetic acid [4], rendering it an ideal loading platform for Lewis bases. In a classical work, Peng *et al.* anchored EDTA molecules into MOF-808 matrix, *via* substituting the original formic acids [12]. The flexibility and adaptivity of EDTA endows the MOF-808-EDTA with wide-spectra chelation affinity for various hard, soft, and borderline Lewis metal ions (Fig. 5b). Similarly, in the work of Yaghi *et al.* [203], three carboxylic molecules including histidine (His), 4-imidazoleacrylic acid (Iza), and 5-benzimidazolecarboxylic acid (Bzz) were incorporated into MOF-808 matrix to fabricate the triangular imidazole-rich regions, for effectively sieving Cu^+ ion based on the N-Cu-O mode.

6.1.3. Rare earth metal ions

Rare earth (RE) elements refer to the total lanthanide series and scandium and yttrium. Trivalent cations, considered as stronger Lewis acids [204], are their most common states in water media. Adsorption and recovery of RE ions from mining water and spent liquor from other industrials are vital to promote the circulation of these rare strategic resources. As known, the separation of RE ions toward common co-existing bivalent and monovalent ions is easy to achieve owing to the large difference in Lewis acidity and coordination ability. The main challenge actually locates at the selective recognition of RE ions-selves, especially for those adjacent ones. Aiming at this situation, rational design of adsorption traps is highly required to enlarge the minor difference in ion diameter and coordination ability. In a 3D mixed-linker framework (NCU-1) assembled by the triazol-derivant and BTC, the two-fold interpenetration creates the dense angstrom-level cavities with adherent adsorption sites of triazol nitrogen and free carboxyl [137]. Meanwhile, it is found that the diameter (3.2 Å) and shape of the cavities better adapt to light RE ions than heavy RE ions, leading to a selective adsorption for the former ones. Constructing anionic frameworks with exchangeable and suitable cations is also a feasible strategy. In a representative work, hydrated $[Zn(H_2O)_6]^{2+}$ ion as a counter-cation was *in-situ* loaded into the ion transport channels of an anionic framework, ATZ-BTC-Zn (ATZ, 4-amino-4H-1,2,4-triazole) (Fig. 5c) [195]. The high configuration similarity with $[Zn(H_2O)_6]^{2+}$ permits the smooth ion exchange and diffusion of the hydrated RE ions. On the other hand, the ion pocket functionalized by terminal -NH_2 and -COOH sensitively distinguishes the minor difference of adjacent light RE ions. As a result, the selectivity factors of La/Nd and Ce/La reach as high as 908 and 543.

6.2. Adsorption of metal anions

Some metal ions are present as anionic states in water media, for examples, the oxometallate classes (*e.g.*, chromate, perrhenate) and metal halide anions (*e.g.*, $AuCl_4^-$). Different with the cations, the overall charge of these anions are negative, and the attached oxygen or halide commonly participate in the coordination. Thus, aiming at their adsorption, the design principles for the framework charge and active sites are rather different with those above.

6.2.1. Oxometallate anions

Toward this class of anions, the dominant design methods for MOF adsorbents can be concluded to the following two routes: (i) *In-situ* incorporation of anions for charge balance in a cationic framework, where the framework-anion interaction should be relatively weaker to ensure feasibility of subsequent ion exchange; (ii) acid-assisted protonation of amino- or hydroxyl–functionalized MOFs. Through a rational induction and comparison, the former one may hold greater advantage in selectivity based on a rational channel tailoring. In this respect, the assembly of soft metal ions (*e.g.*, Ag^+) as well as borderline species (*e.g.*, Zn^{2+}, Ni^{2+}) and nitrogen-donor organic ligands can afford cationic network layers, and in the meantime, anions are *in-situ* embedded into

the interlamination as a counter ion. For example, in the SLUG-21 framework reported by Fei *et al.* [205], Ag^+ ion coordinated with 4,4′-bipyridyl to form the π-π stacking 2D layers and 1,2-ethanedisulfonate (EDS^{2-}) was inserted. Interestingly, the two terminal sulfonates can provide only two oxygens to interact with the Ag atoms; and the O-Ag distance ranges from 2.711 Å to 2.759 Å, exceeding the admissive value of Ag-O covalent bond (median: 2.44 Å). This weak connection renders the EDS^{2-} anion exchangeable by other anions. It is found that exchange affinity follows the order: MnO_4^- > ReO_4^- > ClO_4^- > CrO_4^- > NO_3^- > CO_3^{2-}, rather different with the CO_3^{2-} precedence of traditional double-layer hydroxide.

6.2.2. Noble metal anions

Noble metals refer to gold, silver, and platinum group of metals (*e.g.*, platinum, rhodium, palladium). High scarcity and economic value render their recovery from wastes rather significant. For example, Au is widely distributed in electronic components (*e.g.*, central processing unit, CPU), and Pt-Rh-Pd elements are applied in ternary catalysts. Hydrometallurgy techniques for these solid wastes and ocean gold mining have raised urgent requirements for water-phase MOF adsorbents.

Just like Hg^{2+} ion, Au(I) and Au(III) ions also belong to the soft metal ions. On the basis of Au-S interaction, in an early report, the two ions were successfully adsorbed into the previously discussed L-methionine-derived CuCa-MOF, with a high selectivity than Pd(II), Ni^{2+}, Cu^{2+}, Zn^{2+}, and Al^{3+} ions [206]. Gao *et al.* proposed an interesting idea of "asymmetric electronic structure" for enhancing Au(III) ion adsorption [207]. The introduction of monodentate benzoic acid breaks the symmetric electronic structure of original NH_2-UiO-66, and thereby the -NH_2 group tends to gather electrons and attracts protons to form -NH_3^+ active adsorption site. The adsorption capacity of gold under light irradiation reaches up to 2.04 g/g and selective adsorption over various anions and cations is obtained. Besides the sulfur and amino groups, formamidoxime group also proves its targeted and strong affinity toward this anion. Luo *et al.* prepared a formamidoxime-decorated Ag-based framework, JNM-100-AO, through *in-situ* cyano group introduction and subsequent additive reaction (Fig. 5d) [196]. The nano-level 1D channel promotes the diffusion of guest Au(III) ions, and the targeted chelation of this distinct group permits the effective adsorption. On that basis, selective extraction of ppm- and ppb-level gold from diverse aqueous systems was achieved, including seawater, wastewater, and CPU leaching solution. It is noted that the reduction of ionic-state Au(III) to Au(0) particle is generally accompanied during the adsorption process, may providing a feasible approach to prepare Au(0)-loaded materials.

7. Resource recovery in MOFs

Fu-Xue Wang, Yifei Sun*

The development and production of technologies like batteries, electronics and chemicals rely heavily on minerals and resources [208]. Many resources are not inexhaustible. At the same time, end-of-life devices are often discarded or broken down. Finally, many components are leached into water system in the form of various compounds, resulting in water pollution. Thus, it is urgent need to develop sustainable recycling process and the corresponding functional materials for critical resources recovery, including rare-earth elements (REEs), metals used in energy storage (*e.g.*, lithium, cobalt, nickel) and precious metals (gold, silver, palladium) and so on.

The mechanisms of recovering resources from water primarily involve selective capture of target substances through charge attraction, size exclusion, special coordination interactions with functional groups and catalytic conversion of dissolved compounds into insoluble substance (*e.g.*, nanoparticles, metal oxides). To date, a variety of materials have been applied in critical resource recovery, such as polymeric membranes, graphene oxides, biochar, activated carbon, metal oxides, carbon nanotubes, MOFs and covalent organic frameworks (COFs). These materials and their composite materials have demonstrated promising results in resource recovery application. Nevertheless, their practical implementation remains challenging. This is because many studies are conducted using simulated aqueous solution containing the target compounds, while real wastewater is complex. It is considered that high selectivity is the key technical challenge in resource recovery from water [209].

MOFs exhibit huge potential in critical resource recovery from aqueous environments due to their designable structure and tunable functionality [210]. Their pore sizes are adjustable by using suitable organic ligands. Meanwhile, they can be introduced in functional groups with qualitative and quantitative to enhance their special performances. Consequently, we believe that MOFs will greatly promote the development of critical resource recovery from water. Herein, resource recovery using MOFs is concluded, and some cases are analyzed in depth to illustrate recovery strategies and reaction mechanisms.

7.1. Adsorption

Adsorption technology plays an important role in critical resource recovery from water, since its easy operation, low cost and high efficiency. Adsorption process occurs at solid-liquid interface between adsorbents and water, and the target substance transports from water to adsorbents' active sites *via* physisorption (*e.g.*, hydrophobic interactions, van der Waals and electrostatic) and/or chemisorption (*e.g.*, hydrogen bonding, coordination and chelation reactions). The chemisorption is typically strong and result in high adsorption capacity and fast adsorption rate. MOFs possess huge adsorption potential due to their high specific surface area, high porosity and tunable active sites. The active sites of MOFs can be tuned through post-synthetic functionalization like other adsorbents does [211]. Differently, MOFs can also be adjusted by introducing suitable metal nodes and organic ligands to "tailored to fit" an adsorbent. Consequently, MOFs can exhibit higher resource recovery performance in adsorption rate and selectivity. For instance, 18-crown-6-ether (18Cr6) has specific binding ability towards strontium (Sr^{2+}), which is potential active sites for Sr^{2+}adsorption. However, the ring of crown ether is easy to be occupied in 18Cr6-based adsorbents, inhibiting Sr^{2+}adsorption. Feng *et al.* used an 18Cr6 ligand, 4,4′,5,5′-terabenzoic acid dibenzo-18-crown-6, to synthesize a Ni-MOF (MOF-18Cr6) [193]. The prepared MOF-18Cr6 has three-dimensional framework consisted of uniform one-dimensional channel, enabling fast mass transfer in the channels. Interestingly, the channel walls were decorated with rich crown ethers from the 18Cr6 ligand, which offered natural active sites for Sr^{2+}adsorption (Fig. 6a). The unique structure endowed MOF-18Cr6 with rapid Sr^{2+}adsorption rate (1.42 mg g^{-1} min^{-1}) and high capacity (84.93 mg/g), closed to the theoretical value (84.01 mg/g). Besides, MOF-18Cr6 also exhibited excellent selectivity towards Sr^{2+}. 99.73 % of Sr^{2+} was adsorbed over MOF-18Cr6 in simulated low-level radioactive effluent containing various metal ions. The high Sr^{2+}adsorption capacity and high selectivity were attributed to lower binding energy (−7.86 eV) than other metal ions like Cs^+ (−2.73 eV), as well as the coordination between Sr and six O atoms from crown ether.

Molecular imprinting technology (MIT) is widely researched in enhancing resource adsorption capacity and selectivity over MOFs. MOFs-based MIT has many outstanding advantages compared to traditional adsorbents due to the intrinsic advantages of MOFs. (1) It is feasible to create uniform and well-defined imprinting cavities

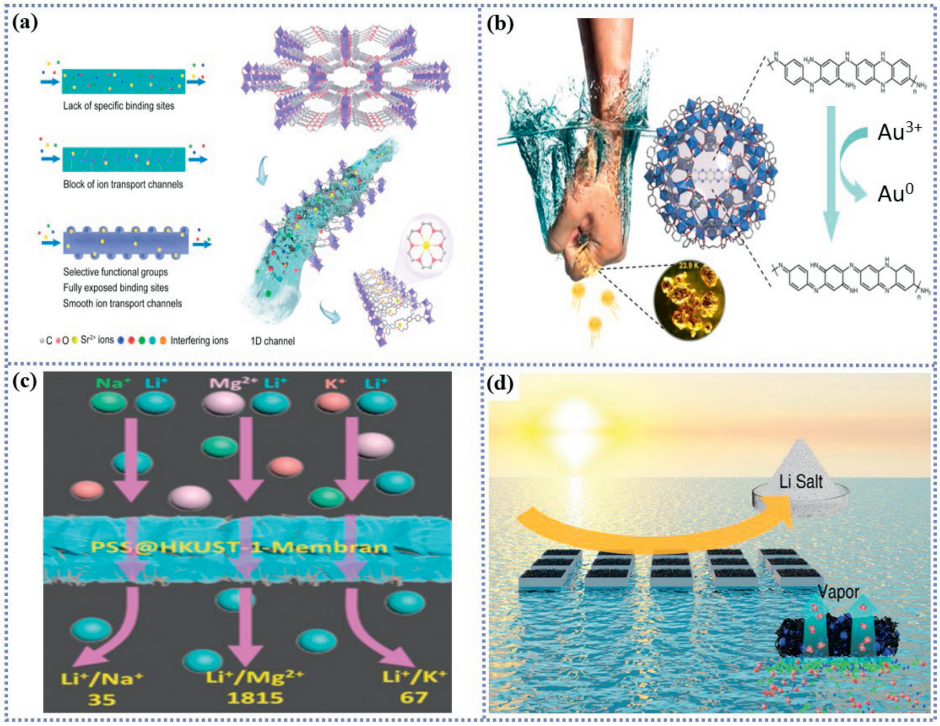


Fig. 6. (a) Mechanism for the efficient separation of Sr^{2+} ions by MOF-18Cr6. Copied with permission [193]. Copyright 2023, Wiley-VCH. (b) Catalytic Au^{3+} reduction on Fe-BTC/PpPDA composite. Copied with permission [213]. Copyright 2028, American Chemical Society. (c) Li^{+} ion selective separation by PSS@HKUST-1 membrane. Copied with permission [216]. Copyright 2016, Wiley-VCH. (d) Lithium salt collection through a photothermal sandwich structured device based on HKUSTST-1 and laser-induced graphene. Copied with permission [221]. Copyright 2024, Wiley-VCH.

due to the highly ordered framework of MOFs. (2) Large range of imprinting molecules sizes can be introduced thanks to the tunable pore sizes of MOFs from micropores to mesopores. (3) Template molecules can be efficiently and rapidly removed due to the interconnected porous network of MOFs. Feng *et al.* reported *in-situ* synthesis of uranyl-imprinted nanocage in UiO-66 analogue for uranium (UO^{2+}) recovery from seawater [212]. The maximum uranium adsorption capacity was up to 475 mg/g in 8 ppm uranium spiked simulated seawater. Meanwhile, the prepared adsorbent exhibited excellent selectivity towards UO^{2+} against interfering metal ions with concentration of 10^5-fold greater than uranyl, including beryllium, cobalt, barium, vanadium, hydrargyrum, lead, chromium, cadmium, silver and cesium. The high adsorption capacity and selectivity were attributed to coordination between uranium with four O atoms from the adsorbent, as well as hydrogen bond between axial O atom of uranyl and H atom from the phenolic hydroxyl group on organic ligand.

The current researches have proven that MOFs possess charming ability for critical resource recovery from water, their formability endows MOFs with excellent adsorption capacity and selectivity to against complex aquatic environment. It is worth noting that desorption is also important for resource recovery and reuse of adsorbents. Consequently, responsive to MOFs to energy like light, ultrasonic wave and heat should be focused in future. Besides, efforts should be pay to develop MOFs-based device to facilitate practical application.

7.2. Catalytic reduction

Catalysis, including electrocatalysis and photocatalysis, is a charming method for critical resource recovery from water. Catalytic technology can reduce metal ions to insoluble compounds, facilitating recycle of resource from water. However, resource recovery from water, such as wastewater and seawater, is difficult due to the complex co-existing mixtures and low concentration of target compounds. MOFs are believed as idea candidate to overcome these challenges since their unique advantages and versatility: (1) High porosity and abundant active sites of MOFs can enrich the target substance, facilitating catalytic reduction. (2) MOFs can be easily functionalized by groups through introducing groups in organic ligands, enhancing catalytic activity. (3) MOFs possess multiple functions like catalysis, adsorption and separation, and realizing efficient resource recovery. (4) MOFs can also act as carrier to combine with other functional materials, further promoting resource recovery efficiency.

Sun *et al.* introduce monomers of polyhydroquinone (PHQ), poly(*para*-phenylenediamine) (PpPDA), polytyramine (PTA) and poly(*meta*-aminophenol) (PmAP) into Fe-BTC for catalytic Au^{3+} reduction from water [213]. The monomer was locked in the pores of Fe-BTC *via* polymerization between $-NH_2$ or -OH from monomer and Fe^{3+} sites from MOF. The pore cages of Fe-BTC were 2.5–2.9 nm in diameter with apertures of 0.5–0.8 nm. Consequently, Au^{3+} can diffuse inside due to its high reduction potential, high polarizability and small hydration shell, while large intereferents such humic acid was inhibited. This reasonable structure helped Fe-BTC/PpPDA to rapidly extract trace amounts of Au^{3+} from complex water mixture, including wastewater, fresh water, ocean water and pickling solution of electronic waste. Subsequently, the captured Au^{3+} was reduced by $-NH_2$ from PpPDA to Au nanoparticle with high purity of 23.9 K (99.6 %), as displayed in Fig. 6b

Photocatalysis is an attractive process for resource recovery from water, since it is possibly operated under solar irradiation. MOFs are excited by light, and the photo-generated electrons transfer from the highest occupied molecular orbital (HOMO) to the lowest unoccupied molecular orbital (LUMO). The electrons initiate reduction reaction, while the holes leaving in HOMO participate in oxidation process [214]. To evaluate the light absorption and charge transfer, Chen *et al.* combined UiO-66-NH_2 and black phosphorus quantum dots (BPQDs) for photocatalytic U(VI) reduction [215]. The photocatalyst was anchored on carboxyl cellu-

lose nanofiber (CNF) aerogel, which showed high porosity (>98 %) to facilitate uranium adsorption. The HOMO of UiO-66-NH_2 and the valence band (VB) of BPQDs are 2.21 and 0.9 eV, respectively. Correspondingly, their LUMO and conduction band (CB) are −0.62 and −0.98 eV. Under light irradiation, photo-generated electrons from HOMO of UiO-66-NH_2 transfer to LUMO. BPQDs were also photo- excited and the charge transferred from VB to CB, further transferred to LUMO of UiO-66-NH_2. Finally, these photo-generated electrons reduced U(VI) to U(IV) oxides.

MOFs as bifunctional materials for catalytic reduction and extraction of valuable metals from water is at an early stage. The catalytic mechanisms still remain elusive. Besides, the stability of MOFs during photocatalysis should also be concerned.

7.3. Membrane separation

Membrane development and its application in critical resource extraction and recovery from water is an emerging research area. Different from wastewater purification, resource recovery requires high selectivity towards goals. However, effective separation of compounds with similar physical and chemical properties is a huge challenge, since the separation process mainly depends on solutes size and surface charge. MOFs' pore sizes can be turned in molecule scale, and their surface charge can be tailored by introducing functional groups. These characters make MOFs membranes charming in critical resource extraction and recovery from water.

Guo *et al.* constructed a membrane using HKUST-1 and a linear polymer polystyrene sulfonate (PSS) for lithium ion (Li^+) recovery [216]. The PSS molecules were encapsulated into HKUST-1 crystals, forming uniform channels for fast ions transfer. This combination also enhanced the stability of the membrane. When immersed in water for two months, the PSS@HKUST-1 membrane was still stable. The high stability of the membrane was possibly due to the protection of labile and accessible Cu sites from PSS. The abundant sulfonate groups resulted in negative charge of the membrane, which enforce the capture of Li^+ from water into HKUST-1 pores through PSS networks. The PSS@HKUST-1 membrane showed higher Li^+conductivity (5.53×10^{-4} S/cm) than that of pristine HKUST-1 (3.80×10^{-9} S/cm). The membrane also exhibited outstanding selectivity towards Li^+. The co-existing Mg^{2+} was excluded due to its large hydrated diameter (0.86 nm), closed to the pore entrance of HKUST-1 (0.9 nm). Although Na^+ (0.72 nm) and K^+ (0.66 nm) have smaller hydrated diameter than that of Li^+, the sulfonate groups had higher binding affinity to Li^+. Consequently, the membrane exhibited significantly high selectivity towards Li^+ than Mg^{2+}, Na^+ and K^+(Fig. 6c).

It is firmly believed that MOFs broaden the application of membrane filtration technology in resource recovery. The versatility also endows MOFs-based membranes with more antifouling property/regeneration strategies. The pollutants/algae can be cleaned *via* (photo/electro)catalytic degradation/removal, light-induced desorption [217,218], realizing convenient regeneration of membranes.

7.4. Extraction by interfacial solar evaporation

Interfacial solar evaporation (ISE) technology, primarily developed for brine mining, has emerged as a promising candidate for resource extraction and recovery from water [219]. Solar evaporation can be easily established to evaporating water and obtain resource without external energy inputs. The evaporating process can be sped up by floating a porous photothermal material on water's surface, which converts solar energy to heat and facilitate water molecules evaporation [220]. Similar to membrane extraction, resource recovery *via* interfacial solar evaporation also demands high selectivity and rapid mass transfer of target substance. Meanwhile, MOFs employed in ISE technology must possess high water stability and thermal stability to withstand the moist and high-temperature reaction environment.

Zhong *et al.* developed a solar-driven extraction device based on HKUST-1 and laser-induced graphene (LIG) for Li^+ recovery from brine water [221]. The extraction device had a sandwich structure, which consisted of LIG-coated cleanroom wipe (light-absorbing layer), HKUST-1 dense film (Li^+ selectivity permeable layer) and pristine cleanroom wipe (water-absorbing layer). During evaporation, water molecules, along with $Li^+$and Mg^{2+}, were permeated into the water-absorbing layer. Then, water molecules and Li^+ further pass through the HKUST-1 film, while Mg^{2+} was excluded due to its larger hydrated diameter than the pore entrance of HKUST-1, as description above (Section 7.3) The water molecules were finally converted into steam because of the excellent photothermal conversion capability of the light-absorbing layer. Meanwhile, the leaving lithium salts crystallized and accumulated in the photothermal layer (Fig. 6d). The maximum lithium capture was up to 1467 mg/m^2 under 1 solar illumination for 25 h. The lithium capture amount was enhanced to 1698.4 mg/m^2 within 20 h under 3 solar illuminations, exhibiting excellent photothermal conversion and lithium recovery capability. Even after 20 cycles, the device still exhibited high selectivity towards Li^+, proving good stability and separation ability of HKUST-1 film.

It is believed that MOFs will significantly accelerate the development and application of ISE technology in the near future, for the following reasons: (1) The uniform pore size of MOFs enhance selectivity towards targets at the nanoscale, (2) MOFs can be turned at the molecule level to better match specific targets, thereby further improving selectivity, (3) during interfacial solar evaporation, MOFs can trigger photocatalytic decontamination, which enhance antifouling properties of the photothermal material/device.

8. Applications of MOFs in radionuclide separation

Yi-Lin Liu*, Qingyi Zeng*

The effective separation of radioactive nuclides such as uranium (U), strontium (Sr), and iodine (I), as well as their fission products, is critical to safeguarding nuclear reactor safety and enabling closed-cycle nuclear fuel reprocessing [222]. MOFs, constructed through the hierarchical assembly of metal nodes and organic ligands, have emerged as transformative materials for targeted radionuclide separation [223,224]. Their programmable pore environments, structural versatility, and host-guest interaction mechanisms offer unparalleled advantages in selectively capturing uranyl ions (UO_2^{2+}), radioiodine isotopes (*e.g.*, ^{129}I, ^{131}I), pertechnetate oxoanions (TcO_4^-), and fission-derived noble metal species such as palladium (Pd) and selenium (Se) [225]. Advanced functionalization strategies such as ligand engineering, pore surface charge modulation, and hierarchical porosity integration enable precise tuning of MOFs' binding site density and interaction energetics [226,227]. These innovations address persistent challenges in conventional adsorbents, including low ion selectivity in complex matrices and sluggish mass transfer kinetics [228]. This section systematically reviews cutting-edge advances in engineered MOFs for radionuclide sequestration, focusing on mechanism-guided designs to optimize uranium/strontium adsorption kinetics, intelligent iodine/technetium capture systems, and multi-mechanistic Pd^{2+}/SeO_3^{2-} separation protocols. The insights herein provide robust theoretical frameworks and practical blueprints for next-generation nuclear waste management technologies.

8.1. Uranium

Recent breakthroughs in seawater uranium extraction have resolved the long-standing trade-off between uranium-vanadium se-

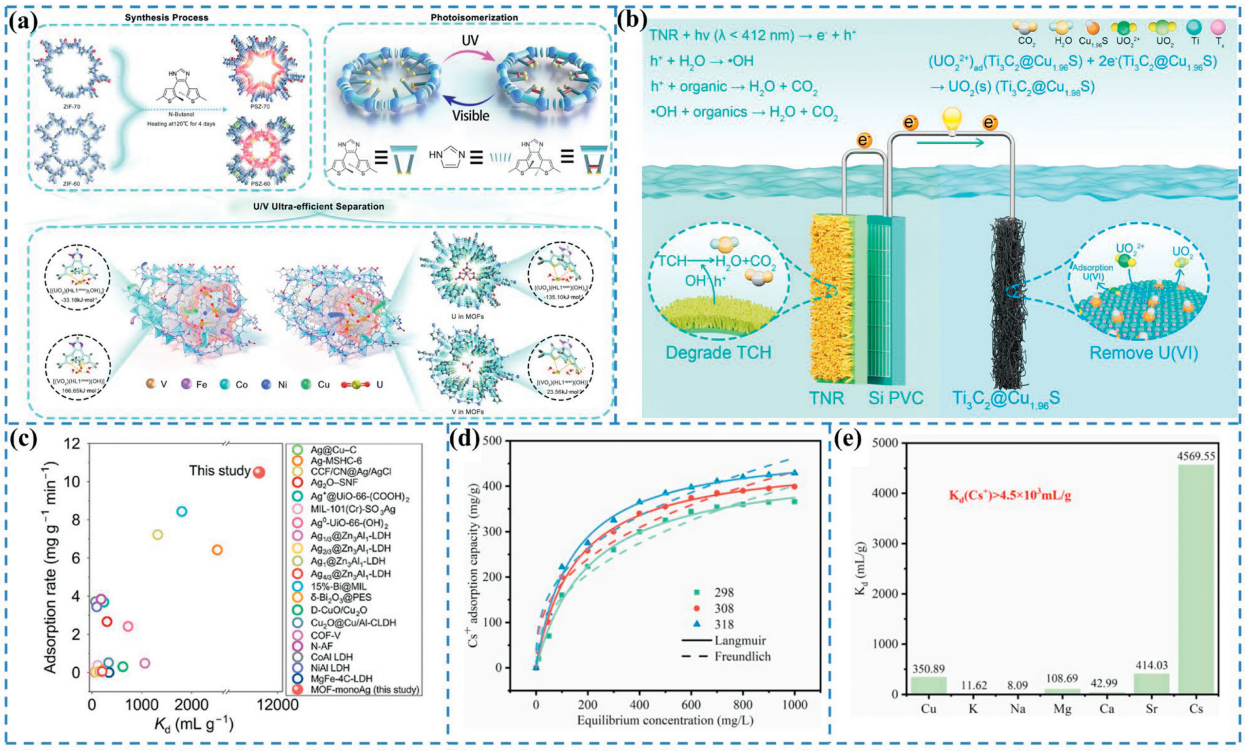


Fig. 7. (a) Construction of a composite photoisomeric material framework and illustration of the selective uranium extraction process. Copied with permission [229]. Copyright 2025, Springer Nature. (b) Mechanistic illustration of synergistic photoredox coupling: Uranyl ion photoreduction, organic substrate oxidation, and photoelectrochemical energy conversion under solar irradiation. Copied with permission [233]. Copyright 2025, Wiley-VCH. (c) Comparison of K_d values and adsorption rates for I^- ions in aqueous solution of available adsorbents. Copied with permission [237]. Copyright 2025, Wiley-VCH. (d) Adsorption isotherms of Cs^+ at 298, 308 and 318 K, along with fitting by Langmuir model (solid lines) and Freundlich model (dash lines). (e) Impact of coexisting ions on Cs^+ adsorption. (d, e) Copied with permission [241]. Copyright 2025, Elsevier.

lectivity and adsorption capacity through multidimensional optimization strategies. Zhang *et al.* [229] developed a light-regulated MOF material employing diarylethene-based dynamic coordination, which enables ultraviolet-visible light modulation of pore topology (Fig. 7a). This photoresponsive system achieved an 8.7-fold enhancement in uranium selectivity over conventional MOFs, with a uranium/vanadium separation factor exceeding 215 while maintaining a record adsorption capacity of 588.24 mg/g. Additionally, Zhang *et al.* [230] designed a π-conjugated two-dimensional uranium organic framework that exhibits outstanding performance. After 20 operational cycles in natural seawater, the residual uranium concentration decreased to 3.3 ppb while maintaining a capture efficiency of 97 %. In parallel, Wan's team [231] engineered a MXene-based heterostructured electrode functionalized with imidazole moieties. This design synergizes hierarchical porosity with chelation effects, achieving a breakthrough adsorption capacity of 2322.4 mg/g under 1.2 V applied potential, coupled with a sustained extraction rate of 1.43 $mg \cdot g^{-1} \cdot d^{-1}$, demonstrating potential for industrial-scale implementation.

For comprehensive radioactive wastewater treatment, Liu *et al.* [232] innovated a ZnS@MXene/carbon felt composite photoanode system. This platform simultaneously enhances uranium enrichment kinetics (22-fold rate improvement, 97 % solar-driven removal) and tetracycline degradation efficiency (4.3-fold increase, 95 % mineralization) while generating electrical power higher density than conventional cathodes. Meanwhile, the Ti_3C_2@$Cu_{1.96}$S-TNR/Si system integrated by Cao *et al.* [233] elucidates multifunctional synergy. H^+/·OH radicals efficiently clease UO_2^{2+}-organic complexes, while photogenerated electrons reduce soluble U(VI) to insoluble U(IV) precipitates (Fig. 7b). These technological advances establish intelligent, adaptive solutions for strategic resource recovery and ecological remediation.

8.2. Strontium

The efficient separation of radioactive strontium isotopes (^{90}Sr, ^{89}Sr) presents a global challenge in nuclear contamination remediation due to their high environmental mobility and prolonged radiological half-lives [234]. Conventional adsorbents often fail to address the dual limitations of poor stability under extreme conditions and inadequate ion selectivity. Recent breakthroughs in advanced material design demonstrate transformative solutions to these challenges. For extreme pH conditions, Zhang *et al.* [235] established complementary layered materials: SZ-4 demonstrated remarkable selectivity with a distribution coefficient of 7.4×10^4 mL/g under 10,000-fold calcium interference in acidic media, while alkaline-optimized SZ-7 achieved 183 mg/g adsorption capacity in 1 mol/L NaOH. This dual-material system enables comprehensive pH-adaptive strontium separation, providing cross-environment applicability from acidic nuclear effluents to alkaline waste streams.

8.3. Iodine

Radioactive iodine contamination remediation faces persistent challenges due to its high environmental mobility and difficulty in enrichment, with conventional adsorbents suffering from low efficiency, poor environmental adaptability, and prohibitive costs. Recent advancements in material engineering offer transformative solutions across multiple operational scenarios [236]. Cao *et al.* [237] developed a single-Ag-site MOF material featuring atomically dispersed active centers, achieving an iodine adsorption kinetic constant of 10.48 mg g^{-1} min^{-1} (Fig. 7c). This material demonstrates exceptional versatility, attaining adsorption capacities of 114.2 mg/g in seawater and removal efficiencies exceeding 98.7 % in

simulated nuclear wastewater. Tian's team [238] employed delignified wood as a hierarchical scaffold to immobilize UiO-66-NH_2 crystals with 36 wt% loading efficiency. The resultant millimeter-scale channel networks enable iodine vapor capture capacities reaching 704 mg/g, addressing gaseous phase remediation demands. In parallel, El-Shahat *et al.* [239] engineered a crosslinked chitosan-MOF composite that achieves 399.68 mg/g iodine adsorption capacity while maintaining 92% cyclic stability under extreme conditions (350 °C, pH 2–10), demonstrating robust environmental resilience. Mechanistic innovations further propel this field. Xiao *et al.* [240] designed a flexible silver-based MOF (FJI-H39) leveraging dynamic pore deformation to induce iodine species reorganization into dense [Ag-I_x] aggregates, achieving a record storage density of 1.72 g/cm^3. This system exhibits 124-fold faster adsorption kinetics than conventional materials while retaining kilogram-scale manufacturability. Collectively, these developments establish an integrated technological chain spanning efficient capture, precise enrichment, and secure sequestration, providing comprehensive solutions for multiscale radioactive iodine contamination management.

8.4. Technetium

The remediation of radioactive technetium (TcO_4^-) and rhenium (ReO_4^-) oxoanion contamination remains a critical challenge due to insufficient detection sensitivity and poor environmental adaptability in conventional methods. Recent innovations in advanced materials address these limitations through precision-engineered structural and mechanistic solutions. Xiao *et al.* [242] developed a pyrimidine-functionalized MOF (ZJU-X8) with tetrahedral anion-sieving capabilities, enabling ultraspecific TcO_4^- recognition at 0.1 ppm concentrations *via* blue-to-yellow fluorescent bathochromic shift responses, coupled with simultaneous adsorption capacities reaching 126.3 mg/g. Wang's team [243] engineered a 2D cationic framework (SCU-103) that achieves 90% TcO_4^- extraction efficiency in Savannah River Site high-level waste simulants (containing 4 mol/L Na^+) at a solid-liquid ratio of 40 mg/mL. The material's molecular confinement effect within layered channels suppresses 97% of competitive anion interference, demonstrating unprecedented selectivity in complex matrices. Zhao *et al.* [244] redefined nuclear waste management paradigms with a thorium-nickel hybrid MOF that maintains structural integrity under 400 kGy irradiation. Its unique [Th_6O_8] cluster-derived d-pπ conjugated system achieves ReO_4^- adsorption capacities of 807 mg/g, while synergistically enabling uranium contaminant removal (>95% efficiency) and CO_2 cycloaddition catalysis (96.7% product yield). This multifunctional system pioneers an integrated approach to radioactive waste treatment and environmental remediation.

8.5. Others

Beyond conventional remediation systems for uranium, iodine, and technetium nuclides, this study highlights innovative application strategies of MOFs in selective adsorption of radioactive nuclides including palladium (Pd), selenium (Se), cesium (Cs), and thorium (Th).

The recovery of radioactive palladium resources faces dual challenges: strong acid corrosion interference and specific recognition requirements for precious metals. To address these issues, Tang's research team [245] developed a coordination pre-modification strategy to construct polydentate chelating MOF materials. These materials demonstrated exceptional Pd^{2+} capture precision in acidic wastewater (pH 4) through nitrogen-oxygen dual functional sites. The adsorption process followed pseudo-second-order kinetics ($K = 0.037$ g mg^{-1} min^{-1}) and Langmuir monolayer model ($Q_{max} = 427$ mg/g). Synchrotron radiation and XPS analyses elucidated a multi-step mechanism involving chelation, electrostatic adsorption, and *in-situ* reduction that converts Pd^{2+} into metallic Pd^0 particles. The material maintained 91% selectivity against 10-fold concentrated interfering ions and retained 92.7% of its initial adsorption efficiency after five consecutive regeneration cycles. This work provides a novel methodology combining efficient recovery with stable regeneration properties for nuclear waste precious metal resource utilization, presenting significant advancements in sustainable nuclear fuel cycle management.

Current remediation systems for radioactive selenium contamination suffer from limited adsorption capacities and inefficient multi-process integration. Guo's research team [246] addressed these limitations through innovative MOF engineering. Their non-nuclear, high-connectivity UPC-183-Eu framework, constructed from heptanuclear europium clusters and dynamic pore-channel architecture, exhibits aqueous stability fivefold greater than conventional MOFs. Single-crystal X-ray diffraction (SXRD) analysis of UPC-183-Eu after SeO_3^{2-} adsorption revealed structural changes and identified the adsorption sites for SeO_3^{2-}. Zhang's team [247] further advanced selenium management through a cobalt-thiol bifunctional MOF design. The engineered metal-sulfur cooperative activation sites enabled 94.1% dynamic removal efficiency within 120 min, representing an eightfold throughput enhancement compared to conventional methods. Their innovatively fabricated MOFs/nanofiltration composite membrane achieved 99.6% selenium retention with ultrahigh water permeability (15.8 L m^2 h^{-1} bar^{-1}) at minimal MOF loading (0.04% w/w). This system creates selective ion-sieving channels through charge-induced effects for smart SO_4^{2-}/Cl^- separation. Demonstrated in steel wastewater treatment, the integrated platform achieved 97.8% total selenium removal, establishing an end-to-end treatment solution from contaminant enrichment to precision separation.

The global remediation of radioactive cesium faces critical challenges from competitive ion interference in complex aquatic systems and inadequate extreme pH resilience. Zhong's team [241] addressed these limitations by developing NH_2−MIL-125@ZIF-8 heterostructured MOFs through molecular interface engineering. The titanium-zinc bimetallic system demonstrated exceptional cesium adsorption capacity (392.62 mg/g) under strong alkaline conditions (pH 11) (Fig. 7d). Mechanistic studies revealed a dual functional mechanism: Titanium-oxo clusters preferentially capture Cs^+ *via* ion exchange, while ZIF-8 pore channels achieve 99.7% Na^+/K^+ rejection through electrostatic sieving effects. With ion selectivity exceeding 4.5×10^3 mL/g magnitude (Fig. 7e), the material provides a dual-effect system combining targeted recognition and gradient enrichment capabilities for precision treatment of nuclear-contaminated waters.

Conventional thorium separation technologies struggle with discriminating ions of similar hydration radii. Song's team [248] engineered the nanopore-trap MOF DBT-DHTA-Cd featuring 5.2 Å lattice-confined spaces that precisely match Th^{4+} hydration radius (5.1 Å). The hydroxyl–N coordinated electron traps exhibit remarkable binding energy depth (−602.7 kJ/mol), enabling ultrafast Th^{4+} detection within 30 s through fluorescence labeling. Adsorption equilibrium reaches 478 mg/g within 45 min, with single-stage Th^{4+} recovery efficiency surpassing 99.2% in breakthrough experiments. Theoretical simulations elucidate a D-f orbital hybridization mechanism that enhances Th^{4+} binding energy by 5.7-fold compared to U^{6+}. This innovative approach synergizes geometric sieving with electronic confinement effects, establishing a molecular recognition paradigm for lanthanide radioactive nuclide management.

9. MOFs for oil-water separation

Yuying Deng*

The improper discharge of oily wastewater has seriously threatened the environment for human survival and caused waste of oil resources [249,250]. Hence, the efficient purification of oily wastewater while simultaneously recovering oil for reuse holds significant social importance in addressing environmental pollution and resource scarcity issues. MOFs have garnered widespread attention in oil-water separation owing to their high surface area, tunable pore structure, and rich surface chemical properties [251]. In particular, high-performance MOF-based adsorbents and membrane materials have demonstrate great application potential in treating oily wastewater. In recent years, with the continuous development of bionics and interfacial science, superwetting materials with different affinities for water and oil have aroused considerable attention, especially for treating emulsified oily wastewater, further promoting in-depth research and widespread application of MOF-based separation materials within this filed.

9.1. MOF-based adsorption separation materials

MOFs, with large specific surface area, high porosity, and highly controllable pore structure, serve as highly efficient adsorbents for oil-water adsorption separation. Through rational ligand design and post synthesis modification (PSM), the water stability, hydrophilicity/hydrophobicity of MOF-based adsorbents can be effectively regulated and optimized, thereby further enhancing their adsorption performance. However, most MOFs exhibit poor structural stability in humid environments, limiting their adsorption performance in aqueous systems. Furthermore, the characteristics of easy agglomeration and difficult recovery of MOF powders hinder their large-scale application in water treatment [20]. To overcome these limitations, researchers have proposed combining MOFs with other inorganic or organic materials to construct MOF-based composites, which can significantly mitigate the limitations of MOFs in water treatment applications through synergistic effects derived from their respective advantages, demonstrating superior adsorption performance and selectivity compared to individual constituents (Fig. 8a) [252,253]. Most of the MOF-based composites currently reported for oil-water separation exhibit hydrophobic and oleophilic properties, which can efficiently adsorb oil substances in oily wastewater for purification, and then recover oil resources through simple extrusion.

Carbon nanomaterials of different dimensions, such as carbon nanotube (CNT), graphene oxide (GO), and porous carbon (PC), are widely used as adsorbents in oil-water separation due to their high porosity and hydrophobicity [254,255]. Among these, CNTs possess a one-dimensional hollow tubular structure formed by the rolled-up graphene layers. The mesoporous and microporous structures present on their surface and within their walls effectively enhance adsorption capacity [256]. Moreover, the hydrophobicity of CNTs contributes to enhancing the moisture sensitivity of MOFs, and endowing CNT@MOF composites with superior hydrophobicity. Similarly, GO with higher aromaticity possesses stronger hydrophobicity than MOFs. However, the internal water transport channels within GO-based materials are tortuous, and the interlayer interactions are relatively weak, resulting in generally low water flux. Combining GO materials with MOFs can maintain the hydrophobicity and stability of the composite material, while effectively improving the mass transfer pathway by embedding MOFs between layers. For instance, Kolleboyina *et al.* prepared a superhydropho-

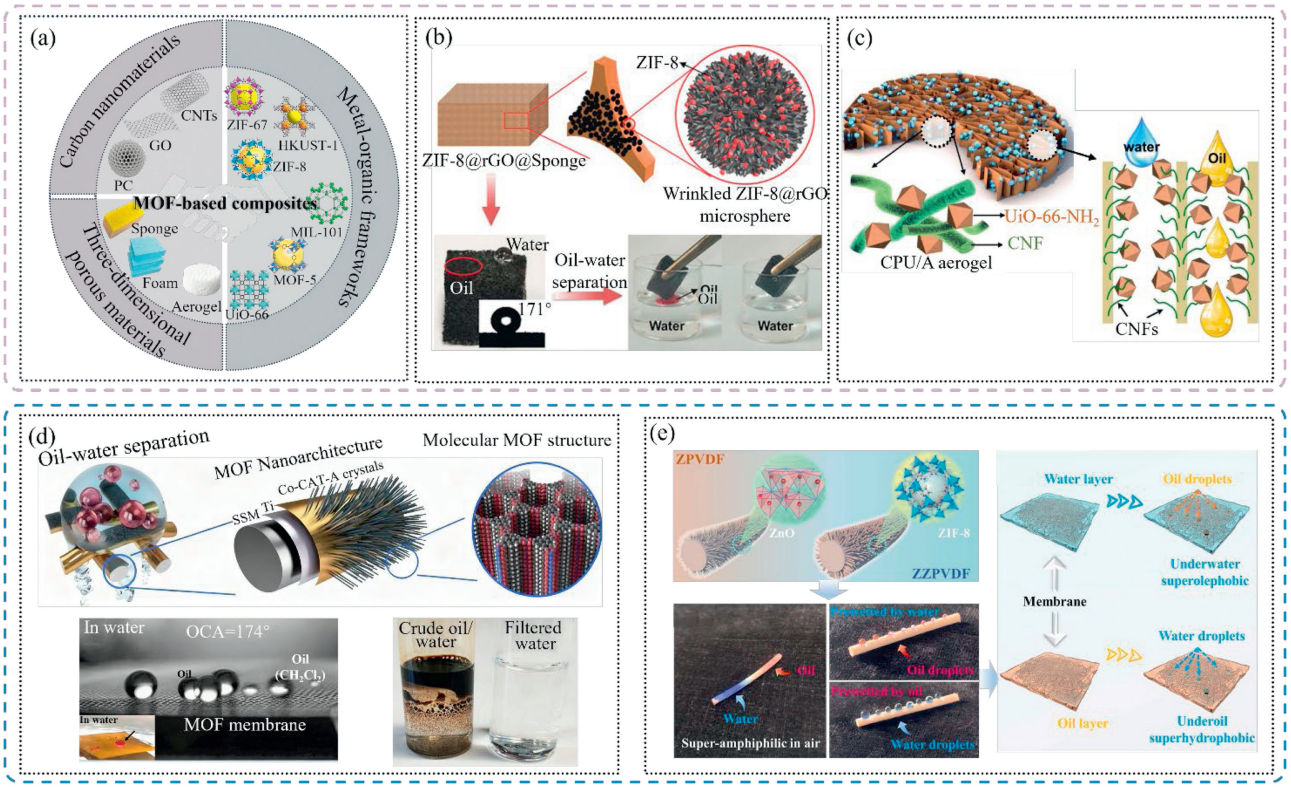


Fig. 8. (a) Schematic illustration of MOF-based composites. (b) Superhydrophobic/superoleophilic ZIF-8@rGO@Sponge composite composed of wrinkled ZIF-8@rGO microspheres and PU sponge for efficient oil-water separation. Copied with permission [260]. Copyright 2019, Wiley-VCH. (c) CPU/A composite aerogel with detailed scaffold structure of CNFs and UiO-66-NH_2 nanoparticles for oil-water separation. Copied with permission [263]. Copyright 2023, Elsevier. (d) Superhydrophilic and underwater superoleophobic Co-CAT-1@Au@SSM membrane for oil-water separation. Copied with permission [268]. Copyright 2021, Wiley-VCH. (e) Schematic illustration of highly efficient on-demand separation by switchable superamphiphilic ZZPVDF tubular nanofiber membrane. Copied with permission [271]. Copyright 2024, Elsevier.

bic/superoleophilic composites HFGO@ZIF-8 comprising highly fluorinated graphene oxide (HFGO) and ZIF-8 [257]. Due to the coordination of zinc ions to oxygen functionalities of HFGO, the controllable growth of ZIF-8 nanocrystals between HFGO layers endows the composite material with a unique micro-mesoporous nanoarchitecture. The composite material reveals prominent adsorption selectivity for nonpolar/polar organic solvents and oils from water.

Three-dimensional porous materials such as sponges, aerogels, and foams are also excellent oil-absorbing materials and loading matrices [258]. Among these, the sponge materials (*e.g.,* melamine sponge, polyurethane sponge, and polydimethylsiloxane sponge) have been extensively studied due to their high porosity, excellent mechanical strength, and outstanding chemical stability. However, most sponge materials exhibit amphiphilic properties (hydrophilic-lipophilic), making it challenging to achieve highly selective oil-water separation. Superhydrophobic three-dimensional porous MOF@sponge composites, prepared *via* loading hydrophobic MOFs, significantly enhance their adsorption selectivity towards oil phases, thus enabling efficient recovery of oil substances from oily wastewater [259]. Meng *et al.* constructed superhydrophobic and superoleophilic MOF@rGO composites with a unique micro/nano hierarchical structure by embedding well-dispersed MOF nanoparticles between crumpled reduced GO (rGO) nanosheets, which display high absorption selectivity and fast absorption rates for organic solvents and oils from water. Furthermore, MOF@rGO@Sponge composite prepared *via* a simple dipping-coating method also showed excellent adsorption performance and good recyclability (Fig. 8b) [260]. Moreover, aerogels, multifunctional materials possessing three-dimensional gel network structure, demonstrate significant potential in oil phase adsorption. Currently reported biomass-based aerogels (*e.g.,* cellulose, lignin, chitosan, sodium alginate) and graphene aerogels exhibit lightweight properties, outstanding mechanical performance, and exceptionally rapid oil absorption capabilities. In view of this, researchers combined MOFs with aerogels to obtain MOF@ aerogels composites with controllable hierarchical structures. The synergistic interaction between MOFs and aerogels is crucial for enhancing mechanical properties, adsorption performance, and stability [261,262]. For instance, Qu *et al.* developed a highly hydrophobic composite aerogel (CPU/A) by incorporating UiO-66-NH_2 into a polyvinyl alcohol (PVA)/cellulose (CNF) composite aerogel (CP/A) (Fig. 8c) [263]. The interconnected porous structure constructed by directional freezing provides ample space for oils and organic solvents storage, thereby enhancing the adsorption capacity of the composite aerogel. A robust three-dimensional network structure with high specific surface area formed by CNF within composite systems endows both CPU/A composite aerogels with excellent mechanical stability and flexibility, facilitating subsequent recovery of adsorbed oil.

9.2. MOF-based membrane separation materials

MOFs and their composites have been extensively loaded onto inorganic substrates (*e.g.,* metal meshes, carbon nanosheets, and metal oxides) or organic substrates (*e.g.,* polymer films, nylon, fabrics, and filter paper) to construct MOF-based membrane materials owing to their outstanding performance in oil-water separation. The MOF layer confers selective separation capabilities, while the substrate layer significantly enhances mechanical strength, thereby expanding their practical application potential. Inspired by the phenomenon of superwetting in nature, endowing membrane surfaces with special wettability has emerged as an effective strategy for achieving efficient and stable oil-water separation [264]. By regulating membrane surface wettability in synergy with the pore-size sieving effect of MOFs, special wetting MOF membranes achieve on-demand, highly efficient oil-water separation.

According to the different wettability of the membrane surface towards oil and water phases, the two most fundamental types of membrane materials in oil-water separation research are superhydrophobic/superoleophilic MOF membranes and superhydrophilic (air)/underwater superoleophobic MOF membranes [265]. Among them, superhydrophobic/superlipophilic MOF membranes can selectively separate oil phase from heavy oil-water mixtures and water in oil (W/O) emulsion through the mechanism of "water blocking and oil permeability". Due to the surface energy of water (72.8 mN/m) is significantly higher than that of oil (30 mN/m), superhydrophobic surfaces typically possess superoleophilicity. A superhydrophobic/superoleophilic surface can be obtained by constructing micro/nano-rough structures on hydrophobic substrates, or modifying surfaces with rough structures using low-surface-energy substances. Pei and Guo *et al.* obtained superhydrophobic (WCA exceeding 159.2°) and superoleophilic (oil contact $\approx$ 0°) MOF-fabric membranes by *in-situ* growth of ultra-narrow bandgap MOF (AgTCNQ) onto fabric substrates, achieving selective separation of toluene-water mixture (98.4%) [266]. MOF membranes with superhydrophilicity in air and superoleophobicity underwater efficiently intercept the oil phase *via* a "water permeability-oil blocking mechanism", making them particularly suitable for treating light oil-water mixtures and oil-in-water (O/W) emulsions. Owing to the extremely high affinity of the superhydrophilic surface for water, water can rapidly spread on the membrane surface to form a continuous and stable hydration layer, effectively suppressing non-specific interactions (adsorption deposition, hydrophobic interactions, and hydrogen bonding) between oil droplets and the membrane surface and significantly enhancing the antifouling performance of the membrane material [267]. Medina's team synthesized a unique nanocolumnar structure of pillar-like Co-CAT-1 MOF crystallites on gold-coated woven stainless teel meshes with large apertures of 50 μm [268]. This mesh membrane with superhydrophilic and underwater superoleophobic properties achieved highly efficient oil-water separation under gravity, with water flux of up to nearly one million L m^{-2} h^{-1}. The membrane demonstrated outstanding separation performance even for crude oil emulsion system (Fig. 8d).

Membrane materials with superhydrophobicity or underwater superhydrophilicity can only achieve oil-water separation *via* a single mechanism of "oil removal" or "water removal". For complex oily wastewater and variable treatment environments, membrane materials with single wettability often fail to meet separation requirements in practical applications. Since the membrane wettability is determined by the synergistic effect between surface nanostructures and chemical composition, it is theoretically feasible to achieve *in situ* regulation of membrane wettability by adjusting chemical composition without altering the surface nanostructure. In recent years, researchers have developed stimuli-responsive smart membrane materials capable of switchable wettability, which can achieve reversible conversion between (super) hydrophobic/(super) oleophilic and (super)hydrophilic/(super)oleophobic under external stimuli (light, heat, electro, pH, pressure, electricity, and moisture), thereby achieving highly efficient, on-demand separation of various oil-water systems [269]. Based on the high designability of MOFs structure and function, responsive molecules are introduced into MOF membranes through pre-modification of organic ligands, in-situ polymerization, and post-modified synthesis, thereby obtaining stimuli-responsive MOF membranes that can simultaneously meet the purification treatment of different types of oily wastewater [270]. For instance, Piao *et al.* [271] fabricated ZIF-8@ZnO/PVDF tubular nanofiber (ZZPVDF) membranes with switchable wettability. The ZZPVDF membrane displayed superamphiphilicity in

air. After prewetted by oil or water, membrane surface demonstrated underwater superoleophobicity or underoil superhydrophobicity for highly efficient, on-demand separation of O/W emulsions (99.85 %) and W/O emulsions (99.92 %), respectively (Fig. 8e). Furthermore, inspired the difference in surface wettability of lotus leaves and desert beetles, Janus materials with asymmetric wettability have been gradually developed and applied to oil-water separation. Within the narrow channel formed by the Janus double membrane layer, emulsion become local enrichment as water permeates through the hydrophilic membrane. While the hydrophobic membrane utilizes these enriched oil droplets to intensify collisions and coalescence, thereby promoting demulsification and separation of emulsion. This synergistic mechanism not only effectively overcomes the concentration polarization (hydrophilic membrane) and flux decline (hydrophobic membrane) issues commonly encountered with single-wettability membranes during separation process, but also enables concurrent oil and water recovery from emulsions, demonstrating unique separation advantages [272,273].

Based on oil-water separation mechanism and solid surface wettability theory, researchers have designed and synthesized various MOF-based adsorption materials and membrane materials with special wettability. Nevertheless, high-performance MOF-based separation materials capable of efficiently treating complex oily wastewater systems remain relatively scarce, and generally face challenges such as high cost, membrane fouling, and low membrane flux. Currently, the preparation and practical application of MOF-based separation materials are mostly still in the laboratory research stage, and promoting their development towards large-scale, low-cost, and green environmental protection has become an inevitable trend. Moreover, the composition of actual oily wastewater is far more complex, with multiple pollutants coexisting. Consequently, developing multifunctional MOF-based separation materials capable of achieving efficient oil-water separation while synergistically removing other contaminants has become an urgent research direction for the future. It is noteworthy that MOFs and their membrane materials have demonstrated outstanding performance in the field of separation, indicating that MOF-based materials hold promise for playing a more critical role in the treatment of oily wastewater.

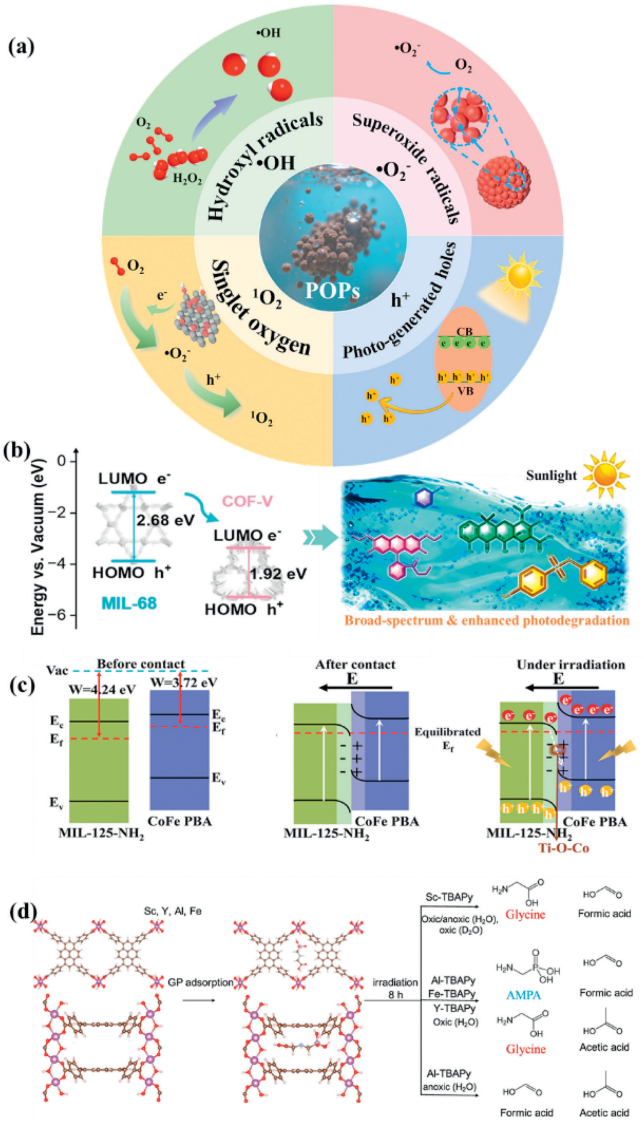


Fig. 9. (a) Schematic diagram of photocatalytic degradation of organic pollutants. (b) Photoinduced electron transfer and pollutant degradation mechanism in MIL-68@COF-V heterojunction. Copied with permission [279]. Copyright 2024, Wiley-VCH. (c) Schematic illustration of S-scheme charges transfer mechanism between MIL-125-NH_2 and CoFe PBA. Copied with permission [280]. Copyright 2023, Wiley-VCH. (d) Product formation by the M^{3+}-TBAPy MOFs under different conditions. Copied with permission [282]. Copyright 2024, Springer Nature.

10. Photocatalytic detoxification of hazardous pollutants in MOFs

Hao Du, Qi Wang*

10.1. Degradation of organic pollutants

Persistent organic pollutants (POPs) which often contain stable aromatic structures, pose a serious threat to environmental safety and human health due to their resistance to biological and conventional treatment processes [274,275]. A promising solution involves using solar energy to mineralize these POPs into CO_2 and H_2O *via* ROS, such as hydroxyl radicals ($^{\bullet}OH$), superoxide radicals ($O_2^{\bullet-}$) and singlet oxygen ($^1O_2$) (Fig. 9a). MOFs, which exhibit inherent semiconductor behavior, have emerged as excellent photocatalysts for this purpose [276,277]. Through atomic-level design, MOFs can be engineered to efficiently decompose recalcitrant organic pollutants, including antibiotics, dyes, phenolic compounds, PFAS.

Constructing heterojunctions is one of the most effective strategies for enhancing charge separation in MOF-based photocatalysts [278]. This approach involves aligning energy bands and forming chemical bonds at material interfaces to achieve directional carrier migration.

Covalent heterojunctions: Zhou *et al.* constructed a core-shell MIL-68@COF-V heterostructure by robust C-C bond [279]. This covalent interface efficiently promotes the transfer of photogenerated electrons from MIL-68 to COF-V (Fig. 9b), enabling spatial charge separation and suppressing electron-hole recombination. This system primarily relies on the generated $O_2^{\bullet-}$ and $^1O_2$ to degrade various pollutants and demonstrates potential for creating reusable films. Strong covalent linkages and shell-localized adsorption sites should be co-designed so that interfacial band alignment and pollutant enrichment occur in the same region, maximizing the utilization of separated charges for surface reactions rather than bulk recombination.

S-Scheme heterojunctions: In a MOF-on-MOF heterojunction (MIL-125-NH_2@CoFe PBA), atomic-level charge transfer channels were created through interfacial Ti-O-Co bonds [280]. Driven synergistically by a built-in electric field, band bending, and Coulomb force, a S-scheme charge transfer mechanism was achieved: electrons in the conduction band (CB) of MIL-125-NH_2 recombine with holes in the valence band (VB) of CoFe PBA (Fig. 9c). This pro-

cess retains highly reducing electrons in the CB of CoFe PBA and strongly oxidizing holes in the VB of MIL-125-NH_2, achieving efficient charge separation while maximizing the system's redox potential to generate ROS ($O_2^{\bullet-}$ and $^{\bullet}OH$) for tetracycline degradation. Here, the spatially separated redox centers strongly reducing sites at the CoFe PBA side and strongly oxidizing sites at the MIL-125-NH_2 side demonstrate how asymmetric band engineering in MOF-on-MOF structures can be used to decouple oxidation and reduction domains and thus tune the degradation pathway and selectivity for different pollutants.

In-situ growth: Chen *et al.* utilized a high-energy electron beam radiation method to synthesize a ZIF-8@ZnO heterojunction *in situ* [281]. This one-step process creates an intimate interface that facilitates improved charge separation. This one-step process creates an intimate interface with conformal contact between the microporous ZIF-8 and ZnO nanoparticles, facilitating improved charge separation and rapid interfacial carrier transfer. The ZIF-8 shell provides size- and polarity-selective adsorption channels, enriching organic substrates near the ZnO surface where electrons and holes are generated. This case highlights the importance of integrating adsorption-selective MOF shells with wide-bandgap semiconductors *via* defect-minimized, *in situ* interfaces to couple molecular sieving with efficient photogenerated charge utilization.

Channel regulation and molecular engineering are powerful strategies for optimizing mass transfer and activation within MOFs, thereby enhancing their photocatalytic efficiency. For instance, in the M^{3+}-TBAPy series of MOFs, *Sc*-TBAPy demonstrates that high surface area is not the sole determinant of performance [282]. Although its surface area is not the highest, *Sc*-TBAPy's unique nanoconfined pores exhibit strong adsorption capacity for glyphosate (GP) through van der Waals forces interactions, effectively enriching reactants near the active sites. Crucially, the pore microenvironment and the properties of the Sc^{3+} metal nodes work in concert to dictate e reaction pathway selectivity. *Sc*-TBAPy selectively generates $^1O_2$, which is key to cleaving the β C-N bond of GP (Fig. 9d). In contrast, other M^{3+}-TBAPy variants such as Al- or Y-TBAPy preferentially form toxic aminomethylphosphonic acid (AMPA). This system clearly reveals a structure performance relationship in which the combination of pore confinement (controlling adsorption geometry and local concentration) and metal-node redox potential (controlling ROS speciation) dictates the reaction pathway and product selectivity.

In a separate approach to molecular engineering, Liu *et al.* constructed a donor-acceptor system by inserting 9,10-dimethylanthracene (DMA) donor molecules into the framework of Sr-NDI MOF, creating an Sr-NDI@DMA eutectic material [283]. The strong charge-transfer interaction between the donor and acceptor not only red-shifts the light absorption into the near-infrared region, but also induces a highly ordered, alternating D-A structure. This arrangement shortens the π-π stacking distance to approximately 3.45 Å, which fosters efficient migration pathways for photo-generated charge carriers. Simultaneously, this structure establishes a strong built-in electric field, which greatly promotes charge separation and leads to the enhanced degradation of pollutants like Rhodamine B. Optimizing the spatial arrangement and stacking distance of donor and acceptor materials is equally important as expanding the light absorption range, as both determine the carrier mobility and separation efficiency under visible near-infrared irradiation.

Beyond direct degradation, the design of MOF photocatalytic systems is expanding towards integrated resource utilization. This approach is particularly beneficial for recalcitrant pollutants like perfluorooctanoic acid (PFOA), where a single reduction or oxidation pathway often proves inefficient. For instance, researchers have demonstrated that MIL-125-NH_2 can simultaneously generate strong reducing hydrated electrons (e_{aq}^-) and oxidizing $^{\bullet}OH$ when using glucose as a sacrificial agent [284]. In this system, e_{aq}^- initiates H/F exchange and chain shortening of PFOA, while $^{\bullet}OH$ plays a key auxiliary role in the hydroxylation step. This synergistic action between reductive and oxidative species achieves efficient degradation and deep defluorination. Furthermore, pollutants can be innovatively utilized as sacrificial agents in H_2 evolution reactions, coupling detoxification with renewable fuel production. In one example, physically mixing MIL-125-NH_2 with the Earth's abundant Ni_2P cocatalyst creates a system where Rhodamine B molecules act as sacrificial electron donors [285]. Under anaerobic conditions, the pollutant is oxidized and degraded by photo-generated holes, while the concurrently generated electrons are efficiently captured by Ni_2P to reduce protons into H_2. Here, the energetic matching between the MOF CB potential and the H_2 evolution cocatalyst, together with the favorable adsorption of dye molecules near oxidative sites, ensures that the thermodynamic driving force for both pollutant oxidation and H_2 generation is fully exploited.

In summary, MOF-based photocatalysts have significant advanced the efficiency, selectivity, and functionality of pollutant degradation through strategies such as constructing heterojunctions, regulating pore microenvironments, and designing novel reaction pathways. Future research should focus on developing more stable, low-cost, and readily scalable MOF materials. By utilizing advanced *in-situ* characterization techniques and theoretical calculations, the field can: (i) Deepen the understanding of the adsorption, activation, and degradation processes of pollutants within MOF pores; (ii) Design more multifunctional photocatalytic systems that can couple pollutant degradation with resource conversion.

10.2. Reduction of heavy metals

The contamination of water bodies by toxic heavy metals such as Cr(VI) and U(VI) poses a severe threat to ecosystems and human health. Cr(VI) is nearly 1000 times more toxic than Cr(III), and U(VI) has strong solubility and high mobility, requiring efficient treatment technologies [286]. While traditional methods like chemical precipitation and filtration are often hampered by high chemical consumption, cost, and sludge generation, photocatalysis offers an attractive alternative due to its high efficiency, environmental friendliness, and minimal secondary pollution [287].

MOFs have demonstrated exceptional performance in removing heavy metal ions, attributable to their high specific surface area, tunable porosity, and abundant active sites. Compared to traditional materials, MOFs offer more metal coordination sites, modifiable organic functional groups, and designable pore structures, enabling multiple interaction mechanisms including electrostatic attraction, coordination binding, electron transfer, and photocatalytic conversion (Fig. S3a in Supporting information) [288]. Critically, through rational structural design, MOFs can achieve selective capture and reduction of specific heavy metal ions, which is of great significance for targeted removal of highly toxic pollutants from complex water matrices.

The core mechanism begins with the generation of electron-hole (e^--h^+) pairs upon photoexcitation of the MOF [289]. Enhancing the reduction efficiency primarily depends on promoting the separation and migration of e^- while suppressing their recombination with h^+. Two predominant strategies are employed: (i) In the sacrificial-agent systems, agents like ethanol are used to scavenge h^+, thereby extending the lifetime of e^- for the direct reduction of heavy metal ions [290]. (ii) The sacrificial-free systems leverage the combined action of both charge carriers, where h^+ participate in generating ROS such as $O_2^{\bullet-}$, which subsequently contribute to the indirect reduction of the target pollutants [291]. In both cases, the spatial correlation between adsorption sites for metal ions and

the locations where e^- or ROS are generated is a key structural factor governing reduction kinetics.

Furthermore, structural modification (such as ligand functionalization to enhance light absorption, or constructing heterojunctions to promote charge space separation using built-in electric fields) can significantly optimize the carrier dynamics [292]. Through these direct and indirect pathways, high toxic and mobile metals like Cr(VI) and U(VI) can be efficiently transformed into less toxic, readily precipitable forms such as Cr(III) and U(IV).

Recent advances in structural regulation and composite design have significantly enhanced the performance of MOFs in the photocatalytic reduction of heavy metals. For instance, Fe-MOFs (MTBDC-TPT-Fe) was constructed for efficient Cr(VI) reduction by strategically incorporating two functional ligands: MTBDC (containing a $-SCH_3$ group) and TPT (a strong electron-withdrawing ligand with a triazine structure) [288]. Under visible light, the $-SCH_3$ group acts as a chromophore to enhance the absorption of visible light and supply electrons to the iron-oxo cluster. Concurrently, the TPT ligand facilitates the spatial separation and migration of electrons from the HOMO (localized on TPT) to the LUMO (localized on the iron-oxo cluster) through its potent electron-withdrawing effect (Fig. S3b in Supporting information). This mechanism significantly suppresses e^--h^+ recombination. In this system, photogenerated e^- and $O_2^{\bullet-}$ were identified as the primary reactive species responsible for reducing Cr(VI). The cooperative roles of MTBDC (light harvesting and electron donation) and TPT (electron withdrawal and transport) exemplify a clear structure performance correlation: Decoupling light absorption and charge-separation functions into different ligands around the same metal cluster is an effective design principle for maximizing the utilization of photogenerated electrons in MOF-based heavy-metal photocatalysts.

In terms of uranium reduction, a highly efficient system integrating complexation and photocatalytic reduction was developed by grafting phosphonic acid and amino functional groups onto the Zr-oxo clusters of photoactive MOF PCN-222 [293]. These functional groups first selectively capture and enrich U(VI) ions from solution. Subsequently, under visible light irradiation, the e^- generated by the excited photosensitive ligands in MOF are transferred to the enriched U(VI) (Fig. S3c in Supporting information). The resulting U(IV) products form insoluble precipitates that are released from the MOF pores. This process vacates the adsorption sites, enabling the material to self-regenerate and establishing a self-sustaining "capture-reduction-release" cycle. This innovative design achieves exceptional selectivity and wide applicability across U(VI) concentrations and pH ranges. More broadly, it illustrates that combining highly specific coordination sites with photoactive chromophores in a single framework allows fine control over both the thermodynamics (selective binding) and kinetics (fast interfacial electron transfer) of heavy-metal detoxification.

Constructing heterojunctions is a highly effective strategy for boosting the photocatalytic performance of MOFs. A prime example is the MIL-101(Fe)/g-C_3N_4 heterojunction, which facilitates the efficient reduction of Cr(VI) *via* a direct Z-type mechanism (Fig. S3d in Supporting information) [292]. Under visible light, this system enriches highly reductive e^- in the conduction band (CB) of g-C_3N_4 and oxidative h^+ in the valence band (VB) of MIL-101(Fe). This spatial charge separation enables the simultaneous reduction of Cr(VI) and mineralization of bisphenol A (BPA). Here, the synergy arises from the complementary band positions and adsorption preferences of the two components, g-C_3N_4 preferentially interacts with anionic Cr(VI), while MIL-101(Fe) provides accessible Fe centers and aromatic linkers that adsorb and activate BPA, enabling a single composite to deliver both reductive and oxidative detoxification.

Beyond binary heterojunctions, more sophisticated systems can be engineered for multifaceted environmental remediation. For instance, a heterojunction composed of UiO-66-NH_2 and black phosphorus quantum dots (BPQDs) was anchored onto a carboxylated cellulose nanofiber aerogel to create a robust BP@CNF-MOF composite [294]. In this architecture, the narrow bandgap BPQDs act as efficient light harvesters, and the generated e^- readily transfer to the CB of UiO-66-NH_2, promoting effective separation of e^--h^+ pairs. These photogenerated e^- reduce soluble U(VI) to insoluble U(IV) oxides, which precipitate on the surface of MOFs. This precipitation releases the binding sites, allowing for continuous adsorption of fresh U(VI) in self-regenerating cycle. Concurrently, the photogenerated h^+ react with H_2O and dissolved oxygen to generate a high yield of ROS. These ROS effectively eliminate marine bacteria, preventing biofouling and thereby enhancing the material's long-term adsorption capacity and operational stability in complex seawater environments. At the same time, combining the layered design combining MOFs, quantum dots and macroscopic aerogels highlights how multiscale structural control (from molecular ligands to porous macrostructures) can be leveraged to balance adsorption, redox activity, mass transport and mechanical robustness.

Despite the considerable promise of MOFs in the photocatalytic reduction of heavy metals, their practical applications faces several significant challenges. Many MOFs exhibit optimal activity under strongly acidic conditions, which severely limits their utility in near neutral water bodies. While sacrificial agents can enhance electron utilization efficiency, their consumption raises operational costs and may introduce secondary pollutants. Furthermore, the typical powdered form of MOFs presents difficulties in recovery and reuse, hindering large-scale application. From a structure performance standpoint, it remains crucial to balance strong binding of target ions (for selectivity) with sufficient reversibility (for regeneration), and to couple these adsorption properties with band structures that provide adequate driving force for reduction under realistic water chemistries.

Future research should focus on addressing these limitations. A primary objective is the development of MOF materials that maintain high photocatalytic activity across a broad pH range, achievable through the strategic design of metal nodes and organic ligands. Concurrently, efforts must be directed toward immobilizing MOFs on scalable substrates, such as membranes or monolithic carriers, to facilitate catalyst recovery and enable continuous-flow processes. Finally, the deep integration of theoretical calculations and simulations will be crucial for the precise, knowledge-driven design of new MOFs with high activity, exceptional stability, and scalability, thereby advancing these materials toward practical environmental remediation. Finally, the deep integration of theoretical calculations and simulations with *in situ* spectroscopic techniques will be crucial for revealing how local coordination environments, adsorption geometries and electronic structures jointly govern heavy-metal reduction pathways. Such knowledge-driven design is expected to yield next-generation MOFs and MOF-based composites with high activity, exceptional stability and scalability, thereby accelerating their deployment in practical environmental remediation.

11. Fenton-like reactions in MOFs

Yixuan Zhai, Xiaodong Zhang*

Fenton-like reactions are a kind of AOPs that can effectively treat the organic pollutants in water [295]. ROSs are produced during the transition metal ions catalytic activation of oxidants such as hydrogen peroxide (H_2O_2), persulfate (PDS), or PMS in Fenton-like reactions [296–299]. Compared to the traditional Fe^{2+}/H_2O_2 Fenton system, Fenton-like reactions exhibit a broader pH applicability range and higher catalytic stability [300]. Owing to their numerous unsaturated sites, tunable metal active sites, and highly organized

porous structures, MOFs are considered as highly suitable Fenton-like catalysts [18].

11.1. Radical pathway

In radical-involved Fenton-like reactions, the free radicals (like •OH) played a crucial role in the efficient degradation of organic pollutants [301]. The generation efficiency of radicals and their reaction pathways directly determined the pollutant degradation performance.

Fe-MOFs are the most widely used MOFs in radical-dominated Fenton-like reactions, because the Fe sites in Fe-MOFs could regulate •OH generation. Zhao *et al.* [302] developed a defective Fe-MOF photocatalyst (MIL53-250) *via* a thermal-assisted synthesis strategy. By precisely modulating the terminal inorganic ligands (OH^-/H_2O), they successfully introduced coordinatively unsaturated Fe sites, thereby tuning the geometric configuration and electronic structure of the active centers. Optimization of the structure of MIL53-250 increased the H_2O_2 adsorption and cleavage of the O-O bond in it. This synergistic effect resulted in a significant increase in •OH generation efficiency. MIL53-250 eliminated 4-chlorophenol (4-CP) in 10 min. These findings highlighted that ligand regulation effectively promoted radical generation in Fenton-like reactions. Duan *et al.* [303] developed an Fe-MOF catalyst containing dual S-coordinated Fe sites, which enabled highly selective •OH generation in Fenton-like reactions. Dual S coordination altered the H_2O_2 adsorption configuration from "end-on" to "side-on," enabling homolytic cleavage of the O-O link and direct splitting of one H_2O_2 molecule into two •OH radicals, resulting in the production of 93.89 % •OH in the Fenton-like system. S-Fe-MOFs demonstrated remarkable practical stability, maintaining 84.66 % BPA removal efficiency over 12 h in a continuous-flow fixed-bed reactor using actual water. These studies demonstrated that the adsorption geometry of oxidants could be effectively modulated by controlling the coordination environment and electronic structure of the Fe center in Fe-MOFs.

Electronic regulation in electro-Fenton systems offers another effective strategy to boost •OH production and catalyst stability. Zhu *et al.* [304] constructed a dual-cathode electro-Fenton system based on a naturally aspirated cathode (NAC). The NAC was treated with nitric acid to obtain a more hydrophilic modified NAC (MNAC), on which Cu-MIL-88B(Fe) was grown *in situ* to form the MNAC@Cu-MIL-88B(Fe) electrode. Cu acted as an electron shuttle mediator in MNAC@Cu-MIL-88B(Fe), resulting in a 93 % Fe^{2+} regeneration rate. Cu doping simultaneously caused the D-band center to move closer to the Fermi level, which improved D-electron hybridization with H_2O_2 and encouraged the production of •OH. The system removed 99.4 % of the pollutants and 70.1 % of the total organic carbon (TOC) during the degradation of 2,4-dichlorophenoxyacetic acid (2,4-D) in 90 min while leaching very little Fe (0.32 mg/L) and Cu (0.03 mg/L). The construction of bimetallic MOF derivatives was also beneficial for stability and catalytic efficiency of catalysts in electro-Fenton processes. Ye *et al.* [305] described a FeS_2/C nanocomposite made by simultaneously carbonizing and sulfidating an Fe-MOF precursor in order to solve the problems of inadequate catalyst stability and high Fe leaching in heterogeneous electro-Fenton processes. The fluoxetine in urban wastewater was almost completely degraded in 60 min and the TOC removal was around 90 % in 6 hours. Moreover, the FeS_2/C catalyst exhibited excellent stability, maintaining its activity over five consecutive cycles, which could be fully recovered by a simple cleaning process. This study provides a highly active and stable catalytic system for heterogeneous electro-Fenton treatment of refractory organic wastewater. Zuo *et al.* [306] designed a FeOCl-MOF yolk–shell reactor to address the bottleneck of the low utilization efficiency of •OH in Fenton-like systems. The MOF shell effectively absorbed BPA *via* π-π interactions, while the FeOCl core activated H_2O_2 to produce •OH, which concentrated both reactive and adsorptive sites in a restricted space. Therefore, the migration distance of •OH was reduced, and the utilization efficiency of •OH was increased to 77.1 %. The FeOCl-MOF/H_2O_2 system steadily broke down BPA in a broad pH range of 3-9. Zhang *et al.* [307] developed a UiO-66-NH_2-(Zr/Fe)/GA catalyst through an *in situ* synthesis strategy with graphene aerogel (GA) as a support. The nanoconfinement effect of GA enriched the reductive intermediates during phenol degradation, which altered the carbon transfer route from the kinetically favored ring-opening route to the thermodynamically favored oligomerization route. This pathway significantly accelerated phenol removal rate and achieved a TOC removal of 92.2 ± 3.7 % within 60 min. The system used over 95 % less H_2O_2 than the conventional Fe(II)/H_2O_2 system. This reduction resulted from nanoconfinement effects, which concentrated reactive intermediates and accelerated Fe(III) reduction. The confined environment improved •OH utilization and minimized the oxidant demand for complete mineralization.

11.2. Non-radical pathway

The non-radical pathway is another important mechanism in Fenton-like reactions, gaining increasing attention because of its distinctive reaction mechanism and high pollutant removal efficiency [308]. Through the rational design of MOFs and their derivatives, the reaction pathway can be precisely controlled to achieve highly efficient non-radical AOPs.

As an important subclass of MOFs, Prussian blue analogues (PBAs) are widely used as precursors for preparing high-performance catalysts [309]. Li *et al.* [310] used Fe-Co PBA ($Fe_{0.5}Co_{0.5}[Co(CN)_6]_{0.67}\cdot nH_2O$) as a precursor to synthesize a porous N-doped graphene catalyst (FeCo-NC-2) through pyrolysis followed by acid leaching. Characterization revealed that Co species in FeCo-NC-2 were coordinated in the CoN_4 configuration. The pyrrolic N sites acted as the main adsorption sites for BPA, while the CoN_4 centers selectively activated PMS to generate $^1O_2$ through a non-radical pathway. This unique adsorption-catalysis dual-site mechanism effectively shortened the migration distance between the generated $^1O_2$ and the adsorbed BPA molecules, resulting in the complete degradation of BPA within 4 min. Electron paramagnetic resonance (EPR) measurements further confirmed the predominance of the non-radical pathway, as no characteristic signals of •OH or sulfate radicals ($SO_4^{\bullet-}$) were detected, whereas a distinct signal of $^1O_2$ was observed [311]. Lan *et al.* [312] synthesized a Co-V bimetallic MOF, $Co_2(V_4O_{12})(bpy)_2$ (bpy = 4,4′-bipyridine), with polyvanadate $[V_4O_{12}]^{4-}$ clusters as the inorganic linkers. This catalyst activated PMS through a non-radical mechanism and degraded multiple typical pollutants, such as OFX, chloroquine phosphate (CQ), tetracycline (TC), and BPA. The Co sites provided electrons from PMS, and the $[V_4O_{12}]^{4-}$ clusters accepted them through hydrogen bonds. This electron transformation generated $^1O_2$. The $Co_2(V_4O_{12})(bpy)_2$/PMS system kept over 90 % OFX removal for 40 h in actual wastewater, which proved the high stability of $Co_2(V_4O_{12})(bpy)_2$ and its potential for real water treatment applications.

To address the issues of structural disorder and heterogeneous active sites in MOF-derived carbons, Lian *et al.* [313] synthesized a MOF-derived crystalline nanocarbon (MCC) by employing NaCl as a template and performing high-temperature pyrolysis of ZIF-8 (Fig. 10a). The obtained MCC possessed a graphite-intercalation-compound-like structure, in which ZnO_x species were intercalated between the graphitic layers. These intercalants stabilized the layered framework and enhanced electron delocalization, thereby improving electron-transfer efficiency. Benefiting from this superior conductivity, MCC efficiently activated PMS through a

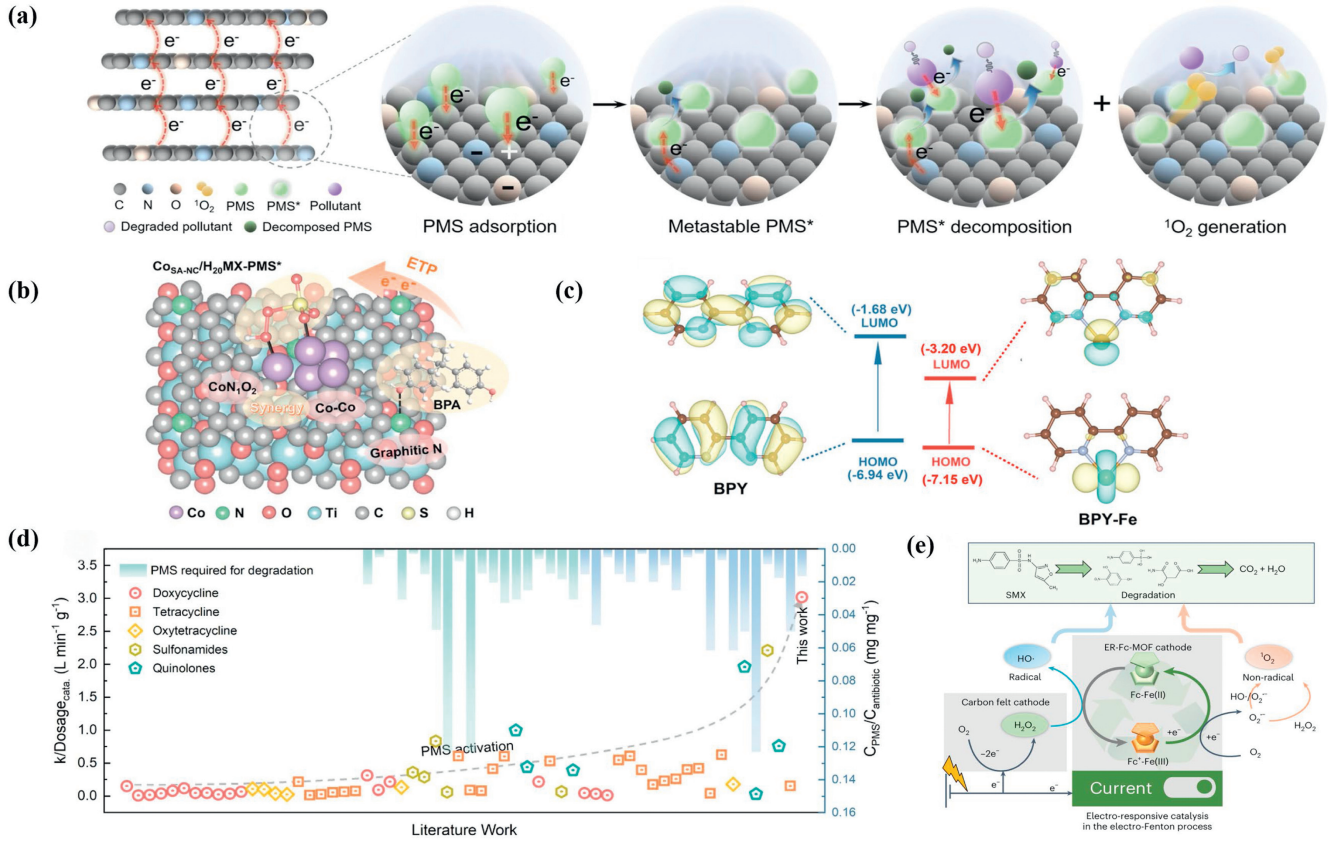


Fig. 10. (a) Proposed PMS activation mechanism at the interfaces of MCC-950, which is adsorbed and then transforms into metastable intermediate PMS*, followed by decomposition and the selective generation of $^1O_2$. Copied with permission [313]. Copyright 2024, Springer Nature. (b) Schematic diagram of the Fenton-like reaction for $Co_{SA\text{-}NC}/H_{20}MX$. Copied with permission [314]. Copyright 2025, Wiley-VCH. (c) The calculated HOMO and LUMO energy of BPY ligand and BPY Fe sites. Copied with permission [316]. Copyright 2025, Wiley-VCH. (d) Comparisons of catalytic efficiency with those of reported catalysts. Copied with permission [318]. Copyright 2023, Springer Nature. (e) Proposed mechanism for the catalytic process in the dual-cathode electro-Fenton system with the ER-Fc-MOF catalytic cathode. Copied with permission [322]. Copyright 2024, Springer Nature.

non-radical pathway dominated by electron transfer to generate $^1O_2$, resulting in rapid degradation of typical pollutants such as ciprofloxacin (CIP) and TC. Guo *et al.* [314] prepared an asymmetric Co single-atom catalyst (CoSA-NC/H_xMX) and pyrolyzed ZnCo-ZIF precursors (Fig. 10b), which was used in the degradation of BPA reacted with PMS by a non-radical electron transfer process (ETP). The critical step was the formation of a surface-confined metastable complex (CoSA-NC/H_{20}MX-PMS*). In the CoSA-NC/H_{20}MX-PMS*, the N-C bond sites adsorbed and concentrated BPA through $\pi-\pi$ interactions, while the bonding between MXene and the graphitic carbon layers promoted fast electron transfer across the interface. The macromolecular products formed during the ETP were deposited on the catalyst surface, leading to efficient BPA degradation within 4 min, and the TOC removal rate reached 78.2%. The study has shown an unusual non-radical type of electron transfer controlled polymerization.

11.3. Synergistic action of radicals and non-radicals

Radical and non-radical processes are combined to enhance the activity of Fenton-like processes [315]. By using the complementary advantages of different reactive species, this hybrid mechanism increases degradation efficiency and expands environmental adaptability.

Duan *et al.* [316] integrated bipyridine-coordinated Fe atoms into the Al-based MOF-253 framework, forming a crystalline Fe-Al bimetallic MOF (MOF-253-Fe) (Fig. 10c). The Fenton-like reaction worked by having H_2O_2 adsorb onto the Fe sites, which triggered an electron transfer reaction and produced bipyridine organic radicals ($^{\bullet}BPY^+$) and the $^{\bullet}OH$. This created a structure of $\bullet BPY^+$-Fe electron pump. The structure accepted electrons from π-electron-rich pollutants such as BPA and 4-CP and transferred them to H_2O_2, enabling continuous and efficient $^{\bullet}OH$ production. Meanwhile, pollutant molecules polymerized on the catalyst surface, which further improved the utilization efficiency of H_2O_2. In a continuous-flow reactor, the catalyst maintained over 90% BPA removal after 10 h of operation. In the same year, Wang *et al.* [317] used a strategy based on site-specific roles to prepare $Co_{0.75}Zn_{0.25}$-NC through pyrolysis using a bimetallic ZIF (ZIF-$Co_{0.75}Zn_{0.25}$) as precursor. Research revealed that Co-Co active sites could activate PMS to generate $SO_4^{\bullet-}$, while Co-N active sites were used in generating $SO_4^{\bullet-}$. TC was fully degraded in 2 min following an adsorption equilibrium. This work made it possible to introduce the concept of synergy between radical and non-radical metals by building two active sites, which helped to understand how to create an efficient and stable system of catalysis with Fenton-like characteristics.

Wang *et al.* [318] designed an S-scheme heterojunction PBA/MoS_2@CSH catalyst to overcome the limitations of conventional Fenton-like systems (Fig. 10d). Chitosan hydrogel (CSH) acted as the support, with PBA and molybdenum disulfide (MoS_2) integrated onto it to create a strong interfacial electric field (IEF). The Fe/Co sites in PBA activated PMS through valence cycling, driving the radical pathway by forming $SO_4^{\bullet-}$ and $^{\bullet}OH$. At the same time, the IEF-induced charge separation supported the non-radical pathway, helping to generate $^1O_2$. Owing to the synergy of radical and non-radical reactions, the PBA/MoS_2@CSH system could main-

tain DC degradation for up to 3000 min. Wang *et al.* [319] reported an S-scheme heterojunction photocatalyst, V_O-M-Co_3O_4@CN_x, by coupling ZIF-67-derived Co_3O_4 containing abundant oxygen vacancies (V_O) with carbon nitride (CN) possessing intrinsic nitrogen vacancies (V_N) *via* polyethylene glycol (PEG). V_O-M-Co_3O_4@CN_x effectively activated PMS under aeration-free conditions through a dual-pathway mechanism. The V_O and V_N defects provided electrons for PMS activation in an anaerobic environment, mainly driving the radical pathway to generate $SO_4^{\bullet-}$ and $^{\bullet}OH$. Meanwhile, the CN_x cooperated with Co sites to promote the formation of $^1O_2$ through the non-radical pathway. Benefiting from this synergistic effect, the catalyst maintained over 98.05 % atrazine (ATZ) removal efficiency for more than 800 min in a continuous-flow reactor. Ren *et al.* [320] fabricate a bifunctional MOF-derived Fe-Cu@biochar composite that integrated adsorption with heterogeneous electro-Fenton oxidation for efficient antibiotic elimination and *in-situ* adsorbent regeneration. The mesoporous biochar, having a high specific surface area, provided stabilization for Fe-Cu dual sites *via* coordination bonds. Concurrently, its abundant oxygen-containing functional groups facilitated rapid TC adsorption through electrostatic and coordination interactions. The mesoporous biochar substrate with a large specific surface area stabilized Fe-Cu dual sites through coordination bonds, while abundant oxygen-containing functional groups enabled rapid TC adsorption *via* electrostatic and coordination interactions. The Fe-Cu dual sites bridged H_2O_2 adsorption through a Fe-O-O-Cu configuration, significantly lowering the adsorption energy barrier and accelerating its dissociation into $^{\bullet}OH$ and $^1O_2$. This synchronous adsorption-oxidation-regeneration system achieved over 99 % TC removal within 20 min across a wide pH range of 3-9, with 70.8 % lower energy consumption compared to the non-adsorption enriched system, demonstrating excellent catalytic activity and stability.

Du *et al.* [321] constructed a magnetic core-shell catalyst, denoted as HOF-on-Fe_3O_4/ZIF-67 (HFZ), by coating a hydrogen-bonded organic framework (HOF) shell on an Fe_3O_4/ZIF-67 core to improve recyclability and stability. The porous HOF shell reduced the diffusion distance between pollutants and active sites while also protecting the Co centers from leaching. The Fe_3O_4 core promoted electron transfer between Co ions, which facilitated the Co^{3+}/Co^{2+} redox cycle and thus enhanced the catalytic efficiency. Under neutral conditions, the HFZ/PMS system was able to completely degrade Rhodamine B (RhB) in 10 min. Notably, the catalyst had a strong activity at a wide pH range of 3 to 9 even after five cycles with Co leaching being very low at 0.14 mg/L. The catalysis of Fenton type was made efficient when it was accompanied by the continuous regeneration of active sites. The efficiency of the Fenton-like system was depended on the continuous regeneration of its catalytic active sites. Yang *et al.* [322] constructed a dual-cathode electro-Fenton system with a two-dimensional electroresponsive ferrocene-based MOF (ER-Fc-MOF) as the catalytic cathode (Fig. 10e). H_2O_2 could be continuously generated by the ER-Fc-MOF cathode in this system. Meanwhile, the Fe sites were present in the ER-Fc-MOF cathode to catalyze the activation of H_2O_2 for generating $^{\bullet}OH$ radicals as the main oxidizing agent. The ferrocene unit was present in a unique sandwich structure, which allowed cathode electrons to directly reduce Fe(III) to Fe(II). Such a process achieved electrically driven regeneration of the active sites and solved the slow cycling problem of traditional Fenton systems. EPR experiments confirmed the presence of the primary ROS of $^{\bullet}OH$ and $^1O_2$. The two species collaborated to degrade SMX at a rapid rate in pH 3.0 to 9.2. Importantly, the process did not produce Fe sludge. This system established a sustainable method for continuous electro-Fenton catalysis.

The combined action of radical and non-radical species occurs in many oxidant activation systems. Liu *et al.* [323] tested MIL-101(Fe), MIL-88B(Fe), MIL-88A(Fe), and MIL-53(Fe) four Fe-MOFs to activate periodate (PI) for TC degradation. Among these Fe-MOFs, MIL-101(Fe) proved to have the best activity for TC remediation due to the synergism of produced Fe(III)-superoxide and pore accessibility of MIL-101(Fe). The high-valent Fe-oxo species (Fe(IV)=O) together with $^{\bullet}OH$ and $O_2^{\bullet-}$ dominated TC decomposition with a removal of 93.3 % in 60 min in MIL-101(Fe)/PI system.

Overall, MOF-based Fenton-like catalysts show high efficiency and good stability under various conditions. Their structural tunability makes them promising materials for future catalytic applications.

12. Photocatalytic reduction of toxic high-valent metals by MOFs

Tao Xia, Jie Li*

Heavy metal pollution in water, including cationic species such as Hg^{2+}, Pb^{2+}, Cd^{2+}, and Cu^{2+}, as well as oxygen-containing anions like chromate/dichromate ($CrO_4^{2-}/Cr_2O_7^{2-}$), selenite/selenate (SeO_3^{2-}/SeO_4^{2-}), and arsenate ($HAsO_4^{2-}/AsO_4^{3-}$) represents a pervasive global challenge, attracting significant scientific and public attention [324]. Unlike organic pollutants, these heavy metal ions resist biodegradation into harmless substances. Consequently, they are readily absorbed by aquatic organisms, entering the food chain and accumulating in living tissues. This bioaccumulation poses severe toxic threats to ecosystems and ultimately threats human health. The variable and complex nature of real-world water systems further complicates remediation, making the effective purification of toxic metals a pressing yet difficult task.

A promising strategy for mitigating certain heavy metals leverages the principle that their toxicity is often valence-dependent. For instance, high-valence states are frequently highly toxic, while their low-valence counterparts may be less toxic or even non-toxic [325]. This creates an opportunity for detoxification through reduction. Photocatalytic technology is ideally suited for this purpose, as it harnesses light energy to drive chemical reactions that reduce pollutants. This process offers a green, efficient, and sustainable pathway for converting highly toxic high-valence metal ions into less harmful low-valence states.

MOFs have emerged as ideal candidate materials for this photocatalytic application. As a class of organic-inorganic hybrids, MOFs possess unique characteristics, including exceptional porosity, vast specific surface areas, and accessible open metal sites [8]. Their photoresponsive nature, capable of light absorption through both organic linkers and metal centers, makes them excellent photocatalysts [326]. Furthermore, their well-defined and tunable topologies promote the rapid transport and precise interaction of target molecules within their pores [327]. Given these advantages, MOFs demonstrate tremendous potential for the photocatalytic reduction of toxic high-valence metals [328–330], positioning them at the forefront of advanced water purification research.

12.1. Photocatalytic mechanism

A typical semiconductor photocatalyst, often an n-type material, possesses a characteristic electronic structure consisting of a valence band (VB), a conduction band (CB), and a band gap between them. The photocatalytic process is initiated when the material absorbs light with photon energy exceeding this band gap. This energy absorption prompts electrons (e^-) in the VB to become excited and jump to the CB, generating positively charged holes (h^+) in the VB and creating photogenerated electron-hole pairs [331]. Initially, these charge carriers are bound by Coulombic attraction [332]. However, under the influence of internal electric fields and diffusion gradients, they can separate and migrate to the catalyst's surface. On the surface, the holes act as powerful oxidants, typically reacting with surface-adsorbed OH^- ions or H_2O molecules to

produce highly reactive hydroxyl radicals (•OH). These radicals are capable of oxidatively degrading a wide range of organic pollutants. Concurrently, the electrons that reach the surface function as potent reductants. They are often captured by adsorbed oxygen (O_2), generating superoxide radicals ($O_2^{\bullet-}$) and other ROS that participate in various redox reactions, including the reduction of heavy metal ions. A competing and detrimental process is the recombination of electrons and holes, either within the material's bulk or on its surface. This recombination releases the absorbed energy as heat, significantly reducing the quantum efficiency of the photocatalytic reaction. Therefore, enhancing photocatalytic activity primarily relies on two key strategies: broadening the range of light absorption and, crucially, suppressing the rate of charge carrier recombination [282,333–335].

Theoretical studies classify MOFs as semiconducting materials with band gaps ranging from 1.0 eV to 5.5 eV [325]. Their crystalline, porous structure provides a high density of well-dispersed active sites that are readily accessible to reactant molecules through open channels. In many ways, the molecular building blocks of MOFs can be viewed as analogous to quantum dots or nanoscale semiconductors, each capable of absorbing light, generating charge carriers, and facilitating catalytic reactions. The organic linkers often serve as efficient "antennas," harvesting light across UV, visible, and even infrared spectra and transferring excitation energy to metal-based catalytic sites *via* a ligand-to-metal charge transfer process. The highly tunable nature of MOFs allows for strategic enhancement of their photocatalytic properties through chemical modification and the construction of composite materials. These strategies are designed to extend light absorption further into the visible spectrum and, more importantly, to minimize the recombination of photogenerated electrons and holes. In recent years, the application of MOFs and MOF-based composites for the photocatalytic reduction of toxic high-valence metals has gained considerable attention, with a particular research focus on remediating hexavalent chromium (Cr(VI)) in aqueous solutions. This section will therefore concentrate on reviewing progress in the MOF-based photocatalytic reduction of toxic high-valent metals over the past three years, using chromium as a primary case study. A summary of the recent research progress on MOF applications for photocatalytic Cr(VI) reduction is provided in Table S1 (Supporting information).

12.2. Photocatalytic reduction of toxic high-valent metals

The pioneering work by Shen and colleagues, who demonstrated the photocatalytic reduction of Cr(VI) to Cr(III) using ammine-functionalized UiO-66 [336], established a foundation for advanced MOF-based photocatalysis. Subsequent research has further validated the superior performance of functionalized MOFs for this application. For instance, Zhang *et al.* developed an anthracene-modified Zn-based MOF (DZU-64) that exhibited exceptional chemical stability across a broad pH range (2–14) and remarkable thermal stability up to 570 °C [337]. In the visible-light photoreduction of Cr(VI) at pH 2, DZU-64 achieved a record-high rate constant of 0.467 min^{-1} and a reduction capacity of 6.68 mg Cr(VI) $g^{-1}{}_{cata}$ min^{-1}. Under direct solar irradiation and with the co-addition of tartaric acid (TA), the material facilitated nearly 100 % reduction of Cr(VI) to Cr(III) within 35 min (Fig. 11a). In a separate study, Zhang's group enhanced the electron "push-pull" dynamics within an Fe-MOF by incorporating 2,5-bis(methylthio)terephthalic acid as an electron-donor and 2,4,6-tri(4-pyridyl)-1,3,5-triazine as an electron-acceptor [288]. The -SCH_3 groups improved light absorption and electron donation to the iron-oxo clusters, while the triazine ligand facilitated the separation and transfer of photogenerated charge carriers. This synergistic effect resulted in enhanced photocatalytic Cr(VI) reduction driven by photoelectrons and $O_2^{\bullet-}$ radicals, without requiring additional scavenging agents. More recently, Zhou *et al.* reported a novel bifunctional Dy-MOF based on a redox-active tetraphenylethylene ligand, capable of both electrochemical detection and visible-light photocatalytic removal of Cr(VI) [338]. The material demonstrated excellent sensing performance for trace Cr(VI), with high sensitivity (2.79 μA L $μmol^{-1}$), a low detection limit (11 nmol/L), and strong anti-interference ability and stability. Concurrently, it functioned as an efficient photocatalyst, achieving 99.1 % Cr(VI) removal within 40 min under visible light, which was attributed to an enhanced ligand-to-metal charge transfer (LMCT) process between the organic linker and the Dy-oxygen clusters.

To address the inherent limitations of MOF photocatalysts, such as their narrow light absorption range and the rapid recombination of photogenerated charge carriers, the construction of homojunctions and heterojunctions has emerged as a highly effective strategy [10]. For example, a Z-scheme DUT-67/Fe_2O_3 heterostructure was fabricated using a straightforward mechanical grinding method [339]. This composite exhibited an increased specific surface area, a broader light absorption range, and most importantly, significantly improved charge carrier separation. These advantages lead to a highly enhanced photocatalytic performance for Cr(VI) reduction, achieving 94 % efficiency within 40 min. This performance was 1.80 times and 5.53 times greater than that of pristine DUT-67 and Fe_2O_3, respectively. DFT calculations illustrated that the exposed Zr sites in DUT-67 showed strong Cr(VI) adsorption and reduction (Fig. 11b).

Practical application requires overcoming the challenges of using MOF powders, such as their tendency to agglomerate and the difficulty of separation and recovery. For this reason, the immobilization of MOFs on solid supports presents a viable solution. In a previous study, MIL-88A(Fe) was successfully anchored onto a polyurethane sponge (denoted as MS) *via* a dip-coating method [340]. The resulting composite could remove 100 % of Cr(VI) from a 10 mg/L solution at its native pH of 5.05, achieving this in just 6.0 min under UV light and 3.0 min under natural solar irradiation, with 0.4 mmol/L tartaric acid. The reduction was driven by photo-induced electrons and radical species ($O_2^{\bullet-}$ and $CO_2^{\bullet-}$). Critically, a fixed-bed experiment demonstrated the exceptional durability of this system, which maintained 100 % activity for over 60 h (Fig. 11c).

12.3. Simultaneous removal of toxic high-valent metals and organic pollutants

The frequent co-occurrence of toxic organic pollutants and heavy metal ions in industrial wastewater necessitates the development of multifunctional photocatalysts capable of their simultaneous removal. A representative study by Li *et al.* addressed this challenge by constructing an innovative plasmonic S-scheme heterojunction (Au/MIL-101(Fe)/BiOBr, denoted as AMB-2) *via* a facile solvothermal-photoreduction method [334]. The synergy between the S-scheme heterojunction and the plasmonic effect of Au nanoparticles significantly enhanced the photocatalytic performance through multiple mechanisms: It increased the number of active sites, broadened visible-light absorption, promoted the efficient separation and redistribution of powerful charge carriers, and elevated the generation of reactive species (Fig. 11d). Consequently, AMB-2 demonstrated durable and high-performance simultaneous removal of Cr(VI) and norfloxacin (NOR) under visible light, achieving removal rates up to 53.3 and 2 times higher than those of pure BiOBr, respectively. Notably, the Cr(VI) removal efficiency in a co-existing Cr(VI)-NOR system surpassed that in a Cr(VI)-only solution, indicating a synergistic utilization of photogenerated carri-

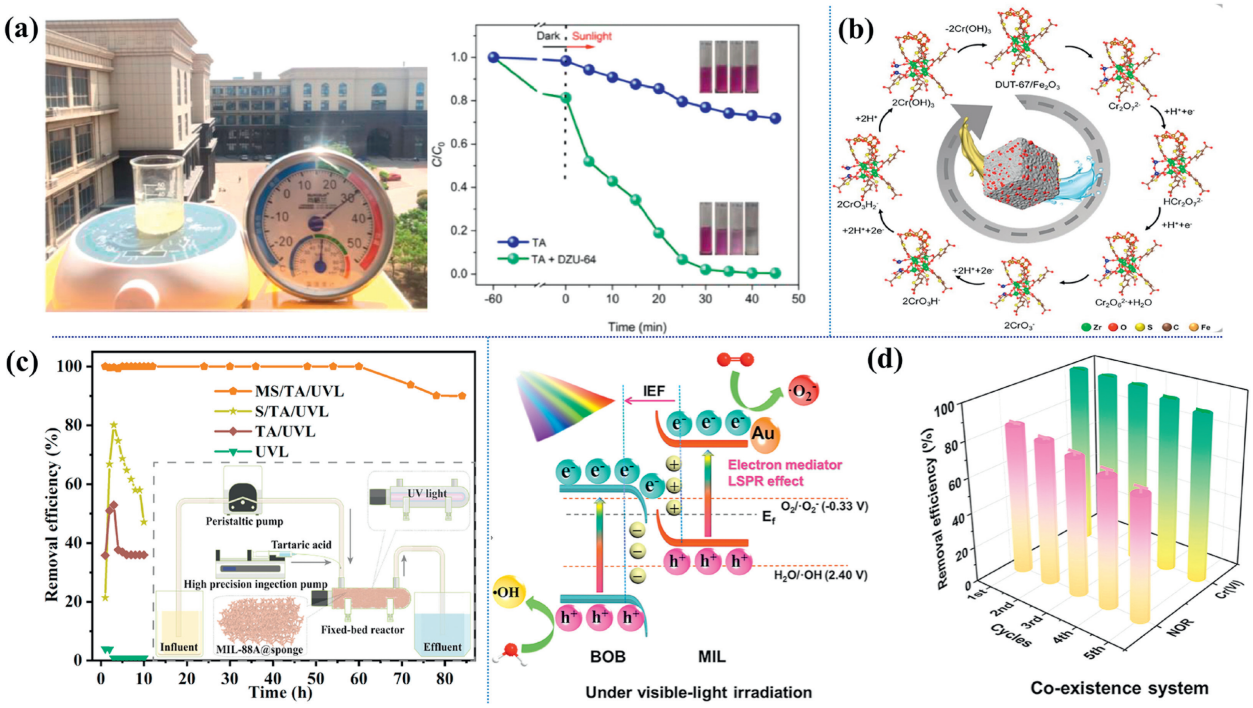


Fig. 11. (a) Cr(VI) photoreduction by DZU-64 under sunlight light conditions. Copied with permission [337]. Copyright 2024, Elsevier. (b) Optimized structural model of the Cr(VI) reduction intermediates. Copied with permission [339]. Copyright 2025, Elsevier. (c) Cr(VI) reduction efficiencies of different system under UV light irradiation during the long-term experiment. Copied with permission [340]. Copyright 2023, Elsevier. (d) Illustration of the S-scheme electron migration mechanism in the AMB-2 heterojunction and stability of AMB-2 when eliminating Cr(VI) and NOR simultaneously. Copied with permission [334]. Copyright 2024, Elsevier.

ers between the two pollutants and the catalyst. This collaborative removal phenomenon was also confirmed in a system containing Cr(VI) and enrofloxacin (ENR) using a MIL-101(Fe)/BiOBr S-scheme photocatalyst, where the MOF enhanced reactive sites and light harvesting while the S-scheme mechanism optimized charge separation and redox power [333]. Further advancing this field, Liu *et al.* grafted MIL-53(Fe) onto a modified $CoTiO_3/BiVO_4$ composite [341]. This configuration facilitated the smooth transfer of photogenerated electrons from $CoTiO_3$ to the $BiVO_4$/Fe-MOF interface. The resulting CT/BV@Fe-MOF composite exhibited remarkable simultaneous removal efficiencies, achieving 98.7 % reduction of Cr(VI) (50 ppm) and 97.5 % degradation of TC (30 ppm) within 90 min under visible light, primarily mediated by $^{\bullet}OH$ and $O_2^{\bullet-}$ radicals.

The development of "round-the-clock" photocatalysts that maintain activity in the dark is a highly sought-after goal, though often limited by short afterglow durations and charge recombination issues. A significant breakthrough was achieved by He *et al.*, who developed a composite by covalently coupling a long-persistent luminescent material ($Zn_3Ga_2Ge_2O_{10}$:0.5 %Mn) with NH_2−MIL-101(Fe) [342]. Leveraging an exceptionally long afterglow time of over 16 days from the phosphor, this composite sustained high photocatalytic activity for the removal of RhB and Cr(VI) for more than 12 h in complete darkness, paving the way for truly continuous water treatment systems.

In summary, MOF-based photocatalysts have proven highly effective for the photocatalytic reduction of Cr(VI), as detailed in Table S1. These materials outperform standard photocatalysts such as TiO_2, primarily due to their superior ability to harvest a wide range of UV–visible light, which is essential for visible-light-driven processes. The principal challenge impeding their large-scale application, however, lies in the regeneration and subsequent recovery of the powdery MOF composites from aqueous media after use.

13. MOFs for PFASs removal

Shaohua Guo, Ning Liu*

PFASs are a class of synthetic fluorinated organic compounds, which are widely used as firefighting foams, surface coatings and papers for food packaging *etc.*, and thus they gradually accumulate in the environment [343]. The highly stable C-F bonds in PFASs enabled them to possess strong environmental persistence, bioaccumulation capacity, high mobility and toxicity [344,345]. Researchers utilized MOFs as adsorbents or catalysts to remove PFASs from water environment.

13.1. Adsorption

MOFs show unique advantages in the field of PFASs adsorption, because of their precisely adjustable pore structures and abundant active sites [15]. The adsorption performance of MOFs for removing PFASs depends on the synergistic regulation of physical mechanisms such as hydrophobic interaction, electrostatic interaction and hydrogen bonding.

Hydrophobic interaction is the most fundamental mechanism for MOFs to capture PFASs, and it is especially crucial for the efficient adsorption of long-chain PFASs [346]. Yang *et al.* [347] studied the adsorption of perfluorooctanoic acid (PFOA) using Fe-BTC, MIL-100(Fe) and MIL-101(Fe) three Fe-MOFs. They identified a positive correlation between the surface hydrophobicity of Fe-MOFs and the carbon chain length of PFASs. They also found that the perfluoroalkyl chain of long-chain PFOA could closely attach to the surface of organic ligands in Fe-MOFs pores through hydrophobic interaction. Computational simulations further confirmed that the energy advantage of adsorption process was concentrated in the hydrophobic binding region between the PFASs alkyl chain and the ligand benzene ring. Among these Fe-MOFs, Fe-BTC had a higher density of hydrophobic sites, with an adsorption capac-

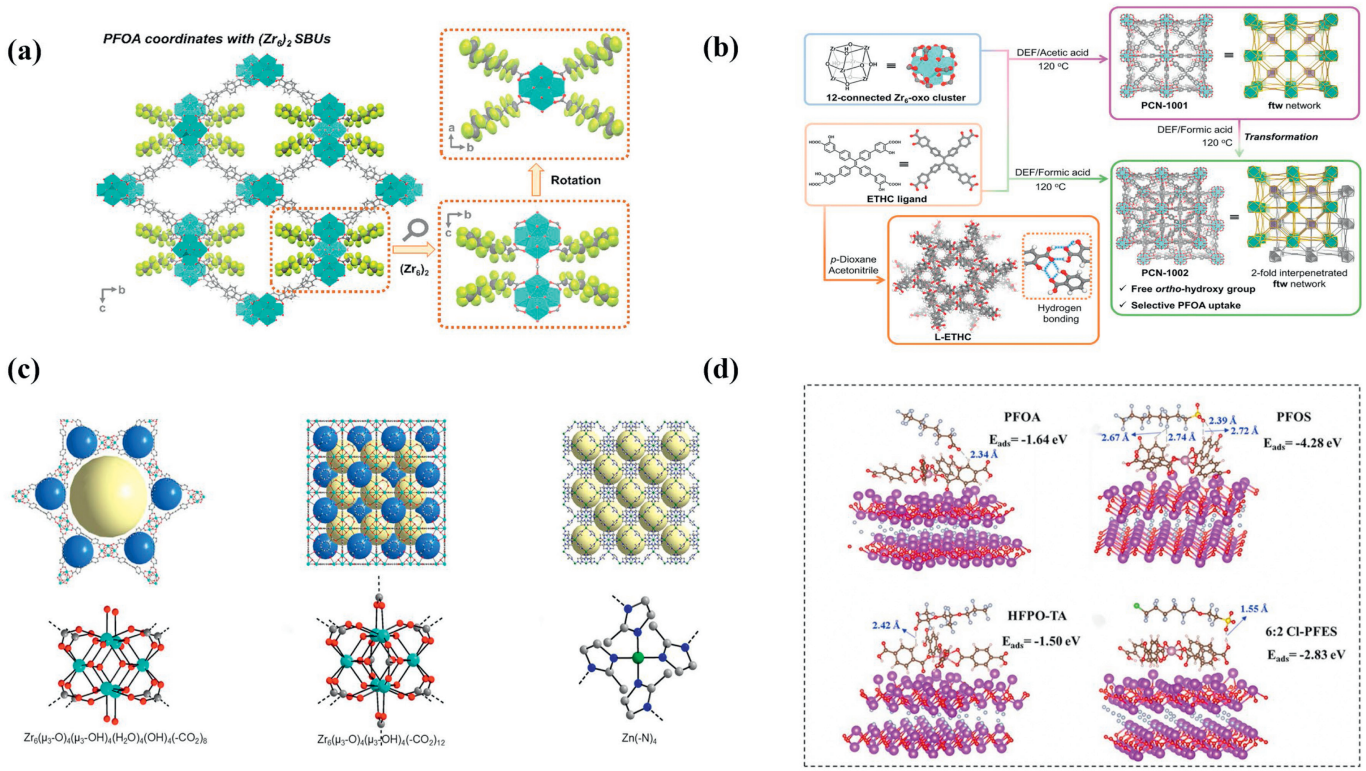


Fig. 12. (a) Structure of single-crystalline PFOA@PCN-999 showing the coordination of PFOA with the $(Zr_6)_2$ SBUs along the axis. C, H, O, F, and Zr atoms are represented in gray, white, red, green, and cyan, respectively. Copied with permission [348]. Copyright 2024, American Chemical Society. (b) Demonstration of the synthesis and crystal structures of L-ETHC, the noninterpenetrated PCN-1001, and the twofold interpenetrated PCN-1002. C, H, O, and Zr atoms are represented by grey, white, red, and cyan, respectively. Copied with permission [352]. Copyright 2024, Wiley-VCH. (c) Crystal structures of MOFs NU-1000, UiO-66, and ZIF-8. Copied with permission [356]. Copyright 2021, American Chemical Society. (d) DFT calculated adsorption energy of several pollutant molecules adsorbed on In-MOF/BiOF. Copied with permission [360]. Copyright 2021, Elsevier.

ity of 418 mg/g for removing PFOA. In addition to Fe-MOFs, Liang *et al.* [348] designed a hierarchical porous structure by constructing PCN-999, a novel Zr-MOFs *via* the ligand desymmetrization strategy to adsorb PFOA. PCN-999 provided sufficient hydrophobic binding spaces for PFOA, achieving a PFOA adsorption capacity of 1089 mg/g. Moreover, PCN-999 maintained stable binding ability even in complex water bodies containing interfering ions, such as Na^+, K^+, Ca^{2+}, Cl^-, NO_3^- and SO_4^{2-}, which further verified the prominent role of hydrophobic interaction for adsorbing PFOA (Fig. 12a). To achieve targeted optimization of hydrophobic interactions through microenvironment regulation, Zhang *et al.* [349] introduced trifluoromethyl groups into UiO-67 series MOFs (UiO-67, UiO-67-NH_2 and UiO-67-2CF_3) to enhance the hydrophobicity of their pores. Among them, UiO-67-2CF_3 showed the best ability. The equilibrium adsorption capacity of the UiO-67-2CF_3 for perfluorohexanoic acid (PFHxA) was enhanced from 987 mg/g to 1386 mg/g, which was significantly higher than that of UiO-67-NH_2, and the adsorption equilibrium time was shortened to 4 min. These results highlighted the dual improvement of hydrophobic interaction regulation on PFHxA adsorption kinetics and capacity.

Electrostatic interaction is another essential mechanism for enhancing the adsorption selectivity of MOFs towards PFASs. Zhao *et al.* [350] systematically investigated the effects of metal nodes and organic ligands of Zr-MOFs on the removal of perfluorooctane sulfonate (PFOS). They found that Zr_6 metal clusters in Zr-MOFs could bind to the sulfonate anions of PFOS through positive charge electrostatic attraction. In addition, amino modification of the ligands could further increase the surface positive charge density, leading to the PFOS adsorption capacity of 320 mg/g. This adsorption efficiency remained above 90 % even under interference from high concentrations of Cl^- and NO_3^-. Ilich *et al.* [351] focused on the removal of trace PFASs by adjusting the dosage of modifiers used in the synthesis of UiO-66, one of the Zr-MOFs. They adjusted the dosage of modifiers, which prevented the phthalic acid ligands from fully coordinating with the Zr(IV) oxo clusters, leading to the formation of "ligand-deficient defects" and Zr^{4+} sites became exposed and turned into positively charged defect sites. The positively charged defect sites introduced on the surface of UiO-66 that increased the adsorption selectivity of trace PFASs (10 ng/L) by nearly 3 times compared to pristine UiO-66. And it exhibited exceptionally fast adsorption kinetics. To address the shortcoming in long-chain PFASs adsorption, Luo *et al.* [138] adopted a structure-directed activation strategy. Oligoalkyl quaternary ammonium salt groups were brought into the pores of UiO-66-NH_2 to enhance surface positive charge, thus obtaining UiO-66-L_3. According to DFT calculations, the oligoalkyl segments induced electronic redistribution elevated the electrostatic potential at adjacent ammonium centers, enabling a selectivity dependent on chain length (2.3–4.9). Consequently, UiO-66-L_3 exhibited rapid kinetics (equilibrium within 5 min) and high adsorption capacities (403–1872 mg/g) towards long-chain PFASs such as PFOA, PFSA, and related derivatives.

Although the individual strength of hydrogen bonding is weak, its synergistic effect with other mechanisms has become a research focus [177]. Related researchers have developed the strategies from the verification of a single interaction to the design of multi-functional sites. Liang *et al.* [352] confirmed the synergistic effect of hydrogen bonding with the Lewis acid-base interaction. They synthesized Zr-MOFs with free ortho–hydroxy groups (PCN-1001, PCN-1002) by a solvothermal method. These MOFs achieved

efficient adsorption of PFOA through multiple hydrogen bonds between the free *ortho*–hydroxy groups, along with the Lewis acid-base interaction. Among them, PCN-1002 possessed a PFOA adsorption capacity of 632 mg/g, which was much higher than that of PCN-94 (no detectable PFOA uptake) without hydroxyl modification (Fig. 12b). In the study of PFOS adsorption by PCN-222 MOFs, Chang *et al.* [353] found that the amino groups of organic ligand could form stable bonds with the sulfonate groups of PFOS through hydrogen bonding. Combined with the large pore size (3.7 nm) of PCN-222, an extremely high adsorption capacity was achieved to be 2257 mg/g. Additionally, the capacity of PCN-222 to adsorb PFOS remained stable within the pH range of 2–10. Lukopoulos *et al.* [354] replaced the formate ligands on the Zr_6 clusters of MOF-808 using trifluoroacetic acid (TFA) and coordinated with their unsaturated sites to obtain TFA-MOF-808 through post-synthetic modification. After the functional modification, the adsorption capacity of TFA-MOF-808 for PFOA was 1341 mg/g, which was 36 % higher than that of the unmodified MOF-808. In the adsorption mechanism, the unsaturated Zr_6 nodes of MOF-808 formed coordinative bonds with PFOA molecules through ligand exchange. Additionally, the -OH and H_2O groups on these nodes engaged in hydrogen bonding with PFOA, which enhanced their binding ability. These hydrogen bonding interactions cooperated with the coordinative bonds to facilitate the adsorption process. Hydrogen bonds can also maintain the structural stability of MOFs to enhance removal of PFASs. Liang *et al.* [355] reported a pyrazolate MOFs PCN-1003, exhibiting an adsorption capacity up to 642 mg/g for PFOA and showing excellent stability in aqueous solutions over a wide pH range (1–12). The two-dimensional layers of PCN-1003 were stacked in a specific way through hydrogen bonding and other interactions to construct a stable lamellar structure and one-dimensional channels. These three aspects together supported its excellent PFOA adsorption capacity. Li *et al.* [356] selected three types of MOFs, NU-1000, UiO-66, and ZIF-8, and investigated the effects of MOFs structure, PFASs properties, and water matrix on the PFASs@MOF adsorption processes based on their distinct pore sizes and metal node characteristics. They found that for anionic PFASs, electrostatic and acid-base interactions played a key role in the PFOA adsorption. Long-chain PFASs were more easily adsorbed than short-chain PFASs, and the adsorption performance was significantly influenced by the nature of the terminal functional groups of PFASs (Fig. 12c). Koli *et al.* [357] fabricated a selective nanofiltration (NF) membrane *via* the integrating an aluminum-based MOFs (MOF 303) into a polyethersulfone (PES) support layer, denoted as PES-MOF 303-TFC, and was used to remove PFOS, PFOA, As(V), and Cr(VI) from water. The PES-MOF 303-TFC membrane displayed superior performance, achieving pure water permeance of 11.68 ± 1.34 LMH bar^{-1}, approximately 1.5 times higher than the pristine PES-TFC membrane. It also exhibited high removal efficiencies of 92 % for PFOA and PFOS in simulated groundwater system.

13.2. Catalytic degradation

MOFs can also be used as the catalysts to degrade PFASs in water environment, and the catalytic PFASs degradation over MOFs can be classified into photocatalysis, electrocatalysis, and photo-electro-Fenton synergistic catalysis [358]. Yan *et al.* [359] developed a Fe-BTC/BiOCl bifunctional Z-scheme heterojunction photocatalyst for PFOA decomposition. Fe-BTC/BiOCl displayed a three-dimensional nano-morphology, strong electronic interaction and staggered energy band characteristics, leading to the generation of a large number of oxygen vacancies and an efficient separation of photogenerated carriers. Under LED light irradiation, a PFOA degradation efficiency of 98.7 % was achieved within 30 min. Wen *et al.* [163] made an effort to extend the range of MOFs materials for PFASs degradation. They chose a titanium-based MOF (MIL-125-NH_2) as photocatalyst, and then examined the performance of this material in the photocatalytic degradation of PFOA. They found that MIL-125-NH_2 could degrade 98.9 % of PFOA and obtain a defluorination efficiency of 66.7 % within 24 h under Hg-lamp irradiation. Further analysis *via* DFT calculations revealed that there were two parallel pathways (chain-shortening and H/F exchange) in PFOA degradation process. The synergistic effect of hydrated electrons and hydroxyl radicals were crucial for the efficient progression of the chain-shortening pathway. MIL-125-NH_2 maintained good crystal structure and pore characteristics after multiple cyclic experiments, demonstrating excellent structural stability. To further optimize the charge separation efficiency of the photocatalytic system, Wang *et al.* [360] synthesized In-MOF/BiOF heterojunctions and improved the performance by adjusting the doping ratio of In-MOF and BiOF. Among the composites, the 20 % In-MOF/BiOF composite showed the best degradation performance for PFOA (15 mg/L) and could achieve complete degradation of PFOA under UV irradiation within 150 min. DFT calculations indicated that the built-in electric field formed at the interface between In-MOF and BiOF significantly promoted the separation of photogenerated charges. Additionally, the adsorption energy of PFOA on the catalyst surface was positively correlated with the degradation rate (Fig. 12d). The strong adsorption can effectively activate pollutant molecules, creating favorable conditions for subsequent catalytic reactions. This finding also provided a new perspective for the research on the "adsorption-degradation" synergistic mechanism in photocatalytic systems.

Besides photocatalysis, electrocatalytic degradation is also an important direction for MOF-based materials to treat PFASs. The electrocatalysts lie in regulating the generation of active species through MOF-modified electrodes. Zhang *et al.* [361] reported a promising catalyst ZIF-67 for electrochemical reductive degradation of PFASs. The ZIF-67 modification to form ZIF-67/C@CP strongly enhanced the adsorption of defluorination of 2-(trifluoromethyl)acrylic acid (TFMAA) on the surface of cathode, resulting in the TFMAA decomposition and defluorination rates of 99.66 % and 97.16 %, respectively, after 48 h treatment. Co-N_4 structure existed ZIF-67/C@CP induced the production of atomic H*, which improved the catalytic defluorination efficiency of TFMAA *via* indirect mechanisms, meanwhile the nitrogen loss because of carbonization further boosted the reductive defluorination.

Photo-electro-Fenton synergistic catalysis integrates the advantages of photocatalysis and electrocatalysis, becoming an emerging direction for MOF-based materials to treat PFASs. Wang *et al.* [22] proposed a solar photo-electro-Fenton system using Fe/Co bimetallic MOFs and carbon nanofibers membrane to prepare MOFs/CNF bifunctional catalytic cathode for PFOA remediation. The fabricated MOFs/CNF composites displayed both excellent photocatalytic and electrocatalytic abilities. H_2O_2 was generated through the two-electron pathway of oxygen reduction reaction (ORR) during the PFOA degradation, leading to 99 % of PFOA degradation and 91 % of TOC removal within 120 min. Wang *et al.* [362] constructed the CoFe alloy nanoparticles with oxygen defects (O*) MOFs on polyacrylonitrile (PAN)-driven carbon nanofiber (CNF) membrane to synthesize the bifunctional photocathode (CoFe-OVs@CNF) with both outstanding abilities of photocatalysis and electrocatalysis to degrade PFOA. When CoFe-OVs@CNF was used as the cathode, the removal efficiency of PFOA reached 95 % after 180 min under the optimal pH 3. Two years later, still the group of Wang [150] prepared a two-dimensional oxygen-vacancy-rich cobalt-iron@natural air diffusion electrode (2D CoFe-OVs@NADE) as photo-electrocatalysts. The abundant unsaturated coordination sites of 2D CoFe-OVs@NADE could accelerate mass transfer and charge transfer processes during the process of PFOA degradation. After 180 min of reaction, 2D CoFe-OVs@NADE realized a 93 %

PFOA degradation efficiency, with a corresponding first-order kinetic constant of 0.546 h^{-1}.

Both adsorption and catalytic degradation enabled the efficient removal of PFASs from aqueous environments *via* distinct mechanisms, thus significantly reducing the environmental accumulation of PFASs and their harmful impacts on living organisms. A fundamental distinction between the two approaches was that adsorption, as a physical process, failed to achieve the complete elimination of PFASs. In contrast, catalytic degradation disrupted the C-F chain structure through chemical pathways, converting PFASs into non-toxic small-molecule byproducts. Overall, these findings offered novel insights into the design of next-generation PFASs adsorbents and catalysts, presenting an effective tailoring strategy while providing unique mechanistic understanding.

14. MOFs for effective adsorption removal of micro/nano plastics

Xiaoning Wang, Chuanxi Yang*

The ubiquitous presence of microplastics (MPs, <5 mm) and nanoplastics (NPs, <1 μm) in aquatic environments, terrestrial ecosystems, and even biological matrices has emerged as a pressing global environmental concern over the past decade [363,364]. These anthropogenic particles originate from the fragmentation of post-consumer plastic wastes (polyethylene terephthalate (PET) bottles, polystyrene (PS) packaging, and polyvinylidene fluoride (PVDF) textiles) and the direct release of microbeads from personal care products [365,366]. Due to their small size, high surface area-to-volume ratio, and chemical stability, MPs/NPs can accumulate in the food chain *via* biomagnification, inducing oxidative stress, inflammatory responses, and neurological dysfunctions in aquatic organisms and humans [367]. Conventional removal technologies often suffer from low removal rate or selectivity, high energy consumption, or secondary pollution, limiting their practical applicability [368,369].

MOFs are a class of crystalline, porous materials composed of metal ions or clusters connected by organic linkers. They have garnered substantial attention for a wide range of applications spanning gas storage, molecular separation, catalysis, chemical sensing, and environmental remediation. Unlike traditional adsorbents, MOFs exhibit unique advantages, including ultrahigh specific surface area (SSA, up to 3000 m^2/g), tunable pore size (from micropores to mesopores), customizable surface chemistry, and excellent chemical stability [4,5]. These features enable MOFs to efficiently capture MPs/NPs through multiple interfacial interactions, while their structural flexibility allows for the design of functional composites (magnetic MOFs, MOF@polymer hybrids) to enhance separation efficiency and reusability [370,371]. Extensive studies have focused on developing MOF-based materials for MPs/NPs removal, covering various MOF types, adsorption mechanisms, and practical application scenarios. This chapter systematically reviews the classifications (pristine MOFs, functionalization MOFs and MOFs-based composites), interactions (hydrophobic interaction, electrostatic attraction, π–π stacking, hydrogen bonding and van der Waals forces) and challenges on MOFs adsorption removal of micro/nano plastics, as shown in Fig. 13.

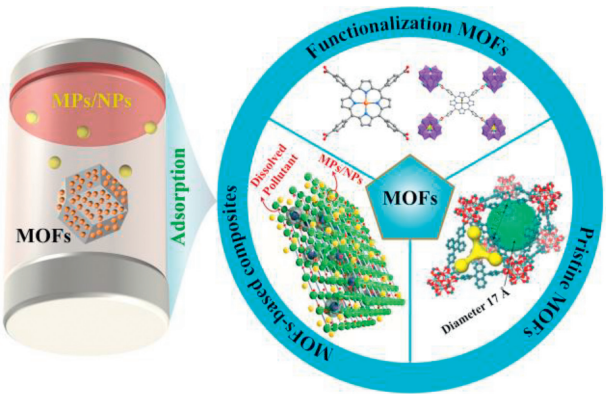


Fig. 13. MOFs for effective adsorption removal of micro/nano plastics.

14.1. Adsorption removal of micro/nano plastics with pristine MOFs

The adsorption performance of MOFs for MPs/NPs is determined by their structural characteristics (pore size, SSA) and surface properties (hydrophobicity, charge). Pristine MOFs refer to unmodified crystalline frameworks synthesized directly from metal ions and organic linkers. Their inherent porosity and surface chemistry make them effective for MPs/NPs adsorption, especially when the pore size matches the diameter of target particles. Representative pristine MOFs used for MPs/NPs removal include zeolitic imidazolate frameworks (ZIFs), Materials of Institut Lavoisier (MILs), and University of Oslo (UiO) series.

ZIFs, constructed from Zn^{2+}/Co^{2+} nodes and imidazole linkers, are among the most widely studied MOFs for MPs/NPs adsorption due to their high chemical stability and tunable hydrophobicity [372]. ZIF-8 (with a pore size of ~1.16 nm) exhibits a removal efficiency of 98 % for PS MPs (1100 nm) at a concentration of 25 mg/L within 5 min [16]. The high efficiency is attributed to the hydrophobic interaction between the aromatic imidazole linkers of ZIF-8 and the benzene rings of PS, as well as electrostatic attraction between the positively charged ZIF-8 surface (ζ-potential: +25 mV) and negatively charged PS MPs (ζ-potential: −30 mV). Similarly, ZIF-67 (Co-based ZIF) achieves a 92.1 % removal efficiency for PS MPs (1000–3000 nm) over a wide pH range (3–12), owing to its mesoporous structure (SSA: 1400 m^2/g) and π–π stacking between Co-imidazole complexes and PS [371].

MILs, typically composed of trivalent metal ions (Cr^{3+}, Fe^{3+}, Al^{3+}) and dicarboxylic acid linkers, are renowned for their high thermal stability and large pore volume, making them suitable for capturing larger MPs. MIL-101(Cr), with a SSA of 2900 m^2/g and mesoporous cages (2.9 nm), removes 96 % of PS NPs (65 nm) at a concentration of 10 ppm [7]. The adsorption process follows the Langmuir isotherm model, with a maximum adsorption capacity of 120 mg/g, which is 2–3 times higher than that of activated carbon (45 mg/g). The superior performance of MIL-101(Cr) is attributed to its hierarchical pore structure, which facilitates the diffusion of PS NPs into the framework, and the strong coordination between Cr^{3+} nodes and oxygen-containing groups on MPs surfaces.

UiO series MOFs (UiO-66(Zr), UiO-66(NH_2)) are another class of pristine MOFs widely used for MPs/NPs removal, thanks to their exceptional chemical stability and defect tolerance. UiO-66(Zr), synthesized from Zr^{4+} and terephthalic acid, exhibits a removal efficiency of 85.7 %–95.5 % for PS, PMMA (polymethyl methacrylate), and PVDF NPs (183–325 nm) [373]. The introduction of amino groups (UiO-66(NH_2)) further enhances the adsorption capacity by 15 %–20 % due to the formation of hydrogen bonds between -NH_2 groups and hydroxyl/carbonyl groups on MPs surfaces. Additionally, UiO-66(Zr) maintains 85 % of its initial adsorption efficiency after 5 cycles, demonstrating good reusability [374].

14.2. Adsorption removal of micro/nano plastics with functionalization MOFs

To address the limitations of pristine MOFs (poor dispersibility in aqueous solutions, low selectivity for specific MPs/NPs), functionalization strategies have been developed to modify their sur-

face properties. Common functionalization approaches include ligand modification, metal node doping, and defect engineering.

Ligand modification involves introducing functional groups (-OH, -COOH, -NH_2) onto the organic linkers of MOFs to enhance specific interactions with MPs/NPs. MIL-53(Al)-OH, a hydroxyl–functionalized MIL derivative, exhibits a 90 % removal efficiency for PVDF MPs (500 nm) at pH 7, which is 25 % higher than that of pristine MIL-53(Al) [375]. The -OH groups on the linker surface form hydrogen bonds with the -CF_2- units of PVDF (bond energy: 2.4 kJ/mol), strengthening the adsorption interaction. Similarly, UiO-66(COOH) modified with carboxylic acid groups shows a selective adsorption capacity of 98 mg/g for PS MPs (200 nm) in the presence of other pollutants (heavy metals, dyes), due to the electrostatic repulsion between -COOH groups and anionic pollutants [376].

Metal node doping involves substituting partial metal ions in MOFs with other transition metals to adjust the surface charge and catalytic activity. Ni-doped ZIF-8 (Ni/ZIF-8) with a Ni/Zn molar ratio of 1:3 exhibits a ζ-potential of +32 mV, which is 18 mV higher than that of pristine ZIF-8 (+14 mV) [377]. This enhanced positive charge significantly improves the electrostatic attraction between Ni/ZIF-8 and negatively charged PS NPs (ζ-potential: −28 mV), leading to a removal efficiency of 99 % within 10 min. Moreover, the doped Ni^{2+} ions can generate ROS under visible light, enabling the simultaneous adsorption and degradation of MPs (photocatalytic degradation efficiency: 85 % for PS MPs within 2 h).

Defect engineering creates intentional defects in MOF frameworks (missing linkers, unsaturated metal nodes) to increase the number of active sites. Defective UiO-66(Zr) prepared by reducing the linker/metal ratio from 2:1 to 1.5:1 exhibits a SSA of 1200 m^2/g, which is 30 % higher than that of defect-free UiO-66(Zr) (920 m^2/g) [378]. The unsaturated Zr^{4+} nodes in defective UiO-66(Zr) act as strong adsorption sites for PS MPs, achieving a maximum adsorption capacity of 150 mg/g with 40 % higher than that of the pristine counterpart. Additionally, the defects facilitate the diffusion of MPs into the framework, reducing the mass transfer resistance.

14.3. Adsorption removal of micro/nano plastics with MOFs-based composites

MOF-based composites integrate MOFs with other materials (polymers, carbon materials, magnetic nanoparticles) to combine their advantages, addressing the poor processability and separation difficulty of pristine MOFs. Common MOF composites for MPs/NPs removal include MOF@polymer hybrids, MOF@carbon composites, and magnetic MOFs [379].

MOF@polymer hybrids leverage the flexibility and mechanical stability of polymers to improve the practical applicability of MOFs. MOF@polydimethylsiloxane (PDMS) membranes fabricated by embedding UiO-66(Zr) into PDMS exhibit a high flux of 80 L m^{-2} h^{-1} and a rejection rate of 99.5 % for PS NPs (100 nm) [380]. The PDMS matrix enhances the membrane's flexibility and water permeability, while UiO-66(Zr) provides abundant adsorption sites. Similarly, MOF@polyacrylonitrile (PAN) nanofibers prepared by electrospinning show a removal efficiency of 98 % for PS MPs (500 nm) in simulated wastewater, with the nanofiber structure facilitating the dispersion of MOF particles and the capture of MPs [381].

MOF@carbon composites combine the high porosity of MOFs with the excellent conductivity and hydrophobicity of carbon materials (graphene, carbon nanotubes (CNTs)). MIL-101(Cr)@CNT composites with a CNT content of 10 wt % exhibit a SSA of 2800 m^2/g and a removal efficiency of 99 % for PS NPs (50 nm) [382]. The CNTs not only enhance the electron transfer capability of the composite but also form a 3D network that traps MPs, preventing their aggregation. Additionally, the hydrophobicity of CNTs strengthens the interaction with nonpolar MPs (PE, PP), further improving adsorption efficiency.

Magnetic MOFs (Fe_3O_4@MOF, $CoFe_2O_4$@MOF) enable rapid separation of MOFs from aqueous solutions using an external magnetic field, addressing the difficulty of recovering powdered MOFs. Fe_3O_4@ZIF-8 composites with a saturation magnetization of 45 emu/g can be completely separated within 30 s under a magnetic field of 0.5 T [383]. The composite exhibits a removal efficiency of 97 % for PS MPs (800 nm) and maintains 90 % efficiency after 6 cycles, with the Fe_3O_4 core facilitating recovery and the ZIF-8 shell providing adsorption sites. Similarly, $CoFe_2O_4$@MIL-53(Al) composites show a magnetic separation efficiency of 98 % and a MPs removal efficiency of 95 %, making them suitable for large-scale wastewater treatment.

14.4. Adsorption mechanisms of MOFs for removal of micro/nano plastics

The adsorption of MPs/NPs onto MOFs is a complex process governed by multiple interfacial interactions, which depend on the properties of MOFs (surface charge, hydrophobicity, pore size) and MPs/NPs (size, surface chemistry, ζ-potential). The main mechanisms include hydrophobic interaction, electrostatic attraction, π–π stacking, hydrogen bonding and Van der Waals forces.

Hydrophobic interaction is one of the dominant mechanisms for the adsorption of nonpolar MPs/NPs (PS, PE, PP) onto MOFs with hydrophobic surfaces. MOFs constructed from aromatic linkers (benzene dicarboxylic acid, imidazole) exhibit strong hydrophobicity with water contact angles (WCAs) >90° ZIF-8 with a WCA of 105° adsorbs PS MPs (WCA: 98°) through hydrophobic interaction, with the adsorption efficiency increasing from 60 % to 98 % as the WCA of MOFs increases from 80° to 110° [16]. The strength of hydrophobic interaction is influenced by the surface roughness of MOFs. MOFs with hierarchical micro/mesoporous structures (MIL-101(Cr), UiO-66(Zr)) exhibit higher surface roughness, increasing the contact area between MOFs and MPs/NPs. MIL-101(Cr) with a surface roughness of 25 nm shows a 30 % higher adsorption capacity for PS MPs than smooth MOFs (surface roughness: 5 nm) [7]. Additionally, the introduction of fluorinated linkers (tetrafluoroterephthalic acid) into MOFs enhances their hydrophobicity (WCA: 120°), further strengthening the hydrophobic interaction with fluorinated MPs (PVDF) [373].

Electrostatic attraction plays a crucial role in the adsorption of charged MPs/NPs onto MOFs with opposite surface charges. The surface charge of MOFs can be tuned by adjusting the metal nodes, linkers, or synthesis conditions. ZIF-67 with a positive ζ-potential (+28 mV) adsorbs negatively charged PS MPs (ζ-potential: −32 mV) through electrostatic attraction, achieving a removal efficiency of 92.1 % [371]. The adsorption capacity increases with the absolute value of the ζ-potential difference between MOFs and MPs/NPs; when the ζ-potential difference increases from 40 mV to 60 mV, the adsorption capacity of ZIF-67 for PS MPs increases from 80 mg/g to 120 mg/g. The pH of the solution significantly affects the surface charge of MOFs and MPs/NPs, thereby influencing electrostatic attraction. UiO-66(NH_2) exhibits a positive ζ-potential (+20 mV) at pH < 7 and a negative ζ-potential (−15 mV) at pH > 9 [376]. As a result, the adsorption efficiency of UiO-66(NH_2) for negatively charged PS MPs is 95 % at pH 5, but decreases to 40 % at pH 10 due to electrostatic repulsion.

π–π stacking occurs between the aromatic rings of MOF linkers (benzene, imidazole) and the conjugated structures of MPs/NPs (PS, polycarbonate (PC)). This interaction is particularly important for the adsorption of aromatic MPs/NPs onto MOFs with aromatic linkers. MIL-53(Al) constructed from benzene dicarboxylic acid linkers adsorbs PS MPs (containing benzene rings) through π–π stacking, with a binding energy of 3.5 kJ/mol [375]. The π–π

stacking strength increases with the number of aromatic rings in the linker; MOFs with naphthalene dicarboxylic acid linkers (MIL-101(Fe)-NDC) exhibit a 20 % higher adsorption capacity for PS MPs than those with benzene dicarboxylic acid linkers. The orientation of aromatic rings also affects $\pi-\pi$ stacking. MOFs with parallel aromatic rings (UiO-66(Zr)) exhibit stronger $\pi-\pi$ stacking with MPs/NPs than those with tilted rings (ZIF-8), as parallel rings maximize the overlap of π orbitals. UiO-66(Zr) shows a $\pi-\pi$ stacking energy of 4.2 kJ/mol for PS MPs, which is 1.2 kJ/mol higher than that of ZIF-8 [378].

Hydrogen bonding occurs between hydrogen atoms covalently bonded to electronegative atoms (O, N) in MOFs and electronegative atoms in MPs/NPs. MIL-53(Al)-NH_2 with -NH_2 groups forms hydrogen bonds with PVDF MPs (containing -CF_2- groups), with a bond energy of 2.8 kJ/mol [375]. This hydrogen bonding strengthens the adsorption interaction, increasing the removal efficiency of PVDF MPs by 25 % compared to pristine MIL-53(Al). The number of hydrogen bonding sites in MOFs affects the adsorption capacity. MOFs with multiple hydrogen bonding groups (UiO-66(COOH)$_2$ with two -COOH groups per linker) exhibit a higher adsorption capacity for PS MPs (containing -OH groups from oxidation) than those with single groups (UiO-66(COOH)) [376]. Additionally, the distance between hydrogen bonding sites in MOFs can be tuned to match the distance between polar groups in MPs/NPs, maximizing the number of hydrogen bonds. UiO-66(NH_2) with a linker spacing of 1.2 nm matches the spacing of -C=O groups in PC MPs (1.1 nm), forming multiple hydrogen bonds and achieving a high adsorption capacity of 110 mg/g.

Van der Waals forces, including London dispersion forces, dipole-dipole interactions, and dipole-induced dipole interactions, contribute to the adsorption of MPs/NPs onto MOFs. MOFs with high SSA (MIL-101(Cr), SSA: 2900 m^2/g) exhibit stronger London dispersion forces with MPs/NPs than those with low SSA (ZIF-67, SSA: 1400 m^2/g), leading to a 50 % higher adsorption capacity [7]. UiO-66(OH) with polar -OH groups (dipole moment: 1.8 D) adsorbs PVDF MPs with polar -CF_2- groups (dipole moment: 1.6 D) through dipole-dipole interactions, with a binding energy of 2.1 kJ/mol [373].

The structure-activity relationships of MOFs for adsorptive removal of MPs/NPs include size matching effect and interaction specificity. First, size matching effect between pore structures of MOFs and size of MPs/NPs is significant. NPs require mesoporous MOFs to achieve rapid diffusion and physical entrapment, however, MPs demand macroporous MOFs to reduce mass transfer resistance and avoid pore blockage. MOFs with high pore volume can provide more adsorption sites, but a balance between pore volume and structural stability must be maintained. Second, interaction specificity between active sites of MOFs and MPs/NPs is meaningful. The active sites of MOFs (metal nodes, ligand functional groups, defect sites) interact with the surface of MPs/NPs through specific forces, which is the key determinant of adsorption selectivity. Therefore, the design principles of MOFs for adsorptive removal of MPs/NPs are proposed. Precisely regulate pore sizes and hierarchical porous structures through ligand modification, post-synthetic etching, and template-assisted synthesis. Utilize pore engineering to address the issues of mass transfer resistance and pore blockage of MPs/NPs. Improve the selectivity for target MPs/NPs and reduce interference from complex wastewater matrices by means of ligand modification, metal node doping, and defect engineering.

14.5. Current challenges on MOFs adsorption removal of micro/nano plastics

Mass production and cost: Most MOFs are synthesized using expensive ligands (terephthalic acid, imidazole) and solvothermal methods, which are not suitable for large-scale production. For example, the cost of UiO-66(Zr) synthesized from $ZrCl_4$ and terephthalic acid is ~500 $/kg, which is much higher than that of activated carbon (~10 $/kg) [374].

Reusability and Stability: Although some MOFs exhibit good reusability in pure water, their stability and efficiency decrease in complex matrices (wastewater with high ionic strength, NOM). For example, ZIF-8 dissolves in acidic wastewater (pH < 4), and its adsorption efficiency for PS MPs decreases by 40 % after 3 cycles [16]. The adsorption of NOM onto MOFs blocks the pores, reducing the accessible active sites and adsorption capacity.

Biological safety: The potential toxicity of MOFs and MPs/MOF composites to aquatic organisms and humans is a major concern. For example, ZIF-8 nanoparticles can accumulate in the gills of fish, inducing oxidative stress and tissue damage [383]. Additionally, the release of metal ions (Zr^{4+}, Cr^{3+}) from MOFs in aqueous solutions can be toxic to microorganisms and aquatic life.

Selectivity: In complex aqueous matrices, MOFs may adsorption other pollutants (heavy metals, dyes) reducing their selectivity for MPs/NPs. UiO-66(NH_2) adsorbs Cu^{2+} (heavy metal) and PS MPs simultaneously, with the adsorption capacity for PS MPs decreasing by 30 % in the presence of 10 mg/L Cu^{2+} [376].

15. MOFs in membrane for water treatment

Yunlong Wang, Jiansheng Li*

Water scarcity and pollution present escalating threats to sustainable development worldwide. Membrane-based water purification has emerged as a promising alternative to conventional thermal and chemical processes, offering superior separation efficiency, modular operation, and reduced energy consumption [384,385]. Nevertheless, the inherent trade-off between permeability, selectivity, and stability in traditional polymeric and ceramic membranes limits their broader implementation [385]. MOFs—crystalline materials assembled from metal nodes and organic linkers—have attracted considerable attention due to their well-defined porosity, tunable pore chemistry, and exceptional surface areas, providing unprecedented opportunities for selective molecular transport [8]. These advantages have stimulated extensive research into MOF-based membranes for desalination, nanofiltration, and wastewater remediation [386]. The unique capability to tailor pore aperture, hydrophilicity, and functionality at the molecular scale distinguishes MOFs from conventional porous materials such as zeolites or activated carbons [8,9]. Recent advances have led to three primary MOF membrane architectures: (i) Continuous MOF layers acting as molecular-sieving barriers; (ii) mixed-matrix membranes (MMMs) incorporating MOF fillers within polymer matrices; and (iii) MOF-derived composite membranes obtained through controlled pyrolysis, offering integrated catalytic-degradation and separation capabilities [387–389]. Each configuration represents a distinct compromise between structural precision, manufacturability, and operational durability [8,388]. This review systematically compares these three membrane types, critically examining synthesis strategies, transport mechanisms, and performance, while identifying crucial challenges in transitioning MOF-based membranes from laboratory prototypes to real-world water treatment applications.

15.1. Polycrystalline MOF membranes

Polycrystalline MOF membranes, composed of densely packed crystalline grains with well-defined pore structures, have garnered considerable interest in water purification owing to their intrinsic porosity, tunable pore architectures, and versatile surface chemistry [390,391]. These membranes facilitate selective molecular transport through synergistic size exclusion and affinity-based interactions [8,392,393]. Among various fabrication approaches, the direct growth of MOF crystals onto porous supports has proven

particularly effective in producing continuous polycrystalline separation layers with minimal defects and strong substrate adhesion [394–396]. This method ensures structural integrity and interfacial continuity, providing a viable route to scalable and chemically robust membranes suitable for challenging aqueous environments [397–399].

The development of polycrystalline MOF membrane fabrication reflects a gradual deepening understanding of interface nucleation and crystal coordination dynamics [400]. Early studies reported *in-situ* solvothermal growth methods, where metal ions and organic linkers assemble together under hydrothermal/solvothermal conditions on porous supports to form continuous MOF thin films directly anchored to the support [392]. Although these pioneering *in-situ* studies established the feasibility of continuous, low-defect MOF layers, challenges remain in controlling crystal orientation, film thickness, and epitaxial growth, as heterogeneous nucleation on the support typically competes with homogeneous nucleation in the solution and is sensitive to additives, solvent composition and temperature [401]. Subsequently, seed-assisted (secondary) growth strategies were developed: A pre-deposited MOF seed layer (from nanoparticles or oriented seed films) provides dense nucleation sites during subsequent solvothermal steps, guiding epitaxial or overgrowth, significantly improving coverage and epitaxial growth while allowing better thickness control [402]. For zirconium-based MOFs, the *in-situ* solvothermal method has been demonstrated to produce highly oriented films when the additives and water content are carefully adjusted, indicating that even in the direct solvothermal growth route, the careful control of solution chemistry can enhance orientation and epitaxial growth [403].

Recent developments in polycrystalline MOF membrane growth have shifted towards the rational design of structurally robust and multifunctional architectures capable of stable operation under practical water treatment conditions. Liu *et al.* first reported high-water-stable UiO-66 membranes on alumina hollow fibers *via* an *in-situ* solvothermal process (Fig. 14a). These membranes achieved rejection rates of 86.3 % for Ca^{2+}, 98.0 % for Mg^{2+}, and 99.3 % for Al^{3+}, maintaining significant stability after 170 h of continuous desalination operation [399]. This study established zirconium-based frameworks as benchmarks for chemically and thermally durable MOF membranes in water purification. Building on this, interface hybridization strategies were developed to overcome the inherent rigidity and limited processability of pure MOF layers. Ma *et al.* embedded UiO-66@graphene oxide (GO) hybrid frameworks into polyethersulfone (PES) supports, resulting in a 351 % increase in water flux and enhanced anti-fouling performance compared to the original PES [404]. The MOF-2D heterogeneous interface promoted hydrophilic pathways and enhanced selective pollutant rejection through electrostatic interactions. Expanding this hierarchical interface synergy concept, Fang *et al.* electrostatically assembled MoS_2/UiO-66-NH_2 composites *via* layer-by-layer deposition, yielding a water permeability of 78.9 L m^{-2} h^{-1} bar^{-1} and >98 % antibiotic rejection, while maintaining structural integrity for over 72 h under acidic and alkaline conditions [405].

Collectively, these studies signify a paradigm shift in the design philosophy for MOF membranes. The focus has shifted beyond merely achieving crystalline continuity to the deliberate construction of multi-component, hierarchically structured hybrid membranes. The integration of molecular sieving, electrostatic selectivity, and catalytic activity within stable frameworks paves the way for tailoring membranes with multifunctionality for water treatment.

15.2. Mixed-matrix MOF membranes

Mixed-matrix membranes (MMMs) that incorporate MOF particles into polymer matrices aim to combine the processability and mechanical resilience of polymers with the tunable porosity and selective affinity of MOFs, thereby offering a practical route to improve permeability and target-specific rejection in water treatment [408–410]. Early *ex-situ* blending approaches, in which pre-synthesized MOF nanoparticles are dispersed in a polymer casting solution and then cast or phase-inverted into flat films or hollow fibers, have shown that modest MOF loadings (typically < 10 wt% in bulk MMMs and frequently ≪ 1 wt% in the selective layer) can increase water permeability and pollutant uptake while preserving mechanical integrity [411–413]. However, these studies also revealed recurring defects such as particle agglomeration, poor particle–polymer adhesion and interfacial "sieve-in-a-cage" voids

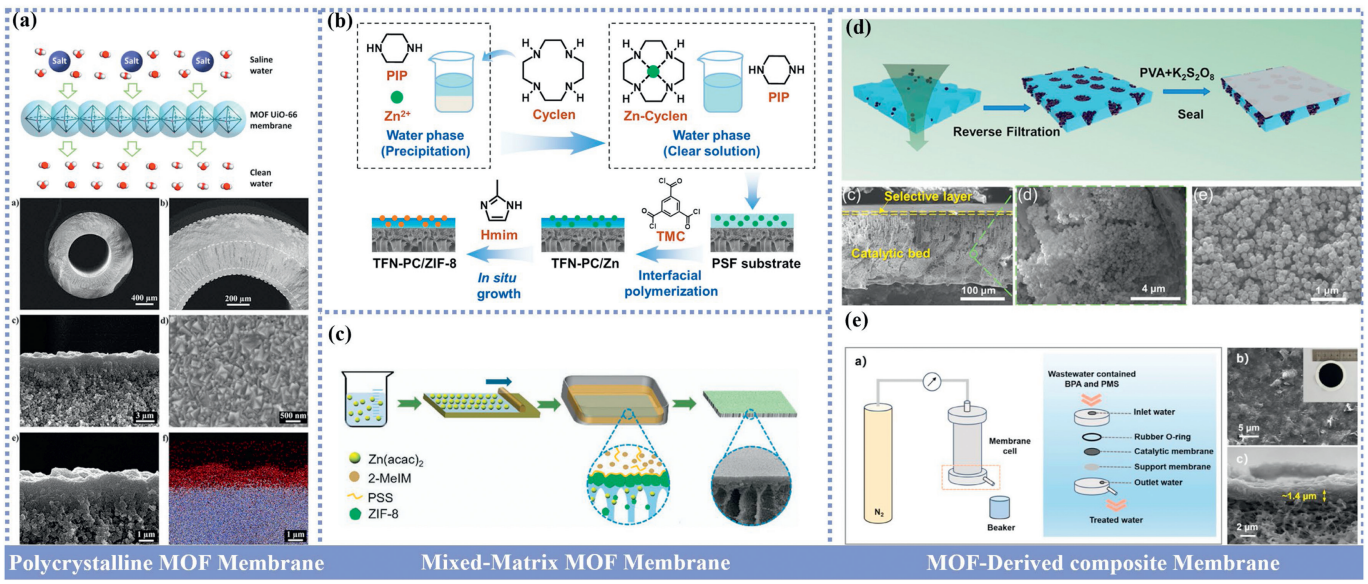


Fig. 14. (a) High water-stable UiO-66 membranes fabricated on alumina hollow fibers. Copied with permission [399]. Copyright 2015, American Chemical Society. (b) *In-situ* nucleation of ZIF-8 nanocrystals inside or on the surface of the polyamide layer. Copied with permission [406]. Copyright 2024, Elsevier. (c) The phase-transformation interfacial-growth (PTIG) method enables the synchronization of polymer phase inversion and MOF crystallization. Copied with permission [395]. Copyright 2021, Royal Society of Chemistry. (d) Preparation process of ordered structural separation catalytic membranes. Copied with permission [407]. Copyright 2021, American Chemical Society. (e) Membrane fabrication *via* coupling of MOF-derived carbon structures with two-dimensional materials. Copied with permission [314]. Copyright 2025, Wiley-VCH.

that create non-selective paths unless filler surface chemistry and particle size are precisely controlled [414–416]. These limitations have motivated a range of complementary strategies including surface functionalisation, compatibilisers, core–shell coatings and in-matrix crystallisation designed to improve interface integrity and preserve selective sieving ability [417–419].

The thin-film nanocomposite (TFN) architecture, in which MOF nanoparticles are introduced into the interfacial-polymerisation chemistry that forms the polyamide active layer, has become the most widely adopted route for desalination and nanofiltration applications because it locates the MOF domains directly at the mass-transfer interface [420,421]. TFNs generally deliver significant flux improvements at very low filler loadings while maintaining salt rejection, provided that nanoparticle hydrophilicity, surface functionality and particle size ($<$ 100–200 nm) are carefully optimised to avoid aggregation and interfacial voids [421–423]. Relevant studies show that hydrophilic or functionalised MOFs can enhance water permeance and fouling resistance *via* enhanced free volume and surface hydration, and that interfacial-polymerisation kinetics must be precisely tuned to minimise defect formation [424–426]. For example, Ni *et al.* introduced a macrocyclic polyamine (Cyclen) into the aqueous monomer phase during PIP/TMC interfacial polymerisation to coordinate Zn^{2+} and induce *in-situ* nucleation of ZIF-8 nanocrystals within or at the surface of the forming polyamide layer [406]. Cyclen acted both as a metal anchor and a nucleation modulator, generating a tightly integrated hybrid selective layer with improved hydrophilicity and polymer–MOF compatibility (Fig. 14b). The optimised TFN achieved a water permeance increase from 17.2 to 31.4 L m^{-2} h^{-1} bar^{-1} while maintaining Na_2SO_4 rejection above ~96%. Ni *et al.* also developed a phase-transformation interfacial-growth (PTIG) method, in which a metal precursor is doped into the polymer casting solution and the organic ligand is placed in the coagulation bath, thereby synchronising polymer phase inversion and MOF crystallisation in one step [395]. In this approach the substrate and the continuous MOF layer form concurrently, leading to a defect-free interface and an integrated polymer/MOF structure (Fig. 14c).

Defect engineering and tailored filler morphology offer additional viable pathways to improve TFN performance [425,427,428]. For instance, amino-functionalised UiO-66 with missing-linker defects improves pore accessibility and offers $–NH_2$ groups for chemical interaction with the polyamide network [427]. After incorporation of defect engineered D-UiO-66-NH_2 into the selective layer, the TFN-DUN membrane exhibited a water permeance of 20.2 L·m^{-2}·h^{-1}·bar^{-1} (48.5% higher than the pristine TFC membrane, 13.6 L·m^{-2}·h^{-1}·bar^{-1}) and an increased Na_2SO_4 rejection of 97.9% compared with 95.5% for the TFC membrane. Similarly, incorporating hydrophilic hollow ZIF-8 nanocubes into the polyamide layer created abundant –OH sites and hollow transport channels, yielding membranes with 19.4 ± 0.6 L m^{-2} h^{-1} bar^{-1} permeance and ~95.2 %± 1.4% Na_2SO_4 rejection [425].

Collectively, the growing body of experimental work establishes consistent design principles for achieving high-performance MOF-based selective layers: (i) Polymer-MOF interfaces must be tightly controlled through covalent grafting, coordination anchoring, or in-situ growth to eliminate nonselective voids; (ii) MOF selection and surface modification should prioritize hydrothermal stability and defect management (*e.g.*, Zr-based or surface-passivated azolate frameworks) to maintain selective sieving ability; (iii) interfacial polymerization kinetics should be finely tuned to control selective-layer morphology and avoid aggregation.

15.3. MOF-derived composite membranes

MOF are widely recognized as tunable precursors for porous carbons, whose inherited porosity, heteroatom doping, and metal species can be tailored to achieve combined adsorption, catalytic, and conductive properties [388,429,430]. Converting MOFs into carbon membranes allows these features to be integrated within a continuous structure, providing hybrid separation layers that couple molecular sieving, adsorption, and catalytic reactivity [313,431]. The advantages of MOF-derived composite membranes include: (i) Hierarchical porosity and large surface area for efficient adsorption and mass transfer; (ii) retention or transformation of metal centers as redox-active sites for catalytic or Fenton-like reactions; (iii) heteroatom doping (N, S, P) from organic linkers that enhances affinity toward polar pollutants; (iv) adjustable mechanical and structural stability when carbons are formed as coatings, fibrous mats, or free-standing layers [432–435].

The fabrication of MOF-derived composite membranes has evolved through several structural design strategies, each contributing distinct advantages to water purification applications [388]. Early studies mainly focused on direct carbonization of MOF-polymer or MOF-ceramic composites, in which MOF crystals were immobilized on porous supports and converted thermally into porous carbon frameworks while preserving the hierarchical morphology of the parent MOFs [436,437]. Such *in situ* carbonization enabled strong interfacial bonding and facilitated the retention of M–N–C active sites beneficial for redox reactions [438]. For instance, Xie *et al.* fabricated a ZIF-67-derived Co/N-doped carbon hollow fiber membrane through a one-step pyrolysis strategy, achieving efficient bisphenol A (BPA) degradation with a modified reaction rate constant of 1260 μmol L^{-1} g_{cat}^{-1} s^{-1} and nearly zero cobalt leaching during 24 h of continuous operation [439]. The hollow fiber architecture offered high permeability, confined reaction microchannels, and enhanced stability under flow-through conditions.

With the increasing complexity and diversification of water treatment demands, multifunctional integrated membranes have been developed with the goal of realizing pollutant separation and catalytic degradation simultaneously within a single membrane unit [440]. This strategy aims to overcome the mass-transfer limitations and secondary interference commonly encountered in suspended catalytic systems. In this context, Xie *et al.* proposed the concept of a sequential ultrafiltration-catalysis membrane (SUCM), marking a milestone in coupling selective filtration with catalytic oxidation in a continuous configuration [407]. In their design, Co_3O_4/C@SiO_2 yolk-shell nanoreactors derived from MOFs were immobilized within the finger-like channels of a polymeric ultrafiltration matrix, forming a hierarchically organized structure (Fig. 14d). The SUC membrane achieved 100% rejection of humic acid and 95% degradation of bisphenol A (BPA) at a flux of 229 L m^{-2} h^{-1} under 0.14 MPa, with degradation kinetics 21.9 times faster than those of conventional batch reactors. The rational spatial arrangement of the separation and catalytic domains effectively prevented natural-organic-matter interference and enhanced mass transfer, thereby establishing a multifunctional paradigm for MOF-derived catalytic membranes. Building upon the concept of sequential separation-catalysis integration, Yang *et al.* further advanced this strategy by employing electrospun MOF-derived carbon nanofibers as functional substrates [441]. They fabricated a sequential separation-catalysis membrane (SSCM) by coating a poly(ether sulfone) ultrafiltration layer on a ZIF-67-derived Co_3O_4/C nanofiber scaffold, achieving over 99% bisphenol A degradation with reaction kinetics nearly 20 times faster than conventional two-step processes. This design demonstrated that integrating MOF-derived carbon nanofibers with polymeric membranes can effectively enhance mass transfer and charge transport, extending the sequential-catalysis concept toward flexible and scalable architectures.

Integrating MOF-derived carbons with two-dimensional conductive materials provides a powerful route to enhance electron

transport, expose more accessible active sites, and achieve atomic-level control of catalytic centers [164,442,443]. Guo *et al.* exemplified this approach by confining asymmetrically coordinated Co single atoms and nanoclusters, derived from a ZnCo–ZIF precursor, onto holey MXene nanosheets to construct a CoSA–NC/H_{20}MX catalytic membrane (Fig. 14e) [314]. This hybrid membrane achieved complete bisphenol A removal in single-pass flow with a hydraulic retention time of only 40 ms. The combination of MOF-derived CoN_1O_2 sites and graphitized conductive layers on MXene promoted an efficient non-radical electron-transfer pathway, enabling ultrafast and stable pollutant degradation. This work highlights the advantages of coupling MOF-derived carbon architectures with two-dimensional materials, demonstrating how MOFs can serve as versatile precursors for constructing hierarchically organized and electronically integrated membranes for advanced water purification.

Collectively, recent studies on MOF-derived composite membranes suggest several general design considerations for achieving high-performance and multifunctional architectures. MOFs can be converted into continuous carbon frameworks with controllable porosity and partially inherited morphology, which may facilitate mass transport and improve mechanical stability. The retained M–N–C coordination structures and heteroatom doping, such as nitrogen, sulfur, or phosphorus, can create redox-active centers that enhance adsorption and catalytic activity. Moreover, integrating MOF-derived carbons with polymers, fibrous supports, or two-dimensional materials can improve interfacial compatibility, electronic conductivity, and structural robustness. Coupling these carbons with conductive substrates such as MXene or graphene also enables more precise control of coordination environments and may promote non-radical electron-transfer processes, resulting in efficient and stable pollutant removal. Overall, these insights highlight the versatility of MOFs as precursors for developing carbon-based membranes that gradually bridge structural hierarchy with catalytic and electronic functionality.

Based on a systematic analysis of three types of MOF membrane materials, this review highlights significant advances in MOF membrane technology across multiple dimensions, including molecular sieving, interface engineering, and catalytic functionalization. Although these membrane structures demonstrate exceptional water treatment potential at the laboratory scale, their path toward large-scale practical application still faces three major challenges: ensuring long-term hydrothermal stability and mechanical reliability, developing large-area and low-cost fabrication processes, and accurately predicting and assessing membrane performance and longevity in complex real-world water environments. Future research should focus on the following frontier directions: (1) Developing MOF materials resistant to harsh aqueous environments including acidic, alkaline, and high-salinity conditions; (2) advancing continuous and environmentally friendly fabrication processes; (3) constructing adaptive water-treatment-responsive MOF membranes. Although MOFs still face numerous technical and application challenges, ongoing technological developments continue to drive their commercialization forward.

16. Multi-path synergistic inhibition of algae: rational design and mechanism of MOFs

Qian Wen, Anping Wang*

Under the combined effect of global warming and eutrophication, the occurrence frequency and intensity of Cyanobacterial Blooms (cyanobacterial Harmful Algal Blooms, CyanoHABs) have significantly increased, and they have become an important global problem threatening the stability of freshwater ecosystems and the safety of drinking water [444–447]. Eutrophic lakes represented by Dianchi Lake in China have long been plagued by water blooms dominated by *Microcystis aeruginosa* [448–450]. Such algal blooms not only deplete the dissolved oxygen in the water body, but also the powerful liver toxins they release directly threaten the safety of drinking water and the health of the water ecosystem [451,452]. However, traditional algaecides have problems such as poor targeting, high required dosage and easy secondary pollution, and their limitations are particularly prominent when treating such complex water bodies [453–455]. Therefore, it is extremely urgent to develop efficient and environmentally friendly alternative technologies.

In recent years, MOFs have become a highly promising type of porous material in the field of environmental remediation. After layered materials such as Zn-Fe-LDH demonstrated potential in the field of photocatalytic algae suppression, MOFs, due to their tunable structure and abundant active sites, are regarded as algae control materials with more promising application prospects. MOFs can not only slowly release biologically toxic metal ions [456,457], inhibiting the growth of *Microcystis aeruginosa* from the source, but also generate multiple ROS *in situ* through an efficient photocatalytic process [458], non-selectively oxidizing and degrading algal cells and the Microcystins (MCs) they release, achieving more thorough control of algal blooms [459]. The outstanding performance of MOFs stems from the fact that it does not rely on a single algae inhibition mechanism, but rather achieves multi-pathway synergistic effects through precise design of components and structures [460–463].

This review summarizes recent advances in using MOFs to control *Microcystis aeruginosa*, emphasizing that their strong algal inhibition arises from multi-path synergistic mechanisms (Fig. 15). The high efficiency is attributed to rational design of metal centers, organic ligands, structural morphology, and stability, and is achieved through the spatio-temporal coordination of “adsorption-enrichment-attack” and the functional synergy of multiple active species. The article discusses key MOF design strategies and the internal logic of these mechanisms to support the targeted development of high-performance anti-algal materials.

16.1. Design and screening of MOFs materials

16.1.1. Selection of antibacterial/algaecidal metal centers

The primary design principle for selecting metal centers in MOFs is to endow the material with either inherent biocidal activity or specific catalytic functions. A common strategy is to introduce metal ions with definite biological toxicity, such as Ag^+ which can damage membrane structure and interfere with enzyme function [464], multivalent metals such as Cu^{2+}/Cu^+ or Fe^{2+}/Fe^{3+} are selected, and the core design intention is to introduce Fenton-like or photo-Fenton reaction active sites. These metal nodes not only promote the separation of photogenerated electron-holes under light, but also their valence state cycles can continuously catalyze the generation of ROS such as H_2O_2 or O_2 to $^{\bullet}OH$, thereby achieving an "in-built" catalytic function [465], and Zn^{2+} which can disrupt microbial metabolism [466]. Therefore, the selection of the metal center is essentially a pre-programming of the dominant attack mode (ionic toxicity *vs.* ROS oxidation). In design, single or dual/multi-metal centers can be adopted to achieve synergistic effects, expand the antibacterial spectrum, and reduce the dosage of single metals and potential toxicity. Among numerous MOFs, Cu-based and Ag-based materials have been widely reported to exhibit excellent algaecidal activity [467]. They can not only release metal ions to directly damage cell membranes, enzymes and proteins, but also form photoseparation interfaces with semiconductors or oxides, significantly enhancing the generation of ROS such as $^{\bullet}OH/O_2^{\bullet-}$ under light exposure. For instance, Wang *et al.* fabricated a floating photocatalyst by loading Bi_2O_3@Cu-MOF with melamine sponge, which exhibited an inhibition rate of ap-

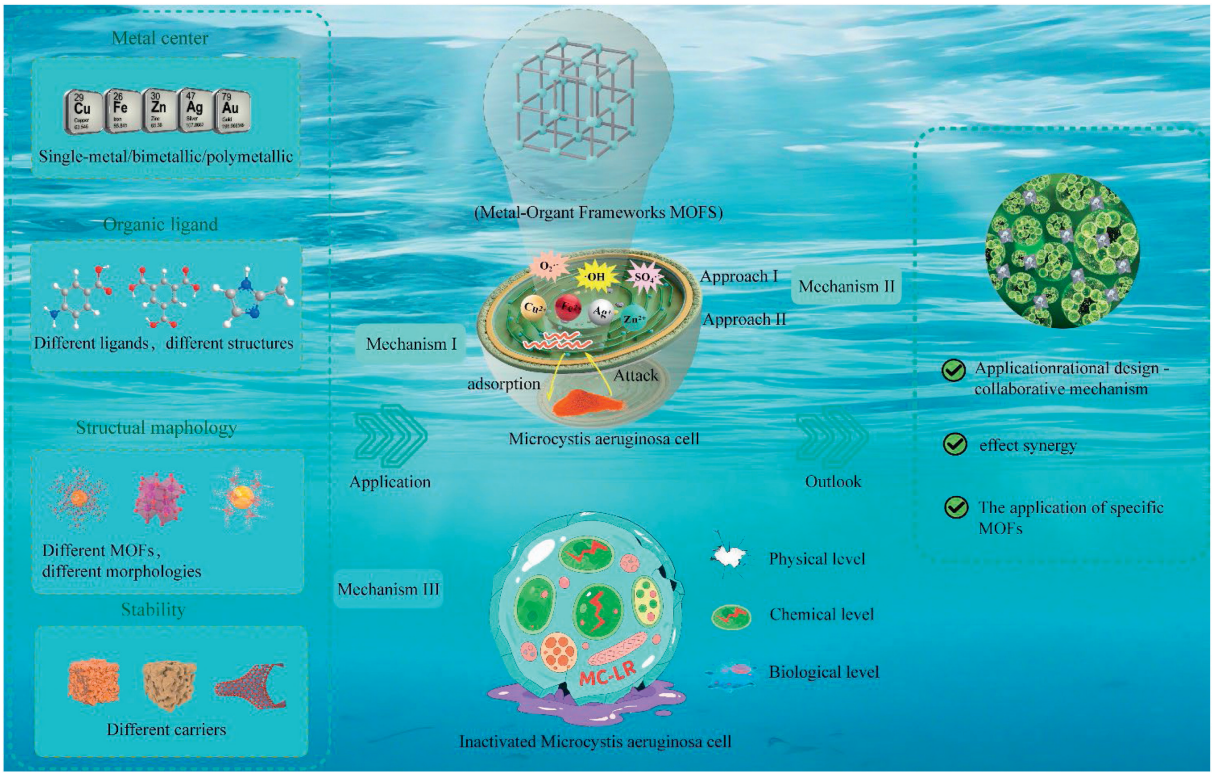


Fig. 15. MOFs for algae control.

proximately 74 % against *Microcystis aeruginosa* under visible light (120 h) [468]. Among them, $^{\bullet}OH$ and $O_2^{\bullet-}$ were the main active species, and the synergistic dissolution of Cu^{2+} played a key role. This design integrates continuous ion release and photocatalytic ROS generation, providing a typical example for the "joint attack of multiple active species" mechanism to be elaborated later. To more systematically compare the characteristics of different metal centers, Table S2 (Supporting information) sorts out the algaecidal advantages and limitations of common metal nodes in representative MOFs.

16.1.2. Functionalization of organic ligands

Organic ligands not only form the supporting framework of MOFs, but their functionalization is also the key to regulating the biological activity of materials. Some fractions themselves possess antibacterial properties, such as nitrogen-containing heterocycles or derivatives of natural products [469]. Ligand functionalization is a key strategy for regulating the algae-inhibiting performance of MOFs, and its design follows a clear structural-activity logic: (1) Enhance electrostatic adsorption with algal cells through charge regulation (such as introducing amino groups), and construct a tight interaction interface; (2) Specific recognition is achieved through affinity modification (such as molecular imprinting), elevating non-selective adsorption to targeted enrichment; (3) By means of photosensitization functions (such as introducing porphyrins), the light response is broadened and it directly participates in the photocatalytic process, converting ligands from structural units into active components. These strategies jointly achieve a collaborative design from interface construction, targeted recognition to photoactivity enhancement. Xiang *et al.* fabricated NH_2−MIL-101(Fe) into MOF@MIP and constructed μCPAD, achieving visual detection of GTX1/4 with a low detection limit, demonstrating the feasibility of the "recognition + catalysis/color development" composite function in practical applications [470]. The principle of high affinity recognition and signal amplification achieved by this strategy has laid a technical foundation for the development of "intelligent" algaecides that can specifically target and efficiently kill algal cells, to more systematically compare the characteristics of different ligands, Table S3 (Supporting information) sorts out the algaecidal advantages and limitations of common ligands in representative MOFs.

16.1.3. Structure and morphology regulation

The algaecidal efficacy of MOFs is closely related to its physical structural parameters, among which specific surface area and pore size play a decisive role [24]. The regulation of the structural morphology of MOFs follows the core principle of "maximizing interfacial mass transfer and exposure of active sites". Optimize the mass transfer pathway by constructing a high specific surface area to provide abundant active sites and precisely designing a multi-level pore system: Mesoporous pores (2–50 nm) mainly promote the enrichment of organic matter and toxins in algae and the diffusion of ROS, while macropores (>50 nm) and macroscopic structures provide spatial carriers for the attachment of algal cells. The two work together to lay the structural foundation for the "adsorption-enrichment – attack" process. For instance, studies have shown that Cu-MOF-74 with one-dimensional macropores can achieve efficient inhibition of *Microcystis aeruginosa* at extremely low concentrations (1 mg/L), and its performance is significantly superior to that of the traditional $CuSO_4$ solution [471]. Furthermore, by regulating the morphology of MOFs, such as nanoscale, two-dimensional lamination or hollow structure [472], the mass transfer efficiency in the interfacial reaction process can be further accelerated on the basis of their intrinsic high specific surface area, and more active sites can be exposed. In addition, moderate defect engineering, such as generating oxygen vacancies, has been proven to effectively regulate the electronic structure of MOFs [473], enhance the separation and migration ability of photogenerated carriers, and thereby increase their photocatalytic ROS production activity. To achieve the practical application of MOFs in

real water environments, integrating them with macroscopic carriers such as floating bodies [474], sponges [259] or fabric-based materials [475] is a crucial strategy. This strategy effectively resolves the engineering bottlenecks of nano-powder materials, such as easy sedimentation, difficult recovery, and insufficient utilization of incident light. For instance, Fan *et al.* developed a recyclable self-floating A-GUN photocatalytic foam that efficiently and stably inactivates *Microcystis aeruginosa* under visible light, providing a new approach for the management of cyanobacterian in water bodies [476].

16.1.4. Stability design

The design principle for MOFs' stability centers on achieving a balance between sustained algicidal efficacy and environmental safety. An unstable MOFs skeleton in water not only leads to a rapid decline in algaecidal activity due to the rapid hydrolysis of metal nodes and the shedding of organic ligands, but also may cause secondary pollution to aquatic ecosystems due to the sudden release of metal ions [477]. The research by Yue *et al.* profoundly revealed the complex correlations among stability, activity and safety [457]. They found that the degradation efficacy of Cu-MOFs on microcystins was significantly size-dependent: as the particle size of Cu-MOFs decreased, the specific surface area of Cu-MOFs increased and the short-term catalytic activity became higher. However, appropriately increasing the particle size helps maintain the structural integrity of the material during the long-term reaction process, thereby demonstrating better sustained algal resistance. This discovery emphasizes that the ideal design is to achieve the "slow release" of metal ions, which requires the MOF skeleton to have moderate dynamic stability in the water environment. To achieve this goal, the macroscopic carrier integration of MOFs has been proven to be an effective strategy for enhancing its application stability. For instance, Wang *et al.* immobilized Cu-MOF onto a SiO_2-TiO_2 composite carrier to construct a floating catalyst [478]. This strategy not only successfully retains the active octahedral structure of Cu-MOF, but also realizes the convenient recycling and reuse of the material, cutting off the environmental leakage risk that the nanomaterials themselves may bring from the engineering level.

However, high-level chemical and physical stability is not the entire connotation of environmental safety. Even for apparently stable MOFs, their interfacial interactions with algal cells may trigger unpredictable biological responses. Li *et al.* have pointed out that although the suspension of UiO-66-NH_2 at a concentration as low as 0.02 mg/L is structurally stable, it can stimulate *Microcystis aeruginosa* to produce and release more algal toxins [479]. This indicates that the assessment of the environmental safety of MOFs must go beyond the traditional category of leaching toxicity and extend to their deeper impact on the physiological behavior of aquatic organisms.

In conclusion, the stability design of MOFs algae-inhibiting materials is a multi-dimensional systematic project: It requires the materials themselves to have a stable framework to ensure long-term effectiveness; It is also necessary to prevent physical loss through engineering mounting. Ultimately, its environmental safety must be confirmed through a more comprehensive ecotoxicological assessment covering algal stress responses and more.

16.2. The algae inhibition mechanism of MOFs materials: multi-path synergistic effect

The inhibitory efficacy of MOFs materials against *Microcystis aeruginosa* is far from the simple addition of the activities of a single component [218]. The essence lies in achieving multi-dimensional coordination in space, time and function through meticulous material design, thereby constructing an efficient and hard-to-defend algae-inhibiting network. This section will analyze its working principle from the two core dimensions of "spatio-temporal synergy" and "functional synergy", and ultimately explain how they jointly lead to the collapse of the "effect synergy" of algal cells.

16.2.1. Spatio-temporal synergy: "Adsorption-enrichment-attack" synergy

The core of this mechanism is to solve the problem of "how to efficiently deliver attack forces to the target position", which is a highly optimized process in space. MOFs has constructed a localized "high-efficiency reaction zone" at the algae-material interface through a series of cascade reactions, achieving a transformation from wide-area pressure application to targeted removal [477].

16.2.1.1. Targeted adsorption and interface construction. The surface of *Microcystis aeruginosa* is usually negatively charged in natural water bodies, while many algaecidal MOFs have a positively charged surface at near-neutral pH [477]. This electrical difference forms a strong electrostatic driving force. Meanwhile, the porous polymer network of alginate sheaths provides physical anchor points for MOFs particles or the components they release, achieving targeted and tight adsorption of algal cells and laying a spatial foundation for subsequent reactions.

16.2.1.2. Specific enrichment in the interface microregion. In the successfully constructed interface microregion, a crucial dual enrichment occurs: (i) Local concentration of metal ions: The metal ions released by MOFs are confined in the limited space between the alginate sheath and the cell wall [480], forming a local high concentration area far exceeding the volume phase concentration, effectively overcoming the diffusion barrier of the alginate sheath; (ii) Enrichment of algal substances: The organic matter and algal toxins produced by the metabolism of *Microcystis aeruginosa* are selectively adsorbed by the MOFs channels [481]. This not only alters the interfacial microenvironment but may also regulate the reaction pathways and efficiency of subsequent attack processes.

16.2.1.3. Multipath cooperative attack and algal disintegration. Based on the above enrichment effect, all attacking behaviors are confined to the surface and periphery of the algal cells to the greatest extent, achieving maximum efficiency: (i) Targeting the photosynthetic system: The *in-situ* generated ROS penetrate the alginate sheath, preferentially destroying the algal bile body and photosystem II, causing degradation of characteristic pigments and a significant reduction in photosynthetic efficiency [482], thereby inhibiting the activity of algal cells at energy source. (ii) Synergistic disruption of cell structure: Local high concentrations of metal ions and ROS jointly induce membrane lipid peroxidation, synergistically destroying the integrity of the cell membrane. Electron microscopy observation can clearly show the cell wall rupture and contents leakage caused by this synergistic effect [483].

16.2.2. Functional synergy: "Joint attack by multiple active species" synergy

The core of this mechanism is to address the issue of "what weapons to use and how to combine attacks", emphasizing the coordination of different algae-inhibiting components in terms of time and function, and forming a three-dimensional attack mode.

16.2.2.1. The sources of diversity for active species. MOFs can simultaneously provide two attack units with distinct natures but complementary functions: (i) Continuous chemical stressors (metal

ions) [483,484]: Slow dissolution from skeleton nodes, by destroying membrane structures, replacing essential elements and inhibiting enzyme activity, constitutes a continuous background toxicity, effectively weakening the defense and repair capabilities of algal cells. (ii) Explosive physicochemical attacks ROS: Mainly generated *in situ* through photocatalytic [482] and enzyme-like catalytic pathways [485], including $^{\bullet}OH$, $O_2^{\bullet-}$. These ROS have extremely high reactivity and can cause indiscriminate and rapid oxidative damage to cell structures.

16.2.2.2. The mechanism and effects of collaborative attacks. Multiple active species form multi-dimensional synergistic effects in terms of time, space and function, jointly promoting the collapse of *Microcystis aeruginosa*. (i) Connection and complementarity in the time dimension: The continuous release of metal ions constitutes "background toxicity", while photocatalytic ROS show light-dependent pulse-like bursts. The combination of the two forms continuous stress. Under dark conditions, enzyme-like catalysis and ionic toxicity can make up for the limitations of photocatalysis. (ii) Internal and external attacks in the spatial dimension: Metal ions preferentially damage the integrity of the cell membrane [457], creating conditions for ROS to enter the cell, and then attack internal targets such as chloroplasts, photosynthetic centers, and genetic material, achieving systematic damage from the surface to the inside. (iii) Cascade amplification in the functional dimension: Metal ions promote the generation of $^{\bullet}OH$ through Fenton-like reactions, membrane damage caused by ROS accelerates ion influx, and the inhibition of antioxidant enzymes such as SOD and CAT by ions further intensifies the accumulation of ROS, forming a cascade amplification effect [468].

16.2.3. The ultimate manifestation of synergy: from physical and chemical destruction to biological functional inactivation

The aforementioned "spatio-temporal synergy" and "functional synergy" do not operate in isolation. They jointly act on algal cells, triggering an irreversible step-by-step destruction chain from physical structure to biological function, which is known as "effect synergy". This mechanism describes the ultimate biological consequences of multi-dimensional collaborative attacks. (i) Physical aspect: The adsorption and shielding effect of MOFs, as well as their direct damage to the cell membrane structure, constitute the initial physical stress. (ii) Chemical level: The synergistic attack of metal ions and ROS has triggered extensive lipid peroxidation, protein denaturation and nucleic acid damage, completely undermining the physicochemical basis for the normal operation of cells. (iii) Biological level: The accumulation of the above-mentioned physical and chemical damages ultimately manifests as irreversible damage to the photosystem II, inactivation of key metabolic enzymes, and disruption of genetic material, leading to the cessation of photosynthesis and paralysis of metabolic functions in algal cells, and ultimately resulting in programmed death or lysis.

As shown in Table S4 (Supporting information), MOFs composed of different metal centers and organic ligands, although they have different focuses in specific synergistic pathways, all follow the core logic of this multi-dimensional synergy, thereby demonstrating algal inhibition efficiency far exceeding that of traditional reagents.

This section establishes a "rational design-collaborative mechanism" framework, revealing that MOFs suppress *Microcystis aeruginosa* efficiently through a customizable multi-dimensional attack network in time, space, and function.

(i) Designable components and structures form the foundation of synergistic algal inhibition. By selecting active metal centers, functional organic ligands, and tuning surface area, pore size, morphology, and macroscopic structure, the photocatalytic activity of MOFs, interfacial behavior, and stability can be precisely optimized, pre-setting the program for efficient algal suppression.

(ii) The multi-dimensional collaborative mechanism is central to the efficient algal inhibition of MOFs. Through spatio-temporal coordination, MOFs form a localized reaction zone at the algae-material interface *via* continuous adsorption, enrichment and attack, while functional synergy enables metal ions and reactive oxygen species to conduct a coordinated three-dimensional assault. These coupled actions generate an irreversible damage chain from physical and chemical disruption to biological inactivation, ultimately causing algal cell collapse. Overall, MOFs represent a shift from traditional "toxic killing" to "intelligent coordinated inhibition," offering a new material platform and theoretical framework for controlling harmful algal blooms.

Based on the above aspects, we offer the following applicability suggestions:

(i) In terms of environmental compatibility and long-term safety, current studies focus mainly on short-term algal inhibition. Future research should move beyond traditional assessments of metal ion leaching toxicity and consider deeper biological stress responses caused by material-algae interactions, such as abnormal toxin release and altered quorum sensing. This will help build a more systematic and comprehensive ecotoxicological evaluation system.

(ii) Materials engineering for practical applications: Develop cost-effective, green large-scale synthesis methods. Optimize macroscopic carrier integration, design immobilized/recyclable devices suitable for various water environments, and address long-term material stability, antibiofouling, and recyclability.

Improving intelligent response and precise targeting: Based on the "adsorption-enrichment-attack" mechanism, design "intelligent" MOFs that selectively recognize *Microcystis aeruginosa* surface polysaccharides or algal toxins, activating algal inhibition only in the presence of target algae to achieve precise targeting and protect aquatic ecosystems.

17. Water capture in MOFs

Ge Shen, Chong-Chen Wang*

Water vapor is present in various industrial and domestic environments. such as drinking water, food preparation, indoor air conditioning and refrigeration, heat pump heating, and agricultural irrigation. In selective adsorption separation and purification systems, the adsorption and desorption processes of water vapor on specific adsorbents, along with their associated thermal effects, have increasingly been applied to atmospheric water harvesting, indoor humidity control, natural gas drying, and thermal conversion. Early adsorbents relied on natural mineral materials like zeolites and silica gels, yet these were constrained by limited adsorption capacity and regeneration performance [486]. Consequently, researchers have shifted their focus to MOFs, which is rich in water-absorbing active sites and possess highly tunable channels facilitating efficient diffusion pathways for the adsorption and desorption of water molecules [8,112]. More importantly, some MOFs display a characteristic steep rise in water uptake near specific relative vapor pressures, indicating that even slight variations in external pressure or temperature can trigger water absorption or release [9]. This distinctive feature allows MOFs to achieve high adsorption capacities surpassing those of conventional adsorbents. This review presents the mechanisms of water adsorption in MOFs, their stability in aqueous environments, strategies to enhance water uptake capacity through reticular chemistry, and demonstrates

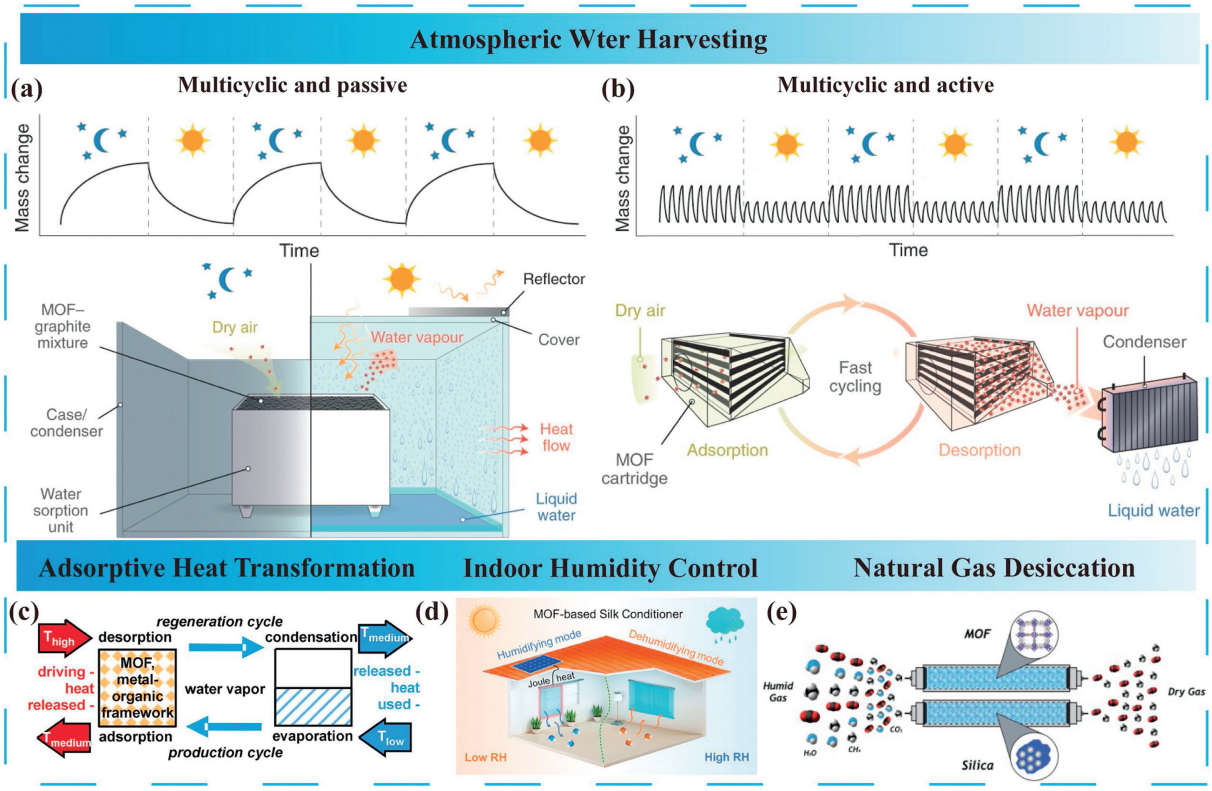


Fig. 16. Application and performance of MOFs for Water Capture. Juxtaposition of two classes of practical MOF water harvesters. (a) A passive, monocyclic (left column). Copied with permission [510], Copyright 2018, American Association for the Advancement of Science. (b) An active, multicyclic (right column). Copied with permission [517], Copyright 2019, American Chemical Society. (c) Principal process in an adsorption of chiller. Copied with permission [526], Copyright 2009, American Chemical Society. (d) Scheme showing the application scenario of MOF/wood composite in passive humidity regulation. Copied with permission [527], Copyright 2024, American Chemical Society. (e) Using MOFs to Dry Natural Gas. Copied with permission [532], Copyright 2021, Elsevier.

their application potential in processes such as water adsorption and desorption (Fig. 16).

17.1. Underlying mechanisms of water capture in MOFs

The adsorption mechanisms of water vapor in MOFs are generally categorized into three types: (1) Chemisorption on open metal sites (OMS) [4,487], (2) water cluster (reversible) formation [488], and (3) capillary condensation [489]. The adsorption of water at OMS of MOFs was accompanied by changes in metal coordination number and/or structural deformation [490]. Water molecules can form strong coordinative bonds with the open metal sites (OMS) through chemisorption, where the water molecules act as a Lewis base and the OMS act as Lewis acids. This mechanism ensured efficient water uptake even in low-humidity environments [491]. Additionally, the formation of water cluster was another key mechanism responsible for the ultrahigh water adsorption capacity in MOFs [403]. As subsequent water molecules diffused into the pores, they preferentially formed hydrogen bonds with the primary water molecules at the OMS [492]. A single water molecule can act as both a donor and an acceptor. This dual role allows it to connect to multiple neighbors, thereby enabling cooperative adsorption and cluster growth [4]. Capillary condensation directly governed the water storage capacity of MOFs in an irreversible way. The formation of a concave meniscus by water clusters in the pores made evaporation more difficult due to the Kelvin effect, thereby causing internal water vapor to condense at a lower pressure [493]. Consequently, the pores were rapidly filled with liquid water, achieving a significant leap in adsorption capacity. The reversibility expressed here is defined by thermodynamics and does not represent the material's stability. This study will discuss the factors affecting the stability of MOFs and methods to enhance their structural stability.

17.2. Stability and design of MOFs for water capture

The water stability of MOFs directly impacts every aspect of their practical applications. MOFs primarily undergo degradation through hydrolysis or ligand displacement [494]. Hydrolysis directly attacks and disrupts metal coordination bonds *via* water molecules. This process yields protonated free ligands and hydroxylated metal nodes [495]. To shield against the hydrolysis effect, researchers employed high-valent metal ions such as Ti^{4+}, Zr^{4+}, and Hf^{4+} (found in UiO-66, MOF-801 [496], or DUT-67 [497]) to synthesize MOFs. This is because high-valent metal ions possess more densely packed coordination spheres. The displacement involved the coordination of water molecules as competitive ligands to the metal nodes. Ultimately, the MOFs lose their complete crystal structure, and their permanent pores collapse. From a thermodynamic perspective, the strength of the metal-ligand bond is the decisive factor in the stability of MOFs.

Therefore, according to the HSAB principle, high-valent metal ions (hard Lewis acids) formed stronger, more break-resistant coordination bonds with carboxylate ligands (hard Lewis bases). Additionally, increasing steric hindrance and providing an additional protective layer of metal ions effectively prevent water molecules from approaching the MOF structure.

The existence of reticular chemistry enables the rational design and assembly of MOFs with significant potential, allowing for the precise design and control of pore size, surface area, and hydrophilicity/hydrophobicity [498]. In this approach, a Zr_6 cluster with multifunctional connectivity serves as the central hub, enabling the construction of diverse stable structures through the uti-

lization of multiple carboxylic acid linkers [499]. Meanwhile, Yaghi and his colleagues pioneered a suitable linker extension strategy by attaching a single vinyl group to the $PZDC^{2-}$ linker (MOF-LA2–1), which achieved a water absorption capacity 1.5 times higher than that of MOF-303 [500]. However, various strategies exist to influence MOF stability. These include employing high-valent metal centers based on the HSAB principle, along with ligand functionalization or linker extension *via* reticular chemistry, and they do not act in isolation. Therefore, the enhancement of MOF stability should be multidimensional.

17.3. Application and performance of MOFs for water capture

The water capture capacity of MOFs is more determined by the shape of the water adsorption isotherm and the material's sorption capacity. According to the standards of the International Union of Pure and Applied Chemistry (IUPAC), water adsorption isotherms were categorized into seven types [501]. In Types I, II, IV, and VI, the water uptake of MOFs increased sharply even at relatively low relative pressures. This is essential for atmospheric water harvesting, which requires high reversible water absorption between 10 % and 30 % relative humidity (RH) [502]. However, the opposite results in Types III, V, and VII suggested that the MOFs possessed moderately hydrophobic pores. Beyond the isotherm shape, the position of their inflection points (α) could also reveal the most suitable practical water absorption applications for MOFs. An extremely low inflection point ($\alpha < 0.05$) indicates a strong interaction between water molecules and the MOF framework. This enables the removal of water molecules over other substances like CO_2 and CH_4, making it suitable for natural gas dehydration [503]. A knee point located in the range of $0.1 < P/P_0 < 0.3$ represents easy desorption characteristics and a suitable relative pressure range, which makes it more applicable for uses such as heat pumps/refrigerators and atmospheric water harvesting [504]. The inflection point on the adsorption branch at $\alpha \approx 0.65$ is better suited for the humidity conditions of human habitation and aligns perfectly with the humidity range of a healthy indoor environment [505]. Therefore, once MOFs with high water adsorption capacity are identified, their application scope can be determined by the shape of their water isotherm, the position of the inflection point, and their water uptake capacity within specific relative humidity (RH) ranges.

17.3.1. MOFs for atmospheric water harvesting (AWH)

Strategies for extracting water from the air primarily include fog collection, condensation, and atmospheric water harvesting based on the adsorption properties of MOFs [506,507]. Hydrophilic MOFs were more suitable for this application, as they could capture water vapor in extremely dry air [508]. Currently, MOF-801 [509,510], MOF-841 [9], Co_2Cl_2BTDD, CAU-10 [511], HKUST-1 [512], NU-1500 [513] and MOF-303 [65] were all demonstrated to achieve high adsorption capacities at relatively low RH levels [514]. Meanwhile, AWH devices applicable for practical use also received significant research attention alongside the development of hydrophilic MOFs [515]. Yaghi and co-workers [516] reported a proof-of-concept MOF water harvester based on a single-cycle, passive adsorption-desorption mode. This device allowed moist air to diffuse into the MOF at night. During the day, when the RH peaked, solar-generated heat was utilized to release water vapor from the MOF, which then condensed on the inner walls of the device [487,509]. However, this single passive collector was highly susceptible to the adsorption capacity of MOFs and the influence of external environments influences (Fig. 16a) [510]. To minimize the impact of external factors on the device, Cordova and co-workers created an adaptive water harvester (Fig. 16b) [517]. In active water adsorption devices, the adsorption and desorption processes are electrically driven, and the uptake and release of water vapor can be initiated on demand [516]. To commercialize the AWH system, in 2024, Wang and co-workers achieved energy-efficient AWH by introducing all-day radiative cooling and designed an integrated hybrid AWH system. This device reduced the production cost per liter of water to $0.11 [518]. However, water produced by such transition metal-based MOF systems may not meet human drinking water standards. Therefore, AWH devices are utilized in many fundamental sectors, such as sustainable agriculture [519]. These AWH systems absorbed water during nighttime when relative humidity was higher and released it for irrigation under natural sunlight during daytime [520].

17.3.2. MOFs for low-temperature heat conversion applications

The water adsorption properties of MOFs are well-suited for low-temperature thermal conversion applications, such as adsorption-based heat pumps (AHP) or thermally driven chillers (TDC) [521]. The working cycle of thermally driven chillers operates as follows: (1) The condensation of water adsorbs heat from the air, thereby reducing the indoor temperature. (2) MOFs adsorb superheated water vapor. (3) The MOFs are heated by solar energy or low-grade waste heat, causing the water within the adsorbent to condense and proceed to the next cycle [522].

To ensure rapid achievement of the material's maximum working capacity during adsorption-desorption cycles, MOFs are required to achieve maximum adsorption and desorption of the working medium within a relative humidity range of 5 % to 32 % [523]. Stock and colleagues developed a green and highly robust reflux synthesis process to produce CAU-10-H. Under full adsorption refrigeration cycle conditions, CAU-10-H requires a regeneration temperature of only 70 °C [524]. Similarly, the physicochemical stability of MOFs has been identified as a key factor to consider in large-scale practical applications [525]. Serre and colleagues utilized Zr_6 and carboxylate ligands (3,3′,5,5′-tetracarboxydiphenylmethane, H_4mdip) to synthesize MIP-200, which features large one-dimensional (1D) hydrophilic channels. The material was subjected to in aqua regia, nitric acid, hydrochloric acid, boiling water, and an ammonia atmosphere, with experiments demonstrating that MIL-200 exhibits ultra-high physicochemical stability (Fig. 16c) [526].

17.3.3. MOFs for autonomous indoor humidity control

The American Society of Heating, Refrigerating and Air-Conditioning Engineers (ASHRAE) recommended that relative humidity should be maintained between 40 % and 65 % to create the most habitable indoor environment. When MOFs were applied as sorbents for indoor humidity control, they adsorbed moisture from the air when the humidity exceeded 65 % RH and rapidly released it when the relative humidity dropped below 45 % RH (Fig. 16d) [527]. Zhu and co-workers fabricated UiO-67–4Me-NH_2–38 % by screening hydrophobic and hydrophilic organic linkers within the pore nano spaces of UiO-66, which exhibited enhanced thermal, hydrolytic, and acid-base stability. This material could precisely control the indoor relative humidity within the range of 45 % RH to 65 % RH [252]. Increasing the pore size of MOFs also enhanced water absorption performance, as larger pores accelerated the rate of capillary condensation. However, this also accelerated the collapse of the MOF framework. Consequently, mesoporous MOFs containing highly inert coordination bonds emerged as the optimal solution. Therefore, Qian and co-workers carried out ligand functionalization with hydrophobic or hydrophilic functional groups to yield both uniform UiO-66 and mixed-linker MOFs [528].

With the progress of time, a more advanced autonomous humidity-control material (AHCM) was developed. It was capable of absorbing/releasing sufficient water vapor under target relative humidity conditions and autonomously maintaining indoor relative

humidity within a range suitable for human survival without external intervention. For Example, Qin and co-workers fabricated MOF-AHCM. The adsorption and desorption trigger points for this MOF occurred at 60 % RH and 40 % RH, respectively, indicating its ability to maintain humidity within the 40 % to 60 % RH range when used as an indoor humidity control material [529].

However, this single-component MOF could hardly adapt rapidly to changes in extreme weather. In contrast, MOF-based nanocomposites could quickly adjust to environmental variations. For instance, Maji and co-workers developed MOF-based nanocomposites (binary composite: CuBTC/AC and ternary composite: CuBTC/AC/GO). This composite material exhibited a water uptake of 0.337 g^{-1} day^{-1} [530]. Ding and co-workers innovatively combined wood with MIL-101(Cr) to create composite material [519,531]. This combination not only enhanced the water absorption capacity of the MOF/wood composite, enabling it to autonomously maintain indoor humidity, but also improved the mechanical strength, dimensional stability, and scalability of the building material. The composite proved highly suitable for building applications and contributed to carbon neutrality in the construction industry.

17.3.4. MOFs for natural gas desiccation

The natural gas industry played a leading role in global energy supply (Fig. 16e) [532]. However, gaseous water in natural gas could combine with CO_2, creating an acidic environment that corroded pipelines and equipment [533]. And the presence of liquid water would form hydrates, reducing the pipeline's transmission capacity [534,535]. Therefore, in 2017, Cadiau and co-workers reported the use of MOFs as desiccants for natural gas dehydration. Even under 95 % humidity, the material synthesized using pyrazine as a ligand and nickel-centered metal salts could remove water from the gas mixture [536]. Beyond this, research on the direct application of MOFs in natural gas dehydration remains limited.

MOFs exhibit excellent water uptake performance, rapid water release kinetics, and high adsorption capacity, which distinguishes them from most other solid adsorbents. However, beyond performance, their usability, economic viability, and acceptability in specific applications must be considered. Enough and acceptable cost are required, while conceptual process design (CPD) and life cycle assessment (LCA) can guide the fundamental direction for further research and development.

18. MOF-derivatives for efficient wastewater treatment

Xun Wang*

Although MOFs have demonstrated excellent and diverse performance in water treatment because of their specific surface area, adjustable porosity and unsaturated active sites, it is undeniable that there are some shortcomings to be faced. For example, most of MOFs are unstable in water, which the collapse of the structure will cause metal ions and organic ligands to be released, posing a threat to wastewater treatment efficiency and environmental health. In some specific catalytic systems (such as O_3 catalysis, H_2O_2-based and PS-based AOPs etc.), the organic ligands of MOFs are also prone to be oxidized. In addition, the pores distribution of most MOFs are microporous instead of mesoporous, which may not be conducive to the mass transfer of pollutants within the MOFs pores [537,538]. With in-depth exploration, MOF-derivatives prepared with MOFs as the precursor are regarded as a promising approach to overcome the above-mentioned shortcomings. MOF-derivatives can not only retain the transition metal elements (such as Ti, Mn, Fe, Co, Cu, etc.) of MOFs and the essential elements of the catalytic system such as C, H, O and N in its ligands, but also inherit the customizable morphology, large surface area, adjustable pore volumes and high porosity of the precursor MOFs, which is conducive to the adsorption and catalysis of pollutants [539,540]. The structurally controllable characteristics of MOFs can be utilized to effectively control the structure, morphology and composition of derivatives, and thereby regulate their catalytic performance. The ordered channels of MOFs can restrict the migration of metal ions and prevent the aggregation, thereby enabling the preparation of metal nanoparticles or single-atom catalysts [541]. Organic ligands in partial MOFs contain heteroatoms such as nitrogen and sulfur. After pyrolysis, they will form nitrogen-doped carbon or sulfur-doped carbon, which can interact strongly with metal components through chemical bonds, such as C-N-Metal, C-S-Metal, further stabilizing the dispersion of metal composition. In addition, the MOF-derivatives exhibit improved stability in water [542]. Based on the above advantages, various MOF-derivatives have stepped onto the broad stage of removing pollutants from water.

18.1. Preparation strategies of MOF-derivatives

Up to now, MOF-derivatives including metal oxides, metal nitrides, metal sulfides, metal-carbon composites, metal selenides, metal phosphides and metal free carbon materials can be prepared through different approaches such as pyrolysis, sulfidation, phosphorylation and selenidation.

Pyrolysis in an atmosphere of oxidizing gases (O_2, air and water vapor), inert gases (N_2 and argon) or reducing gases (H_2, HN_3 and CO), MOFs can be directly used as precursors for the preparation of metal oxides, metal/carbon materials and metal nitrides [19,543]. Adding the corresponding components during the pyrolysis process, derivatives such as metal sulfides and metal phosphides can also be obtained by sulfidation, phosphating or selenidation of metal elements with high-temperature vapor generated from S, P and Se sources. The precisely regulation of the composition, morphology and specific surface area of the derivatives are closely related to the gas atmosphere, pyrolysis temperature, heating rate, holding time and pyrolysis stage [544]. As there are no organic solvents and the morphology of MOF precursors can be maintained, Pyrolysis is widely used in the preparation of MOF-derivatives. However, the harsh pyrolysis conditions and the low yield of the catalyst are unsatisfactory.

For metal sulfides, metal selenides and metal phosphides, solvothermal/hydrothermal methods is another promising strategy. The vulcanization time, phosphorus source amount and selenification temperature have been reported to be the key factors affecting the physicochemical properties of derivatives [545]. Due to the short required time and low temperature, sulfidation is the most common method for MOF-derived metal sulfides. However, the release of toxic gas H_2S and the use of organic solvents will cause secondary pollution to the environment. Phosphating is similar to selenification, with the advantages of low required temperature and high catalyst yield, and the disadvantages of the extensive use of solutions and the relatively long reaction time [546]. In general, each preparation method of MOF-derivatives has unique superiority and scruples that should be deeply considered. During the application, specific scenario requirements should be taken into account and applied flexibly.

18.2. Applications in removal of pollutants from water

In recent years, MOF-derivatives have been reported to be mainly applied to the removal of organic pollutants in wastewater, including but not limited to bisphenol A (BPA), thiamethoxam (TMX), direct acid-proof red (4BS), tetracycline (TC), naproxen (NPX), tetracycline hydrochloride (TCH), sulfamethoxazole (SMX), through adsorption and catalytic technologies.

18.2.1. Adsorption

Adsorption has attracted widespread attention in the removing pollutants from water due to the easy operation and high efficient. Some MOF-derivatives inherit the large specific surface area of MOFs precursors and may expose more adsorption sites during the derivation process, thus becoming potential adsorption materials [547]. Wang *et al.* reported ZIF-8/agarose-derived nitrogen-doped carbon aerogels (ZIF-8/AG-CA) with the highly interconnected porous labyrinth structure through simple mixing, freeze-drying and pyrolysis procedure [548]. ZIF-8 helped maintain the two-dimensional layer of AG, while AG pulled ZF-8 "outward", thus forming the porous hollow structure during the carbonization process. The interaction between AG and ZIF-8 enabled ZIF-8/AG-CA to have the low density of 24 mg/cm^3, high specific surface area of 516 m^2/g, and the large pore volume of 0.58 cm^{-3} g^{-1}. Based on these advantages, ZIF-8/AG-CA exhibited excellent adsorption capacity for a variety of organic solvents such as toluene, mineral oil, tetrahydrofuran, ethyl acetate, *etc*. Furthermore, the large-scale synthesis of ZF-8/AG-CA had been realized, which was expected to be used in practical applications. This sustainable preparation strategy had also been extended to other MOFs materials. For example, a carbon aerogels prepared from a ZIF-67/AG aerogel was obtained by the same method.

18.2.2. Catalysis

Catalytic elimination of organic pollutants in water is an efficient and sustainable advanced technology. By using the catalyst to lower the activation energy of the reaction, accelerating the decomposition of oxidants to generate strong oxidizing free radicals or non-free radical species, the rapid mineralization or transformation of organic pollutants have been realized [549].

Due to the asymmetric molecular structure (H−O−O−SO_3^-) of PMS, it readily decomposes into reactive oxygen species-like free radicals ($SO_4^{\bullet-}$, $^{\bullet}OH$ and $O_2^{\bullet-}$) after accepting electrons from the catalyst. In addition, PMS can also act as an electron donor to undergo oxidation and generate PMS anion radicals ($SO_5^{\bullet-}$), which react with water molecules to produce $^1O_2$, the PMS-based AOPs of wastewater over MOF-derivatives become increasingly widespread. ZIFs are a classic type of MOFs material. During the preparation of derivatives, it can maintain structural integrity and high porosity, providing abundant active sites for the catalytic reactions. In addition, the chemical properties of ZIFs can be flexibly adjusted through post-synthesis modification to meet different application requirements. Pei *et al.* confined I within the N−C scaffold derived from ZIF-8 (I−NC) by chemical vapor deposition [550]. This structure featured a unique C-I coordination that optimized the electronic structure of the carbon sites adjacent to nitrogen, thus reducing the energy barrier for the rate-limiting step of $SO_5{\cdot}^-$ generation in I-NC (1.45 eV), compared with NC (1.65 eV), which was conducive to promoting the generation of $^1O_2$. Ciprofloxacin (CIP) was almost completely degraded by the I-NC/PMS system within 10 min, while only about 35 % of CIP degradation was observed in the NC/PMS system. Despite the addition of iodide ions, the performance improvement of the NC/PMS system was negligible, highlighting the crucial role of the limiting effect of N−C derived from ZIF-8 in enhancing PMS activation and promoting CIP degradation. Yu and the co-workers proposed that due to the generation of a large number of inherent defects at the edge position, the thermally stable edge-supported Zn-N_4 single-atom catalyst (ZnN_4−Edge) was formed (Fig. 17a) [551]. The regulation of the edge moiety greatly enhanced the atomic utilization efficiency of ZnN_4−Edge, which was ∼10^4 times higher than the equivalent amount of the catalyst without edge sites (ZnN_4). DFT calculations showed that the edge sites not only promote the decomposition of HSO_5^-, but also significantly reduce the activation barrier for $^{\bullet}OH$ generation at Zn sites, endowing ZnN_4−Edge with excellent catalytic properties for phenol decomposition (Fig. 17b). By using a simple NaCl-assisted strategy, the highly organized crystal nanoporous carbons (NPC) was synthesized *via* sealing monoclinic ZIF-8 with NaCl crystals and then conducting heat treatment, completing the first successful attempt of the third-generation MOF-derived NPCs [313]. Thanks to interfacial $^1O_2$ and surface-activated PMS, dyes such as methylene blue, rhodamine B and acid orange 7 could be completely degraded within approximately 5 s, phenolic compounds such as phenol, bisphenol A, *p*-nitrophenol and 4-hydroxybenzoic acid and inert antibiotics such as ciprofloxacin and tetracycline were achieved 100 % removal efficiency within around 90 s.

In Fenton-like catalysis, precisely adjusting the electronic structure and coordination environment of the metal center was crucial to enhance the activation kinetics. The relationship between the single-atom coordination number of Co and the Fenton-like performance of Co-N_x was investigated by using a series of atomic dispersion Co catalysts with different Co−N coordination numbers [552]. Experimental and theoretical results indicated that the single Co atom, pyridinic N-bonded C atoms as well as the nitrogen vacancies in the adjacent unsaturated Co-pyridinic N_2 portion served the reduction and oxidation of PMS to the generation of radicals and $^1O_2$, respectively (Fig. 17c). Therefore, reducing the coordination number had been increased the electron density of the single Co atom in Co−N_x, which was conducive to the Fenton-like performance of the Co−N_x catalyst. Furthermore, the long-term degradation of BPA and the treatment of actual kitchen wastewater were achieved by using a continuous-flow reactor composed of silica sand columns filled with Co−N_2 catalyst. The single-atom catalysts (CoSAs-ZnO) with surface hydroxylation and isolated asymmetric Co−O−Zn structure had the significant activation effect on PMS and PAA, and can selectively and efficiently generate $SO_4^{\bullet-}$ or $^1O_2$ in the different systems due to the activation effect of the Co−O−Zn structure on asymmetric oxidants and the regulation of the adsorption configuration of $SO_4^{\bullet-}$ or $^1O_2$ by the hydroxyl groups on the surface of ZnO [553]. The PMS activation system dominated by $SO_4^{\bullet-}$ showed high efficiency in treating benzoic acid wastewater, while the PAA activation system dominated by $^1O_2$ demonstrated a significant ability to convert benzyl alcohol into benzaldehyde. Guo *et al.* found that when single atoms and nanoclusters coexisted, Co nanoclusters synergistically enhanced the adsorption and activation PMS ability of asymmetric CoN_1O_2 single atoms sites, significantly accelerating the interfacial charge transfer [314].

The Fenton-like activity of MOF-derivatives could also be enhanced by introducing additional metal components to accelerate electron transfer and increase the generation of free radicals or non-free radicals. Li and co-workers synthesized a series of Mo-doped Co_3O_4 catalysts through controlled pyrolysis of Mo-ZIF-67 and found that the synergistic effect of Mo and Co promoted the directional transfer of electrons from Co^{2+} and Co^{3+} to Mo^{6+}, meanwhile increasing the spin states of Mo and Co and adjusting the center of the Co D-band from 0.14 eV to −0.29 eV, ultimately optimizing the adsorption of PMS and the interfacial electron transfer on Mo−Co_3O_4 [554]. The research by Zhou *et al.* also confirmed the positive role of *Mo species* [555]. The presence of Mo simultaneously accelerated the Fe^{2+}/Fe^{3+}−Mo^{4+}/Mo^{6+} REDOX cycle and lowered the energy barrier for PMS activation, which was conducive to the generation of $^1O_2$. Therefore, the reaction kinetics of 2,4-dichlorophenol (2,4-DCP) over FeMo−N−*C* was 20.67 times higher than Fe−N−*C*. By constructing a dual-electron migration pathway, Cu-Co_3O_4/OVs, derived by Cu-ZIF-67, demonstrated outstanding efficiency in degrading a variety of micropollutants [308]. Specifically, in addition to the electron contribution from the Co center, electrons could migrate from micropollutants to the Co sites

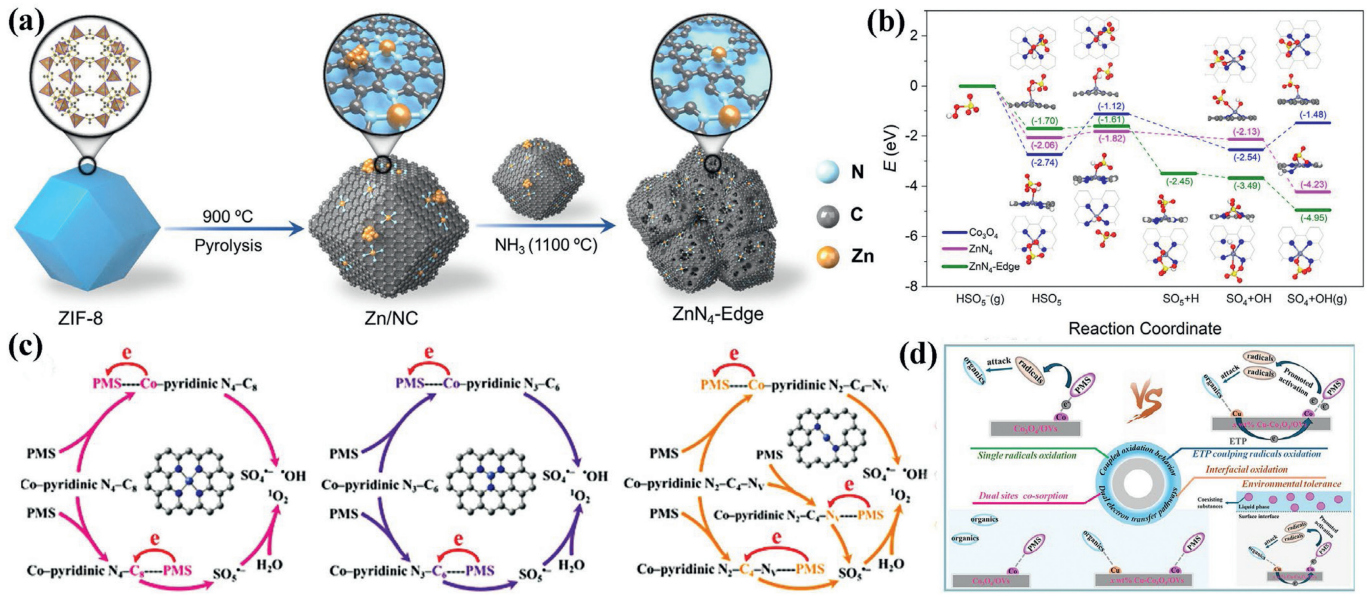


Fig. 17. (a) Schematic diagram of the preparation of ZnN_4-Edge. (b) The energy distribution map of the most favorable pathway for the dissociation of PMS into OH radicals under neutral conditions. Copied with permission [551]. Copyright 2023, National Academy of Sciences. (c) The free energy plots of PMS activates on FeMo−N−C and Fe−N−C. Copied with permission [552]. Copyright 2018, Wiley-VCH. (d) The summary of the functions of dual sites and the synergistic effects of free radicals and non-free radicals. Copied with permission [308]. Copyright 2025, Wiley-VCH.

via the Cu, acting as an extra electron source to assist in the activation of PMS. Besides, the utilization efficiency of active substances had been enhanced because of the shortened migration distance of free radicals (Fig. 17d).

In addition to the ZIF series, other members of the large MOFs family have also been reported as precursors of the derivatives for efficient Fenton-like catalytic treatment of wastewater. For example, Xu *et al.* successfully fixed electron-rich Ru diatomic sites on N-doped carbon (Ru_2N_6-C, derived from MET-6) [556]. The presence of Ru diatomic sites not only provided more electrons for PMS but also promoted the cleavage of O−O bonds, leading to an increase in the generation of $^{\bullet}SO_4^-$ and $^{\bullet}OH$. Thanks to this, derivative catalysts exhibited excellent NPX degradation performance with 153.95 min^{-1} L mol^{-1} turnover frequency. The development of membrane reactors based on Ru_2N_6-C had further enhanced the practical application potential. Similarly, double reaction site FeCo-NC had also shown the potential in the catalytic oxidation of stubborn organic substances because this dual reaction sites were conducive to reducing the migration distance of active substances [310]. Concretely, the CoN_4 site with a single Co atom acted as the active sites with optimal binding energy for PMS activation, while the adjacent pyrrolic N site adsorbed organic molecules.

Photocatalysis has demonstrated to be an environmentally friendly and efficient technology for removal pollutant in wastewater. How to suppress the recombination of photo-generated carriers to improve photocatalytic performance has always been the research hotspot. Organic nitrogen-encapsulated MOFs could be transformed into N-doped Fe_3O_4@C by chemical vapor deposition-induced super-assembly method [557]. Compared with Fe_3O_4@C, the abundant pyrrole-N and oxygen vacancies at the carbon interface of N-Fe_3O_4@C promoted the transfer of photo-generated carriers and the activation of H_2O_2, thus 96.9% removal of TMX could observed at 60 min, higher than the 30% removal of Fe_3O_4@C. Wang *et al.* coated a thin/soft silica layer on the surface of the octahedron NH_2−MIL-125 to synthesize hollow TiO_2 octahedrons (H-TiO_2) with concave surfaces, high specific surface area and abundant oxygen vacancy [558]. Ascribed to the above advantages, H-TiO_2 has better MB degradation performance than cracked TiO_2 fragments (C-TiO_2), produced by coating thick/rigid silica, or solid TiO_2 particles (S-TiO_2), prepared *via* direct calcination.

In conclusion, because MOF-derivatives can inherit many merits of the MOFs predecessors, such as customizable morphology, large surface area, adjustable pore volume and high porosity, and can take advantage of the structural controllability of MOFs to pre-regulate the structure, morphology and composition as well as exhibit higher stability, MOF-derivatives have expanded the application of MOFs in removing pollutants from water. However, the further development of MOF-derivatives also needs to take into account some issues, including the optimization of the physicochemical properties of MOF-derivatives, the simple and high-throughput preparation strategy, the removal of extremely trace amounts of refractory pollutants, the development of MOF-derivatives macroscopic system to catalytic degrade actual water environmental pollutants and so on.

19. Toxic risk assessment of MOFs in the aqueous environment

Meng Yang, Xuchun Qiu*

MOFs have demonstrated impressive versatility across a range of applications, including adsorption, separation, catalysis, chemical sensing, biomedical delivery, and proton conduction, due to their high specific surface area, customizable pore size, and ease of functionalization [335,559]. In aqueous environments, MOFs show considerable promise for water remediation, particularly in pollutant removal, harmful algal bloom control, and water regeneration [335]. Nonetheless, the widespread use of MOFs might lead to their release into the environment and subsequently into aqueous ecosystems, raising concerns about their effects on aquatic organisms [560–563]. Therefore, understanding their toxic effects on aquatic organisms is essential for evaluating the ecological risks associated with MOF applications [561,562]. Such assessments are critical for ensuring the large-scale and sustainable applications of these materials.

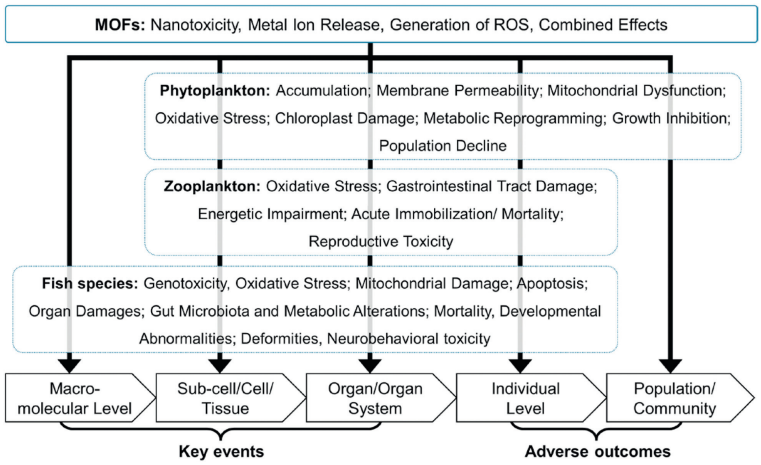


Fig. 18. Toxic effects of MOFs on aquatic organisms.

19.1. Toxic effects of MOFs on aquatic organisms

Recent studies, most of which are based on laboratory exposure tests at relatively high concentrations, have demonstrated that MOFs exhibit complex toxic effects on aquatic organisms (Fig. 18).

Toxic effects on phytoplankton: The effects of MOFs on harmful microalgae have been well documented, since these materials exhibited great potential in controlling and mitigating harmful algal blooms. It has been shown that MOFs have a notable impact on freshwater algae, leading to growth inhibition, reduced chlorophyll content, and metabolic reprogramming [477,560,564]. The mechanisms of toxicity include the direct physical interactions, release of metal ions, generation of ROS, and the adsorption of essential nutrients [477,560,564]. For example, high concentration (50 mg/L) of MIL-101 could significantly reduce algal viability, inhibit photosynthesis, and impact metabolic pathways in *Chlamydomonas reinhardtii*, while low concentrations (0.1 mg/L) of this MOF do not produce any noticeable physiological changes [565]. The bimetallic Hofmann MOF (NiCo-PYZ) released 87 % of its nickel and 96 % of its cobalt ions into the algal medium within 72 h, which was sufficient to account for nearly all observed toxicity to *C. reinhardtii* [477]. However, it should be noted that algae are the critical primary producers in the aquatic ecosystem and contribute approximately 50 % of the global net primary productivity [566]. Therefore, clarifying the toxic effects of MOFs on non-target algae is crucial for accurately assessing their ecological risks. Furthermore, MOFs can be absorbed or internalized by algae, which influences bioavailability to higher trophic levels [560,563]. For example, aggregates formed by MOFs and algae may be ingested by zooplankton or directly compete for food resources, leading to growth inhibition due to starvation [477,562].

Toxic effects on zooplankton: Zooplankton act as key links in mediating the transfer of energy and substances in aquatic ecosystems. Using *Daphnia magna* and *Moina mongolica* as the model species, several recent studies demonstrated that the toxic effects of MOFs are significantly influenced by the exposure concentration and route [560,563]. For example, a study on MIL-101(Cr)-NH_2 demonstrated that *D. magna* directly ingested this MOF from the water column, with body burdens reaching 1 %–9 % of its dry weight, classifying it as very bioaccumulative [560]. The accumulated MOF was primarily located in the gut at lower concentrations ($\leq$1 mg/L), while at higher concentrations (10 mg/L), large MOF aggregates attached extensively to the carapace, antennae, and appendages, potentially impairing mobility and molting [560]. In another study, Li, Liu, Cui, Qu and Xia [563] reported that algae exhibit a protective role against the toxicity of MIL-88B(Fe) at low concentrations (0.1–1 mg/L) to *M. mongolica*, while a high-concentration dietary exposure (10 mg/L) induces synergistic toxicity, enhancing MOF bioaccumulation by 44.6 % compared to the waterborne exposure [560]. The findings emphasize that a thorough assessment of MOF ecological impacts requires evaluation across multiple trophic levels, thus providing a more reliable forecast of their environmental effects under actual exposure situations.

Toxic effects on fish: As the high-level consumers in the aquatic ecosystems, the physiological and behavioral responses directly reflect the ecotoxicological effects of pollutants, making them ideal indicator organisms for assessing the environmental safety of MOFs [567]. Current research primarily uses zebrafish (*Danio rerio*) and medaka (*Oryzias* spp.) as model species to evaluate the toxic effects of MOFs, spanning multiple life stages, from embryonic development to adult behavior [567–571]. Generally, different metal types of MOFs exhibit significant differences in toxicity to fish [567], and synergistic toxicity may occur when MOFs are co-exposed to other pollutants [571].

Taking the toxic effects of ZIF-8 as an example, although this MOF substance exhibited low acute toxicity to zebrafish, it can induce various adverse effects at sublethal concentrations. For example, embryos exposed to ZIF-8 ($\geq$90 mg/L) exhibited delayed hatching and a significant decrease in heart rate [568], while adult fish exposed to ZIF-8 (30–90 mg/L) showed decreased locomotor activity and increased oxidative stress in the brain [569]. Furthermore, co-exposure of ZIF-8 and cetylpyridinium chloride (CPC) could induce synergistic toxicity, characterized by increased heart rate, larval hyperactivity, and oxidative stress in zebrafish larvae [571]. In addition, combined exposure to ZIF-8 and copper further reduced zebrafish survival and caused gut microbiota dysbiosis. Those findings highlight the potential risks of MOFs as a pollutant carrier in real aquatic environments [571]. In the marine model organism of *Oryzias melastigma*, the toxicity contrast between Cu-MOF and Zn-MOF was even more pronounced [572]. The Cu-MOF significantly increased the mortality rate of adult fish and was accompanied by oxidative stress at $\geq$4.0 mg/L, while Zn-MOF only produced similar effects at $\geq$80 mg/L [572]. Those studies demonstrated that the toxicity of MOFs to fish exhibits obvious metal type dependence, life stage specificity, and a combined physical-chemical mechanism [567–571]. Case comparisons further reveal that different fish species have different sensitivities to the same MOFs [571,572]. Therefore, considering species differences in the toxicity of MOFs may provide a potential way to balance the ecological benefits and risks of MOF application. Furthermore, the interactions between MOFs and co-existing pollutants should not be

ignored; their behavior as carriers in the environment may amplify the ecological risks of existing pollutants.

19.2. Mechanisms involved in MOF toxicity to aquatic organisms

Physical interactions and surface functional groups: The properties of MOFs, particularly their size, morphology, and surface properties, play a crucial role in their interactions with biological organisms [573]. Generally, the smaller particles (nano-MOFs) are more likely to penetrate physiological barriers, such as skin, the alveolar-capillary barrier, and the blood-brain barrier [574]. While the increased surface area-to-volume ratio is often advantageous for targeted drug delivery [575], it concurrently elevates the risk of nanotoxicity of MOF by enhancing cellular uptake and increasing chemical reactivity [561]. On the other hand, MOF particles can aggregate in aqueous environments or within biological systems, which may reduce their nanotoxicity but alter their bioavailability and associated toxicological implications [560,562]. Moreover, although the functionalization can considerably enhance the effectiveness of MOFs in environmental remediation and water treatment, introducing functional groups may also significantly alter their bioavailability and overall toxicity [565,574]. Given these considerations, developing effective recovery methods for MOFs is crucial to minimize the possible risks of MOFs and support their sustainable application.

Metal ion release: The chemical toxicity of MOFs primarily results from the release of metal ions embedded within their structure [477]. MOFs with different metal centers exhibit varying rates and extents of ion release in aquatic environments and organisms [495,576], leading to distinct toxic effects. For example, Cu-MOFs release copper ions gradually into aquatic environments, which can cause lipid peroxidation, protein denaturation, and DNA damage in zebrafish larvae by triggering significant oxidative stress [567]. In contrast, although Zn-MOFs also release zinc ions, their toxicity is much lower than that of copper ions. Even at certain concentrations in fish tissues, zinc ions do not typically cause notable toxic reactions. This disparity in stability explains the drastically different toxicity profiles observed among various MOFs under similar experimental conditions [567,572]. Consequently, enhancing the stability of MOFs is essential not only for improving their application performance but also for effectively reducing their ecological risks.

Generation of ROS and other effects: Generation of ROS is a dual-mechanism pathway that contributes to the toxicity of MOFs toward organisms [559]. Certain MOFs, especially those featuring specific metal centers or structural defects, can directly generate ROS when suspended in aquatic media [577]. The ROS released into the surrounding environment may damage external biological interfaces, such as the cell membranes, epithelium, and mucous layers, making the organism more susceptible to physical damage and the uptake of other toxicants [54,567]. Once internalized, MOF particles or released metal ions can directly disrupt crucial cellular components, leading to mitochondrial dysfunction, promoting the generation of excessive intracellular ROS, and finally resulting in oxidative stress [559]. Such stress can lead to damage to critical cellular components, including DNA, lipids, and proteins, ultimately inducing cellular apoptosis and dysfunction within tissues [578]. On the other hand, some indirect effects of MOFs on the growth of phytoplankton were also reported. For example, the high porosity of MOFs facilitates the effective adsorption of essential nutrients in aqueous environments, leading to the depletion of free nutrients, thereby indirectly inhibiting the growth of algae or bacteria [477]. Additionally, suspended MOF particles or their aggregates may attach to algal cell surfaces, creating a light-shielding effect that disrupts photosynthesis [480].

Combined toxic effects: MOFs do not exist alone in either experimental systems or actual aquatic ecosystems. Owing to their pronounced adsorption affinity, MOFs can adsorb co-existing pollutants and act as a Trojan horse, facilitating the intracellular uptake of these contaminants and thereby enhancing their bioaccumulation and joint toxic effects [579]. Compared with individual exposure, combined exposure of zebrafish to ZIF-8 and Cu^{2+} leads to more severe toxicity, revealing a synergistic impact [54]. Similarly, ZIF-8 also exhibited more severe toxicity in early-life stage zebrafish when co-exposed with CPC [571]. Those findings highlight the need to update ecological risk assessment frameworks to incorporate scenarios of combined exposure and to develop predictive models for assessing the joint toxicity of MOF-pollutant complexes.

Given that MOFs exhibit certain toxic effects on aquatic organisms, a proactive risk assessment strategy is crucial to ensure their sustainable application. For example, Gao *et al.* [580] developed high-performance Bi-MOFs for the degradation of bisphenol pollutants and assessed the toxicities of the degradation intermediates using mung beans and zebrafish embryos as model species. The results proved that the toxicities of degradation intermediates were significantly reduced, demonstrating that their systems can not only remove contaminants effectively but also reduce environmental risks. Additionally, using medaka fish as the model species for safety assessment, Nikzad *et al.* [572] successfully determined the optimal dosage for application of Cu-MOF and Zn-MOF in controlling the toxigenic microalga *Alexandrium minutum* that maintained relative safety towards non-target organisms. These examples suggested that, through effective design and comprehensive risk assessment, MOFs can play a considerable role in environmental governance by balancing their benefits against potential ecological risks.

Nevertheless, current ecotoxicological assessments of MOFs in aquatic systems reveal several critical knowledge gaps that limit the accuracy of their ecological risk evaluation [561,562]. First, most of the toxic information of MOFs was derived from acute exposure tests under laboratory conditions, failing a comprehensive evaluation of their long-term effects and impacts on ecosystems [569,575]. Second, there remains a limited understanding of how complex environmental factors (such as pH, salinity, dissolved organic matter, and co-existing pollutants) influence MOF toxicity [576]. Another significant gap concerns the toxicological evaluation of transformation products generated during MOF application, including both structural degradation intermediates and metabolites of target pollutants, whose ecological impacts remain largely uncharacterized [580]. Compounding these issues is the absence of standardized testing protocols tailored to the unique physicochemical properties of MOFs, which substantially undermines the comparability and reliability of findings across different studies [561,562].

To enhance the predictive capabilities of MOFs risk assessments and address current deficiencies, future research should prioritize several directions: First, it is critical to conduct chronic, low-dose exposure studies to clarify the relationships among MOF characteristics, environmental persistence, and toxic potency, which will lay a foundational framework for the computational design of eco-compatible MOFs [581]. In addition, it is imperative to develop standardized testing guidelines and evaluate species sensitivity across various developmental stages [561]. Second, expanding toxicological endpoints to encompass sublethal and sensitive responses (*e.g.*, neurodevelopmental impairment, endocrine disruption, and transgenerational effects.) will provide a more comprehensive approach to their risk assessment [565,571]. Third, the implementation of microcosm and mesocosm simulation systems will facilitate a more accurate investigation of MOF behavior and the combined effects of other pollutants in multi-media aquatic en-

vironments [577]. Furthermore, the establishment of quantitative structure–activity relationship (QSAR) models that include systematic material characterization, environmental aging protocols, and transformation tracking to ensure data consistency [561,562]. Finally, intensified research on the transformation pathways of MOFs under environmentally realistic conditions, along with mechanistic toxicological evaluations of key degradation products, will substantially enhance our ability to predict long-term ecological impacts and inform the sustainable use of MOF-based technologies [580]. These scientific approaches will provide the essential knowledge needed to ensure that the deployment of MOFs maximizes environmental remediation benefits while protecting aquatic ecosystems.

20. Computational chemistry helping environmental applications of MOFs

Yu-Hang Li, Haodong Ji*

Density functional theory (DFT) calculations are fundamentally a theoretical approach to calculate the many-electron Schrödinger equation [582]. In recent years, researchers have not only developed numerous approximated exchange-correlation functionals to support DFT calculations [583], but also created suitable computational software toward different calculated systems [584–586]. Among these, Gaussian and the Vienna Ab-initio Simulation Package (VASP) are two of the most widely used software tools in the fields of chemistry and materials science.

In the studies of MOFs for wastewater remediation, theoretical calculations have been widely used to investigate the microscopic electronic properties of MOFs and targeted pollutants, adsorption processes, redox reaction mechanisms and so on [307,587–589]. For instance, calculating the electronic properties of organic molecules can help to predict their electron-rich sites, radical attack sites, nucleophilic reaction sites [46,590]. which is crucial for investigating the degradation pathways of organic pollutants. For material calculations, MOFs with the highly tunable structural properties can achieve atomic level metal doping, metal cluster modification, organic ligand substitution, vacancy construction and other adjustments. Using DFT calculations can theoretically determine the optimal doping/substitution sites or vacancy locations [591,592]. Additionally, the corresponding electronic properties can be derived from these optimal models, which help to explain the structure-activity relationship [593,594]. Moreover, theoretical calculations can identify potential adsorption sites, catalytic sites in MOF structure and reaction pathways [306,595], which can then be cross-verified with experimental and characterization results to support the investigation of reaction mechanisms. Therefore, this section will elaborate on the application of different computational modules in analyzing the intrinsic electronic properties of targeted pollutants and MOFs as well as assisting in the exploration of redox reaction mechanisms.

20.1. Gaussian computations

Due to the increasing attention given to emerging contaminants and their perniciousness in water, researchers have developed various effective techniques for removing these pollutants from water, including adsorption, catalysis, photocatalysis and advanced oxidation process [12–14]. In the mechanisms exploration of pollutants' degradation, the Gaussian computational program based on the Gaussian platform and combined with Multiwfn can calculate a series of electronic properties for organic molecules, such as the highest occupied molecular orbital (HOMO), the lowest unoccupied molecular orbital (LUMO), electrostatic potential (ESP), Fukui index, dipole moment, ionization potential (IP), electron affinity (EA) and so on [596,597]. Many previous studies have reported: a higher HOMO value indicates that the organic molecule is more likely to perform the single electron transfer reaction with electrophilic radicals [308,598]. Additionally, a smaller energy gap (LUMO-HOMO) suggests the lower chemical stability of the organic molecules, which will cause them to be eliminated [554]. IP and EA represent the energy required for an organic contaminant to lose or gain an electron, respectively, which helps assess its tendency to participate in redox reactions [599]. By calculating the Fukui indices and electrostatic potential of the targeted pollutant, it can identify electrophilic/nucleophilic reaction sites and predict the points that are more vulnerable to attack by reactive species (Fig. S4a in Supporting information), which can help identify degradation intermediates *via* combining with the non-targeted screening and determine the major degradation pathways [600–603]. Furthermore, Gaussian calculations can also simulate the attack pathways of active radicals on organic pollutants, deeply revealing the radical-mediated reaction mechanism from the molecular orbital level *via* dynamic electron distribution analyses [602,603]. As shown in Fig. S4b (Supporting information), Zhang *et al.* exhibited that the single electron transfer reaction happened between N14 site from sulfacetamide (SCT^-) and $CH_3COO^•$, significantly enhancing the knowledge of the reaction of alkoxy radicals produced by peracetic acid on attacking organic contaminants at the molecular orbital level [603].

20.2. First-principles calculations

20.2.1. Formation energy

Some MOFs like UiO-66, ZIF-67 and MIL-88 are considered as the "star materials" in the field of water pollution control [604,605], thereby many studies focus on their modification by using these frameworks as the intrinsic materials. While some characterizations like XPS or XAFS can reveal the changes in electronic properties before and after modification, the optimal structure after modification can be determined by calculating the formation energies of different coordination structures. For instance, Li *et al.* constructed MIL-88B(Fe) doped with 4-aminonicotinic acid for PDS activation [606]. Based on the results of formation energy calculations, the authors found that both the pyridine nitrogen and amine nitrogen of 4-amino nicotinic acid can all coordinate with Fe atoms (Fig. 19a). The differences in the coordination angles between 4-amino nicotinic acid, terephthalic acid, and the Fe-O clusters led to the morphological change from nanorods (MIL-88B(Fe)) to spindles (De-MIL-88B(Fe)-1.25). Moreover, after doping heteroatoms, modifying clusters or creating vacancies in the MOF structure, the possible modification sites can also be identified through formation energy calculations [607], which can further assist in explaining the structural characterization results.

20.2.2. Adsorption energy

The calculation of adsorption energy is commonly utilized to study the interactions between adsorbate molecules and MOFs. By subtracting the energy of all pre-adsorption models from that of the post-adsorption model, the specific adsorption energy value can be obtained. Specifically, the negative value indicates that the adsorbates can be spontaneously captured by the sorption sites from MOFs, while the positive value suggests the non-spontaneous adsorption. In recent studies, MOFs have been used to efficiently adsorb target pollutants such as emerging contaminants, heavy metal ions, phosphates, owing to the large specific surface area and rich sorption sites of MOFs [15,608]. The calculation of adsorption energy aids researchers in determining the optimal adsorption sites and adsorption modes as well as investigating the adsorption/selective adsorption mechanisms [582,609]. Li *et al.* used DFT calculations to construct different phosphate sorption

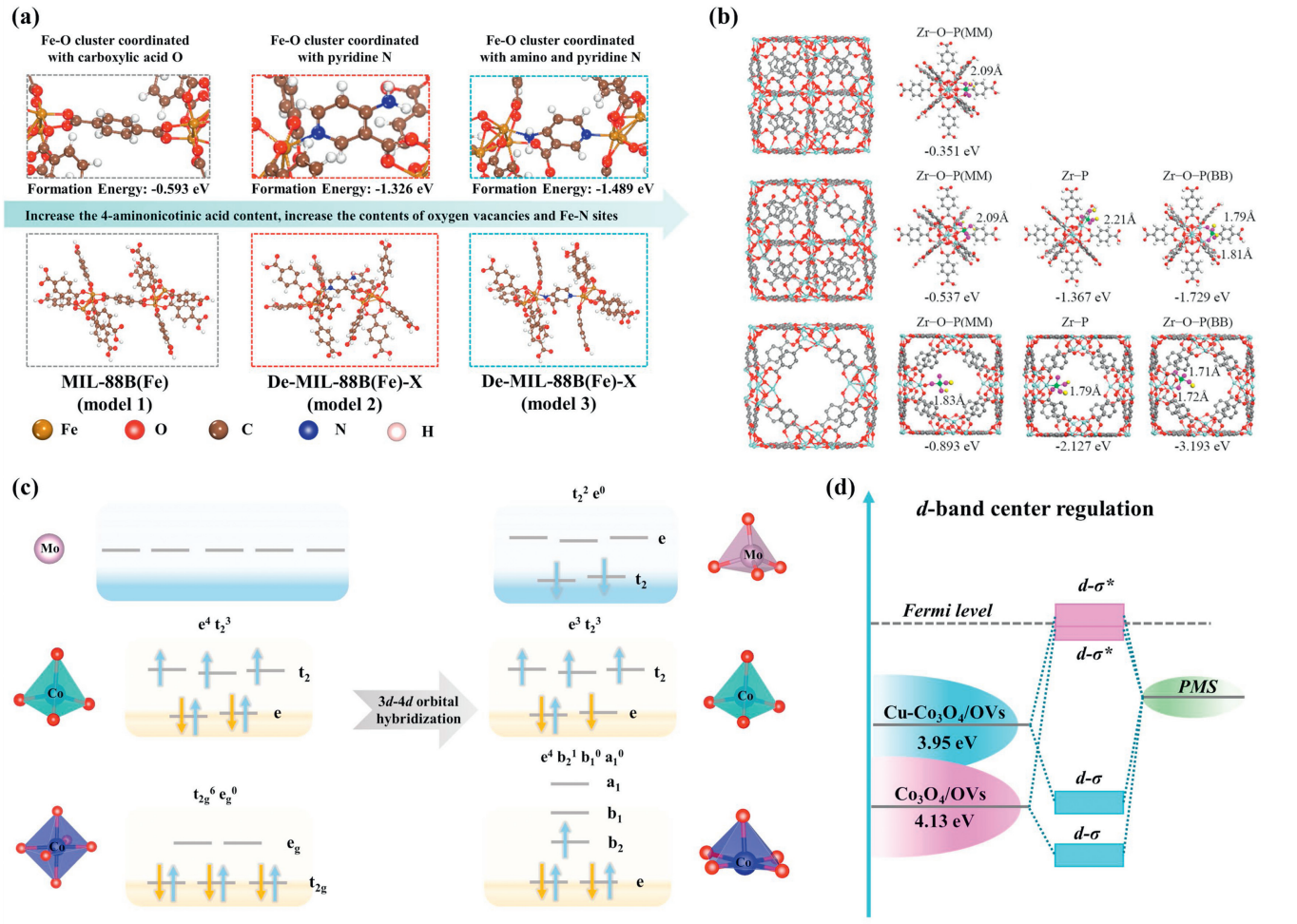


Fig. 19. Theoretical calculations of different modules. (a) The calculations of formation energies of different coordination models. Copied with permission [606]. Copyright 2023, Elsevier. (b) Phosphate adsorption in perfect and defective UiO-66 with different sorption sites as well as the corresponding adsorption energy calculations. Copied with permission [595]. Copyright 2021, American Chemical Society. (c) The variation in d orbitals after 3*d*-4*d* hybridization from Co and Mo sites. Copied with permission [554]. Copyright 2025, Wiley-VCH. (d) D-band center regulation before and after Cu doping. Copied with permission [308]. Copyright 2025, Wiley-VCH.

models (Fig. 19b), confirming that the binuclear bidentate sorption mode was the most stable (adsorption energy: −3.193 eV) [595]. Additionally, comparing values of adsorption energy can help explain the mechanism behind selective adsorption. For instance, Li *et al.* calculated that the adsorption energy for Pb(II) on defective UiO-66-NH_2 was higher than that for other heavy metal ions, which explained why defective UiO-66-NH_2 preferentially adsorbed Pb(II) in the presence of other heavy metal ions [582].

Adsorption energy is also frequently utilized to reveal the interactions between guest oxidants and the catalytic sites of MOFs in advanced oxidation systems. For example, the molecular structure of the oxidant PMS contains oxygen atoms of different types, which will lead to differences in adsorption energy values due to the different interaction models between PMS and the catalytic sites [312]. Constructing the optimal PMS adsorption model facilitates to analyze subsequent production pathway of active species, as the interaction between the catalytic site and PMS induces changes in the bond lengths of the PMS model. Usually, the regions where bond length changes are more significant are more likely to be the main areas for the acceptance or loss of electrons, which can be further validated through the identification experiments of active species to support the oxidation mechanism of the system.

20.2.3. Density of states (DOS)

DOS, including both total DOS (TDOS) and projected DOS (PDOS), is a significant calculation tool for analyzing the electronic properties of materials. First, the TDOS spectrum, particularly in the vicinity of the Fermi level, allows for a qualitative assessment of the bandgap of MOFs [610], which is indicative of their electrical conductivity. On the other hand, PDOS represents the contribution to the TDOS from each atomic orbital after projecting the TDOS onto individual atomic orbitals [611]. This approach provides a detailed view of what different elements, atoms, or even specific atomic orbitals contribute to the overall DOS. For example, in MOF-based Fenton oxidation systems, comparing the PDOS spectra before and after the bonding of the catalytic site with the oxidant can reveal the orbital hybridization, further allowing for the determination of the electron transfer direction [611]. Additionally, transition metal-based MOFs often can exhibit the strong spin polarization, and the PDOS spectra can be used to assess the spin states of the transition metal sites [612], helping to investigate whether the transition metal sites are more likely to donate or accept electrons. For instance, Fig. 19c reveals that the electron arrangement of the d orbital from Co and Mo atoms after 3*d*-4*d* orbital hybridization, leading to the synchronous increase in spin-state at both the Co and Mo sites [554]. Furthermore, the PDOS spectrum can also pro-

vide information about the D-band center of the metal sites [308]. The position and broadening of the d-band center are crucial factors that directly influence the adsorption and catalytic activities of the MOFs. As shown in Fig. 19d, the upward shift of the d-band center brings Co sites from Cu doped Co_3O_4 (obtained by ZIF-67 pyrolysis) closer to the Fermi level, causing that Cu doped Co_3O_4 displays better PMS adsorption and electron transport ability compared to pristine Co_3O_4 [308].

20.2.4. Charge analyses and electron density difference

Atomic charges provide insights into the charge distribution at reactive sites, and common methods for analyzing charge distribution include the Bader charge, Mulliken charge, and Hirshfeld charge [613–615]. In a previous study, Li *et al.* found that defective UiO-66 with zirconium vacancies exhibited more negative charges on the oxygen atoms adjacent to the zirconium vacancies by comparing to the perfect UiO-66 (Fig. S4c in Supporting information), indicating a stronger tendency of defective UiO-66 for capturing the cationic heavy metal ions [609]. In Fenton-like catalytic systems, the adsorption of oxidants will lead to significant changes in the charge at the catalytic sites, which can thus be used as a descriptor for catalytic activity [616].

Electron density difference (EDD) refers to the charge transfer occurring between interacting host and guest substances, with the strength of the interaction determining the extent of charge transfer. In studies involving the construction of MOF-based heterojunctions, the calculation of electron density difference can investigate the direction of electron transfer between the host and guest catalysts, helping to determine the type of heterojunction in conjunction with experimental and characterization analyses [617]. In the field of adsorption, electron density difference can also be assessed by examining the overlap strength of electron cloud densities and the specific number of electrons transferred, which helps to evaluate the strength of interactions formed between the adsorbates and the sorption sites [609]. In advanced oxidation systems, the interaction between oxidants and catalytic sites triggers the electron transfer, and the electron density difference results can exhibit the direction of electron transfer, which further helps to identify the types of active species that may be generated [312]. Lan *et al.* fabricated a Co-based MOF containing polyvanadate $[V_4O_{12}]^{4-}$ cluster ($Co_2(V_4O_{12})(bpy)_2$), which displayed superior elimination activity toward various micropollutants. DFT calculations (Fig. S4d in Supporting information) exhibited that the electron aggregation region was concentrated on the O-H bond from PMS, explaining why PMS can transform into the singlet oxygen intermediate ($SO_5^{\bullet-}$ radical) [312].

20.2.5. Crystal overlap hamiltonian population (COHP)

COHP analysis can be used for the quantitative evaluation of bonding strength between atoms [618]. When two adjacent atoms interact, bonding orbitals and anti-bonding orbitals will be formed. If the anti-bonding orbitals below the Fermi level are occupied, the bonding strength is weakened, meaning that the bond will lack strong chemical stability. As a quantitative measure, a smaller ICOHP value obtained through integration indicates a stronger bonding strength [619,620]. Additionally, a positive COHP value near the Fermi level suggests that the active sites possess a strong electron-donating ability [621], which can accelerate catalytic reactions.

20.2.6. Gibbs free energy

Gibbs free energy (ΔG) is commonly used to explain the formation pathways of active species *via* combining with active species quenching experiments [611,622]. In the DFT calculations, the calculation of Gibbs free energy requires the consideration of zero-point vibrational energy and entropy changes of surface adsorbates. The change in Gibbs free energy determines whether a reaction is spontaneous and the difficulty of the reaction process. In the field of Fenton-like catalysis, Gibbs free energy diagrams can be used to assess the relative ease of generating various active species [623], which helps to identify the main active species responsible for removing target contaminants. Furthermore, by calculating the difference in free energy for different MOFs or catalytic sites along the same reaction pathway, it can determine the rate-limiting step of the reaction and compare the catalytic activity of different MOFs or catalytic sites [606].

DFT calculations have broad applications in the field of MOFs for water pollution control [624]. Specifically, DFT calculations can assist researchers in characterizing the microscopic electronic properties of MOFs, which is valuable for exploring the structure-activity relationship and redox reaction mechanisms. However, there are several considerations in performing these calculations: (i) The periodicity of MOF structures, which involves a large number of atoms, can make calculations more challenging. Therefore, it is essential to optimize the structure reasonably without altering its intrinsic properties. For example, we can choose to perform non-periodic calculations on a single cell of the MOF, while ensuring the integrity of the organic ligands [625]. (ii) For transition metal-based MOFs, especially MOFs containing Fe, Co, Ni or Mn, it is crucial to account for the spin polarization of those transition metal atoms and apply DFT+U corrections during the calculation process [626], which avoids the significant errors in the calculated properties [176].

In practical applications, researchers currently tend to use DFT calculations to validate the results of experiments or characterizations. In future studies, DFT calculations can be combined with preliminary experiments to facilitate the initial screening of catalysts [627,628]. For instance, when experimental results show that the pristine MOF exhibits high redox activity after metal doping, we can utilize the DFT calculations to pre-screen other suitable doping metal elements for comparative studies, which can provide the theoretical guidance for the design of MOF-based catalysts. In conclusion, the development and rational use of DFT will play a unique role in the application of MOFs for water environmental remediation.

21. AI for environmental applications of MOFs

Mingjia Xu, Xuedong Du*

The pursuit of clean water through advanced materials has positioned MOFs at the forefront of environmental research. Their unparalleled structural and chemical tunability presents a virtually infinite design space for targeting diverse aquatic pollutants, from heavy metals and emerging pharmaceuticals to microplastics and antibiotic resistance genes. However, this very virtue of customizability constitutes a fundamental challenge: navigating this colossal chemical universe to discover optimal materials for specific applications has far surpassed the reach of traditional, sequential "trial-and-error" methodologies [629]. Even conventional computational screening, while powerful, becomes computationally prohibitive when grappling with millions of potential structures and the complex, multi-component nature of real-world wastewater.

Concurrently, the field is generating an unprecedented deluge of data, spanning from high-throughput computational simulations of aqueous-phase adsorption and catalysis to vast repositories of synthetic recipes and characterization results. This data-rich landscape presents both a challenge and an unparalleled opportunity [630]. It is at this critical juncture that Artificial Intelligence (AI), particularly machine learning (ML), emerges not merely as an incremental tool, but as a transformative force poised to orchestrate a paradigm shift in MOFs research. AI serves as a strategic accelerator and an intelligent decision-making core, capable of distill-

ing hidden structure-property relationships from complex, multi-dimensional datasets [631]. This chapter articulates how AI is forging a closed-loop, intelligent R&D framework that seamlessly integrates four pivotal stages: AI-guided in-silico design and discovery of target-specific MOFs; intelligent optimization of synthesis pathways to bridge digital models with physical reality; smart prediction and mechanistic decoding of performance in aquatic environments; and finally, system-level optimization and knowledge generation for deployable water treatment technologies. By moving beyond isolated applications, this AI-driven ecosystem is fundamentally reshaping the landscape of MOFs development, enabling a rapid, rational, and holistic approach to solving one of humanity's most pressing challenges, ensuring water security for all.

21.1. The foundation of AI in MOFs research

21.1.1. Multifaceted data as the fuel for AI

The genuine power of AI in MOFs-based water remediation research stems from its ability to synergistically integrate multifaceted data sources, thereby constructing a self-improving, intelligent R&D ecosystem. This ecosystem is founded upon three pillars of data [632]: experimental data (encompassing synthesis parameters, structural characterization, and aqueous performance metrics) forms the empirical backbone, reflecting material behavior in real-world, complex environments. Computational simulation data, such as binding energies, diffusion pathways, and electronic structures, acts as both a mechanistic probe and a performance extender, providing molecular-scale insights and high-throughput predictions to fill experimental gaps. Most prospectively, text-mined data, extracted *via* natural language processing from the vast scientific literature, captures unstructured, tacit knowledge. For instance, it can systematically identify critical negative data obscured by publication biases, such as "failed synthesis in aqueous phase" or "structural collapse at low pH". These three pillars form a powerful strategic closed loop: hypotheses generated from text mining (*e.g.*, a specific functional group improves the selective capture of heavy metal ions or organic contaminants.) can be preliminarily screened and mechanistically validated through computational simulations, which then guide targeted experimental synthesis and performance testing. The resulting experimental data, both positive and negative, continuously feeds back to calibrate the computational models and enrich the textual knowledge graph [633]. This cycle not only dramatically accelerates the discovery of high-performance MOFs but also elevates AI's role from a mere predictive tool to a strategic scientific partner capable of generating novel, testable hypotheses.

21.1.2. Core algorithms for decoding MOFs complexity

The integration of AI into MOFs-based water remediation research is fundamentally powered by a sophisticated algorithmic engine, which can be categorized into two complementary paradigms: predictive and generative models. In the realm of predictive modeling, ML algorithms are trained to establish complex, non-linear mappings between MOFs structures and their functional properties in aqueous environments. While traditional models like Random Forest rely heavily on carefully crafted feature engineering (*e.g.*, surface area, pore size, functional group identity), the emergence of Graph Neural Networks (GNNs) represents a transformative advancement. GNNs natively interpret a MOF's crystal structure as a mathematical graph, where metal clusters and organic linkers serve as nodes and edges, respectively [634]. Through iterative message-passing mechanisms, these networks learn to aggregate information from local atomic environments, autonomously capturing profound, high-level descriptors critical for predicting performance metrics such as the adsorption affinity for specific pharmaceuticals, heavy metal ion selectivity, or photocatalytic degradation efficiency for organic pollutants. This capability is well-supported by leading studies, where GNNs have demonstrated superior performance over conventional methods in predicting gas separation and storage properties, establishing a solid foundation that makes their extension to aqueous-phase prediction both a logical progression and a highly promising research frontier.

Building upon this predictive foundation, generative models facilitate a paradigm shift from high-throughput screening to genuine inverse design. Techniques such as Variational Autoencoders (VAEs) and Generative Adversarial Networks (GANs) learn the underlying probability distribution of existing MOFs structures from large databases. Once this "latent space" is mastered, these models can sample from it to propose novel, chemically plausible MOFs architectures that have never been seen before. The most powerful application is conditional generation, where the model is guided by specific performance targets as input constraints. For instance, a researcher can direct the model to "generate a MOFs structure with maximum adsorption capacity for PFOA at neutral pH and superior hydrolytic stability" [635]. The generative model then acts as a prolific in-silico designer, producing candidate structures that are intrinsically biased toward meeting these exact requirements. Pioneering studies have showcased this potential for designing diverse functional materials, heralding a new era of tailor-made MOFs for complex water treatment challenges. Together, these predictive and generative algorithms form a cohesive, intelligent core that not only interprets complex data but also proactively generates targeted, innovative material solutions, dramatically accelerating the R&D cycle for advanced water remediation technologies.

21.2. AI in action for environmental MOFs: key application domains

21.2.1. Accelerated discovery of high-performance MOFs

AI has fundamentally transformed the R&D paradigm for high-performance MOFs in water remediation, shifting it from a slow, serendipity-dependent experimental process to a rapid, rational, and predictive discovery cycle by integrating intelligent virtual screening with generative inverse design. In intelligent virtual screening, the core objective is to leverage high-performance predictive models to efficiently identify candidate materials with exceptional properties from vast MOFs databases. Taking gas adsorption as an illustrative example, recent Transformer-based models such as Uni-MOF proposed by Wang *et al.* have demonstrated remarkable multi-task predictive capability. Through self-supervised pre-training on over 630,000 three-dimensional structures of MOFs/COFs, the model autonomously extracts material features and incorporates multi-system conditions (such as gas type, temperature, and pressure) to achieve highly accurate predictions of gas adsorption capacities (*e.g.*, achieving an R^2 up to 0.98 on simulated data) [636]. Notably, it also exhibits exceptional generalization, with an R^2 of 0.85 even for previously unseen gas adsorption predictions. Importantly, this modeling framework is highly transferable: since the adsorption behavior of aqueous pollutants (*e.g.*, heavy metals and organic molecules) is analogous in physical mechanism to gas adsorption, both relying on interactions between the material's pore structure, surface chemistry, and target molecules, the structure representation learning and multi-condition integration approach employed by Uni-MOF can be seamlessly extended to the screening of adsorbents for water treatment. This provides a reliable computational foundation for the efficient and precise development of novel MOF-based water purification materials. Generative AI has overcome the limitations of conventional screening in existing MOFs databases by enabling performance-targeted "inverse design". While traditional machine learning methods, such as XGBoost in the study by Li *et al.*, can efficiently predict the adsorption performance of known

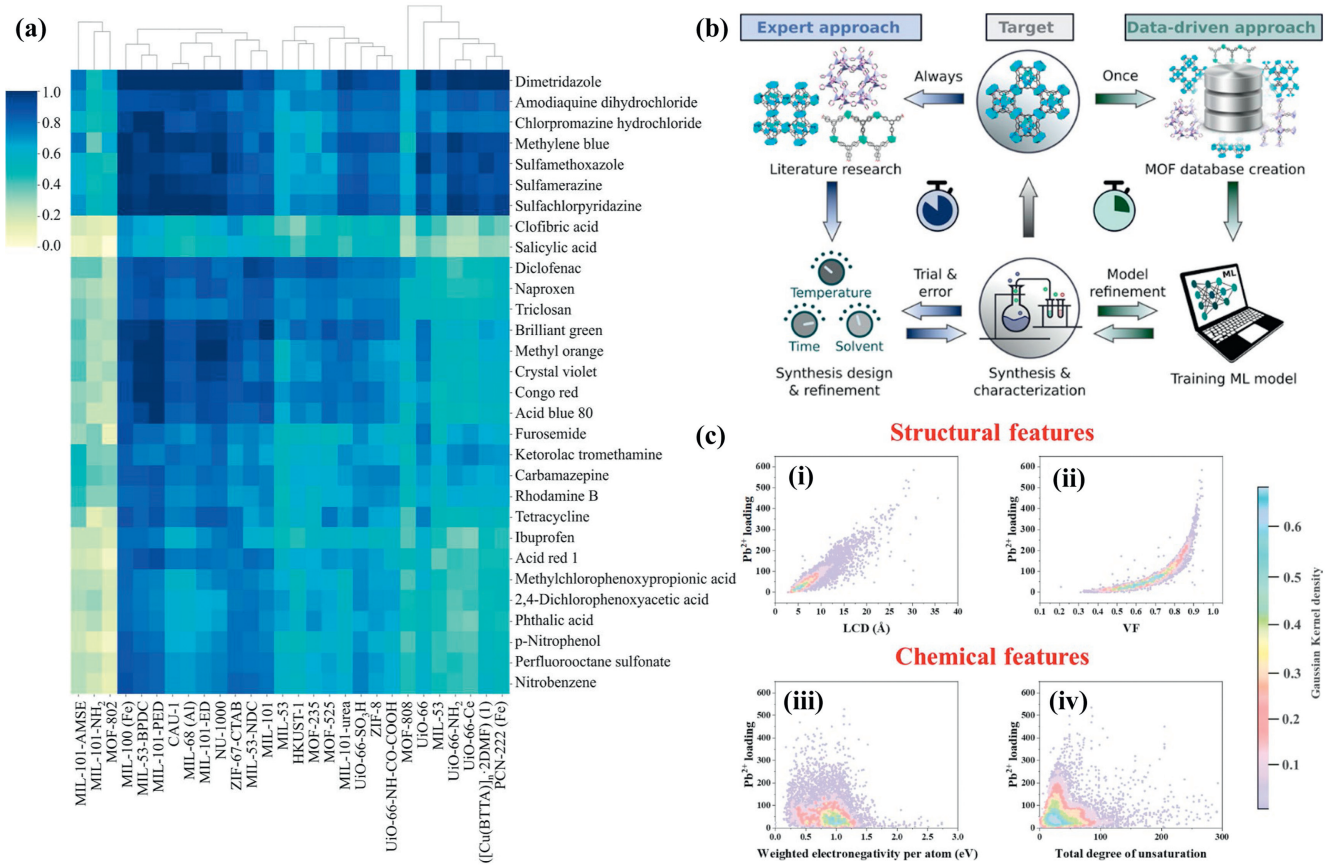


Fig. 20. (a) Heatmap of the predicted removal rate of all 28 MOFs for 30 pollutants. Copied with permission [637]. Copyright 2023, the American Chemical Society. (b) A data-driven approach (right loop), where a ML model is trained on a library of automatically extracted literature data, to then suggest synthesis conditions in a data-driven MOF discovery cycle. Copied with permission [638]. Copyright 2022, Wiley-VCH. (c) The relationships between (i) largest cavity diameter and Pb^{2+} loading; (ii) void fraction and Pb^{2+} loading; (iii) weighted electronegativity per atom and Pb^{2+} loading; (iv) Total degree of unsaturation and Pb^{2+} loading. Pb^{2+} loading is the calculated result from MS simulation, indicates the number of Pb^{2+} adsorbed by per cell. The colored contours describe the Gaussian kernel density of different MOFs, which represent density contours of MOF numbers. Copied with permission [639]. Copyright 2024, Elsevier.

MOFs (Fig. 20a), their effectiveness heavily relies on the availability of existing experimental data [637]. In contrast, generative models (including diffusion models and variational autoencoders) learn the structure-property relationships from large datasets of known MOFs, thereby constructing a continuous "chemical design space". Researchers can input complex multi-objective performance requirements, for example, "Design a Zr- or Fe-based MOFs that exhibits high adsorption capacity and high removal efficiency for clofibric acid and sulfonamide contaminants in aqueous solution under near-neutral pH, with electrostatic and π-π interactions as the dominant mechanisms". The model can then perform targeted exploration and optimization within this space, directly generating novel MOFs topologies and linker-node combinations that satisfy all predefined constraints. This offers an intelligent design pathway beyond existing databases, facilitating the development of MOFs capable of adsorbing specific pollutants that are otherwise challenging to remove using conventional materials.

21.2.2. Decoding and optimizing synthesis pathways

Deciphering and optimizing the synthesis pathways of MOFs has long been a challenge, primarily dependent on researcher experience and iterative experimentation. Luo and co-workers introduce a data-driven methodology to transform this paradigm (Fig. 20b) [638]. They first constructed a specialized MOFs synthesis database by automatically extracting critical parameters (such as metal source, linker, solvent, and temperature) from scientific literature using natural language processing. This structured data resource enabled the training of machine learning models to predict synthesis conditions directly from a MOF's crystal structure. The models, employing representations like molecular fingerprints and graph-based features, learned underlying patterns linking structure to synthesis. They demonstrated significant predictive capability for continuous variables like temperature and time. For complex choices like solvents, the model successfully recommended options based on physicochemical properties rather than a fixed list. Impressively, these computational predictions surpassed the estimation accuracy of human experts, highlighting the potential of data-driven guidance. An online tool was developed to provide the research community with immediate synthesis condition forecasts for custom MOFs structures. Throughout this process, AI is not merely decoding the "black box" of MOFs synthesis but is actively learning to control it. By predicting feasible pathways and efficiently optimizing complex recipes, AI ensures that promising materials designed in silico can be reliably and reproducibly manufactured in the laboratory, thereby paving the way for their practical deployment in water remediation technologies.

21.2.3. Unraveling complex mechanisms at the molecular level

While the predictive and generative capabilities of AI are transforming material design and synthesis, its most profound scientific contribution may lie in deciphering the fundamental molecular-level mechanisms governing MOFs interactions with aquatic

pollutants. The exceptional performance of MOFs in adsorbing or degrading pollutants stems from complex, often synergistic, interactions at the molecular scale. Traditional characterization techniques provide snapshots, while molecular simulations offer dynamics but at a prohibitive computational cost for exploring vast chemical spaces. AI bridges this gap by extracting hidden patterns from simulation data and providing real-time analysis. Yuan *et al.* unraveled the complex mechanisms of Pb^{2+} adsorption in aqueous solution by MOFs at the molecular level through an integrated approach combining machine learning, molecular simulation, and experimental validation [639]. Fig. 20c delineated two dominant adsorption trends: a direct, positive correlation of Pb^{2+} loading with structural descriptors (largest cavity diameter, void fraction), and a distinct non-linear, volcanic relationship with chemical descriptors (weighted electronegativity per atom, total degree of unsaturation), highlighting the interplay between pore accessibility and optimized affinity. This study identified pore accessibility, characterized by the largest cavity diameter, as the most critical structural descriptor, underscoring the necessity of minimizing steric hindrance for ion diffusion. Concurrently, the chemical landscape of the framework, quantified by metrics like the weighted electronegativity, was found to dictate the binding strength, exhibiting a non-linear relationship with adsorption capacity. Furthermore, evaluation under aqueous conditions highlighted the indispensable role of hydrostability; many computationally promising MOFs were deemed unsuitable due to structural degradation or competitive water adsorption. Among the hydrostable frontrunners, a statistical recurrence of specific topological patterns and a high density of carboxyl groups were observed. These carboxyl groups are posited to serve dual roles: as electron-withdrawing units that generate a favorable electrostatic potential and as potent chelating sites for direct metal ion coordination, thereby significantly enhancing the adsorption affinity and capacity for Pb^{2+}. In photocatalytic or Fenton-like reactions for pollutant degradation, understanding the electronic structure and reaction pathways is paramount [640]. AI is dramatically accelerating these discoveries. ML models can be trained to predict key electronic properties (*e.g.*, band gap, density of states, oxidation state of metal centers) directly from the MOFs structure, bypassing the need for expensive DFT calculations on every candidate material. This allows for the high-throughput screening of MOFs for photocatalytic activity [641]. For MOFs involved in AOPs, AI can help map the complex reaction pathways of ROS generation and their subsequent attack on pollutant molecules. By analyzing the trajectories and energies from a limited set of DFT-based MD simulations, ML models can identify transition states and intermediate species that are difficult to capture experimentally, providing atomistic blueprint for designing more efficient catalytic MOFs [642].

21.2.4. Towards intelligent water treatment systems

The integration of AI culminates in the transformation of molecular discoveries into intelligent water treatment ecosystems, creating a seamless pipeline from nanoscale design to macroscale system optimization. At the systems level, AI establishes predictive process models that translate fundamental material properties of MOFs into actionable engineering insights. These sophisticated models accurately forecast dynamic breakthrough behaviors and adsorption kinetics under variable operational conditions, enabling precise determination of column lifespan and regeneration requirements. Furthermore, AI-driven multi-objective optimization algorithms navigate the complex trade-offs between competing parameters, including removal efficiency, energy consumption, operational costs, and waste management, to identify Pareto-optimal solutions for specific application scenarios. The most advanced manifestation of this intelligence emerges through dynamic digital twins, where AI creates and maintains virtual replicas of physical treatment systems that continuously calibrate themselves using real-time sensor data. These digital counterparts enable predictive maintenance and adaptive control strategies, allowing systems to autonomously respond to fluctuating water quality and pollutant loads while maintaining optimal treatment performance. This systems-level intelligence effectively closes the research and development loop, where operational data from field deployments continuously informs subsequent generations of AI-designed materials and processes. Through this integrated approach, AI transcends its role as a design tool to become the core orchestrator of responsive, efficient, and self-optimizing water purification infrastructure that dynamically adapts to both present challenges and future environmental demands, ultimately establishing a new paradigm for sustainable water management [643].

21.3. Evolving frontiers and future pathways

Looking ahead, the development of AI in the MOFs-based water treatment field is poised to reshape the research paradigm along three critical directions [644]. First, AI-driven multi-objective optimization will advance material design beyond the pursuit of single performance metrics (*e.g.*, adsorption capacity) toward systematically balancing multiple often-conflicting goals, such as capacity, selectivity, stability, cost, and regeneration energy, enabling holistic optimization of material performance. Second, deeper integration with robotics and automation will give rise to "self-driving laboratories", forming a closed-loop R&D cycle where AI proposes candidate materials and synthesis routes, robotic platforms execute high-throughput synthesis and testing, and experimental data feedback refines the AI models, significantly accelerating the iteration from conceptual design to experimental validation. Finally, the development of large-scale foundation models for chemistry (*e.g.*, a "MOFs Chemistry GPT"), pre-trained on vast chemical knowledge, will equip models with profound molecular understanding and reasoning capabilities, leading to faster convergence and superior generalization in specific water treatment tasks. The synergistic progress along these three directions will collectively establish an efficient, intelligent, and sustainable new ecosystem for MOFs material development.

22. Challenges and prospectives of MOFs for clean water

Jiaxing Wu*

MOFs have emerged as a highly versatile and efficient class of materials with remarkable potential [645–647]. MOFs are crystalline compounds made of metal ions or metal clusters coordinated to organic ligands, forming a robust, porous structure with high surface areas and tunable chemical properties [648–650]. These unique characteristics make MOFs excellent candidates for applications in water purification, especially in the removal of contaminants such as heavy metals, organic pollutants, salts, and dyes.

However, while the potential of MOFs is vast, there are several challenges that hinder their large-scale application in water treatment [268,651]. Issues such as material stability, scalability, high cost of synthesis, selectivity in contaminant removal, and their ability to withstand harsh environmental conditions need to be addressed [652,653]. This review provides a comprehensive analysis of the challenges and prospects of MOFs for clean water, with a focus on their application in contaminant removal, desalination, and purification. By examining the current state of research and future opportunities, this section aims to present a clear view of the current progress and the potential future advancements of MOFs in clean water technologies.

22.1. Mechanisms of MOFs for water purification

The application of MOFs for water purification involves several mechanisms that enable them to remove contaminants effectively. These include:

(1) Adsorption: MOFs can adsorb a wide variety of contaminants through physical and chemical adsorption. Their high surface area and tunable pores provide ample space for contaminants such as heavy metals, organic pollutants, and gases to adhere to the surface of the MOF. Adsorption is often the primary mechanism by which MOFs remove pollutants from water [654].
(2) Ion Exchange: Some MOFs have metal centers that can exchange ions with the surrounding aqueous solution. This process is particularly effective for removing toxic heavy metals such as arsenic, cadmium, lead, and fluoride. The metal ions within the MOF framework can be swapped with toxic ions from the water, thus eliminating contaminants.
(3) Catalysis: MOFs can also serve as catalysts in breaking down harmful organic pollutants. Certain MOFs exhibit photocatalytic properties, enabling the degradation of organic contaminants like dyes, pesticides, and pharmaceutical residues when exposed to light. This catalytic behavior can be beneficial for water purification, especially for contaminants that are difficult to remove through conventional methods.
(4) Desalination: In addition to contaminant removal, MOFs can be used in desalination processes, specifically in the creation of membranes for reverse osmosis or forward osmosis. MOFs' high surface area and selective permeability make them suitable for separating water molecules from salt and other impurities.

22.2. Challenges in the use of MOFs for clean water

Despite their numerous advantages, there are significant challenges that hinder the widespread use of MOFs for water purification. These challenges revolve around issues such as material stability, scalability, cost, selectivity, and regeneration. Below, we discuss these challenges in greater detail.

22.2.1. Stability in aqueous environments

One of the primary challenges associated with MOFs is their stability in aqueous environments. Many MOFs are susceptible to hydrolysis, a process in which water molecules break the metal-ligand bonds, leading to the collapse of the MOF structure. This degradation significantly reduces the material's adsorption capacity and structural integrity, which limits its effectiveness in real-world water treatment applications.

For example, MOFs such as ZIF-8 (Zinc-based) are stable under dry conditions but degrade rapidly when exposed to water . Similarly, MIL-53 (Aluminum-based) can undergo hydrolytic instability when exposed to water at high temperatures, which may cause the loss of the material's porosity and functionality.

The Hard and Soft Acids and Bases (HSAB) theory provides a framework for designing MOFs with enhanced water stability. By selecting metal centers and organic ligands based on their acid-base characteristics (hard and soft), one can achieve more stable interactions, especially in aqueous environments. Enhancing the water stability of MOFs can be achieved through post-synthesis modifications or derivation strategies. This approach involves modifying the MOF structure after its synthesis to increase its resistance to water-induced degradation. Loading or functionalizing MOFs with specific guest molecules or materials can enhance their resistance to water-induced degradation. These loaded MOFs have added functionalities that protect the framework or reduce its interaction with water.

To overcome this challenge, research is focusing on developing more stable MOFs using more resilient metals like iron, magnesium, and calcium, which are less prone to hydrolysis. Additionally, strategies like the incorporation of inorganic clusters or hybrid composites (MOFs combined with materials like graphene oxide or carbon nanotubes) can enhance the structural stability of MOFs in aqueous environments. By leveraging the principles of the HSAB theory, deriving MOFs through post-synthesis modifications, and loading functional species into the MOF structure, we can design more stable MOFs for use in water-sensitive applications. These strategies can significantly enhance the durability of MOFs in aqueous environments, making them suitable for applications such as catalysis, gas storage, and environmental sensing. However, ongoing research is essential to overcome the challenges of scalability and long-term stability in real-world conditions.

22.2.2. Scalability and cost-effectiveness

While MOFs show remarkable performance in laboratory settings, their scalability and cost-effectiveness remain significant challenges. The synthesis of MOFs often requires precise control over reaction conditions such as temperature, solvent, and pressure [655]. These controlled conditions, while necessary for achieving high-quality MOFs, also make large-scale production expensive and energy-intensive.

Additionally, the use of precious metals (*e.g.*, platinum or gold) as metal centers in some MOFs further increases the cost. The reliance on these rare and expensive materials makes MOF-based technologies less feasible for large-scale water purification applications, especially in low-income regions where cost is a major constraint.

When designing water-stable MOFs, it's important not only to consider low-cost metals but also to incorporate low-cost, green ligands. These green ligands, such as natural small organic acids, purines, and other bio-based molecules, can contribute to the creation of environmentally friendly and cost-effective MOFs. This approach aligns with sustainable chemistry principles and reduces the overall environmental footprint of MOF production. Low-cost metals play a crucial role in developing affordable and scalable MOFs. The choice of ligands significantly affects the structure, stability, and sustainability of MOFs. Green ligands, especially those derived from natural sources, offer a cost-effective and environmentally friendly alternative to synthetic organic ligands. Several green ligands, including natural small organic acids and purine derivatives, have been explored for MOF synthesis. By combining low-cost, green metals with natural small organic acids and purine derivatives, we can design green MOFs that are not only environmentally friendly but also cost-effective and water-stable.

To address these issues, there is a growing emphasis on developing low-cost synthesis methods and using earth-abundant metals (*e.g.*, iron, magnesium, zinc) instead of precious metals. Researchers are also exploring green chemistry approaches and continuous-flow synthesis methods that could make the production of MOFs more scalable, sustainable, and cost-effective. The integration of low-cost, green metals and ligands—such as natural small organic acids and purine derivatives—into the design of MOFs offers a path toward sustainable, cost-effective, and water-stable materials. These green MOFs hold promise for applications in areas such as catalysis, environmental remediation, and energy storage, aligning with the principles of green chemistry and sustainable materials development. Moving forward, advances in synthesis techniques and the scalability of green ligands will be key to unlocking the full potential of these environmentally friendly MOFs.

22.2.3. Regeneration and reusability

For MOFs to be economically viable in water treatment, they need to be regenerated and reused multiple times without significant loss of performance. However, regenerating MOFs can be challenging due to their structural fragility and chemical instability under harsh regeneration conditions. The processes typically used to regenerate MOFs, such as thermal desorption, chemical washing, or electrochemical regeneration, often lead to irreversible damage to the MOF structure or loss of metal ions, which limits their ability to retain their adsorption capacity.

For example, thermal regeneration may involve heating the MOF to high temperatures to remove adsorbed contaminants, but this can cause the MOF to collapse or lose its functional properties. Chemical regeneration can involve the use of harsh solvents or acidic conditions, which may also degrade the MOF material.

To overcome these challenges, researchers are focusing on developing more stable MOFs that can withstand repeated regeneration cycles without degradation. Strategies such as designing MOFs with higher thermal stability or exploring gentler regeneration methods like electrochemical desorption could enhance the material's reusability and make MOF-based water treatment systems more cost-effective in the long run.

22.2.4. Selectivity and efficiency in contaminant removal

Another challenge in using MOFs for water purification is their selectivity in contaminant removal. While MOFs can adsorb a wide variety of pollutants, achieving high selectivity for specific contaminants remains difficult. In real-world water, multiple contaminants, such as heavy metals, organic compounds, and minerals, are often present, and MOFs may compete for the same adsorption sites.

For instance, while MOFs are highly effective at removing arsenic or lead, they may also adsorb essential ions like calcium, magnesium, and potassium, which are important for human health. This lack of selectivity can lead to inefficient water treatment and undesired outcomes, such as the removal of beneficial minerals from drinking water.

Researchers are working on designing MOFs with selective adsorption properties that can target specific contaminants while avoiding the uptake of essential ions. This could involve functionalizing the MOF surface with specific chemical groups that bind only to target contaminants or adjusting the pore size to selectively capture particular molecules.

22.3. Prospects of MOFs in clean water applications

Despite the challenges, the prospects for the use of MOFs in clean water applications remain highly promising. Ongoing advancements in MOF design, synthesis techniques, and hybrid materials are paving the way for overcoming many of the limitations associated with these materials. In this section, we will explore the exciting opportunities for MOFs in addressing the global water crisis.

22.3.1. Design and engineering of stable MOFs

The development of stable MOFs that can withstand exposure to water, pH fluctuations, and other environmental conditions is a key area of research. Several strategies have been proposed to improve the stability of MOFs, including the use of metal-organic composites or hybrids that combine the best properties of MOFs with other materials such as carbon nanotubes, graphene oxide, and polymers. These hybrid materials exhibit enhanced mechanical strength, chemical stability, and resilience under harsh conditions.

Moreover, the use of iron-based MOFs, which are more stable in water than other metal-based frameworks, is showing promise. Fe-MOFs, such as Fe-MOF-74, are gaining attention for their potential use in water purification, particularly for the removal of arsenic and fluoride ions.

22.3.2. Hybrid materials and composite MOFs

Hybrid MOFs that combine the adsorption capabilities of MOFs with the mechanical strength and chemical stability of other materials, such as graphene oxide, are an exciting prospect for clean water applications. These composites offer enhanced performance in water treatment, with improved regeneration ability, adsorption efficiency, and long-term stability. The development of MOF-carbon composites is an active area of research, especially for desalination and heavy metal removal.

For example, MOF-graphene composites have shown improved water permeation and salt rejection in desalination applications, making them potential candidates for reverse osmosis membranes.

22.3.3. Integration of MOFs with existing water treatment technologies

MOFs can be integrated into existing water purification systems to enhance their performance. For example, MOFs can be used as an additional filtration or adsorption layer in multi-stage filtration systems, combining with traditional methods such as activated carbon filtration, UV disinfection, and reverse osmosis. This integration can enhance the efficiency of water treatment systems, making them more effective at removing a broad range of contaminants.

In desalination, the use of MOF-based membranes has the potential to reduce the energy consumption and cost associated with traditional reverse osmosis systems. MOFs' selectivity and permeability make them ideal candidates for water filtration and desalination applications, offering a potential breakthrough in sustainable water purification.

22.3.4. Sustainable and eco-friendly water purification

As concerns about environmental sustainability grow, MOFs offer a green alternative for water purification. MOFs can be synthesized from renewable materials and designed to be easily regenerated and recycled. This makes them an attractive option for sustainable water treatment systems that can be operated with minimal environmental impact.

Researchers are working on developing zero-waste water treatment systems that use MOFs to remove pollutants from water, after which the MOFs can be regenerated and reused without producing harmful waste or requiring significant energy input. This approach could revolutionize water purification by providing a more energy-efficient and sustainable alternative to conventional methods.

23. Conclusion and outlook

Jiaxing Wu*

MOFs demonstrate significant potential in clean water applications, yet their implementation faces challenges while offering broad prospects for development. The following provides a detailed analysis:

23.1. Challenges

(1) Insufficient stability: MOFs exhibit poor water resistance and corrosion resistance in complex aquatic environments, prone to degradation during prolonged use or under harsh conditions, thereby impacting performance and service life.
(2) High cost: Complex preparation processes involving precise assembly of metal ions and organic ligands result in elevated material costs, limiting large-scale adoption.

(3) Unclear mechanisms: The microscopic mechanisms governing adsorption and catalytic processes remain incompletely elucidated, hindering targeted optimization and design of high-performance materials.
(4) Recovery challenges: MOFs are predominantly powder-based, making post-reaction recovery and reuse difficult, thereby increasing costs and environmental burdens.
(5) Limited selectivity: Adsorption or catalytic selectivity for certain pollutants is insufficient, potentially requiring integration with other technologies.

23.2. Prospects

(1) Technological innovation: Develop novel immobilization techniques, such as *in-situ* growth and secondary growth methods, to enhance material recovery rates and stability, enabling engineering applications.
(2) Functional modification: Enhance selective adsorption and catalytic performance through surface modification and composite methods, improving removal efficiency for specific pollutants.
(3) Cost Optimization: Optimize preparation processes and explore low-cost metal ions and organic ligands to reduce material costs, driving large-scale adoption.
(4) Mechanism research: Deepen understanding of adsorption and catalytic mechanisms to provide theoretical support for material design, enabling development of more efficient and stable MOFs.
(5) Multi-technology integration: Combine with advanced oxidation processes and membrane separation technologies to build integrated water treatment systems, improving treatment effectiveness and efficiency.
(6) Application scenario expansion: Beyond atmospheric water harvesting and wastewater treatment, extend applications to seawater desalination and groundwater remediation to meet diverse scenario demands.

MOFs present a promising and versatile solution for addressing the global clean water crisis. With their unique properties, such as high surface area, tunable pore sizes, and chemical versatility, MOFs offer a wide range of potential applications in water purification, including the removal of heavy metals, organic contaminants, salts, and dyes. However, several challenges, including material stability, scalability, regeneration, and selectivity, need to be addressed for MOFs to be adopted on a large scale.

Ongoing research into stable MOF designs, hybrid materials, cost-effective synthesis methods, and integration with existing water treatment technologies holds great promise for overcoming these challenges. As research progresses, MOFs could play a crucial role in providing clean, safe, and sustainable water solutions for communities worldwide, contributing to a more sustainable future for water purification.

This review offers an in-depth analysis of the challenges and prospects of MOFs for clean water applications. It emphasizes both the barriers that need to be overcome and the opportunities that exist for these materials to revolutionize water purification. In summary, while MOFs face challenges in the field of clean water, technological innovation, mechanism research, and multi-technology integration hold promise for overcoming these difficulties. This approach could enable broader applications and provide robust support for addressing the global water crisis.

CRediT authorship contribution statement

Xiao-Hong Yi: Writing – original draft, Investigation. **Hong-Yu Chu:** Writing – review & editing. **Chao-Yang Wang:** Writing – original draft, Investigation. **Hang Ren:** Writing – original draft, Investigation. **Li-hong Zhou:** Writing – original draft, Investigation. **Yujie Zhao:** Writing – review & editing. **Fu-Xue Wang:** Writing – original draft, Investigation. **Hao Du:** Writing – original draft, Investigation. **Yixuan Zhai:** Writing – original draft, Investigation. **Tao Xia:** Writing – original draft, Investigation. **Shaohua Guo:** Writing – original draft, Investigation. **Xiaoning Wang:** Writing – original draft, Investigation. **Yunlong Wang:** Writing – original draft, Investigation. **Qian Wen:** Writing – original draft, Investigation. **Ge Shen:** Writing – original draft. **Meng Yang:** Writing – review & editing. **Yu-Hang Li:** Writing – original draft, Investigation. **Mingjia Xu:** Writing – original draft, Investigation. **Xiaoyuan Zhang:** Writing – review & editing, Funding acquisition, Formal analysis. **Hao Wang:** Writing – review & editing, Formal analysis. **Xudong Zhao:** Writing – review & editing, Formal analysis. **Yifei Sun:** Writing – review & editing, Formal analysis. **Yi-Lin Liu:** Writing – review & editing, Formal analysis. **Qingyi Zeng:** Writing – review & editing, Formal analysis. **Yuying Deng:** Writing – review & editing, Formal analysis. **Qi Wang:** Writing – review & editing, Formal analysis. **Xiaodong Zhang:** Writing – review & editing, Formal analysis. **Jie Li:** Writing – review & editing, Funding acquisition, Formal analysis. **Ning Liu:** Writing – review & editing, Formal analysis. **Chuanxi Yang:** Writing – review & editing, Formal analysis. **Jiansheng Li:** Writing – review & editing, Funding acquisition, Formal analysis. **Anping Wang:** Writing – review & editing, Formal analysis. **Xun Wang:** Writing – review & editing, Formal analysis. **Xuchun Qiu:** Writing – review & editing, Writing – original draft, Formal analysis. **Haodong Ji:** Writing – review & editing, Formal analysis. **Xuedong Du:** Writing – review & editing, Funding acquisition, Formal analysis. **Jiaxing Wu:** Writing – review & editing, Funding acquisition, Formal analysis. **Chong-Chen Wang:** Writing – review & editing.

Acknowledgments

This work was supported by the National Natural Science Foundation of China (Nos. 22176012, 52370025, 42377047, 22276096 and 52470082), Jing-Jin-Ji Regional Integrated Environmental Improvement-National Science and Technology Major-Project (2024ZD1200503), Hebei Natural Science Foundation (No. E2023203123), Open Research Fund of Hubei Key Laboratory of Pollutant Analysis & Reuse Technology (No. PA250220) and Talent Introduction Project of Hubei Normal University.

Supplementary materials

Supplementary material associated with this article can be found, in the online version, at doi:10.1016/j.cclet.2025.112243.

References

[1] K.T. Smith, A.K. Yadav, K.C. Stylianou, Nat. Commun. 16 (2025) 7986.
[2] S.R. Batten, N.R. Champness, X.-M. Chen, et al., CrystEngComm 14 (2012) 3001–3004.
[3] S.R. Batten, N.R. Champness, X.-M. Chen, et al., Pure Appl. Chem. 85 (2013) 1715–1724.
[4] H. Furukawa, F. Gándara, Y.-B. Zhang, et al., J. Am. Chem. Soc. 136 (2014) 4369–4381.
[5] Q. Huang, Q. Niu, X.F. Li, et al., Sci. Adv. 8 (2022) eadd5598.
[6] C. Wang, X. Liu, N. Keser Demir, J.P. Chen, K. Li, Chem. Soc. Rev. 45 (2016) 5107–5134.
[7] S. Modak, M. Kasula, M.R. Esfahani, ACS Appl. Eng. Mater. 1 (2023) 744–755.
[8] H. Furukawa, K.E. Cordova, M. O'Keeffe, O.M. Yaghi, Science 341 (2013) 1230444.
[9] X. Liu, X. Wang, F. Kapteijn, Chem. Rev. 120 (2020) 8303–8377.
[10] R.X. Mei, P. Wang, X.H. Yi, C.C. Wang, Environ. Sci.: Nano (2025), doi:10.1039/D5EN00657K.
[11] R.G. Pearson, J. Am. Chem. Soc. 85 (1963) 3533–3539.
[12] Y. Peng, H. Huang, Y. Zhang, et al., Nat. Commun. 9 (2018) 187.
[13] Y.J. Zhang, J.-S. Tao, Y. Hu, et al., Nat. Water 2 (2024) 770–781.

[14] C.C. Wang, J.R. Li, X.L. Lv, Y.Q. Zhang, G. Guo, Energy Environ. Sci. 7 (2014) 2831–2867.
[15] J. Li, G. Lin, H. Liang, et al., Coord. Chem. Rev. 545 (2025) 217010.
[16] F. Pasanen, R.O. Fuller, F. Maya, Chem. Eng. J. 455 (2023) 140405.
[17] Z.X. Liu, H.Y. Chu, X.H. Yi, et al., Environ. Sci.: Nano (2025), doi:10.1039/D5EN00739A.
[18] N. Kolobov, M.G. Goesten, J. Gascon, Angew. Chem. Int. Ed. 60 (2021) 26038–26052.
[19] W. Qu, T. Jin, K. Huang, et al., Adv. Mater. (2025) e12877, doi:10.1002/adma.202512877.
[20] Y. Song, W. Zhu, C. Wang, et al., Adv. Mater. 37 (2025) 2504364.
[21] F. Ahmadijokani, A. Ghaffarkhah, H. Molavi, et al., Adv. Funct. Mater. 34 (2024) 2305527.
[22] Y. Wang, M. Zhao, C. Hou, et al., Chem. Eng. J. 414 (2021) 128940.
[23] H.Y. Chu, Z.X. Liu, J.F. Wang, et al., Water Res (2025) 125008, doi:10.1016/j.watres.2025.125008.
[24] H.Y. Chu, Z.M. Huang, G. Shen, Y. Dong, C.C. Wang, Environ. Sci.: Nano 12 (2025) 2901–2910.
[25] Z. Han, Y. Yang, J. Rushlow, et al., Chem. Soc. Rev. 54 (2025) 367–395.
[26] S. Yuan, L. Feng, K. Wang, et al., Adv. Mater. 30 (2018) 1704303.
[27] N. Stock, S. Biswas, Chem. Rev. 112 (2012) 933–969.
[28] A.U. Czaja, N. Trukhan, U. Müller, Chem. Soc. Rev. 38 (2009) 1284–1293.
[29] O.M. Yaghi, A. Phoenix, United States patents, 1997, US005648508A.
[30] P. Du, L. Yuan, T. Bao, et al., Chin. Chem. Lett. 36 (2025) 110472.
[31] Y. Wang, C. Lu, D. Jiao, et al., Chin. Chem. Lett. (2025) 111979, doi:10.1016/j.cclet.2025.111979.
[32] D.E. Akporiaye, I.M. Dahl, A. Karlsson, R. Wendelbo, Angew. Chem. Int. Ed. 37 (1998) 609–611.
[33] K. Jin, X. Huang, L. Pang, et al., Chem. Commun. (2002) 2872–2873.
[34] T.J. Azbell, T.A. Pitt, M.M. Bollmeyer, et al., Angew. Chem. Int. Ed. 62 (2023) e202218252.
[35] X. Sang, J. Zhang, J. Xiang, et al., Nat. Commun. 8 (2017) 175.
[36] U. Mueller, M. Schubert, F. Teich, et al., J. Mater. Chem. 16 (2006) 626–636.
[37] Y. Liu, Y. Wei, M. Liu, et al., Angew. Chem. Int. Ed. 60 (2021) 2887–2891.
[38] Y. Gao, F. Wang, C.-C. Wang, X.-H. Yi, Surf. Interfaces 44 (2024) 103724.
[39] Z. Ni, R.I. Masel, J. Am. Chem. Soc. 128 (2006) 12394–12395.
[40] H. Zhang, J. Zhong, G. Zhou, et al., J. Nanomater. 2016 (2016) 9648386.
[41] C.Y. Wang, C.C. Wang, H.Y. Chu, et al., Sep. Purif. Technol. 331 (2024) 125589.
[42] J.M. Marrett, F. Effaty, X. Ottenwaelder, T. Friščić, Adv. Mater. (2025) 2418707, doi:10.1002/adma.202418707.
[43] A. Pichon, A. Lazuen-Garay, S.L. James, CrystEngComm 8 (2006) 211–214.
[44] X.H. Yi, S.Q. Ma, X.D. Du, et al., Chem. Eng. J. 375 (2019) 121944.
[45] X. Du, X. Yi, P. Wang, J. Deng, C.C. Wang, Chin. J. Catal. 40 (2019) 70–79.
[46] X.H. Yi, H. Ji, C.C. Wang, et al., Appl. Catal. B: Environ. 293 (2021) 120229.
[47] C.Y. Wang, C.C. Wang, H.Y. Chu, P. Wang, Sci. Total Environ. 1003 (2025) 180730.
[48] L.G. Qiu, Z.Q. Li, Y. Wu, et al., Chem. Commun. (2008) 3642–3644.
[49] S. Hajra, M. Sahu, A.M. Padhan, et al., Adv. Funct. Mater. 31 (2021) 2101829.
[50] R. Ameloot, F. Vermoortele, W. Vanhove, et al., Nat. Chem. 3 (2011) 382–387.
[51] J.O. Kim, W.T. Koo, H. Kim, et al., Nat. Commun. 12 (2021) 4294.
[52] I.A. Ibarra, P.A. Bayliss, E. Pérez, et al., Green Chem 14 (2012) 117–122.
[53] L. Peng, J. Zhang, Z. Xue, et al., Nat. Commun. 5 (2014) 4465.
[54] K. Yu, T. Ji, M. Wu, et al., Angew. Chem. Int. Ed. 64 (2025) e202422709.
[55] J. Troyano, C. Çamur, L. Garzón-Tovar, et al., Acc. Chem. Res. 53 (2020) 1206–1217.
[56] A. Carné-Sánchez, K.C. Stylianou, C. Carbonell, et al., Adv. Mater. 27 (2015) 869–873.
[57] J.J. Richardson, K. Liang, F. Lisi, et al., Eur. J. Inorg. Chem. 2016 (2016) 4499–4504.
[58] M. Chang, Y. Wei, D. Liu, J.X. Wang, J.F. Chen, Angew. Chem. 133 (2021) 26594–26600.
[59] X. Jiang, Z.e. Lin, X. Zeng, et al., Chem. Commun. 55 (2019) 12192–12195.
[60] S. Liu, C. Dun, F. Yang, et al., Nat. Commun. 15 (2024) 9365.
[61] E.G. Rasmussen, J. Kramlich, I.V. Novosselov, ACS Sustainable Chem. Eng. 8 (2020) 9680–9689.
[62] P. Zhang, X. Kang, L. Tao, et al., CCS Chemistry 5 (2023) 1462–1469.
[63] Y.K. Seo, J. Yoon, J. Lee, et al., Microporous Mesoporous Mater. 157 (2012) 137–145.
[64] D. Crawford, J. Casaban, R. Haydon, et al., Chem. Sci. 6 (2015) 1645–1649.
[65] Z. Zheng, H.L. Nguyen, N. Hanikel, et al., Nat. Protoc. 18 (2023) 136–156.
[66] C. Van Goethem, M. Mertens, F.G. Cirujano, et al., Chem. Commun. 54 (2018) 7370–7373.
[67] H.Y. Chu, M.Y. Wang, C.C. Wang, et al., Sep. Purif. Technol. 340 (2024) 126800.
[68] H.K. Pham, Y. Sim, M. Carboni, D. Meyer, N. Mathews, J. Environ. Chem. Eng. 10 (2022) 108346.
[69] J.J. Roy, S. Rarotra, V. Krikstolaityte, et al., Adv. Mater. 34 (2022) 2103346.
[70] M. Yeganeh, M. Farzadkia, A.J. Jafari, et al., J. Environ. Manage. 345 (2023) 118755.
[71] S. Pathan, J. Raveendran, M. Memon, et al., Chem. Eng. J. 511 (2025) 162217.
[72] X. Zhao, C. Zhang, B. Liu, et al., Resour. Conserv. Recy. 188 (2023) 106647.
[73] P. Dong, T. Maneerung, W.C. Ng, et al., J. Hazard. Mater. 321 (2017) 62–72.
[74] G. Zhan, W.C. Ng, W.Y. Lin, S.N. Koh, C.H. Wang, Environ. Sci. Technol. 52 (2018) 3008–3015.
[75] Y. Yao, C. Liu, C. Xiao, et al., Chem. Eng. J. 519 (2025) 165620.
[76] M. El-Shahat, R.M. Abdelhameed, Appl. Catal. A: Gen. 635 (2022) 118558.
[77] J.N. Joshi, C.M. Moran, H.P. Feininger, J.M. Dow, K.S. Walton, Cryst. Growth Des. 19 (2019) 5097–5104.
[78] T.S. Crickmore, H.B. Sana, H. Mitchell, M. Clark, D. Bradshaw, Chem. Commun. 57 (2021) 10592–10595.
[79] F. Awaja, D. Pavel, Eur. Polym. J. 41 (2005) 1453–1477.
[80] C.A. Trickett, K.J. Gagnon, S. Lee, et al., Angew. Chem. Int. Ed. 54 (2015) 11162–11167.
[81] S. Zhang, Y. Zhuo, C.I. Ezugwu, et al., Environ. Sci. Technol. 55 (2021) 8341–8350.
[82] X. Xie, L. Peng, H. Yang, et al., Adv. Mater. 33 (2021) 2101038.
[83] D. Salionov, O.O. Semivrazhskaya, N.P. Casati, et al., Nat. Commun. 13 (2022) 3762.
[84] C.Y. Wang, H.Y. Chu, C.C. Wang, Coord. Chem. Rev. 518 (2024) 216106.
[85] R.J.A. Bool, G.C. Luwalhati, N.E.Y. Tan, A.P. Aquino, R.D. Maalihan, Mater. Today: Proc. 65 (2022) 3312–3320.
[86] W.P. Deleu, I. Stassen, D. Jonckheere, R. Ameloot, D.E. De Vos, J. Mater. Chem. A 4 (2016) 9519–9525.
[87] X. Dyosiba, J. Ren, N.M. Musyoka, et al., Ind. Eng. Chem. Res. 58 (2019) 17010–17016.
[88] X. Dyosiba, J. Ren, N.M. Musyoka, et al., Sustain. Mater. Techno. 10 (2016) 10–13.
[89] A. Ghosh, G. Das, J. Environ. Chem. Eng. 9 (2021) 105288.
[90] B. Slater, S.O. Wong, A. Duckworth, et al., Chem. Commun. 55 (2019) 7319–7322.
[91] S.Y. Pan, Y.Y. Hsiao, S. Negi, B.M. Matsagar, K.C.W. Wu, ACS Sustainable Chem. Eng. 12 (2024) 17793–17805.
[92] D.M. Kabtamu, Y.N. Wu, Q. Chen, et al., ACS Sustainable Chem. Eng. 8 (2020) 12443–12452.
[93] P. He, Z. Hu, Z. Dai, et al., ChemSusChem 16 (2023) e202201935.
[94] P. Waribam, T.R. Katugampalage, M. Ogawa, et al., ACS Sustainable Chem. Eng. 13 (2025) 9576–9587.
[95] J. Ren, X. Dyosiba, N.M. Musyoka, et al., Int. J. Hydrogen Energy 41 (2016) 18141–18146.
[96] Y. Heng, Z. Fang, J. Li, et al., J. Colloid Interface Sci. 650 (2023) 836–845.
[97] P. Dubey, V. Shrivastav, P.H. Maheshwari, et al., J. Energy Storage 68 (2023) 107828.
[98] Y. Kim, P. Kalimuthu, G. Nam, J. Jung, Environ. Res. 224 (2023) 115532.
[99] M. Sharma, P. Sharma, V.C. Janu, R. Gupta, J. Mater. Chem. A 12 (2024) 26833–26847.
[100] L. Bazzi, K. Boukayouht, S. Mansouri, S. El Hankari, Process Saf. Environ. 191 (2024) 750–759.
[101] P. Waribam, T.R. Katugampalage, P. Opaprakasit, et al., Chem. Eng. J. 473 (2023) 145349.
[102] X. Zhang, Q. Cao, J. Xu, Y. Zhang, W. Xiang, J. Environ. Chem. Eng. 13 (2025) 118626.
[103] H. Bai, P. He, L. Hao, et al., Chem. Eng. J. 456 (2023) 140994.
[104] B. Chen, L. Liu, Y. Song, et al., Mater. Today Sustain. 24 (2023) 100561.
[105] X. Zhang, K. Yue, R. Rao, et al., Appl. Catal. B: Environ. 310 (2022) 121300.
[106] L. Karam, A. Miglio, S. Specchia, et al., Mater. Adv. 2 (2021) 2750–2758.
[107] J. Yang, J. Wu, P. Feng, et al., J. Clean. Prod. 261 (2020) 121235.
[108] F. Hiroyasu, K. Nakeun, G. Yong Bok, et al., Science 329 (2010) 424–428.
[109] I. Pacheco-Fernández, P. González-Hernández, J. Pasán, J.H. Ayala, V. Pino, Handbook of Smart Materials in Analytical chemistry 2019, pp. 463–502.
[110] J.R. Li, J. Sculley, H.C. Zhou, Chem. Rev. 112 (2012) 869–932.
[111] D. Perl, S.J. Lee, A. Ferguson, G.B. Jameson, S.G. Telfer, Nat. Chem. 15 (2023) 1358–1364.
[112] O.M. Yaghi, M. O'Keeffe, N.W. Ockwig, et al., Nature 423 (2003) 705–714.
[113] M. Eddaoudi, D.B. Moler, H. Li, et al., Acc. Chem. Res. 34 (2001) 319–330.
[114] Z. Wang, S.M. Cohen, Chem. Soc. Rev. 38 (2009) 1315–1329.
[115] Z. Wang, S.M. Cohen, J. Am. Chem. Soc. 129 (2007) 12368–12369.
[116] M. Kalaj, S.M. Cohen, ACS Central Sci 6 (2020) 1046–1057.
[117] J. Koo, I.C. Hwang, X. Yu, et al., Chem. Sci. 8 (2017) 6799–6803.
[118] D. Jędrzejowski, M. Ryndak, G. Jajko-Liberka, et al., Chem. Mater. 37 (2025) 5206–5216.
[119] D. Ge, H.K. Lee, J. Chromatogr. A 1263 (2012) 1–6.
[120] S. Yang, C. Chen, Z. Yan, Q. Cai, S. Yao, J. Sep. Sci. 36 (2013) 1283–1290.
[121] X.F. Chen, H. Zang, X. Wang, et al., Analyst 137 (2012) 5411–5419.
[122] I. Guerra-Martín, A. Gutiérrez-Serpa, A.I. Jiménez-Abizanda, J. Pasán, V. Pino, Microchem. J. 195 (2023) 109502.
[123] N. Li, L. Zhang, L. Nian, et al., J. Agric. Food Chem. 63 (2015) 2154–2161.
[124] J. Gao, C. Huang, Y. Lin, P. Tong, L. Zhang, J. Chromatogr. A 1436 (2016) 1–8.
[125] M. Li, X. Ren, Y. Gao, et al., Chin. Chem. Lett. 35 (2024) 109699.
[126] J. Zhu, Y. Hao, Z. Song, et al., Chin. Chem. Lett. 36 (2025) 111290.
[127] D. Ge, H.K. Lee, J. Chromatogr. A 1218 (2011) 8490–8495.
[128] Y. Hu, Z. Huang, J. Liao, G. Li, Anal. Chem. 85 (2013) 6885–6893.
[129] L. Pang, H. Feng, X. Hu, et al., Microchem. J. 215 (2025) 114468.
[130] C. Hu, M. He, B. Chen, C. Zhong, B. Hu, J. Chromatogr. A 1310 (2013) 21–30.
[131] Q. Han, T. Aydan, L. Yang, et al., Anal. Chim. Acta 1009 (2018) 48–55.
[132] M. Jian, R. Qiu, Y. Xia, et al., Sci. Adv. 6 (2020) eaay3998.
[133] Y.Y. Zhou, X.P. Yan, K.N. Kim, S.W. Wang, M.G. Liu, J. Chromatogr. A 1116 (2006) 172–178.
[134] H. Furukawa, Y.B. Go, N. Ko, et al., Inorg. Chem. 50 (2011) 9147–9152.
[135] M.J. Katz, Z.J. Brown, Y.J. Colón, et al., Chem. Commun. 49 (2013) 9449–9451.
[136] L. Hua, M.B. Solomon, D.M. D'Alessandro, W.A. Donald, J. Hazard. Mater. 494 (2025) 138679.
[137] Q.H. Hu, A.M. Song, X. Gao, et al., Nat. Commun. 15 (2024) 1558.

[138] J. Luo, F. Luo, H. Li, et al., Angew. Chem. Int. Ed. 137 (2025) e202514746.
[139] Y. Yu, N. Xu, J. Zhang, et al., ACS Appl. Mater. Interfaces 12 (2020) 16903–16911.
[140] K. Alt, F. Carraro, E. Jap, et al., Adv. Mater. 34 (2022) 2106607.
[141] J.G. Nguyen, S.M. Cohen, J. Am. Chem. Soc. 132 (2010) 4560–4561.
[142] Y. Liang, X. Yang, X. Wang, et al., Nat. Commun. 14 (2023) 5223.
[143] R. Ahmad, A.G. Wong-Foy, A.J. Matzger, Langmuir 25 (2009) 11977–11979.
[144] S.-S. Liu, C.-X. Yang, S.-W. Wang, X.-P. Yan, Analyst 137 (2012) 816–818.
[145] S.K. Firooz, D.W. Armstrong, Anal. Chim. Acta 1234 (2022) 340208.
[146] S. Ehrling, C. Kutzscher, P. Freund, et al., Microporous Mesoporous Mater 263 (2018) 268–274.
[147] F. Fan, X. Lu, X. Liang, L. Wang, Y. Guo, J. Chromatogr. A 1662 (2022) 462745.
[148] T. Si, S. Wang, H. Zhang, et al., Microchim. Acta 188 (2021) 76.
[149] A.A. Lahcen, S.G. Surya, T. Beduk, et al., ACS Appl. Mater. Interfaces 14 (2022) 49399–49424.
[150] H. Hu, Y. Wang, TrAC, Trends Anal. Chem. 171 (2024) 117520.
[151] Y. Kong, Y. Sun, Z. Tian, S. Liu, N. Li, Colloids Surf., B 252 (2025) 114670.
[152] L. Zeng, H. Cui, J. Chao, et al., Microchim. Acta 187 (2020) 142.
[153] H. Liu, T. Ni, L. Mu, et al., Sensor. Actuat. B: Chem. 256 (2018) 1038–1044.
[154] Z. Iskierko, P.S. Sharma, D. Prochowicz, et al., ACS Appl. Mater. Interfaces 8 (2016) 19860–19865.
[155] X. Yang, J. Chen, H. Liu, X. Li, S. Zhong, Colloids Surf., A 570 (2019) 244–250.
[156] Q. Qiu, H. Chen, Y. Wang, Y. Ying, Coord. Chem. Rev. 387 (2019) 60–78.
[157] G. Chen, X. Kou, S. Huang, et al., Angew. Chem. Int. Ed. 59 (2020) 2867–2874.
[158] Y. Feng, H. Wang, S. Zhang, et al., Adv. Mater. 31 (2019) 1805148.
[159] D. Wei, D. Xiong, N. Zhu, et al., Anal. Chem. 94 (2022) 12981–12989.
[160] S. Huang, Z. Chen, Y. Wang, et al., J. Hazard. Mater. 480 (2024) 135824.
[161] C. Yim, H. Lee, S. Lee, S. Jeon, RSC Adv. 7 (2017) 1418–1422.
[162] M. Sun, W. Wan, X. Zhao, et al., Adv. Funct. Mater. 35 (2025) 2500553.
[163] Y. Shi, Q. Wu, W. Li, et al., J. Hazard. Mater. 432 (2022) 128605.
[164] H. Zhao, X. Tan, H. Chai, et al., Chin. Chem. Lett. 36 (2025) 110571.
[165] S. Ding, X. Wang, Chem. Eng. J. 464 (2023) 142751.
[166] S. Bhattacharjee, R. Das, T. Chakraborty, et al., Chem. Eng. J. 473 (2023) 145238.
[167] Y. Dong, J. Hao, Y. Wang, et al., Chin. Chem. Lett. (2025) 111564, doi:10.1016/j.cclet.2025.111564.
[168] T. Du, J. Wang, L. Zhang, et al., Chem. Eng. J. 431 (2022) 134050.
[169] D. Chen, H. Qiao, S. Fang, J. Rare Earths 43 (2025) 1026–1034.
[170] X. Yu, D.I. Pavlov, A.A. Ryadun, et al., Angew. Chem. Int. Ed. 63 (2024) e202410509.
[171] T. Gao, Z. Ma, Y. Ren, et al., J. Rare Earths 42 (2024) 303–313.
[172] Y.F. Xia, H.Q. Yuan, Z.Q. Cai, et al., Chem. Eng. J. 503 (2025) 158669.
[173] L. Yu, L. Feng, L. Xiong, et al., J. Hazard. Mater. 434 (2022) 128914.
[174] Z.D. Zhou, C.Y. Wang, G.S. Zhu, et al., J. Mol. Struct. 1251 (2022) 132009.
[175] X. Yu, A.A. Ryadun, D.I. Pavlov, T.Y. Guselnikova, A.S. Potapov, V.P. Fedin, Adv. Mater. 36 (2024) 2311939.
[176] S. Zhou, H. Li, H. Gao, et al., Chin. Chem. Lett. 36 (2025) 110142.
[177] T. Chen, Y. Chen, W. Li, et al., Chin. Chem. Lett. 36 (2025) 110214.
[178] Y. Dong, T. Li, H. Su, X. Zhang, J. Zhang, J. Hazard. Mater. 477 (2024) 135281.
[179] Y. Huang, L. Gong, C. Xie, et al., Chem. Eng. J. 506 (2025) 160046.
[180] T. Su, F. Kong, J. Guo, et al., Chem. Eng. J. 521 (2025) 166891.
[181] J. Li, R. Yao, B. Deng, et al., Chem. Eng. J. 464 (2023) 142626.
[182] D. Chen, Y. Xu, J. Wei, et al., Nano Res 17 (2024) 9980–9989.
[183] Y. Zhang, X. Cui, X. Wang, et al., Chem. Eng. J. 474 (2023) 145804.
[184] C.-Y. Wang, C.-C. Wang, X.-W. Zhang, et al., Chin. Chem. Lett. 33 (2022) 1353–1357.
[185] H. Liu, B. Xiao, Y. Zhao, W. Wang, Q. Jia, Chin. Chem. Lett. 36 (2025) 110619.
[186] B. Li, Y. Cheng, X. Ma, et al., Chin. Chem. Lett. 37 (2026) 111134.
[187] J. Lu, H. Zhang, J. Hou, et al., Nat. Mater. 19 (2020) 767–774.
[188] M. Plabst, L.B. McCusker, T. Bein, J. Am. Chem. Soc. 131 (2009) 18112–18118.
[189] X. Zhao, X. Zhang, X. Xing, et al., Adv. Funct. Mater. 35 (2025) 2416628.
[190] C.J. Pedersen, Science 241 (1988) 536–540.
[191] A.A. Lysova, D.G. Samsonenko, P.V. Dorovatovskii, et al., J. Am. Chem. Soc. 141 (2019) 17260–17269.
[192] D.W. Lim, S.A. Chyun, M.P. Suh, Angew. Chem. Int. Ed. 126 (2014) 7953–7956.
[193] L. Feng, X. Chen, M. Cao, et al., Angew. Chem. Int. Ed. 62 (2023) e202312894.
[194] L. Li, K. Kang, T.-S. Chee, et al., Adv. Sci. 11 (2024) 2308663.
[195] A.M. Song, M.J. Yang, Z. Wu, et al., Adv. Funct. Mater. 35 (2025) 2419093.
[196] J. Luo, X. Luo, M. Xie, et al., Nat. Commun. 13 (2022) 7771.
[197] K.-K. Yee, N. Reimer, J. Liu, et al., J. Am. Chem. Soc. 135 (2013) 7795–7798.
[198] M. Mon, F. Lloret, J. Ferrando-Soria, et al., Angew. Chem. Int. Ed. 128 (2016) 11333–11338.
[199] R. Bruno, M. Mon, P. Escamilla, et al., Adv. Funct. Mater. 31 (2021) 2008499.
[200] S. Yang, L. Peng, O.A. Syzgantseva, et al., J. Am. Chem. Soc. 142 (2020) 13415–13425.
[201] M. Mon, R. Bruno, E. Tiburcio, et al., J. Am. Chem. Soc. 141 (2019) 13601–13609.
[202] X. Li, Z. Jin, H. Lu, et al., Adv. Funct. Mater. 35 (2025) 2501311.
[203] J. Baek, B. Rungtaweevoranit, X. Pei, et al., J. Am. Chem. Soc. 140 (2018) 18208–18216.
[204] S. Abednatanzi, P. Gohari Derakhshandeh, H. Depauw, et al., Chem. Soc. Rev. 48 (2019) 2535–2565.
[205] H. Fei, M.R. Bresler, S.R.J. Oliver, J. Am. Chem. Soc. 133 (2011) 11110–11113.
[206] M. Mon, J. Ferrando-Soria, T. Grancha, et al., J. Am. Chem. Soc. 138 (2016) 7864–7867.
[207] J. Cao, Z. Xu, Y. Chen, et al., Angew. Chem. Int. Ed. 62 (2023) e202302202.
[208] J. Guo, C. Luo, P. Li, et al., Chin. Chem. Lett. 37 (2026) 112116.
[209] O.A. Kazi, W. Chen, J.G. Eatman, et al., Adv. Mater. 35 (2023) 2300913.
[210] C.-C. Wang, X. Xu, Chin. Chem. Lett. 36 (2025) 111287.
[211] Y.H. Li, C.C. Wang, X. Zeng, et al., Chem. Eng. J. 442 (2022) 136276.
[212] L. Feng, H. Wang, T. Feng, et al., Angew. Chem. Int. Ed. 61 (2022) e202101015.
[213] D.T. Sun, N. Gasilova, S. Yang, E. Oveisi, W.L. Queen, J. Am. Chem. Soc. 140 (2018) 16697–16703.
[214] F.X. Wang, X.H. Yi, C.C. Wang, J.G. Deng, Chin. J. Catal. 38 (2017) 2141–2149.
[215] M. Chen, T. Liu, X. Zhang, et al., Adv. Funct. Mater. 31 (2021) 2100106.
[216] Y. Guo, Y. Ying, Y. Mao, X. Peng, B. Chen, Angew. Chem. Int. Ed. 55 (2016) 15120–15124.
[217] F.X. Wang, Z.W. Zhang, Z.C. Zhang, et al., Chem. Eng. J. 487 (2024) 150506.
[218] H.Y. Chu, G.C. Liu, F.X. Wang, L.S. Cui, C.C. Wang, Chin. Chem. Lett. 36 (2025) 110745.
[219] K. Yang, M. Yang, H. Chen, et al., Sci. Adv. 11 (2025) eadx3242.
[220] Y. Song, S. Fang, N. Xu, J. Zhu, Nat. Rev. Clean Technol. 1 (2025) 55–74.
[221] H. Zhong, Q. Zhao, Z. Lai, et al., Adv. Funct. Mater. 35 (2025) 2418358.
[222] X. Li, K. Chen, R. Guo, Z. Wei, Chem. Rev. 123 (2023) 10432–10467.
[223] K. Jin, B. Lee, J. Park, Coord. Chem. Rev. 427 (2021) 213473.
[224] S. Dutta, E. Lizundia, J. Goscianska, et al., Adv. Mater. (2025) e18734, doi:10.1002/adma.202418734.
[225] Y. Wu, H. Pang, W. Yao, et al., Sci. Bull. 63 (2018) 831–839.
[226] K.C. Park, C.R. Martin, G.A. Leith, et al., J. Am. Chem. Soc. 144 (2022) 16139–16149.
[227] Y.E. Jung, J.H. Yang, M.-S. Yim, J. Hazard. Mater. 467 (2024) 133777.
[228] P. Cao, Y.-L. Liu, Q. Zhang, et al., Coord. Chem. Rev. 545 (2025) 217018.
[229] Y. Jian, J. Zhang, X. Cao, et al., Nat. Commun. 16 (2025) 9241.
[230] Q.Y. Zhang, L.J. Zhang, J.Q. Zhu, et al., Nat. Commun. 15 (2024) 453.
[231] K. Wan, S. Yuan, J. Zhang, et al., Water Res 285 (2025) 124149.
[232] Y.L. Liu, P. Cao, Q. Zhang, et al., Water Res 286 (2025) 124254.
[233] P. Cao, Y.L. Liu, Q. Zhang, et al., Adv. Funct. Mater. (2025) e14318, doi:10.1002/adfm.202514318.
[234] W. Xiao, D. Pan, Z. Niu, et al., Chin. Chem. Lett. 33 (2022) 3413–3421.
[235] J. Zhang, L. Chen, X. Dai, et al., Chem. Commun. 57 (2021) 8452–8455.
[236] X. Cao, Y. Jin, H. Wang, et al., Chin. Chem. Lett. 35 (2024) 109201.
[237] X. Cao, J. Zhang, J. Pan, et al., Adv. Sci. (2025) e17224, doi:10.1002/advs.202517224.
[238] S. Tian, Z. Yi, J. Chen, S. Fu, J. Hazard. Mater. 443 (2023) 130236.
[239] M. El-Shahat, A.E. Abdelhamid, R.M. Abdelhameed, Carbohydr. Polym. 231 (2020) 115742.
[240] C. Xiao, J. Tian, F. Jiang, et al., Small 20 (2024) 2311181.
[241] W. Zhong, N. Wang, F. Huang, et al., Chem. Eng. J. 522 (2025) 166789.
[242] K. Kang, X. Dai, N. Shen, et al., Chem.-Eur. J. 27 (2021) 5632–5637.
[243] N. Shen, Z. Yang, S. Liu, et al., Nat. Commun. 11 (2020) 5571.
[244] H. Xu, C.S. Cao, H.S. Hu, et al., Angew. Chem. Int. Ed. 58 (2019) 6022–6027.
[245] J. Tang, J. Zhao, S. Wang, et al., Chem. Eng. J. 407 (2021) 127223.
[246] B. Guo, H. Liu, J. Pang, et al., J. Hazard. Mater. 436 (2022) 129094.
[247] H. Zhang, Q. Liu, P. Zhou, et al., J. Hazard. Mater. 485 (2025) 136836.
[248] A.M. Song, M.J. Yang, Z. Wu, et al., Adv. Funct. Mater. 34 (2024) 2406932.
[249] B.Q. Huynh, L.H. Kwong, M.V. Kiang, et al., Nat. Sustain. 4 (2021) 1084–1091.
[250] Z. Chu, Y. Feng, S. Seeger, Angew. Chem. Int. Ed. 54 (2015) 2328–2338.
[251] X.H. Yi, C.C. Wang, Chin. Chem. Lett. 35 (2024) 109094.
[252] N.X. Zhu, Z.W. Wei, C.X. Chen, et al., Angew. Chem. Int. Ed. 61 (2021) e202112097.
[253] Y. Zhao, Y. Cui, X. Meng, J. Ding, H. Hou, Coord. Chem. Rev. 473 (2022) 214815.
[254] L. Jiao, Z. Pan, D. Li, et al., Adv. Funct. Mater. (2025) e12912, doi:10.1002/adfm.202512912.
[255] J. Peng, Y. He, C. Zhou, S. Su, B. Lai, Chin. Chem. Lett. 32 (2021) 1626–1636.
[256] X. Mao, Y. Wang, Z. Gao, et al., ACS Appl. Nano Mater. 6 (2023) 22363–22372.
[257] K. Jayaramulu, K.K.R. Datta, C. Rösler, et al., Angew. Chem. Int. Ed. 55 (2016) 1178–1182.
[258] G. Zheng, X. Kang, H. Ye, et al., Chin. Chem. Lett. 35 (2024) 108817.
[259] X.H. Yi, G.C. Liu, H.Y. Chu, et al., Chem. Commun. 60 (2024) 9530–9533.
[260] J. Gu, H. Fan, C. Li, J. Caro, H. Meng, Angew. Chem. Int. Ed. 131 (2019) 5351–5355.
[261] T. Guo, H. Mashhadimoslem, L. Choopani, et al., Small 20 (2024) 2402942.
[262] Z. Qin, Z. Wang, D. Li, et al., Adv. Mater. Technol. 8 (2023) 2300739.
[263] W. Qu, Z. Wang, M. Qin, et al., Sep. Purif. Technol. 325 (2023) 124673.
[264] S. Gao, F. Zhang, J. Jin, ACS Nano 19 (2025) 11489–11500.
[265] Y. Deng, Y. Wu, G. Chen, et al., Chem. Eng. J. 405 (2021) 127004.
[266] J. Liu, K. Pei, Y. Zhou, et al., Adv. Funct. Mater. (2025) e13624, doi:10.1002/adfm.202513624.
[267] Y. Zhao, X. Yang, Z. Cheng, et al., Nat. Commun. 14 (2023) 2679.
[268] A. Mähringer, M. Hennemann, T. Clark, T. Bein, D.D. Medina, Angew. Chem. Int. Ed. 60 (2021) 5519–5526.
[269] Y. Wang, S. Yang, J. Zhang, et al., Nat. Commun. 14 (2023) 1108.
[270] Q. Guan, Y. Fang, X. Wu, et al., Mater. Today 64 (2023) 138–164.
[271] H. Piao, J. Zhao, Y. Tang, et al., Appl. Catal. B: Environ. 341 (2024) 123300.
[272] H.C. Yang, Y.Z. Chen, K. Li, et al., Angew. Chem. Int. Ed. 64 (2025) e202509503.
[273] X.Y. Guo, L. Zhao, H.N. Li, et al., Science 386 (2024) 654–659.
[274] S.A. Sapchenko, R.V. Belosludov, I.J. Vitoria-Irezabal, et al., Nat. Commun. 16 (2025) 1578.
[275] S.Y. Gu, T. Feng, F.Y. Gang, et al., Chin. Chem. Lett. 36 (2025) 110957.
[276] H. Du, Y. Hui, B. Shen, et al., Appl. Catal. B: Environ. Energy 380 (2026) 125793.

[277] M.I. Severino, A. Al Mohtar, C. Vieira Soares, et al., Angew. Chem. Int. Ed. 62 (2023) e202211583.
[278] X.L. Yang, J. Hu, H. Zhong, et al., Chin. Chem. Lett. 36 (2025) 110120.
[279] S. Zhou, Y. Kuang, H. Yang, et al., Angew. Chem. Int. Ed. 63 (2024) e202412279.
[280] L. Yuan, C. Zhang, Y. Zou, et al., Adv. Funct. Mater. 33 (2023) 2214627.
[281] J. Chen, M. Zhang, S. Zhang, et al., Angew. Chem. 134 (2022) e202212532.
[282] N.C. Chiu, J.M. Lessard, E.N. Musa, et al., Nat. Commun. 15 (2024) 1459.
[283] K. Liu, L. Wang, S. Li, et al., Adv. Funct. Mater. 33 (2023) 2306871.
[284] Y. Wen, Á. Rentería-Gómez, G.S. Day, et al., J. Am. Chem. Soc. 144 (2022) 11840–11850.
[285] S. Kampouri, T.N. Nguyen, M. Spodaryk, et al., Adv. Funct. Mater. 28 (2018) 1806368.
[286] X. Yang, W. Sun, L. Chen, et al., Angew. Chem. 137 (2025) e202519402.
[287] J.V. Burykina, I.I. Surzhikova, R.R. Shaydullin, et al., J. Am. Chem. Soc. 147 (2025) 22796–22805.
[288] H. Zhang, Y.-H. Luo, F.-Y. Chen, et al., J. Hazard. Mater. 441 (2023) 129875.
[289] Z. Qian, R. Zhang, Y. Xiao, et al., Adv. Energy Mater. 13 (2023) 2300086.
[290] Q. Wang, Y. Hui, X. Ma, et al., Chem. Eng. J. 507 (2025) 160487.
[291] A. Liu, X. Ma, B. Shen, et al., Chem. Eng. J. 504 (2025) 158929.
[292] F. Zhao, Y. Liu, S.B. Hammouda, et al., Appl. Catal. B: Environ. 272 (2020) 119033.
[293] H. Li, F. Zhai, D. Gui, et al., Appl. Catal. B: Environ. 254 (2019) 47–54.
[294] M. Chen, T. Liu, X. Zhang, et al., Adv. Funct. Mater. 31 (2021) 2100106.
[295] Q. Tian, Y. Jiang, X. Duan, et al., Water Res 268 (2025) 122621.
[296] C.-H. Gu, M. Du, R.-Y. Han, et al., Angew. Chem. Int. Ed. 64 (2025) e202423629.
[297] Y.N. Wu, D.H. Huang, D.X. Li, X. Qian, J. Niu, Adv. Mater. (2025) e16166, doi:10.1002/adma.202516166.
[298] H. Xu, M. Zhang, Q. Zhang, et al., Angew. Chem. Int. Ed. 64 (2025) e202509527.
[299] X. Zhang, C. Zhou, J. Zhang, et al., Chin. Chem. Lett. (2025) 111630, doi:10.1016/j.cclet.2025.111630.
[300] J.R. Guo, B.Y. Gao, Q. Li, et al., Adv. Mater. 36 (2024) 2403965.
[301] Y. Lei, Y.F. Yu, X. Lei, et al., Environ. Sci. Technol. 57 (2023) 5433–5444.
[302] Y. Zhao, S. Li, S. Tang, et al., Appl. Catal. B: Environ. Energy 378 (2025) 125529.
[303] L.M. Duan, H.H. Jiang, B.R. Cai, et al., Water Res 282 (2025) 123653.
[304] S. Zhu, J. Qiang, L. Hu, et al., Adv. Funct. Mater. (2025) e02912, doi:10.1002/adfm.202502912.
[305] Z.H. Ye, J.A. Padilla, E. Xuriguera, et al., Environ. Sci. Technol. 54 (2020) 4664–4674.
[306] S. Zuo, Y. Ding, L. Wu, et al., Water Res 231 (2023) 119631.
[307] X. Zhang, J. Tang, L. Wang, et al., Nat. Commun. 15 (2024) 917.
[308] Y.H. Li, C.Y. Chen, S. Gao, et al., Angew. Chem. Int. Ed. 64 (2025) e202507772.
[309] J. Peng, W. Zhang, Q.N. Liu, et al., Adv. Mater. 34 (2022) 2108384.
[310] X. Li, X. Huang, S. Xi, et al., J. Am. Chem. Soc. 140 (2018) 12469–12475.
[311] S. Chen, Y. Xiang, Q. Yang, et al., Chin. Chem. Lett. (2025) 111838, doi:10.1016/j.cclet.2025.111838.
[312] M.Y. Lan, Y.H. Li, C.C. Wang, et al., Nat. Commun. 15 (2024) 7208.
[313] T. Lian, L. Xu, D. Piankova, et al., Nat. Commun. 15 (2024) 6199.
[314] X. Guo, H. Zhang, Y. Wang, et al., Angew. Chem. Int. Ed. 64 (2025) e202511266.
[315] C. Jin, B. Han, C. Luo, et al., Water Res 287 (2025) 124420.
[316] L.M. Duan, H.H. Jiang, B.R. Cai, et al., Adv. Funct. Mater. (2025) e09337, doi:10.1002/adfm.202509337.
[317] Z. Wang, M. Zhang, J. Wang, et al., Environ. Sci. Technol. 59 (2025) 7389–7398.
[318] A.W. Wang, M. Du, J.X. Ni, et al., Nat. Commun. 14 (2023) 6733.
[319] Y. Wang, L. Li, P. Zhou, et al., Angew. Chem. Int. Ed. 64 (2025) e202419680.
[320] X. Ren, C. Zhang, X. Zhang, Y. Zhang, M. Zhou, Water Res 287 (2025) 124408.
[321] Y. Du, C. Ding, C. Deng, S. Banerjee, S. Agarwal, Adv. Funct. Mater. (2024) 2416686, doi:10.1002/adfm.202416686.
[322] C. Yang, S. Shang, L. Lin, et al., Nat. Water 2 (2024) 793–802.
[323] N. Liu, J.W. Xu, Y.X. Zhai, et al., Green Energy Environ (2025), doi:10.1016/j.gee.2025.10.006.
[324] J.O. Nriagu, Science 272 (1996) 223-223.
[325] Z. Li, L. Wang, L. Qin, et al., Chemosphere 285 (2021) 131432.
[326] P. Stanley, J. Haimerl, N. Shustova, R. Fischer, J. Warnan, Nat. Chem. 14 (2022) 1342–1356.
[327] S. Karmakar, S. Barman, F.A. Rahimi, et al., Nat. Commun. 14 (2023) 4508.
[328] V. Kumar, V. Singh, K.-H. Kim, E.E. Kwon, S.A. Younis, Coord. Chem. Rev. 447 (2021) 214148.
[329] C.C. Wang, X.D. Du, J. Li, et al., Appl. Catal. B: Environ. 193 (2016) 198–216.
[330] P.D. Harvey, Sep. Purif. Technol. 322 (2023) 124214.
[331] H. Wang, Y. Shi, J. Guo, et al., Chin. Chem. Lett. 36 (2025) 110779.
[332] Y. Hou, F. Liu, C. Nie, Z. Li, M. Tong, Environ. Sci. Technol. 57 (2023) 11675–11686.
[333] S. Li, C. Wang, K. Dong, et al., Chin. J. Catal. 51 (2023) 101–112.
[334] S. Li, K. Dong, M. Cai, X. Li, X. Chen, eScience 4 (2024) 100208.
[335] E. Svensson Grape, A.J. Chacón-García, S. Rojas, et al., Nat. Water 1 (2023) 433–442.
[336] L. Shen, S. Liang, W. Wu, R. Liang, L. Wu, Dalton Trans 42 (2013) 13649–13657.
[337] Y. Zhang, Y. Zhang, C.-X. Jia, et al., Chin. Chem. Lett. 35 (2024) 109756.
[338] W. Zou, Q. Li, Q. Wu, Z. Zhang, Y. Zhou, Chem. Eng. J. 505 (2025) 159428.
[339] Y. Xiang, X. Ji, X. Dong, et al., Chem. Eng. J. 509 (2025) 161196.
[340] X.-H. Yi, Y. Gao, C.-C. Wang, et al., Chin. Chem. Lett. 34 (2023) 108029.
[341] X. Liu, S. Naraginti, F. Zhang, et al., Carbon Neutrality 3 (2024) 15.
[342] F. He, A. Abulimiti, B. Li, et al., ACS Appl. Nano Mater. 6 (2023) 12871–12881.
[343] M.G. Evich, M.J.B. Davis, J.P. McCord, et al., Science 375 (2022) eabg9065.
[344] N.N. Adarsh, M. Wriedt, Nat. Water 2 (2024) 1157–1165.
[345] D. Xia, H. Zhang, Y. Ju, et al., J. Am. Chem. Soc. 146 (2024) 11266–11271.
[346] S. Wei, X. Li, C. Huang, et al., Chin. Chem. Lett. (2025) 111858.
[347] Y. Yang, Z. Zheng, W. Ji, J. Xu, X. Zhang, J. Hazard. Mater. 395 (2020) 122686.
[348] R.-R. Liang, S. Xu, Z. Han, et al., J. Am. Chem. Soc. 146 (2024) 9811–9818.
[349] X. Zhang, X. Zeng, M. Rong, et al., J. Hazard. Mater. 498 (2025) 139877.
[350] C. Zhao, Y. Xu, F. Xiao, et al., Chem. Eng. J. 406 (2020) 126852.
[351] N. Ilić, K. Tan, F. Mayr, et al., Adv. Mater. 37 (2024) 2413120.
[352] R.R. Liang, Y. Yang, Z. Han, et al., Adv. Mater. 36 (2024) 2407194.
[353] P.H. Chang, R. Mukhopadhyay, B. Zhong, et al., J. Colloid Interface Sci. 636 (2023) 459–469.
[354] E. Loukopoulos, S. Marugán-Benito, D. Raptis, et al., Adv. Funct. Mater. 34 (2024) 2409932.
[355] R.-R. Liang, Y. Fu, Z. Han, et al., Nat. Water 2 (2024) 1218–1225.
[356] R. Li, S. Alomari, T. Islamoglu, et al., Environ. Sci. Technol. 55 (2021) 15162–15171.
[357] M. Koli, B. Kanwar, S.R. Wickramasinghe, S.P. Singh, Desalination 616 (2025) 119392.
[358] Z. Liu, M. Liao, L. Wang, S. Zhuang, Rev. Environ. Sci. Bio/Technol. 23 (2024) 63–95.
[359] C. Yan, Z. Zhong, J. Wang, K. Feng, D. Xing, Chem. Eng. J. 513 (2025) 163085.
[360] J. Wang, C.-S. Cao, J. Wang, Y. Zhang, L. Zhu, Appl. Catal. B: Environ. 304 (2022) 121013.
[361] X. Zhang, H. Wu, Y. Wang, et al., Water Res 265 (2024) 122276.
[362] Y. Wang, S. Li, Y. Shao, et al., Chem. Eng. J. 443 (2022) 136514.
[363] A.D. Vethaak, J. Legler, Science 371 (2021) 672–674.
[364] W. Zhao, S. Shao, H. Ma, et al., Chin. Chem. Lett. 36 (2025) 110846.
[365] V. Nava, S. Chandra, J. Aherne, et al., Nature 619 (2023) 317–322.
[366] P. Stegmann, V. Daioglou, M. Londo, D.P. van Vuuren, M. Junginger, Nature 612 (2022) 272–276.
[367] R.C. Thompson, Y. Olsen, R.P. Mitchell, et al., Science 304 (2004) 838-838.
[368] D.M. Mitrano, P. Wick, B. Nowack, Nat. Nanotecchnol. 16 (2021) 491–500.
[369] C.C. Wang, Z.C. Zhang, X.H. Yi, Chin. Chem. Lett. 34 (2023) 108182.
[370] B.N.T. Nguyen, T.T.Y. Tan, K.I. Otake, S. Kitagawa, J.Y.C. Lim, Angew. Chem. Int. Ed. 64 (2025) e202504017.
[371] S. Wan, S. Zhao, H. Shi, et al., Fuel 399 (2025) 135580.
[372] X. Lin, Y. Zhou, J. Hong, et al., Chin. Chem. Lett. 35 (2024) 109835.
[373] D. You, Y. Zhao, W. Yang, Q. Pan, J. Li, Chem. Res. Chin. Univ. 38 (2022) 186–191.
[374] M. Jiang, Y. Yang, Y. Wang, et al., Chem. Eng. Sci. 317 (2025) 122101.
[375] F. Liu, X. Gao, R. Shi, et al., Angew. Chem. Int. Ed. 62 (2023) e202300094.
[376] Y. Chen, S. Zhang, S. Cao, et al., Adv. Mater. 29 (2017) 1606221.
[377] H. Guo, D.-H. Si, H.-J. Zhu, et al., eScience 2 (2022) 295–303.
[378] J. Ding, T. Fan, K. Shen, Y. Li, Appl. Catal. B: Environ. 292 (2021) 120174.
[379] M. Haris, M.W. Khan, A. Zavabeti, N. Mahmood, N. Eshtiaghi, Chem. Eng. J. 455 (2023) 140390.
[380] Y. Liu, J. Guo, J.-W. Wang, et al., Chem. Eng. J. 467 (2023) 143389.
[381] L. Han, J. Mao, A.-Q. Xie, et al., Sep. Purif. Technol. 309 (2023) 123003.
[382] W. Li, D. Xiao, X. Gong, et al., Chem. Eng. J. 480 (2024) 148087.
[383] K. Zhang, X. Zhang, B. Zou, et al., Chem. Commun. 58 (2022) 7070–7073.
[384] M.A. Shannon, P.W. Bohn, M. Elimelech, et al., Nature 452 (2008) 301–310.
[385] J.R. Werber, C.O. Osuji, M. Elimelech, Nat. Rev. Mater. 1 (2016) 16018.
[386] Y. Cheng, S.J. Datta, S. Zhou, et al., Chem. Soc. Rev. 51 (2022) 8300–8350.
[387] X. Shi, H. Li, T. Chen, et al., Nat. Chem. Eng. 1 (2024) 483–493.
[388] S. Shahzadi, M. Akhtar, M. Arshad, M.H. Ijaz, M.R.S.A. Janjua, RSC Adv. 14 (2024) 27575–27607.
[389] S. Qiu, M. Xue, G. Zhu, Chem. Soc. Rev. 43 (2014) 6116–6140.
[390] Q. Xing, X. Xu, H. Li, et al., Molecules 29 (2024) 3885.
[391] L. Wang, J. Huang, Z. Li, Z. Han, J. Fan, Polymers (Basel) 15 (2023) 1950.
[392] S. Hermes, F. Schröder, R. Chelmowski, C. Wöll, R.A. Fischer, J. Am. Chem. Soc. 127 (2005) 13744–13745.
[393] Y. Liu, Z. Zhao, M. Li, Z. Zhao, J. Mater. Chem. C 12 (2024) 3394–3409.
[394] Y. Sun, R. Zhang, C. Zhao, et al., RSC Adv 4 (2014) 33007–33012.
[395] Q. Li, J. Li, X. Fang, et al., Chem. Commun. 54 (2018) 3590–3593.
[396] E. Virmani, J.M. Rotter, A. Mähringer, et al., J. Am. Chem. Soc. 140 (2018) 4812–4819.
[397] R. Wei, H.-Y. Chi, X. Li, et al., Adv. Funct. Mater. 30 (2020) 1907089.
[398] F. Yan, J. Yan, Y. Sun, et al., Eur. J. Inorg. Chem. 26 (2023) e202200679.
[399] X. Liu, N.K. Demir, Z. Wu, K. Li, J. Am. Chem. Soc. 137 (2015) 6999–7002.
[400] D. Zacher, O. Shekhah, C. Wöll, R.A. Fischer, Chem. Soc. Rev. 38 (2009) 1418–1429.
[401] M.L. Ohnsorg, C.K. Beaudoin, M.E. Anderson, Langmuir 31 (2015) 6114–6121.
[402] X. Wu, Y. Yang, X. Lu, Z. Wang, J. Membr. Sci. 613 (2020) 118518.
[403] A. Lamaire, J. Wieme, S. Vandenhaute, et al., Nat. Commun. 15 (2024) 9997.
[404] J. Ma, X. Guo, Y. Ying, D. Liu, C. Zhong, Chem. Eng. J. 313 (2017) 890–898.
[405] S.Y. Fang, J.L. Gong, L. Tang, et al., Chem. Eng. J. 449 (2022) 137808.
[406] L. Ni, M. Li, X. Guo, et al., J. Membr. Sci. 709 (2024) 123149.
[407] J. Xie, Z. Liao, M. Zhang, et al., Environ. Sci. Technol. 55 (2021) 2652–2661.
[408] B. Seoane, J. Coronas, I. Gascon, et al., Chem. Soc. Rev. 44 (2015) 2421–2454.
[409] H.L. Choi, Y. Jeong, H. Lee, T.-H. Bae, JACS Au 4 (2024) 253–262.

[410] S. Sorribas, P. Gorgojo, C. Téllez, J. Coronas, A.G. Livingston, J. Am. Chem. Soc. 135 (2013) 15201–15208.
[411] C. Zhang, Y. Dai, J.R. Johnson, O. Karvan, W.J. Koros, J. Membr. Sci. 389 (2012) 34–42.
[412] J. Dechnik, J. Gascon, C.J. Doonan, C. Janiak, C.J. Sumby, Angew. Chem. Int. Ed. 56 (2017) 9292–9310.
[413] A. Elrasheedy, N. Nady, M. Bassyouni, A. El-Shazly, Membranes (Basel) 9 (2019) 88.
[414] K. Kamali, T. Mohammadi, S. Zarghami, Ind. Eng. Chem. Res. 64 (2025) 16299–16311.
[415] D.L. Zhao, F. Feng, L. Shen, et al., Chem. Eng. J. 454 (2023) 140447.
[416] B. Zhu, S. He, Y. Yang, et al., Nat. Commun. 14 (2023) 1697.
[417] M.M. Jia, J.H. Feng, W. Shao, et al., J. Membr. Sci. 694 (2024) 122418.
[418] X. Li, Matter 1 (2019) 1112.
[419] N. Hosono, W. Guo, K. Omoto, H. Yamada, S. Kitagawa, Chem. Lett. 48 (2019) 597–600.
[420] Z. Wang, Z. Wang, S. Lin, et al., Nat. Commun. 9 (2018) 2004.
[421] C. Echaide-Górriz, Y. Aysa-Martínez, M. Navarro, C. Téllez, J. Coronas, ACS Appl. Mater. Interfaces 13 (2021) 7773–7783.
[422] M. Kadhom, W. Hu, B. Deng, Membranes (Basel) 7 (2017) 31.
[423] J. Duan, Y. Pan, F. Pacheco, et al., J. Membr. Sci. 476 (2015) 303–310.
[424] M. Pejman, M. Dadashi Firouzjaei, S. Aghapour Aktij, et al., ACS Appl. Mater. Interfaces 12 (2020) 36287–36300.
[425] Z. Liao, X. Fang, J. Xie, et al., ACS Appl. Mater. Interfaces 11 (2019) 5344–5352.
[426] X. Yang, ACS Omega 4 (2019) 13824–13833.
[427] L. Ni, Z. Liao, K. Chen, et al., Chem. Commun. 56 (2020) 8372–8375.
[428] J. Zhu, L. Qin, A. Uliana, et al., ACS Appl. Mater. Interfaces 9 (2017) 1975–1986.
[429] S. Singh, N. Sivaram, B. Nath, et al., npj Clean Water 7 (2024) 124.
[430] C. Wang, J. Kim, J. Tang, et al., Chem 6 (2020) 19–40.
[431] H. Fan, M. Peng, I. Strauss, et al., Nat. Commun. 12 (2021) 38.
[432] S.J. Yang, T. Kim, J.H. Im, et al., Chem. Mater. 24 (2012) 464–470.
[433] Y. Xue, N.N.T. Pham, G. Nam, et al., Chem. Eng. J. 408 (2021) 127305.
[434] F. Zhan, S. Liu, Q. He, et al., Energy Storage Mater 52 (2022) 685–735.
[435] Y.N. Wu, F. Li, H. Liu, et al., J. Mater. Chem. 22 (2012) 16971–16978.
[436] M. Kim, R. Xin, J. Earnshaw, et al., Nat. Protoc. 17 (2022) 2990–3027.
[437] J. Shui, C. Chen, L. Grabstanowicz, D. Zhao, D.-J. Liu, Proc. Natl. Acad. Sci. 112 (2015) 10629–10634.
[438] X. Liu, L. Zhang, J. Wang, J. Materiomics 7 (2021) 440–459.
[439] J. Xie, Y. Yang, H. Zhang, et al., Chem. Eng. J. 451 (2023) 138403.
[440] S. Pan, J. Li, O. Noonan, et al., Environ. Sci. Technol. 51 (2017) 5098–5107.
[441] Y. Yang, J. Xie, Y. Yao, et al., ACS ES&T Water 3 (2023) 1884–1892.
[442] Z. Guo, P. Ren, F. Yang, et al., ACS Appl. Mater. Interfaces 15 (2023) 7308–7318.
[443] H. Saini, N. Srinivasan, V. Šedajová, et al., ACS Nano 15 (2021) 18742–18776.
[444] Y. Wang, D. Zhao, R.I. Woolway, et al., Natl. Sci. Rev. 12 (2025) nwaf011.
[445] L. Feng, Y. Wang, X. Hou, et al., Nat. Rev. Earth Environ. 5 (2024) 631–644.
[446] C. Mays, S. McLoughlin, T.D. Frank, et al., Nat. Commun. 12 (2021) 5511.
[447] Y. Chen, J. Li, J. Wei, et al., J. Hazard. Mater. 321 (2016) 888–895.
[448] Y. Wang, Theore. Natur. Sci. 6 (2023) 371–375.
[449] J.H. Wang, Y.N. Wang, G.H. Dao, et al., Ecol. Indic 115 (2020) 106425.
[450] Y. Wu, L. Li, N. Gan, et al., J. Environ. Sci. 26 (2014) 1921–1929.
[451] S. Pavagadhi, S. Natera, U. Roessner, R. Balasubramanian, Environ. Sci. Technol. 47 (2013) 14376–14384.
[452] K. Zhang, T.F. Lin, T. Zhang, C. Li, N. Gao, J. Environ. Sci. 25 (2014) 1539–1548.
[453] X. Mamatimin, W. Song, M. Yilimulati, T. Zhang, N. Habibul, J. Hazard. Mater. 494 (2025) 138766.
[454] B. Balaji-Prasath, Y. Wang, Y.P. Su, et al., Environ. Chem. Lett. 20 (2022) 3133–3152.
[455] H. Ma, Z. Yin, Q. Wang, et al., Chin. Chem. Lett. (2025) 112174, doi:10.1016/j.cclet.2025.112174.
[456] C. Li, P. Li, H. Fu, et al., Sci. Total Environ. 871 (2023) 161995.
[457] L. Yue, M. Tao, L. Xu, et al., J. Hazard. Mater. 462 (2024) 132799.
[458] J. Wang, S.P. Teong, S.N. Riduan, et al., J. Am. Chem. Soc. 146 (2023) 599–608.
[459] S. Qing, X. Lu, Y. Jiang, et al., Chin. Chem. Lett. 37 (2024) 110576.
[460] Y. Liang, X. Yang, X. Wang, et al., Nat. Commun. 14 (2023) 5223.
[461] Y. Hou, Z. Su, Y. Wu, J. Ma, Sep. Purif. Technol. 358 (2024) 130310.
[462] Z. Yu, Y. Shi, J. Lin, et al., Int. J. Biol. Macromol. 319 (2025) 145130.
[463] H.Y. Chu, G.C. Liu, F.X. Wang, L.S. Cui, C.C. Wang, Chin. Chem. Lett. 36 (2025) 110745.
[464] I.L. Hsu, F.H. Yeh, Y.C. Chin, et al., Chem. Eng. J. 409 (2020) 128266.
[465] Y. Shangguan, R. Wang, H. Tang, et al., Small (2025) 2411116, doi:10.1002/smll.202411116.
[466] L. Guo, J. Zhou, R. Liu, et al., ACS Appl. Mater. Interfaces 17 (2025) 46803–46819.
[467] L. Zheng, J. Zhu, J. Chen, Y. Xu, L. Jiang, J. Inorg. Organomet. Polym. Mater. 35 (2024) 570–582.
[468] M. Wang, J. Chen, Y. Wei, et al., J. Hazard. Mater. 465 (2024) 133273.
[469] P. Roszkowski, A. Bielenica, J. Stefańska, et al., Biomed. Pharmacother. 179 (2024) 117439.
[470] J. Xiang, J. Qi, D. Hu, et al., J. Hazard. Mater. 469 (2024) 133969.
[471] G. Fan, L. Hong, X. Zheng, et al., RSC Adv 8 (2018) 35314–35326.
[472] B. Yu, Y. Liu, Z. Li, et al., Chem. Eng. J. 455 (2022) 140840.
[473] X. Dai, Z. Hu, Y. Wu, et al., Appl. Catal. B: Environ. Energy 379 (2025) 125667.
[474] J. Cui, C. Dou, X. Cong, et al., Sep. Purif. Technol. 364 (2025) 132536.
[475] J. Liang, S. Luo, D. Pan, et al., Chem. Eng. J. 464 (2023) 142646.
[476] G. Fan, J. Zhang, J. Zhan, et al., J. Hazard. Mater. 419 (2021) 126407.
[477] Y. Li, S. Shang, J. Shang, W.-X. Wang, Environ. Pollut. 291 (2021) 118199.
[478] R. Wang, L. Hu, M. Wang, et al., Chemosphere 343 (2023) 140276.
[479] Y. Li, W.-X. Wang, Environ. Pollut. 346 (2024) 123595.
[480] G. Fan, M. Bao, X. Zheng, et al., J. Hazard. Mater. 367 (2019) 529–538.
[481] G. Fan, J. Zhou, X. Zheng, et al., Chemosphere 239 (2020) 124721.
[482] X. Cao, G. Fan, J. Luo, et al., J. Hazard. Mater. 478 (2024) 135461.
[483] X. Wang, K. Huang, J. Gao, et al., Sci. Total Environ. 792 (2021) 148247.
[484] N. Gu, J. Gao, K. Wang, et al., J. Taiwan Inst. Chem. Eng. 64 (2016) 189–195.
[485] A. Dhakshinamoorthy, Z. Li, S. Yang, H. Garcia, Chem. Soc. Rev. 53 (2024) 3002–3035.
[486] M. Wang, E. Liu, T. Jin, et al., Water Res 250 (2024) 121052.
[487] H. Kim, S. Yang, S.R. Rao, et al., Science 356 (2017) 430–434.
[488] M.A. van der Veen, S. Canossa, M. Wahiduzzaman, et al., Adv. Mater. 36 (2023) 2210050.
[489] J.J. Oppenheim, M. Dincă, J. Am. Chem. Soc. 146 (2024) 20615–20626.
[490] C. Jia, Q.M. Junaid, G.-Y. Han, et al., Adv. Funct. Mater. 35 (2025) 2505730.
[491] A.J. Rieth, A.M. Wright, M. Dincă, Nat. Rev. Mater. 4 (2019) 708–725.
[492] Y. Han, P. Das, Y. He, et al., J. Am. Chem. Soc. 144 (2022) 19567–19575.
[493] S.R. Shin, H.S. Cho, Y. Lee, et al., J. Am. Chem. Soc. 143 (2021) 20747–20757.
[494] N.C. Burtch, H. Jasuja, K.S. Walton, Chem. Rev. 114 (2014) 10575–10612.
[495] M. Ding, X. Cai, H.-L. Jiang, Chem. Sci. 10 (2019) 10209–10230.
[496] C. Yang, H. Wu, J. Yun, et al., Adv. Mater. 35 (2023) 2210235.
[497] V. Bon, I. Senkovska, J.D. Evans, et al., J. Mater. Chem. A 7 (2019) 12681–12690.
[498] H. Lyu, Z. Ji, S. Wuttke, O.M. Yaghi, Chem 6 (2020) 2219–2241.
[499] H. Jiang, D. Alezi, M. Eddaoudi, Nat. Rev. Mater. 6 (2021) 466–487.
[500] M. Zhai, F. Moghadam, T. Gosiamemang, J.Y.Y. Heng, K. Li, Nat. Commun. 15 (2024) 10264.
[501] L. Valenzano, B. Civalleri, S. Chavan, et al., Chem. Mater. 23 (2011) 1700–1718.
[502] K. Yang, T. Pan, Q. Lei, et al., Environ. Sci. Technol. 55 (2021) 6542–6560.
[503] Y. Li, Y. Liu, Y. Chen, et al., Green Chem 18 (2015) 1010–1018.
[504] M.S. Kang, I. Heo, S.H. Park, et al., Nat. Commun. 15 (2024) 9793.
[505] L. Ge, Y. Feng, Y. Xue, et al., Small Struct 4 (2023) 2300055.
[506] J. Wang, L. Hua, C. Li, R. Wang, Energy Environ. Sci. 15 (2022) 4867–4871.
[507] H. Kim, S.R. Rao, E.A. Kapustin, et al., Nat. Commun. 9 (2018) 1191.
[508] N. Hanikel, M.S. Prévot, O.M. Yaghi, Nat. Nanotecchnol. 15 (2020) 348–355.
[509] A. Fuchs, F. Knechtel, H. Wang, et al., J. Am. Chem. Soc. 145 (2023) 14324–14334.
[510] F. Fathieh, M.J. Kalmutzki, E.A. Kapustin, et al., Sci. Adv. 4 (2018) eaat3198.
[511] H. Reinsch, M.A. van der Veen, B. Gil, et al., Chem. Mater. 25 (2012) 17–26.
[512] S.S.Y. Chui, S.M.F. Lo, J.P.H. Charmant, A.G. Orpen, I.D. Williams, Science 283 (1999) 1148–1150.
[513] Z. Chen, P. Li, X. Zhang, et al., J. Am. Chem. Soc. 141 (2019) 2900–2905.
[514] W. Xu, O.M. Yaghi, ACS Central Sci 6 (2020) 1348–1354.
[515] L.G. Gordeeva, Y.D. Tu, Q. Pan, et al., Nano Energy 84 (2021) 105946.
[516] W. Song, Z. Zheng, A.H. Alawadhi, O.M. Yaghi, Nat. Water 1 (2023) 626–634.
[517] N. Hanikel, M.S. Prévot, F. Fathieh, et al., ACS Central Sci 5 (2019) 1699–1706.
[518] J. Xu, X. Huo, T. Yan, et al., Energy Environ. Sci. 17 (2024) 4988–5001.
[519] A. Ghaffarkhah, M. Panahi-Sarmad, S. Rostami, et al., Adv. Funct. Mater. 35 (2025) 2506427.
[520] H. Zou, X. Yang, J. Zhu, et al., Nat. Water 2 (2024) 663–673.
[521] D. Lenzen, J. Zhao, S.J. Ernst, et al., Nat. Commun. 10 (2019) 3025.
[522] K.H. Cho, D.D. Borges, U.H. Lee, et al., Nat. Commun. 11 (2020) 5112.
[523] B. Han, A. Chakraborty, Renewable Sustainable Energy Rev 198 (2024) 114411.
[524] D. Lenzen, P. Bendix, H. Reinsch, et al., Adv. Mater. 30 (2017) 1705869.
[525] J. Canivet, A. Fateeva, Y. Guo, B. Coasne, D. Farrusseng, Chem. Soc. Rev. 43 (2014) 5594–5617.
[526] S.K. Henninger, H.A. Habib, C. Janiak, J. Am. Chem. Soc. 131 (2009) 2776–2777.
[527] K. Tu, Z. Zhang, C.H. Dreimol, et al., Mater. Horiz. 11 (2024) 5786–5797.
[528] F.F. Lu, X.W. Gu, E. Wu, B. Li, G. Qian, J. Mater. Chem. A 11 (2023) 1246–1255.
[529] M. Qin, O.S. Rasmussen, J. Chen, L. Wadsö, Build. Environ. 261 (2024) 111757.
[530] S. Laha, T.K. Maji, Adv. Funct. Mater. 32 (2022) 2203093.
[531] X. Liu, D. Beysens, T. Bourouina, ACS Mater. Lett. 4 (2022) 1003–1024.
[532] K.M.C. Santos, T.R. Menezes, M.R. Oliveira, et al., Sep. Purif. Technol. 276 (2021) 119409.
[533] H.A.A. Farag, M.M. Ezzat, H. Amer, A.W. Nashed, Alexandria Eng. J. 50 (2011) 431–439.
[534] A.C. Ferrari, F. Bonaccorso, V. Fal'ko, et al., Nanoscale 7 (2015) 4598–4810.
[535] J.S. Yun, Z.H. Lee, N.N.k. Odilova, et al., Korean. J. Chem. Eng. 42 (2025) 1845–1859.
[536] A. Cadiau, Y. Belmabkhout, K. Adil, et al., Science 356 (2017) 731–735.
[537] X. Wang, Z. Li, R. Gao, et al., Environ. Sci. Technol. 58 (2024) 17190–17200.
[538] G. Cai, P. Yan, L. Zhang, H.-C. Zhou, H.-L. Jiang, Chem. Rev. 121 (2021) 12278–12326.
[539] X. Wang, L. Wu, Z. Wang, et al., Appl. Catal. B: Environ. 322 (2023) 122075.
[540] G.-C. Liu, X.-Y. Liu, X.-H. Yi, et al., Water Res 289 (2026) 124791.
[541] M. Chen, J. Ma, X. Chen, et al., Chin. Chem. Lett. (2025) 111637, doi:10.1016/j.cclet.2025.111637.
[542] Y. Chai, F. Wang, Y. Gao, et al., Environ. Res. 282 (2025) 122099.
[543] Z.C. Zhang, R.-X. Mei, F.X. Wang, et al., Environ. Sci.: Nano 12 (2025) 4843–4849.
[544] X. Wang, Z. Wang, Y. Liu, et al., Top. Catal. (2024) 1–22, doi:10.1007/s11244-024-01947-3.
[545] W. Yang, X. Li, Y. Li, R. Zhu, H. Pang, Adv. Mater. 31 (2019) 1804740.
[546] X. Xu, J. Liu, J. Liu, et al., Adv. Funct. Mater. 28 (2018) 1707573.
[547] X. Wang, Y. Liu, H. Dai, et al., Green Energy Environ 10 (2025) 1674–1691.

[548] C. Wang, J. Kim, J. Tang, et al., Angew. Chem. Int. Ed. 59 (2020) 2066–2070.
[549] Q. Yan, C. Lian, K. Huang, et al., Angew. Chem. Int. Ed. 60 (2021) 17155–17163.
[550] J. Pei, J. Liu, K. Fu, et al., Nat. Commun. 16 (2025) 800.
[551] X. Yu, H. Liu, Y. Huang, et al., Proc. Natl. Acad. Sci. 120 (2023) e2221228120.
[552] X. Liang, D. Wang, Z. Zhao, et al., Adv. Funct. Mater. 32 (2022) 2203001.
[553] Z.Q. Zhang, P.-J. Duan, C.W. Bai, et al., Nat. Commun. 16 (2025) 2376.
[554] Y.H. Li, T. Li, X. Hu, et al., Adv. Funct. Mater. (2025) e14549, doi:10.1002/adfm.202514549.
[555] X. Zhou, Y. Zhou, S. Zhao, et al., Adv. Funct.ater. (2025) e13232, doi:10.1002/adfm.202513232.
[556] S. Xu, X. Mi, P. Wang, et al., Adv. Funct. Mater. 33 (2023) 2308204.
[557] Y. Yang, X. Mao, R. Li, et al., Adv. Funct. Mater. 33 (2023) 2210265.
[558] J. Wang, L. Yuan, C. Zhang, et al., Adv. Funct. Mater. 31 (2021) 2107260.
[559] W. Bao, M. Liu, J. Meng, et al., Nat. Commun. 12 (2021) 6399.
[560] Y. Li, W.X. Wang, Environ. Sci. Technol. 57 (2023) 118–127.
[561] R. Ettlinger, U. Lächelt, R. Gref, et al., Chem. Soc. Rev. 51 (2022) 464–484.
[562] X. Lu, Z. Yan, F. Hao, et al., Eco-Environ Health 4 (2025) 100191.
[563] Y. Li, Z. Liu, Z. Cui, K. Qu, B. Xia, J. Hazard. Mater. 498 (2025) 139859.
[564] G. Fan, J. Zhou, X. Zheng, W. Chen, Appl. Organomet. Chem 32 (2018) e4600.
[565] M. Wang, B. Xia, Z. Cui, K. Qu, Y. Li, Aquat. Toxicol. 285 (2025) 107421.
[566] C.B. Field, M.J. Behrenfeld, J.T. Randerson, P. Falkowski, Science 281 (1998) 237–240.
[567] L. Yang, H. Chen, A.E. Kaziem, et al., ACS Nano 18 (2024) 25425–25445.
[568] Y. Shi, X. Rong, C. Chen, et al., J. Fac. Agr., Kyushu Univ. 66 (2021) 211–216.
[569] L. Jin, S. Wang, C. Chen, X. Qiu, C.C. Wang, Antioxidants 12 (2023) 1345.
[570] W. Li, W. Xiong, S. He, et al., Environ. Res. 269 (2025) 120922.
[571] X. Qiu, L. Liu, W. Xu, et al., Antioxidants 11 (2022) 945.
[572] M.S. Nikzad, J. Qiu, G. Wang, et al., Aquat. Toxicol. 287 (2025) 107529.
[573] X. Li, X. Shu, Y. Shi, H. Li, X. Pei, Chin. Chem. Lett. 34 (2023) 107986.
[574] L. Liu, X. Bai, M.-V. Martikainen, et al., Nat. Commun. 12 (2021) 5726.
[575] R. Mohammadpour, M.A. Dobrovolskaia, D.L. Cheney, K.F. Greish, H. Ghandehari, Advanced Drug Deliver. Rev. 144 (2019) 112–132.
[576] L. He, Z. Wang, H. Wang, Y.-n. Wu, Coord. Chem. Rev. 526 (2025) 216361.
[577] A. Carboni, D.L. Slomberg, M. Nassar, et al., Environ. Sci. Technol. 55 (2021) 16270–16282.
[578] N. Chandimali, S.G. Bak, E.H. Park, et al., Cell Death Discov 11 (2025) 19.
[579] K. Chen, A. Zhou, X. Zhou, et al., Sci. Adv. 10 (2024) eadk3201.
[580] Y. Gao, F. Wang, J. Tang, et al., Chem. Eng. J. 495 (2024) 153631.
[581] H. Wang, Y. Li, X. Xuan, et al., Environ. Sci. Technol. 59 (2025) 6361–6378.
[582] X. Liao, R. Lu, L. Xia, et al., Energy Environ. Mater. 5 (2022) 157–185.
[583] J.P. Perdew, J.A. Chevary, S.H. Vosko, et al., Phys. Rev. B 46 (1992) 6671.
[584] S.J. Clark, M.D. Segall, C.J. Pickard, et al., Z. Kristallogr. Cryst. Mater. 220 (2005) 567–570.
[585] G. Kresse, D. Joubert, Phys. Rev. B 59 (1999) 1758.
[586] B.G. Johnson, P.M. Gill, J.A. Pople, J. Chem. Phys. 98 (1993) 5612–5626.
[587] Y. Li, Z. Yang, Y. Wang, et al., Nat. Commun. 8 (2017) 1354.
[588] G. Liu, Y. Guo, C. Chen, et al., Nat. Mater. 22 (2023) 769–776.
[589] K. Fu, X. Liu, C. Lv, et al., Environ. Sci. Technol. 56 (2022) 2677–2688.
[590] L. Chen, J. Hu, A.G. Borthwick, et al., Nat. Water 2 (2024) 453–463.
[591] L.B. Vilhelmsen, K.S. Walton, D.S. Sholl, J. Am. Chem. Soc. 134 (2012) 12807–12816.
[592] X. Song, D. Mei, Phys. Chem. Chem. Phys. 22 (2020) 23645–23656.
[593] J. Zhou, L. Xu, H. Gai, et al., Angew. Chem. Int. Ed. 136 (2024) e202409449.
[594] Y. Chen, X. Zhang, X. Wang, et al., J. Am. Chem. Soc. 143 (2021) 4302–4310.
[595] M. Li, Y. Liu, F. Li, et al., Environ. Sci. Technol. 55 (2021) 13209–13218.
[596] A.O. Zacharias, A. Varghese, K. Akshaya, M. Savitha, L. George, J. Mol. Struct. 1158 (2018) 1–13.
[597] T. Lu, F. Chen, J. Comput. Chem. 33 (2012) 580–592.
[598] J. Guo, Y. Wang, Y. Shang, et al., Proc. Natl. Acad. Sci. 121 (2024) e2313387121.
[599] Z. Chen, F. An, Y. Zhang, et al., Proc. Natl. Acad. Sci. 120 (2023) e2305933120.
[600] W. Liu, Y. Li, F. Liu, et al., Water Res 151 (2019) 8–19.
[601] H. Ji, P. Du, D. Zhao, et al., Appl. Catal. B: Environ. 263 (2020) 118357.
[602] H. Zhang, C. Xie, L. Chen, et al., Water Res 229 (2023) 119392.
[603] H. Zhang, L. Chen, P. Du, F. Li, W. Liu, Environ. Sci. Technol. 58 (2024) 3506–3519.
[604] Y.-H. Li, C.-C. Wang, X.-H. Yi, H.-Y. Chu, Environ. Funct. Mater. 2 (2023) 93–132.
[605] H.S. Jadhav, H.A. Bandal, S. Ramakrishna, H. Kim, Adv. Mater. 34 (2022) 2107072.
[606] Y.-H. Li, C.-C. Wang, F. Wang, et al., Appl. Catal. B: Environ. 331 (2023) 122699.
[607] W. Orellana, J. Phys. Chem. C 128 (2024) 6471–6477.
[608] S. Rojas, P. Horcajada, Chem. Rev. 120 (2020) 8378–8415.
[609] Y.-H. Li, S. Gao, L. Zhang, et al., Chin. Chem. Lett. 35 (2024) 109894.
[610] F.-X. Wang, C.-C. Wang, X. Du, et al., Chem. Eng. J. 429 (2022) 132495.
[611] R. Su, Y. Gao, L. Chen, et al., Proc. Natl. Acad. Sci. 121 (2024) e2319427121.
[612] K. Sun, Y. Huang, Q. Wang, et al., J. Am. Chem. Soc. 146 (2024) 3241–3249.
[613] R.F. Bader, Chem. Rev. 91 (1991) 893–928.
[614] R.S. Mulliken, J. Chem. Phys. 23 (1955) 1833–1840.
[615] F.L. Hirshfeld, Theor. Chim. Acta 44 (1977) 129–138.
[616] Z. Zhao, P. Wang, C. Song, et al., Angew. Chem. Int. Ed. 62 (2023) e202216403.
[617] Z. Fang, Y. Liu, J. Qi, et al., Appl. Catal. B: Environ. 320 (2023) 121979.
[618] R. Dronskowski, P.E. Bloechl, J. Phys. Chem. 97 (1993) 8617–8624.
[619] S. Kielar, C. Li, H. Huang, et al., Nat. Commun. 15 (2024) 6981.
[620] R.Y. Rohling, I.C. Tranca, E.J. Hensen, E.A. Pidko, J. Phys. Chem. C 123 (2019) 2843–2854.
[621] H. Wang, Y. Liu, L. Li, et al., Angew. Chem. 137 (2025) e202506960.
[622] T. Liu, S. Xiao, N. Li, et al., Nat. Commun. 14 (2023) 2881.
[623] X. Li, Y. Gao, J. Qi, et al., Adv. Funct. Mater. 35 (2025) 2502680.
[624] S. Chen, H. Lin, Z. Zhao, et al., Chin. Chem. Lett. (2025) 111982, doi:10.1016/j.cclet.2025.111982.
[625] X. Ren, C.C. Wang, Y. Li, P. Wang, S. Gao, J. Hazard. Mater. 445 (2023) 130552.
[626] S. Bhattacharjee, U.V. Waghmare, S.-C. Lee, Sci. Rep. 6 (2016) 35916.
[627] C. Bozal-Ginesta, S. Pablo-García, C. Choi, A. Tarancón, A. Aspuru-Guzik, Nat. Rev. Chem. 9 (2025) 601–616.
[628] H. Xu, D. Cheng, D. Cao, X.C. Zeng, Nat. Catal. 7 (2024) 207–218.
[629] S.T. Khan, S.M. Moosavi, Nat. Commun. 16 (2025) 5642.
[630] R. Batra, L. Song, R. Ramprasad, Nat. Rev. Mater. 6 (2021) 655–678.
[631] B. Madika, A. Saha, C. Kang, et al., ACS Nano 19 (2025) 27116–27158.
[632] R. Du, R. Xin, H. Wang, et al., Chem. Eng. J. 490 (2024) 151828.
[633] Z. Zhang, A.S. Palakkal, X. Wu, J. Jiang, Z. Jiang, Environ. Sci. Technol. 59 (2025) 9123–9133.
[634] M. Jalali, A.D.D. Wonanke, C. Wöll, J. Cheminf. 15 (2023) 94.
[635] Q. Wang, Z. Xiao, C. Fan, J. Environ. Chem. Eng. 13 (2025) 118503.
[636] J. Wang, J. Liu, H. Wang, et al., Nat. Commun. 15 (2024) 1904.
[637] J. Li, J. Wang, H. Mu, et al., ACS ES&T Engg 3 (2023) 1258–1266.
[638] Y. Luo, S. Bag, O. Zaremba, et al., Angew. Chem. Int. Ed. 61 (2022) e202200242.
[639] L. Yuan, M. Xu, Y. Zhang, et al., Sep. Purif. Technol. 339 (2024) 126732.
[640] W. Li, Z. Sun, Y. Chen, et al., Chin. Chem. Lett. (2025) 111791, doi:10.1016/j.cclet.2025.111791.
[641] M. Gheytanzadeh, A. Baghban, S. Habibzadeh, et al., Sci. Rep. 12 (2022) 6615.
[642] N. Li, W. Gao, B. Yan, et al., Sci. Bull. 70 (2025) 811–814.
[643] C.E. Richards, A. Tzachor, S. Avin, R. Fenner, Nat. Water 1 (2023) 422–432.
[644] A. Ozcan, F.-X. Coudert, S.M.J. Rogge, et al., J. Am. Chem. Soc. 147 (2025) 23367–23380.
[645] Q. Ma, P. Yin, M. Zhao, et al., Adv. Mater. 31 (2019) 1808249.
[646] Y. Feng, L. Ge, Y. Zhao, et al., Energy Environ. Sci. 17 (2024) 1083–1094.
[647] M. Najafi, S. Abednatanzi, P. Gohari Derakhshandeh, et al., Coord. Chem. Rev. 454 (2022) 214332.
[648] M.R. Azhar, Y. Arafat, M. Khiadani, S. Wang, Z. Shao, Composites, Part B 192 (2020) 107985.
[649] P. Bhadane, S. Chakraborty, Coord. Chem. Rev. 535 (2025) 216669.
[650] M. Panahi-Sarmad, T. Guo, S.A. Hashemi, et al., Adv. Mater. (2025) 2413353, doi:10.1002/adma.202413353.
[651] C. Ji, M. Xu, H. Yu, L. Lv, W. Zhang, J. Hazard. Mater. 424 (2022) 127684.
[652] S. Dutta, S. Fajal, S.K. Ghosh, Acc. Chem. Res. 57 (2024) 2546–2560.
[653] T. Zhang, P. Li, S. Ding, X. Wang, J. Hazard. Mater. 424 (2022) 127742.
[654] X. Zhao, Y. Wang, X. Gao, et al., Chin. Chem. Lett. 36 (2025) 109901.
[655] W. Zhang, B. Yang, Z. Xiang, Chin. Chem. Lett. 36 (2025) 109630.